Simulations of the Effect of Integrated Metal Nanoparticles on the Optical Absorptance of Perovskite Photovoltaic Solar Cells

Torbjørn Egeland-Eriksen

Thesis presented for the
Master's Degree in Energy
Renewable Energy

University of Bergen
Faculty of Mathematics and Natural Sciences
Geophysical Institute
June 2018
Main supervisor: Professor Dr. Bodil Holst

Abstract

The negative effects from the use of fossil fuels that are evident in the ongoing climate change and pollution challenges necessitates a shift from fossil fuels to renewable energy technologies. The most promising of these is probably photovoltaic solar cells, and one of the most promising photovoltaic technologies is perovskite solar cells. These are a type of thin film solar cells that has shown the most rapid increase in power conversion efficiency of any photovoltaic technology in history. They are also relatively cheap and easy to produce, as well as light-weight and flexible, which makes them a promising candidate for building integrated solar cells. However, they are still in the research stage and require further development to achieve long-term stability and to scale up to commercial sizes.

Plasmonic effects that arise from the integration of metal nanoparticles within the perovskite solar cells is a very promising method for increasing the power conversion efficiency of these solar cells. This thesis used computer simulations to investigate how these plasmonic effects alter the fraction of light that is absorbed by the solar cell, since light absorptance is the most important factor affecting the power conversion efficiency. Close to 400 simulations are performed using the Lumerical FDTD Solutions software. The materials used for the nanoparticles are gold, silver, aluminum and platinum, and the shapes used are spheres, cubes, rods (cylinders) and pyramids. Simulations using core-shell particles with a silicon dioxide shell, and simulations where the position and number of nanoparticles is adjusted are also performed. Material data from research articles are imported and used for the various layers of the solar cell structure.

The absorptance increases in almost all the simulations where nanoparticles are used. Relatively large nanoparticles usually show the highest absorptance. The thinnest solar cell, where the thickness of the active perovskite layer is 200 nm, show a larger increase in absorptance relative to the reference solar cell without nanoparticles than the thicker solar cell (500 nm perovskite) does. These two thicknesses (200 and 500 nm) for the perovskite layer was used in the simulations because those are the lower and upper limit of the thicknesses that are usually used in published research literature on the topic, and because the 200 nm layer showed the highest absorptance per nm while the 500 nm layer showed the highest total absorptance. The largest total absorptance was achieved by using a platinum nanoparticle shaped like a pyramid in the thickest solar cell, while the largest relative absorptance increase was achieved by using a platinum nanoparticle shaped like a cube in the thinnest solar cell. The former achieved a total absorptance of 0.861 (86.1% of incident photons were absorbed), while the latter achieved a 52.9% increase in absorptance relative to the reference solar cell without nanoparticles. However, the reduced price and higher availability of aluminum could make it more beneficial to replace the platinum nanoparticles with aluminum, which resulted in a

total absorptance of 0.848 (as opposed to 0.861 for platinum) for the thickest solar cell and a relative absorptance increase of 47.6% (as opposed to 52.9% for platinum) for the thinnest solar cell.

All simulation results in this thesis strongly indicate that the integration of metal nanoparticles in perovskite solar cells will increase the absorptance of the solar cell, and consequently increase the power conversion efficiency. Utilizing plasmonic effects therefore seem to be a very promising route towards creating high-efficiency thin film solar cells.

Acknowledgements

I would like to thank my main supervisor, Professor Dr. Bodil Holst, and my co-supervisor, Dr. Martin Møller Greve, for valuable guidance throughout the writing process. I would also like to thank M.Sc. Vårin Renate Andvik Holm for dedicating the better part of two of her busy days to giving me an introduction to the Lumerical software. It was very helpful and no doubt saved me a lot of time.

Most of all I would like to thank my family, and particularly my wife Hilde for putting up with a husband who had to spend the majority of nights and weekends on studies for six continuous years. This would not have been possible without you.

Contents

1 Introduction **1**
- 1.1 Background . . . 1
- 1.2 Thesis Objectives . . . 4
- 1.3 Methods and Tools . . . 4
- 1.4 Thesis Outline . . . 5
- 1.5 Definitions . . . 5

2 Photovoltaic Solar Cells **6**
- 2.1 History . . . 6
- 2.2 Working Principle . . . 8
- 2.3 The pn Junction . . . 9
- 2.4 Characteristics of PV Cells . . . 10
- 2.5 Types of PV cells . . . 14
  - 2.5.1 Three Generations of PV cells . . . 14
  - 2.5.2 Crystalline Silicon (*c*-Si) . . . 14
  - 2.5.3 Gallium Arsenide (GaAs) . . . 15
  - 2.5.4 Amorphous Silicon (*a*-Si) . . . 15
  - 2.5.5 Cadmium Telluride (CdTe) . . . 16
  - 2.5.6 Copper Indium Gallium Selenide (CIGS) and Copper Indium Selenide (CIS) . . . 16
  - 2.5.7 Organic PV cells . . . 16
  - 2.5.8 Dye-Sensitized Solar Cells (DSSC) . . . 17
  - 2.5.9 Perovskite . . . 17
  - 2.5.10 Quantum Dots (QD) . . . 17

3 Perovskite PV Cells **19**
- 3.1 History . . . 19
- 3.2 Materials and Architecture . . . 20
  - 3.2.1 The Organic Cation (A) . . . 21
  - 3.2.2 The Metal Cation (B) . . . 22
  - 3.2.3 The Halide Anion (X) . . . 23
  - 3.2.4 The Mesoporous Scaffold Architecture . . . 24
  - 3.2.5 The Planar Architecture . . . 24
- 3.3 Working principle . . . 25
- 3.4 Challenges and future possibilities . . . 27

4 Plasmonic PV Cells **32**
4.1 Working Principle . . . 32
4.1.1 Light Scattering . . . 33
4.1.2 Near-Field Enhancement . . . 34
4.1.3 Plasmon-Induced Energy Transfer . . . 35
4.2 Plasmonic Perovskite PV Cells . . . 36

5 Computer Simulation Model **40**
5.1 Lumerical FDTD Solutions . . . 40
5.2 Simulation Settings . . . 42

6 Simulation Results **49**
6.1 Comparison with Existing Work . . . 49
6.2 Perovskite Without Nanoparticles . . . 52
6.3 Solid Gold Spheres . . . 54
6.4 Solid Silver Spheres . . . 57
6.5 Solid Aluminum Spheres . . . 59
6.6 Solid Platinum Spheres . . . 61
6.7 Solid Gold Cubes . . . 63
6.8 Solid Silver Cubes . . . 66
6.9 Solid Aluminum Cubes . . . 68
6.10 Solid Platinum Cubes . . . 71
6.11 Solid Gold Rods . . . 73
6.12 Solid Silver Rods . . . 76
6.13 Solid Aluminum Rods . . . 78
6.14 Solid Platinum Rods . . . 81
6.15 Solid Gold Pyramids . . . 83
6.16 Solid Silver Pyramids . . . 86
6.17 Solid Aluminum Pyramids . . . 88
6.18 Solid Platinum Pyramids . . . 91
6.19 Gold Sphere Variations . . . 93
6.20 Silver Sphere Variations . . . 97
6.21 Aluminum Sphere Variations . . . 101
6.22 Platinum Sphere Variations . . . 105
6.23 Gold Cube Variations . . . 109
6.24 Silver Cube Variations . . . 113
6.25 Aluminum Cube Variations . . . 117
6.26 Platinum Cube Variations . . . 121
6.27 Gold Rod Variations . . . 125
6.28 Silver Rod Variations . . . 129
6.29 Aluminum Rod Variations . . . 133
6.30 Platinum Rod Variations . . . 137
6.31 Gold Pyramid Variations . . . 141
6.32 Silver Pyramid Variations . . . 145
6.33 Aluminum Pyramid Variations . . . 149
6.34 Platinum Pyramid Variations . . . 153
6.35 Results Summary . . . 157
6.35.1 Maximum Absorptance . . . 158
6.35.2 Spheres . . . 159

6.35.3 Cubes 160
6.35.4 Rods 161
6.35.5 Pyramids 162
6.35.6 Core-Shell and Other Variations 163
6.35.7 Overall 164

7 Summary, Conclusion and Future Work **167**

A Calculation and Plotting Methods **175**

List of Figures

1.1 GHG emissions grouped by economic sector. Figure is taken from [1]. 2
1.2 Forecast of the world's final energy demand by energy carrier. Figure is taken from [2]. 2
1.3 Forecast of the world's electricity generation by source. Figure is taken from [2]. 3
1.4 Forecast of the world's primary energy supply by source. Figure is taken from [2]. 3

2.1 Global installed photovoltaic power capacity [3]. 7
2.2 Predicted global electricity production in 2050 [2]. 8
2.3 Cross-section of a basic silicon PV cell [4]. 9
2.4 The pn junction after the n-type and p-type semiconductor layers have been combined. The full black circles and empty black circles are the free electrons and holes, respectively. The plus signs and minus signs are the positively and negatively charged ions, respectively. The depletion layer is shown in the middle and the electric field will be from the right to the left in the figure. The figure is taken from [5]. . 10
2.5 A typical J-V curve for a PV cell. The short circuit current density, J_{sc}, and the open circuit voltage, V_{oc}, is shown along with the maximum power point and the corresponding current, J_{m}, and voltage, V_{m}. The gray curve is the power density, and the peak of this curve has the voltage value V_{m}. See the text in section 2.4 for further details. The figure is taken from [6]. 11
2.6 PCE development of different PV technologies [7]. 12
2.7 The standard solar spectra. AM0 is the irradiance above the atmosphere (solar constant), AM1.5 Direct is the irradiance at the earth surface with the sun at an angle of 48 degrees with only direct light, and AM1.5 Global is AM1.5 Direct plus the irradiance from diffuse light. AM1.5 Global is the spectrum that is used as Standard Test Condition (STC) for PV cells. Plot is taken from [8]. 13
2.8 Map of global irradiance [9]. 14

3.1 a) The ABX_3 perovskite crystal structure, also showing a BX_6 octahedral. b) The unit cell of one of the most common perovskite materials in PV cells. Methylammonium ($CH_3NH_3^+$) is the organic cation (A), lead (Pb^{2+}) is the metal cation (B) and iodide (I^-) is the halide anion (X), resulting in $CH_3NH_3PbI_3$. Figure taken from [10]. . 20

3.2 The absorbance and band gap of some of the different perovskite materials. a) Absorbance of perovskite with different metal cations (pure Pb, pure Sn and mixtures of both. b) Band gap for various perovskite materials. Figure taken from [11]. 22
3.3 Two different architectures for perovskite PV cells. The arrows symbolize incident sunlight. a) Mesoporous/mesoscopic scaffold architecture, b) planar architecture. Figure taken from [11]. 25
3.4 a) Energy diagram for a typical perovskite PV cell, also showing movements of electrons and holes. b) Band bending of energy levels during separation of charges. Figure taken from [12]. 26
3.5 Average PCE for perovskite PV cells with (S1) and without (S2) excess PbI_2 in ambient air at 60% relative humidity (RH) as a function of time with a) alternating simulated sunlight in 10 hour dark/14 hour sunlight cycles at room temperature, and b) at 85°C and under constant simulated illumination. Figure taken from [13]. 28
3.6 *I-V* curve of a standard perovskite PV cell showing hysteresis. The blue dots show the reverse scan and the red dots show the forward scan. Figure taken from [12]. 30

4.1 Number of scientific publications reported in the Scopus database by searching for "plasmonic solar cells". Figure taken from [14]. 33
4.2 Different plasmonic light trapping configurations for thin film PV cells. a) Metal nanoparticles on the surface of the PV cell. b) Metal nanoparticles embedded in the active layer of the PV cell. c_1) Metal nanoparticles at the interface between the metal electrode and the active layer. c_2) Metal arrays at the interface between the metal electrode and the active layer. Figure taken from [14]. 34
4.3 A) SPP near-field on a gold film. B) LSPR near-field on gold spheres. C) The dispersion plot of LSPR (LSP) and SPP together with light. Figure is taken from [15]. 36

5.1 The Yee cell with the different components of the electric and magnetic fields. The simulation space in Lumerical is divided into numerous Yee cells. Figure taken from [16]. 42
5.2 The basic structure used in the simulations in this thesis. The red layer is perovskite (active layer), the green layer is TiO_2 (ETM) and the blue layer is spiro-OMeTAD (HTM). The purple arrow indicates the direction of the incident light, which is perpendicular to the surface of the structure. Everything inside the orange box is the simulation region, the yellow square at the top is a monitor that records reflectance and the yellow square at the bottom is a monitor that records transmittance. 46

6.1 The reflectance and transmittance for the perovskite material deposited on a glass substrate. The thickness of the perovskite film is 305.68 nm. (a) Simulation from this thesis, using Lumerical. (b) Experimental and modeled results from [17]. 50

6.2 The absorptance of a perovskite PV cell, both simulated in [18, 19] and in this thesis. (a) Perovskite with thickness 300 nm, no nanoparticle. (b) Perovskite with thickness 300 nm, gold sphere with diameter 240 nm. (c) Perovskite with thickness 300 nm, aluminum sphere with diameter 240 nm. (d) Perovskite with thickness 600 nm, two gold spheres with diameter 180 nm and 10 nm gap between spheres. . 51
6.3 Absorptance for perovskite PV cell without nanoparticles. Seven different simulations are shown with various layer thicknesses. t_p is the thickness of the perovskite layer. The thicknesses of the TiO_2 layer (ETM) and spiro-OMeTAD layer (HTM) is given in table 6.2 53
6.4 Absorptance for the 310 nm PV cell with solid Au nanospheres of various diameters included. The thick blue line is the absorptance of the reference PV cell without nanoparticles. 56
6.5 Absorptance for the 880 nm PV cell with solid Au nanospheres of various diameters included. The thick red line is the absorptance of the reference PV cell without nanoparticles. 56
6.6 Absorptance for the 310 nm PV cell with solid Ag nanospheres of various diameters included. The thick blue line is the absorptance of the reference PV cell without nanoparticles. 58
6.7 Absorptance for the 880 nm PV cell with solid Ag nanospheres of various diameters included. The thick red line is the absorptance of the reference PV cell without nanoparticles. 58
6.8 Absorptance for the 310 nm PV cell with solid Al nanospheres of various diameters included. The thick blue line is the absorptance of the reference PV cell without nanoparticles. 60
6.9 Absorptance for the 880 nm PV cell with solid Al nanospheres of various diameters included. The thick red line is the absorptance of the reference PV cell without nanoparticles. 61
6.10 Absorptance for the 310 nm PV cell with solid Pt nanospheres of various diameters included. The thick blue line is the absorptance of the reference PV cell without nanoparticles. 62
6.11 Absorptance for the 880 nm PV cell with solid Pt nanospheres of various diameters included. The thick red line is the absorptance of the reference PV cell without nanoparticles. 63
6.12 Absorptance for the 310 nm PV cell with solid Au nanocubes with various side lengths included (s is side length). The thick blue line is the absorptance of the reference PV cell without nanoparticles. 65
6.13 Absorptance for the 880 nm PV cell with solid Au nanocubes with various side lengths included (s is side length). The thick red line is the absorptance of the reference PV cell without nanoparticles. 65
6.14 Absorptance for the 310 nm PV cell with solid Ag nanocubes with various side lengths included (s is side length). The thick blue line is the absorptance of the reference PV cell without nanoparticles. 67
6.15 Absorptance for the 880 nm PV cell with solid Ag nanocubes with various side lengths included (s is side length). The thick red line is the absorptance of the reference PV cell without nanoparticles. 68

6.16 Absorptance for the 310 nm PV cell with solid Al nanocubes with various side lengths included (s is side length). The thick blue line is the absorptance of the reference PV cell without nanoparticles. 70
6.17 Absorptance for the 880 nm PV cell with solid Al nanocubes with various side lengths included (s is side length). The thick red line is the absorptance of the reference PV cell without nanoparticles. 70
6.18 Absorptance for the 310 nm PV cell with solid Pt nanocubes with various side lengths included (s is side length). The thick blue line is the absorptance of the reference PV cell without nanoparticles. 72
6.19 Absorptance for the 880 nm PV cell with solid Pt nanocubes with various side lengths included (s is side length). The thick red line is the absorptance of the reference PV cell without nanoparticles. 73
6.20 Absorptance for the 310 nm PV cell with solid Au nanorods with various diameters and lengths included (d is diameter, L is length). The thick red line is the absorptance of the reference PV cell without nanoparticles. 75
6.21 Absorptance for the 880 nm PV cell with solid Au nanorods with various diameters and lengths included (d is diameter, L is length). The thick red line is the absorptance of the reference PV cell without nanoparticles. 75
6.22 Absorptance for the 310 nm PV cell with solid Ag nanorods with various diameters and lengths included (d is diameter, L is length). The thick red line is the absorptance of the reference PV cell without nanoparticles. 77
6.23 Absorptance for the 880 nm PV cell with solid Ag nanorods with various diameters and lengths included (d is diameter, L is length). The thick red line is the absorptance of the reference PV cell without nanoparticles. 78
6.24 Absorptance for the 310 nm PV cell with solid Al nanorods with various diameters and lengths included (d is diameter, L is length). The thick red line is the absorptance of the reference PV cell without nanoparticles. 80
6.25 Absorptance for the 880 nm PV cell with solid Al nanorods with various diameters and lengths included (d is diameter, L is length). The thick red line is the absorptance of the reference PV cell without nanoparticles. 80
6.26 Absorptance for the 310 nm PV cell with solid Pt nanorods with various diameters and lengths included (d is diameter, L is length). The thick red line is the absorptance of the reference PV cell without nanoparticles. 82
6.27 Absorptance for the 880 nm PV cell with solid Pt nanorods with various diameters and lengths included (d is diameter, L is length). The thick red line is the absorptance of the reference PV cell without nanoparticles. 83
6.28 Absorptance for the 310 nm PV cell with solid Au nanopyramids with various side lengths and heights included (s is side length, h is height). The thick red line is the absorptance of the reference PV cell without nanoparticles. 85

6.29 Absorptance for the 880 nm PV cell with solid Au nanopyramids with various side lengths and heights included (s is side length, h is height). The thick red line is the absorptance of the reference PV cell without nanoparticles. 85
6.30 Absorptance for the 310 nm PV cell with solid Ag nanopyramids with various side lengths and heights included (s is side length, h is height). The thick red line is the absorptance of the reference PV cell without nanoparticles. 87
6.31 Absorptance for the 880 nm PV cell with solid Ag nanopyramids with various side lengths and heights included (s is side length, h is height). The thick red line is the absorptance of the reference PV cell without nanoparticles. 88
6.32 Absorptance for the 310 nm PV cell with solid Al nanopyramids with various side lengths and heights included (s is side length, h is height). The thick red line is the absorptance of the reference PV cell without nanoparticles. 90
6.33 Absorptance for the 880 nm PV cell with solid Al nanopyramids with various side lengths and heights included (s is side length, h is height). The thick red line is the absorptance of the reference PV cell without nanoparticles. 90
6.34 Absorptance for the 310 nm PV cell with solid Pt nanopyramids with various side lengths and heights included (s is side length, h is height). The thick red line is the absorptance of the reference PV cell without nanoparticles. 92
6.35 Absorptance for the 880 nm PV cell with solid Pt nanopyramids with various side lengths and heights included (s is side length, h is height). The thick red line is the absorptance of the reference PV cell without nanoparticles. 93
6.36 Absorptance for various setups of the 310 nm PV cell. (a) Total absorptance of the Au@SiO_2 core-shell nanospheres (thin lines) compared to the Au sphere of the same size but without a SiO_2 shell (thick lines). d is the diameter of the Au sphere and t is the thickness of the SiO_2 shell. (b)Total absorptance for Au nanosphere at bottom interface, top interface, double nanospheres side by side, double nanospheres over/under, compared to the centered Au nanosphere of the same size (thick line) from section 6.3. d is the diameter of the sphere and g is the gap between the two spheres. 96
6.37 Absorptance for various setups of the 880 nm PV cell. (a) Total absorptance of the Au@SiO_2 core-shell nanospheres (thin lines) compared to the Au sphere of the same size but without a SiO_2 shell (thick lines). d is the diameter of the Au sphere and t is the thickness of the SiO_2 shell. (b)Total absorptance for Au nanosphere at bottom interface, top interface, double nanospheres side by side, double nanospheres over/under, compared to the centered Au nanosphere of the same size (thick line) from section 6.3. d is the diameter of the sphere and g is the gap between the two spheres. 96

6.38 Absorptance for various setups of the 310 nm PV cell. (a) Total absorptance of the Ag@SiO_2 core-shell nanospheres (thin lines) compared to the Ag sphere of the same size but without a SiO_2 shell (thick lines). d is the diameter of the Ag sphere and t is the thickness of the SiO_2 shell. (b)Total absorptance for Ag nanosphere at bottom interface, top interface, double nanospheres side by side, double nanospheres over/under, compared to the centered Ag nanosphere of the same size (thick line) from section 6.4. d is the diameter of the sphere and g is the gap between the two spheres. 100
6.39 Absorptance for various setups of the 880 nm PV cell. (a) Total absorptance of the Ag@SiO_2 core-shell nanospheres (thin lines) compared to the Ag sphere of the same size but without a SiO_2 shell (thick lines). d is the diameter of the Ag sphere and t is the thickness of the SiO_2 shell. (b)Total absorptance for Ag nanosphere at bottom interface, top interface, double nanospheres side by side, double nanospheres over/under, compared to the centered Ag nanosphere of the same size (thick line) from section 6.4. d is the diameter of the sphere and g is the gap between the two spheres. 100
6.40 Absorptance for various setups of the 310 nm PV cell. (a) Total absorptance of the Al@SiO_2 core-shell nanospheres (thin lines) compared to the Al sphere of the same size but without a SiO_2 shell (thick lines). d is the diameter of the Al sphere and t is the thickness of the SiO_2 shell. (b)Total absorptance for Al nanosphere at bottom interface, top interface, double nanospheres side by side, double nanospheres over/under, compared to the centered Al nanosphere of the same size (thick line) from section 6.5. d is the diameter of the sphere and g is the gap between the two spheres. 104
6.41 Absorptance for various setups of the 880 nm PV cell. (a) Total absorptance of the Al@SiO_2 core-shell nanospheres (thin lines) compared to the Al sphere of the same size but without a SiO_2 shell (thick lines). d is the diameter of the Al sphere and t is the thickness of the SiO_2 shell. (b)Total absorptance for Al nanosphere at bottom interface, top interface, double nanospheres side by side, double nanospheres over/under, compared to the centered Al nanosphere of the same size (thick line) from section 6.5. d is the diameter of the sphere and g is the gap between the two spheres. 104
6.42 Absorptance for various setups of the 310 nm PV cell. (a) Total absorptance of the Pt@SiO_2 core-shell nanospheres (thin lines) compared to the Pt sphere of the same size but without a SiO_2 shell (thick lines). d is the diameter of the Pt sphere and t is the thickness of the SiO_2 shell. (b)Total absorptance for Pt nanosphere at bottom interface, top interface, double nanospheres side by side, double nanospheres over/under, compared to the centered Pt nanosphere of the same size (thick line) from section 6.6. d is the diameter of the sphere and g is the gap between the two spheres. 108

6.43 Absorptance for various setups of the 880 nm PV cell. (a) Total absorptance of the Pt@SiO_2 core-shell nanospheres (thin lines) compared to the Pt sphere of the same size but without a SiO_2 shell (thick lines). d is the diameter of the Pt sphere and t is the thickness of the SiO_2 shell. (b)Total absorptance for Pt nanosphere at bottom interface, top interface, double nanospheres side by side, double nanospheres over/under, compared to the centered Pt nanosphere of the same size (thick line) from section 6.6. d is the diameter of the sphere and g is the gap between the two spheres. 108
6.44 Absorptance for various setups of the 310 nm PV cell. (a) Total absorptance of the Au@SiO_2 core-shell nanocubes (thin lines) compared to the Au cube of the same size but without a SiO_2 shell (thick lines). s is the side length of the Au cube and t is the thickness of the SiO_2 shell. (b)Total absorptance for Au nanocube at bottom interface, top interface, double nanocubes side by side, double nanocubes over/under, compared to the centered Au nanocube of the same size (thick line) from section 6.7. s is the side length of the cube and g is the gap between the two cubes. 112
6.45 Absorptance for various setups of the 880 nm PV cell. (a) Total absorptance of the Au@SiO_2 core-shell nanocubes (thin lines) compared to the Au cube of the same size but without a SiO_2 shell (thick lines). s is the side length of the Au cube and t is the thickness of the SiO_2 shell. (b)Total absorptance for Au nanocube at bottom interface, top interface, double nanocubes side by side, double nanocubes over/under, compared to the centered Au nanocube of the same size (thick line) from section 6.7. s is the side length of the cube and g is the gap between the two cubes. 112
6.46 Absorptance for various setups of the 310 nm PV cell. (a) Total absorptance of the Ag@SiO_2 core-shell nanocubes (thin lines) compared to the Ag cube of the same size but without a SiO_2 shell (thick lines). s is the side length of the Ag cube and t is the thickness of the SiO_2 shell. (b)Total absorptance for Ag nanocube at bottom interface, top interface, double nanocubes side by side, double nanocubes over/under, compared to the centered Ag nanocube of the same size (thick line) from section 6.8. s is the side length of the cube and g is the gap between the two cubes. 116
6.47 Absorptance for various setups of the 880 nm PV cell. (a) Total absorptance of the Ag@SiO_2 core-shell nanocubes (thin lines) compared to the Ag cube of the same size but without a SiO_2 shell (thick lines). s is the side length of the Ag cube and t is the thickness of the SiO_2 shell. (b)Total absorptance for Ag nanocube at bottom interface, top interface, double nanocubes side by side, double nanocubes over/under, compared to the centered Ag nanocube of the same size (thick line) from section 6.8. s is the side length of the cube and g is the gap between the two cubes. 116

6.48 Absorptance for various setups of the 310 nm PV cell. (a) Total absorptance of the Al@SiO_2 core-shell nanocubes (thin lines) compared to the Al cube of the same size but without a SiO_2 shell (thick lines). s is the side length of the Al cube and t is the thickness of the SiO_2 shell. (b)Total absorptance for Al nanocube at bottom interface, top interface, double nanocubes side by side, double nanocubes over/under, compared to the centered Al nanocube of the same size (thick line) from section 6.9. s is the side length of the cube and g is the gap between the two cubes. 120
6.49 Absorptance for various setups of the 880 nm PV cell. (a) Total absorptance of the Al@SiO_2 core-shell nanocubes (thin lines) compared to the Al cube of the same size but without a SiO_2 shell (thick lines). s is the side length of the Al cube and t is the thickness of the SiO_2 shell. (b)Total absorptance for Al nanocube at bottom interface, top interface, double nanocubes side by side, double nanocubes over/under, compared to the centered Al nanocube of the same size (thick line) from section 6.9. s is the side length of the cube and g is the gap between the two cubes. 120
6.50 Absorptance for various setups of the 310 nm PV cell. (a) Total absorptance of the Pt@SiO_2 core-shell nanocubes (thin lines) compared to the Pt cube of the same size but without a SiO_2 shell (thick lines). s is the side length of the Pt cube and t is the thickness of the SiO_2 shell. (b)Total absorptance for Pt nanocube at bottom interface, top interface, double nanocubes side by side, double nanocubes over/under, compared to the centered Pt nanocube of the same size (thick line) from section 6.10. s is the side length of the cube and g is the gap between the two cubes. 124
6.51 Absorptance for various setups of the 880 nm PV cell. (a) Total absorptance of the Pt@SiO_2 core-shell nanocubes (thin lines) compared to the Pt cube of the same size but without a SiO_2 shell (thick lines). s is the side length of the Pt cube and t is the thickness of the SiO_2 shell. (b)Total absorptance for Pt nanocube at bottom interface, top interface, double nanocubes side by side, double nanocubes over/under, compared to the centered Pt nanocube of the same size (thick line) from section 6.10. s is the side length of the cube and g is the gap between the two cubes. 124
6.52 Absorptance for various setups of the 310 nm PV cell. (a) Total absorptance of the Au@SiO_2 core-shell nanorods (thin lines) compared to the Au rod of the same size but without a SiO_2 shell (thick lines). d is the diameter of the Au rod and t is the thickness of the SiO_2 shell. (b)Total absorptance for Au nanorod at bottom interface, top interface, double nanorods side by side, double nanorods over/under, compared to the centered Au nanorod of the same size (thick line) from section 6.11. d is the diameter of the rod and g is the gap between the two rods. All rods in this thesis have a length that is equal to three times its diameter (aspect ratio is 3). 128

6.53 Absorptance for various setups of the 880 nm PV cell. (a) Total absorptance of the Au@SiO_2 core-shell nanorods (thin lines) compared to the Au rod of the same size but without a SiO_2 shell (thick lines). d is the diameter of the Au rod and t is the thickness of the SiO_2 shell. (b)Total absorptance for Au nanorod at bottom interface, top interface, double nanorods side by side, double nanorods over/under, compared to the centered Au nanorod of the same size (thick line) from section 6.11. d is the diameter of the rod and g is the gap between the two rods. All rods in this thesis have a length that is equal to three times its diameter (aspect ratio is 3). 128
6.54 Absorptance for various setups of the 310 nm PV cell. (a) Total absorptance of the Ag@SiO_2 core-shell nanorods (thin lines) compared to the Ag rod of the same size but without a SiO_2 shell (thick lines). d is the diameter of the Ag rod and t is the thickness of the SiO_2 shell. (b)Total absorptance for Ag nanorod at bottom interface, top interface, double nanorods side by side, double nanorods over/under, compared to the centered Ag nanorod of the same size (thick line) from section 6.12. d is the diameter of the rod and g is the gap between the two rods. All rods in this thesis have a length that is equal to three times its diameter (aspect ratio is 3). 132
6.55 Absorptance for various setups of the 880 nm PV cell. (a) Total absorptance of the Ag@SiO_2 core-shell nanorods (thin lines) compared to the Ag rod of the same size but without a SiO_2 shell (thick lines). d is the diameter of the Ag rod and t is the thickness of the SiO_2 shell. (b)Total absorptance for Ag nanorod at bottom interface, top interface, double nanorods side by side, double nanorods over/under, compared to the centered Ag nanorod of the same size (thick line) from section 6.12. d is the diameter of the rod and g is the gap between the two rods. All rods in this thesis have a length that is equal to three times its diameter (aspect ratio is 3). 132
6.56 Absorptance for various setups of the 310 nm PV cell. (a) Total absorptance of the Al@SiO_2 core-shell nanorods (thin lines) compared to the Al rod of the same size but without a SiO_2 shell (thick lines). d is the diameter of the Al rod and t is the thickness of the SiO_2 shell. (b)Total absorptance for Al nanorod at bottom interface, top interface, double nanorods side by side, double nanorods over/under, compared to the centered Al nanorod of the same size (thick line) from section 6.13. d is the diameter of the rod and g is the gap between the two rods. All rods in this thesis have a length that is equal to three times its diameter (aspect ratio is 3). 136

6.57 Absorptance for various setups of the 880 nm PV cell. (a) Total absorptance of the Al@SiO_2 core-shell nanorods (thin lines) compared to the Al rod of the same size but without a SiO_2 shell (thick lines). d is the diameter of the Al rod and t is the thickness of the SiO_2 shell. (b)Total absorptance for Al nanorod at bottom interface, top interface, double nanorods side by side, double nanorods over/under, compared to the centered Al nanorod of the same size (thick line) from section 6.13. d is the diameter of the rod and g is the gap between the two rods. All rods in this thesis have a length that is equal to three times its diameter (aspect ratio is 3). 136
6.58 Absorptance for various setups of the 310 nm PV cell. (a) Total absorptance of the Pt@SiO_2 core-shell nanorods (thin lines) compared to the Pt rod of the same size but without a SiO_2 shell (thick lines). d is the diameter of the Pt rod and t is the thickness of the SiO_2 shell. (b)Total absorptance for Pt nanorod at bottom interface, top interface, double nanorods side by side, double nanorods over/under, compared to the centered Pt nanorod of the same size (thick line) from section 6.14. d is the diameter of the rod and g is the gap between the two rods. All rods in this thesis have a length that is equal to three times its diameter (aspect ratio is 3). 140
6.59 Absorptance for various setups of the 880 nm PV cell. (a) Total absorptance of the Pt@SiO_2 core-shell nanorods (thin lines) compared to the Pt rod of the same size but without a SiO_2 shell (thick lines). d is the diameter of the Pt rod and t is the thickness of the SiO_2 shell. (b)Total absorptance for Pt nanorod at bottom interface, top interface, double nanorods side by side, double nanorods over/under, compared to the centered Pt nanorod of the same size (thick line) from section 6.14. d is the diameter of the rod and g is the gap between the two rods. All rods in this thesis have a length that is equal to three times its diameter (aspect ratio is 3). 140
6.60 Absorptance for various setups of the 310 nm PV cell. (a) Total absorptance of the Au@SiO_2 core-shell nanopyramids (thin lines) compared to the Au pyramid of the same size but without a SiO_2 shell (thick lines). s is the side length of the Au pyramid and t is the thickness of the SiO_2 shell. (b)Total absorptance for Au nanopyramid at bottom interface, top interface, double nanopyramids side by side, double nanopyramids over/under, compared to the centered Au nanopyramid of the same size (thick line) from section 6.15. s is the side length of the pyramid and g is the gap between the two pyramids. All pyramids in this thesis have a height that is equal to its side length. 144

6.61 Absorptance for various setups of the 880 nm PV cell. (a) Total absorptance of the Au@SiO_2 core-shell nanopyramids (thin lines) compared to the Au pyramid of the same size but without a SiO_2 shell (thick lines). s is the side length of the Au pyramid and t is the thickness of the SiO_2 shell. (b)Total absorptance for Au nanopyramid at bottom interface, top interface, double nanopyramids side by side, double nanopyramids over/under, compared to the centered Au nanopyramid of the same size (thick line) from section 6.15. s is the side length of the pyramid and g is the gap between the two pyramids. All pyramids in this thesis have a height that is equal to its side length. 144
6.62 Absorptance for various setups of the 310 nm PV cell. (a) Total absorptance of the Ag@SiO_2 core-shell nanopyramids (thin lines) compared to the Ag pyramid of the same size but without a SiO_2 shell (thick lines). s is the side length of the Ag pyramid and t is the thickness of the SiO_2 shell. (b)Total absorptance for Ag nanopyramid at bottom interface, top interface, double nanopyramids side by side, double nanopyramids over/under, compared to the centered Ag nanopyramid of the same size (thick line) from section 6.16. s is the side length of the pyramid and g is the gap between the two pyramids. All pyramids in this thesis have a height that is equal to its side length. 148
6.63 Absorptance for various setups of the 880 nm PV cell. (a) Total absorptance of the Ag@SiO_2 core-shell nanopyramids (thin lines) compared to the Ag pyramid of the same size but without a SiO_2 shell (thick lines). s is the side length of the Ag pyramid and t is the thickness of the SiO_2 shell. (b)Total absorptance for Ag nanopyramid at bottom interface, top interface, double nanopyramids side by side, double nanopyramids over/under, compared to the centered Ag nanopyramid of the same size (thick line) from section 6.16. s is the side length of the pyramid and g is the gap between the two pyramids. All pyramids in this thesis have a height that is equal to its side length. 148
6.64 Absorptance for various setups of the 310 nm PV cell. (a) Total absorptance of the Al@SiO_2 core-shell nanopyramids (thin lines) compared to the Al pyramid of the same size but without a SiO_2 shell (thick lines). s is the side length of the Al pyramid and t is the thickness of the SiO_2 shell. (b)Total absorptance for Al nanopyramid at bottom interface, top interface, double nanopyramids side by side, double nanopyramids over/under, compared to the centered Al nanopyramid of the same size (thick line) from section 6.17. s is the side length of the pyramid and g is the gap between the two pyramids. All pyramids in this thesis have a height that is equal to its side length. 152

6.65 Absorptance for various setups of the 880 nm PV cell. (a) Total absorptance of the Al@SiO_2 core-shell nanopyramids (thin lines) compared to the Al pyramid of the same size but without a SiO_2 shell (thick lines). s is the side length of the Al pyramid and t is the thickness of the SiO_2 shell. (b)Total absorptance for Al nanopyramid at bottom interface, top interface, double nanopyramids side by side, double nanopyramids over/under, compared to the centered Al nanopyramid of the same size (thick line) from section 6.17. s is the side length of the pyramid and g is the gap between the two pyramids. All pyramids in this thesis have a height that is equal to its side length. 152
6.66 Absorptance for various setups of the 310 nm PV cell. (a) Total absorptance of the Pt@SiO_2 core-shell nanopyramids (thin lines) compared to the Pt pyramid of the same size but without a SiO_2 shell (thick lines). s is the side length of the Pt pyramid and t is the thickness of the SiO_2 shell. (b)Total absorptance for Pt nanopyramid at bottom interface, top interface, double nanopyramids side by side, double nanopyramids over/under, compared to the centered Pt nanopyramid of the same size (thick line) from section 6.18. s is the side length of the pyramid and g is the gap between the two pyramids. All pyramids in this thesis have a height that is equal to its side length. 156
6.67 Absorptance for various setups of the 880 nm PV cell. (a) Total absorptance of the Pt@SiO_2 core-shell nanopyramids (thin lines) compared to the Pt pyramid of the same size but without a SiO_2 shell (thick lines). s is the side length of the Pt pyramid and t is the thickness of the SiO_2 shell. (b)Total absorptance for Pt nanopyramid at bottom interface, top interface, double nanopyramids side by side, double nanopyramids over/under, compared to the centered Pt nanopyramid of the same size (thick line) from section 6.18. s is the side length of the pyramid and g is the gap between the two pyramids. All pyramids in this thesis have a height that is equal to its side length. 156
6.68 Percentage increase in total absorptance for the PV cells with integrated nanospheres. (a) 310 nm PV cell. (b) 880 nm PV cell. 160
6.69 Percentage increase in total absorptance for the PV cells with integrated nanocubes. (a) 310 nm PV cell. (b) 880 nm PV cell. 161
6.70 Percentage increase in total absorptance for the PV cells with integrated nanorods. The height is equal to three times the diameter for all rods in this thesis. (a) 310 nm PV cell. (b) 880 nm PV cell. 162
6.71 Percentage increase in total absorptance for the PV cells with integrated nanopyramids. The height is equal to the side length for all pyramids in this thesis. (a) 310 nm PV cell. (b) 880 nm PV cell. . . . 163

List of Tables

4.1 Summary of published research articles investigating the effect of nanoparticles in perovskite PV cells. All percentage increases are relative to the same PV cell without the given nanoparticles. 39

5.1 Summary of simulation settings used in Lumerical FDTD Solutions. . 48

6.1 Total reflectance, transmittance and absorptance for the seven different PV cells without nanoparticles. The values in the right column gives the total absorptance divided by the thickness of the active layer (perovskite). As shown, the absorptance per nanometer decreases as the thickness of the active layer increases. 53

6.2 Thicknesses of the various layers for the simulations of the PV cell without nanoparticles. Perovskite is the active layer, TiO_2 is the ETM and spiro-OMeTAD is the HTM. 54

6.3 Total reflectance, transmittance and absorptance for the 310 nm PV cell with Au nanospheres with various diameters, as well as the percentage increase in absorptance ($\%\Delta A$) relative to the reference cell. The first row is the reference PV cell without nanosphere. 55

6.4 Total reflectance, transmittance and absorptance for the 880 nm PV cell with Au nanospheres with various diameters, as well as the percentage increase in absorptance ($\%\Delta A$) relative to the reference cell. The first row is the reference PV cell without nanosphere. 57

6.5 Total reflectance, transmittance and absorptance for the 310 nm PV cell with Ag nanospheres with various diameters, as well as the percentage increase in absorptance ($\%\Delta A$) relative to the reference cell. The first row is the reference PV cell without nanosphere. 57

6.6 Total reflectance, transmittance and absorptance for the 880 nm PV cell with Ag nanospheres with various diameters, as well as the percentage increase in absorptance ($\%\Delta A$) relative to the reference cell. The first row is the reference PV cell without nanosphere. 59

6.7 Total reflectance, transmittance and absorptance for the 310 nm PV cell with Al nanospheres with various diameters, as well as the percentage increase in absorptance ($\%\Delta A$) relative to the reference cell. The first row is the reference PV cell without nanosphere. 60

6.8 Total reflectance, transmittance and absorptance for the 880 nm PV cell with Al nanospheres with various diameters, as well as the percentage increase in absorptance ($\%\Delta A$) relative to the reference cell. The first row is the reference PV cell without nanosphere. 61

6.9 Total reflectance, transmittance and absorptance for the 310 nm PV cell with Pt nanospheres with various diameters, as well as the percentage increase in absorptance ($\%\Delta A$) relative to the reference cell. The first row is the reference PV cell without nanosphere. 62
6.10 Total reflectance, transmittance and absorptance for the 880 nm PV cell with Pt nanospheres with various diameters, as well as the percentage increase in absorptance ($\%\Delta A$) relative to the reference cell. The first row is the reference PV cell without nanosphere. 63
6.11 Total reflectance, transmittance and absorptance for the 310 nm PV cell with Au nanocubes with various side lengths, as well as the percentage increase in absorptance ($\%\Delta A$) relative to the reference cell. The first row is the reference PV cell without nanocube. 64
6.12 Total reflectance, transmittance and absorptance for the 880 nm PV cell with Au nanocubes with various side lengths, as well as the percentage increase in absorptance ($\%\Delta A$) relative to the reference cell. The first row is the reference PV cell without nanocube. 66
6.13 Total reflectance, transmittance and absorptance for the 310 nm PV cell with Ag nanocubes with various side lengths, as well as the percentage increase in absorptance ($\%\Delta A$) relative to the reference cell. The first row is the reference PV cell without nanocube. 67
6.14 Total reflectance, transmittance and absorptance for the 880 nm PV cell with Ag nanocubes with various side lengths, as well as the percentage increase in absorptance ($\%\Delta A$) relative to the reference cell. The first row is the reference PV cell without nanocube. 68
6.15 Total reflectance, transmittance and absorptance for the 310 nm PV cell with Al nanocubes with various side lengths, as well as the percentage increase in absorptance ($\%\Delta A$) relative to the reference cell. The first row is the reference PV cell without nanocube. 69
6.16 Total reflectance, transmittance and absorptance for the 880 nm PV cell with Al nanocubes with various side lengths, as well as the percentage increase in absorptance ($\%\Delta A$) relative to the reference cell. The first row is the reference PV cell without nanocube. 71
6.17 Total reflectance, transmittance and absorptance for the 310 nm PV cell with Pt nanocubes with various side lengths, as well as the percentage increase in absorptance ($\%\Delta A$) relative to the reference cell. The first row is the reference PV cell without nanocube. 72
6.18 Total reflectance, transmittance and absorptance for the 880 nm PV cell with Pt nanocubes with various side lengths, as well as the percentage increase in absorptance ($\%\Delta A$) relative to the reference cell. The first row is the reference PV cell without nanocube. 73
6.19 Total reflectance, transmittance and absorptance for the 310 nm PV cell with Au nanorods with various diameters and lengths, as well as the percentage increase in absorptance ($\%\Delta A$) relative to the reference cell. The first row is the reference PV cell without nanorod. . . . 74
6.20 Total reflectance, transmittance and absorptance for the 880 nm PV cell with Au nanorods with various diameters and lengths, as well as the percentage increase in absorptance ($\%\Delta A$) relative to the reference cell. The first row is the reference PV cell without nanorod. . . . 76

6.21 Total reflectance, transmittance and absorptance for the 310 nm PV cell with Ag nanorods with various diameters and lengths, as well as the percentage increase in absorptance ($\%\Delta A$) relative to the reference cell. The first row is the reference PV cell without nanorod. . . . 77
6.22 Total reflectance, transmittance and absorptance for the 880 nm PV cell with Ag nanorods with various diameters and lengths, as well as the percentage increase in absorptance ($\%\Delta A$) relative to the reference cell. The first row is the reference PV cell without nanorod. . . . 78
6.23 Total reflectance, transmittance and absorptance for the 310 nm PV cell with Al nanorods with various diameters and lengths, as well as the percentage increase in absorptance ($\%\Delta A$) relative to the reference cell. The first row is the reference PV cell without nanorod. . . . 79
6.24 Total reflectance, transmittance and absorptance for the 880 nm PV cell with Al nanorods with various diameters and lengths, as well as the percentage increase in absorptance ($\%\Delta A$) relative to the reference cell. The first row is the reference PV cell without nanorod. . . . 81
6.25 Total reflectance, transmittance and absorptance for the 310 nm PV cell with Pt nanorods with various diameters and lengths, as well as the percentage increase in absorptance ($\%\Delta A$) relative to the reference cell. The first row is the reference PV cell without nanorod. . . . 82
6.26 Total reflectance, transmittance and absorptance for the 880 nm PV cell with Pt nanorods with various diameters and lengths, as well as the percentage increase in absorptance ($\%\Delta A$) relative to the reference cell. The first row is the reference PV cell without nanorod. . . . 83
6.27 Total reflectance, transmittance and absorptance for the 310 nm PV cell with Au nanopyramids with various side lengths and heights, as well as the percentage increase in absorptance ($\%\Delta A$) relative to the reference cell. The first row is the reference PV cell without nanopyramid. 84
6.28 Total reflectance, transmittance and absorptance for the 880 nm PV cell with Au nanopyramids with various side lengths and heights, as well as the percentage increase in absorptance ($\%\Delta A$) relative to the reference cell. The first row is the reference PV cell without nanopyramid. 86
6.29 Total reflectance, transmittance and absorptance for the 310 nm PV cell with Ag nanopyramids with various side lengths and heights, as well as the percentage increase in absorptance ($\%\Delta A$) relative to the reference cell. The first row is the reference PV cell without nanopyramid. 87
6.30 Total reflectance, transmittance and absorptance for the 880 nm PV cell with Ag nanopyramids with various side lengths and heights, as well as the percentage increase in absorptance ($\%\Delta A$) relative to the reference cell. The first row is the reference PV cell without nanopyramid. 88

6.31 Total reflectance, transmittance and absorptance for the 310 nm PV cell with Al nanopyramids with various side lengths and heights, as well as the percentage increase in absorptance ($\%\Delta A$) relative to the reference cell. The first row is the reference PV cell without nanopyramid. 89
6.32 Total reflectance, transmittance and absorptance for the 880 nm PV cell with Al nanopyramids with various side lengths and heights, as well as the percentage increase in absorptance ($\%\Delta A$) relative to the reference cell. The first row is the reference PV cell without nanopyramid. 91
6.33 Total reflectance, transmittance and absorptance for the 310 nm PV cell with Pt nanopyramids with various side lengths and heights, as well as the percentage increase in absorptance ($\%\Delta A$) relative to the reference cell. The first row is the reference PV cell without nanopyramid. 92
6.34 Total reflectance, transmittance and absorptance for the 880 nm PV cell with Pt nanopyramids with various side lengths and heights, as well as the percentage increase in absorptance ($\%\Delta A$) relative to the reference cell. The first row is the reference PV cell without nanopyramid. 93
6.35 Total reflectance, transmittance and absorptance for the 310 nm PV cell with Au nanosphere with SiO_2 shell, Au nanosphere at perovskite/HTM interface, Au nanosphere at perovskite/ETM interface, two Au nanospheres side by side, two Au nanospheres over/under, as well as the two PV cells with standard setup Au nanosphere at center. The absorptance change for the various setups is given relative to the two PV cells with standard setup (from section 6.3). d is diameter, t is shell thickness and g is the gap between the two nanospheres. . . . 95
6.36 Total reflectance, transmittance and absorptance for the 880 nm PV cell with Au nanosphere with SiO_2 shell, Au nanosphere at perovskite/HTM interface, Au nanosphere at perovskite/ETM interface, two Au nanospheres side by side, two Au nanospheres over/under, as well as the two PV cells with standard setup Au nanosphere at center. The absorptance change for the various setups is given relative to the two PV cells with standard setup (from section 6.3). d is diameter, t is shell thickness and g is the gap between the two nanospheres. . . . 97
6.37 Total reflectance, transmittance and absorptance for the 310 nm PV cell with Ag nanosphere with SiO_2 shell, Ag nanosphere at perovskite/HTM interface, Ag nanosphere at perovskite/ETM interface, two Ag nanospheres side by side, two Ag nanospheres over/under, as well as the two PV cells with standard setup Ag nanosphere at center. The absorptance change for the various setups is given relative to the two PV cells with standard setup (from section 6.4). d is diameter, t is shell thickness and g is the gap between the two nanospheres. . . . 99

6.38 Total reflectance, transmittance and absorptance for the 880 nm PV cell with Ag nanosphere with SiO_2 shell, Ag nanosphere at perovskite/HTM interface, Ag nanosphere at perovskite/ETM interface, two Ag nanospheres side by side, two Ag nanospheres over/under, as well as the two PV cells with standard setup Ag nanosphere at center. The absorptance change for the various setups is given relative to the two PV cells with standard setup (from section 6.4). d is diameter, t is shell thickness and g is the gap between the two nanospheres. . . . 101
6.39 Total reflectance, transmittance and absorptance for the 310 nm PV cell with Al nanosphere with SiO_2 shell, Al nanosphere at perovskite/HTM interface, Al nanosphere at perovskite/ETM interface, two Al nanospheres side by side, two Al nanospheres over/under, as well as the two PV cells with standard setup Al nanosphere at center. The absorptance change for the various setups is given relative to the two PV cells with standard setup (from section 6.5). d is diameter, t is shell thickness and g is the gap between the two nanospheres. 103
6.40 Total reflectance, transmittance and absorptance for the 880 nm PV cell with Al nanosphere with SiO_2 shell, Al nanosphere at perovskite/HTM interface, Al nanosphere at perovskite/ETM interface, two Al nanospheres side by side, two Al nanospheres over/under, as well as the two PV cells with standard setup Al nanosphere at center. The absorptance change for the various setups is given relative to the two PV cells with standard setup (from section 6.5). d is diameter, t is shell thickness and g is the gap between the two nanospheres. 105
6.41 Total reflectance, transmittance and absorptance for the 310 nm PV cell with Pt nanosphere with SiO_2 shell, Pt nanosphere at perovskite/HTM interface, Pt nanosphere at perovskite/ETM interface, two Pt nanospheres side by side, two Pt nanospheres over/under, as well as the two PV cells with standard setup Pt nanosphere at center. The absorptance change for the various setups is given relative to the two PV cells with standard setup (from section 6.6). d is diameter, t is shell thickness and g is the gap between the two nanospheres. 107
6.42 Total reflectance, transmittance and absorptance for the 880 nm PV cell with Pt nanosphere with SiO_2 shell, Pt nanosphere at perovskite/HTM interface, Pt nanosphere at perovskite/ETM interface, two Pt nanospheres side by side, two Pt nanospheres over/under, as well as the two PV cells with standard setup Pt nanosphere at center. The absorptance change for the various setups is given relative to the two PV cells with standard setup (from section 6.6). d is diameter, t is shell thickness and g is the gap between the two nanospheres. 109
6.43 Total reflectance, transmittance and absorptance for the 310 nm PV cell with Au nanocube with SiO_2 shell, Au nanocube at perovskite/HTM interface, Au nanocube at perovskite/ETM interface, two Au nanocubes side by side, two Au nanocubes over/under, as well as the two PV cells with standard setup Au nanocube at center. The absorptance change for the various setups is given relative to the two PV cells with standard setup (from section 6.7). s is side length, t is shell thickness and g is the gap between the two nanocubes. 111

6.44 Total reflectance, transmittance and absorptance for the 880 nm PV cell with Au nanocube with SiO_2 shell, Au nanocube at perovskite/HTM interface, Au nanocube at perovskite/ETM interface, two Au nanocubes side by side, two Au nanocubes over/under, as well as the two PV cells with standard setup Au nanocube at center. The absorptance change for the various setups is given relative to the two PV cells with standard setup (from section 6.7). s is side length, t is shell thickness and g is the gap between the two nanocubes. 113
6.45 Total reflectance, transmittance and absorptance for the 310 nm PV cell with Ag nanocube with SiO_2 shell, Ag nanocube at perovskite/HTM interface, Ag nanocube at perovskite/ETM interface, two Ag nanocubes side by side, two Ag nanocubes over/under, as well as the two PV cells with standard setup Ag nanocube at center. The absorptance change for the various setups is given relative to the two PV cells with standard setup (from section 6.8). s is side length, t is shell thickness and g is the gap between the two nanocubes. 115
6.46 Total reflectance, transmittance and absorptance for the 880 nm PV cell with Ag nanocube with SiO_2 shell, Ag nanocube at perovskite/HTM interface, Ag nanocube at perovskite/ETM interface, two Ag nanocubes side by side, two Ag nanocubes over/under, as well as the two PV cells with standard setup Ag nanocube at center. The absorptance change for the various setups is given relative to the two PV cells with standard setup (from section 6.8). s is side length, t is shell thickness and g is the gap between the two nanocubes. 117
6.47 Total reflectance, transmittance and absorptance for the 310 nm PV cell with Al nanocube with SiO_2 shell, Al nanocube at perovskite/HTM interface, Al nanocube at perovskite/ETM interface, two Al nanocubes side by side, two Al nanocubes over/under, as well as the two PV cells with standard setup Al nanocube at center. The absorptance change for the various setups is given relative to the two PV cells with standard setup (from section 6.9). s is side length, t is shell thickness and g is the gap between the two nanocubes. 119
6.48 Total reflectance, transmittance and absorptance for the 880 nm PV cell with Al nanocube with SiO_2 shell, Al nanocube at perovskite/HTM interface, Al nanocube at perovskite/ETM interface, two Al nanocubes side by side, two Al nanocubes over/under, as well as the two PV cells with standard setup Al nanocube at center. The absorptance change for the various setups is given relative to the two PV cells with standard setup (from section 6.9). s is side length, t is shell thickness and g is the gap between the two nanocubes. 121
6.49 Total reflectance, transmittance and absorptance for the 310 nm PV cell with Pt nanocube with SiO_2 shell, Pt nanocube at perovskite/HTM interface, Pt nanocube at perovskite/ETM interface, two Pt nanocubes side by side, two Pt nanocubes over/under, as well as the two PV cells with standard setup Pt nanocube at center. The absorptance change for the various setups is given relative to the two PV cells with standard setup (from section 6.10). s is side length, t is shell thickness and g is the gap between the two nanocubes. 123

6.50 Total reflectance, transmittance and absorptance for the 880 nm PV cell with Pt nanocube with SiO_2 shell, Pt nanocube at perovskite/HTM interface, Pt nanocube at perovskite/ETM interface, two Pt nanocubes side by side, two Pt nanocubes over/under, as well as the two PV cells with standard setup Pt nanocube at center. The absorptance change for the various setups is given relative to the two PV cells with standard setup (from section 6.10). s is side length, t is shell thickness and g is the gap between the two nanocubes. 125
6.51 Total reflectance, transmittance and absorptance for the 310 nm PV cell with Au nanorod with SiO_2 shell, Au nanorod at perovskite/HTM interface, Au nanorod at perovskite/ETM interface, two Au nanorods side by side, two Au nanorods over/under, as well as the two PV cells with standard setup Au nanorod at center. The absorptance change for the various setups is given relative to the two PV cells with standard setup (from section 6.11). d is diameter, t is shell thickness and g is the gap between the two nanorods. All rods in this thesis have a length that is equal to three times its diameter (aspect ratio is 3). 127
6.52 Total reflectance, transmittance and absorptance for the 880 nm PV cell with Au nanorods with SiO_2 shell, Au nanorod at perovskite/HTM interface, Au nanorod at perovskite/ETM interface, two Au nanorods side by side, two Au nanorods over/under, as well as the two PV cells with standard setup Au nanorod at center. The absorptance change for the various setups is given relative to the two PV cells with standard setup (from section 6.11). d is diameter, t is shell thickness and g is the gap between the two nanorods. All rods in this thesis have a length that is equal to three times its diameter (aspect ratio is 3). . . 129
6.53 Total reflectance, transmittance and absorptance for the 310 nm PV cell with Ag nanorod with SiO_2 shell, Ag nanorod at perovskite/HTM interface, Ag nanorod at perovskite/ETM interface, two Ag nanorods side by side, two Ag nanorods over/under, as well as the two PV cells with standard setup Ag nanorod at center. The absorptance change for the various setups is given relative to the two PV cells with standard setup (from section 6.12). d is diameter, t is shell thickness and g is the gap between the two nanorods. All rods in this thesis have a length that is equal to three times its diameter (aspect ratio is 3). 131
6.54 Total reflectance, transmittance and absorptance for the 880 nm PV cell with Ag nanorods with SiO_2 shell, Ag nanorod at perovskite/HTM interface, Ag nanorod at perovskite/ETM interface, two Ag nanorods side by side, two Ag nanorods over/under, as well as the two PV cells with standard setup Ag nanorod at center. The absorptance change for the various setups is given relative to the two PV cells with standard setup (from section 6.12). d is diameter, t is shell thickness and g is the gap between the two nanorods. All rods in this thesis have a length that is equal to three times its diameter (aspect ratio is 3). . . 133

6.55 Total reflectance, transmittance and absorptance for the 310 nm PV cell with Al nanorod with SiO_2 shell, Al nanorod at perovskite/HTM interface, Al nanorod at perovskite/ETM interface, two Al nanorods side by side, two Al nanorods over/under, as well as the two PV cells with standard setup Al nanorod at center. The absorptance change for the various setups is given relative to the two PV cells with standard setup (from section 6.13). d is diameter, t is shell thickness and g is the gap between the two nanorods. All rods in this thesis have a length that is equal to three times its diameter (aspect ratio is 3). 135
6.56 Total reflectance, transmittance and absorptance for the 880 nm PV cell with Al nanorods with SiO_2 shell, Al nanorod at perovskite/HTM interface, Al nanorod at perovskite/ETM interface, two Al nanorods side by side, two Al nanorods over/under, as well as the two PV cells with standard setup Al nanorod at center. The absorptance change for the various setups is given relative to the two PV cells with standard setup (from section 6.13). d is diameter, t is shell thickness and g is the gap between the two nanorods. All rods in this thesis have a length that is equal to three times its diameter (aspect ratio is 3). 137
6.57 Total reflectance, transmittance and absorptance for the 310 nm PV cell with Pt nanorod with SiO_2 shell, Pt nanorod at perovskite/HTM interface, Pt nanorod at perovskite/ETM interface, two Pt nanorods side by side, two Pt nanorods over/under, as well as the two PV cells with standard setup Pt nanorod at center. The absorptance change for the various setups is given relative to the two PV cells with standard setup (from section 6.14). d is diameter, t is shell thickness and g is the gap between the two nanorods. All rods in this thesis have a length that is equal to three times its diameter (aspect ratio is 3). 139
6.58 Total reflectance, transmittance and absorptance for the 880 nm PV cell with Pt nanorods with SiO_2 shell, Pt nanorod at perovskite/HTM interface, Pt nanorod at perovskite/ETM interface, two Pt nanorods side by side, two Pt nanorods over/under, as well as the two PV cells with standard setup Pt nanorod at center. The absorptance change for the various setups is given relative to the two PV cells with standard setup (from section 6.14). d is diameter, t is shell thickness and g is the gap between the two nanorods. All rods in this thesis have a length that is equal to three times its diameter (aspect ratio is 3). 141

6.59 Total reflectance, transmittance and absorptance for the 310 nm PV cell with Au nanopyramid with SiO_2 shell, Au nanopyramid at perovskite/HTM interface, Au nanopyramid at perovskite/ETM interface, two Au nanopyramids side by side, two Au nanopyramids over/under, as well as the two PV cells with standard setup Au nanopyramid at center. The absorptance change for the various setups is given relative to the two PV cells with standard setup (from section 6.15). s is side length, t is shell thickness and g is the gap between the two nanopyramids. All pyramids in this thesis have a height that is equal to its side length. 143

6.60 Total reflectance, transmittance and absorptance for the 880 nm PV cell with Au nanopyramids with SiO_2 shell, Au nanopyramid at perovskite/HTM interface, Au nanopyramid at perovskite/ETM interface, two Au nanopyramids side by side, two Au nanopyramids over/under, as well as the two PV cells with standard setup Au nanopyramid at center. The absorptance change for the various setups is given relative to the two PV cells with standard setup (from section 6.15). s is side length, t is shell thickness and g is the gap between the two nanopyramids. All pyramids in this thesis have a height that is equal to its side length. 145

6.61 Total reflectance, transmittance and absorptance for the 310 nm PV cell with Ag nanopyramid with SiO_2 shell, Ag nanopyramid at perovskite/HTM interface, Ag nanopyramid at perovskite/ETM interface, two Ag nanopyramids side by side, two Ag nanopyramids over/under, as well as the two PV cells with standard setup Ag nanopyramid at center. The absorptance change for the various setups is given relative to the two PV cells with standard setup (from section 6.16). s is side length, t is shell thickness and g is the gap between the two nanopyramids. All pyramids in this thesis have a height that is equal to its side length. 147

6.62 Total reflectance, transmittance and absorptance for the 880 nm PV cell with Ag nanopyramids with SiO_2 shell, Ag nanopyramid at perovskite/HTM interface, Ag nanopyramid at perovskite/ETM interface, two Ag nanopyramids side by side, two Ag nanopyramids over/under, as well as the two PV cells with standard setup Ag nanopyramid at center. The absorptance change for the various setups is given relative to the two PV cells with standard setup (from section 6.16). s is side length, t is shell thickness and g is the gap between the two nanopyramids. All pyramids in this thesis have a height that is equal to its side length. 149

6.63 Total reflectance, transmittance and absorptance for the 310 nm PV cell with Al nanopyramid with SiO_2 shell, Al nanopyramid at perovskite/HTM interface, Al nanopyramid at perovskite/ETM interface, two Al nanopyramids side by side, two Al nanopyramids over/under, as well as the two PV cells with standard setup Al nanopyramid at center. The absorptance change for the various setups is given relative to the two PV cells with standard setup (from section 6.17). s is side length, t is shell thickness and g is the gap between the two nanopyramids. All pyramids in this thesis have a height that is equal to its side length. 151
6.64 Total reflectance, transmittance and absorptance for the 880 nm PV cell with Al nanopyramids with SiO_2 shell, Al nanopyramid at perovskite/HTM interface, Al nanopyramid at perovskite/ETM interface, two Al nanopyramids side by side, two Al nanopyramids over/under, as well as the two PV cells with standard setup Al nanopyramid at center. The absorptance change for the various setups is given relative to the two PV cells with standard setup (from section 6.17). s is side length, t is shell thickness and g is the gap between the two nanopyramids. All pyramids in this thesis have a height that is equal to its side length. 153
6.65 Total reflectance, transmittance and absorptance for the 310 nm PV cell with Pt nanopyramid with SiO_2 shell, Pt nanopyramid at perovskite/HTM interface, Pt nanopyramid at perovskite/ETM interface, two Pt nanopyramids side by side, two Pt nanopyramids over/under, as well as the two PV cells with standard setup Pt nanopyramid at center. The absorptance change for the various setups is given relative to the two PV cells with standard setup (from section 6.18). s is side length, t is shell thickness and g is the gap between the two nanopyramids. All pyramids in this thesis have a height that is equal to its side length. 155
6.66 Total reflectance, transmittance and absorptance for the 880 nm PV cell with Pt nanopyramids with SiO_2 shell, Pt nanopyramid at perovskite/HTM interface, Pt nanopyramid at perovskite/ETM interface, two Pt nanopyramids side by side, two Pt nanopyramids over/under, as well as the two PV cells with standard setup Pt nanopyramid at center. The absorptance change for the various setups is given relative to the two PV cells with standard setup (from section 6.18). s is side length, t is shell thickness and g is the gap between the two nanopyramids. All pyramids in this thesis have a height that is equal to its side length. 157

Chapter 1

Introduction

This chapter will give a short introduction to the thesis. A description of the background is given in section 1.1, thesis objectives are given in section 1.2, methods and tools used in the thesis are described in section 1.3, section 1.4 describes the outline of the whole thesis, and section 1.5 gives some important definitions.

1.1 Background

One of the biggest challenges that humanity faces at the present time is to ensure the supply of clean and sustainable energy for the planet's population, now and in the future. This is reflected in the United Nations Sustainable Development Goals [20], where "Goal 7: Affordable and Clean Energy" is directly related to this. Energy also has a significant effect on several of the other sustainable development goals, e.g. "Goal 13: Climate Action". The ongoing climate change and related challenges is a subject that is well known in the general population by now. Raised temperatures will raise the level of the oceans, thereby flooding whole regions of the planet and making them inhabitable. More extreme weather events are likely to become more common. The heat itself can also render some of the warmer regions of the world almost inhabitable. It can cause droughts, hunger, and consequently huge migrations of refugees, wars and destabilization of societies across the whole planet.

There is very high consensus among the world's scientists that at least some of the climate change is caused by human activity. The main problem has been the enormous amounts of the so-called greenhouse gases (GHG) that human activity has released into the atmosphere since the dawn of the industrial age, with the majority of this having been released over the course of the last few decades. By far the biggest of these anthropogenic GHGs is carbon dioxide (CO_2), and the main source of its release is the burning of fossil fuels, i.e. coal, oil and natural gas. A big portion of this is burned to generate electricity. As shown in figure 1.1, approximately 25% of all GHG emissions comes from the generation of electricity and heat. This means that cutting the GHG releases from this sector will be a very important part of mitigating the anthropogenic climate change. Electricity is also expected to supply a much larger portion of the world's energy in the coming decades, making it even more crucial to clean up the electricity sector. As seen in figure 1.2, DNV GL predicts in their recent report [2] that primary energy demand will peak around the year 2030, and that electricity will be by far the biggest energy

carrier by the year 2050.

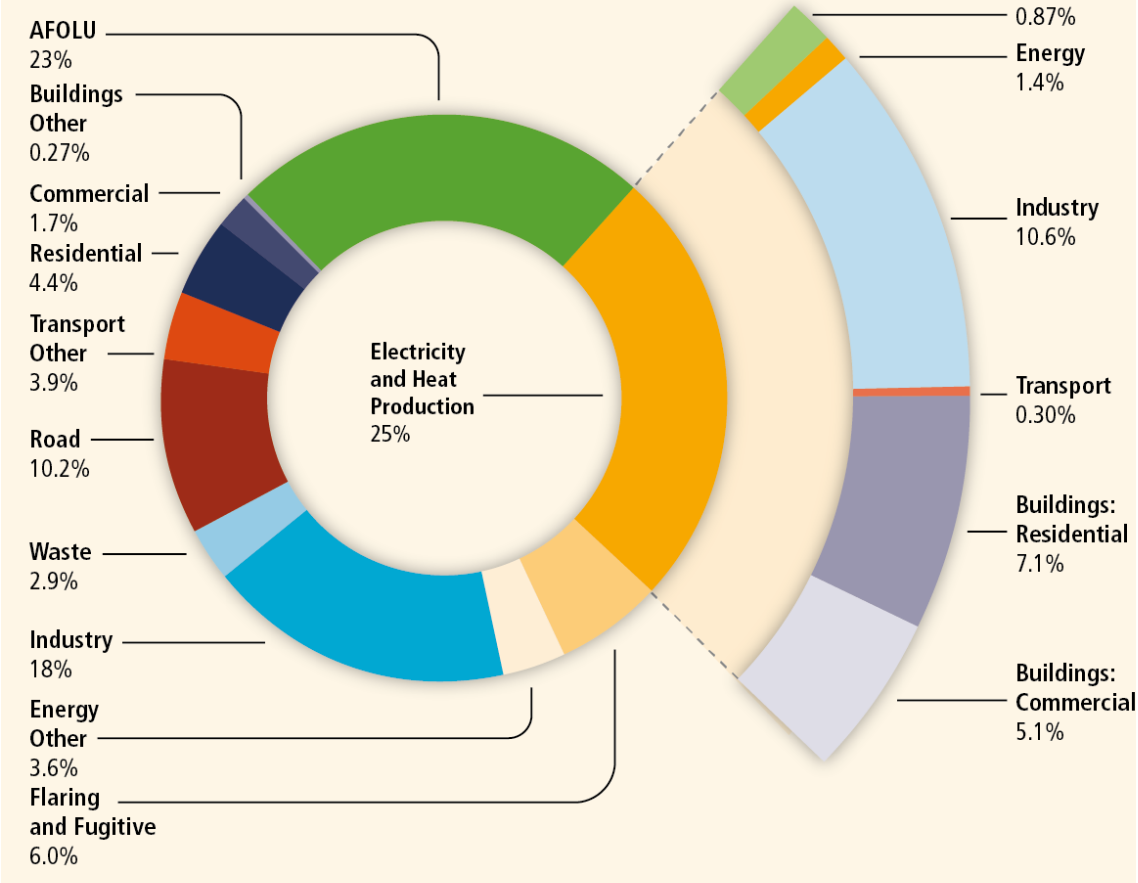

Figure 1.1: GHG emissions grouped by economic sector. Figure is taken from [1].

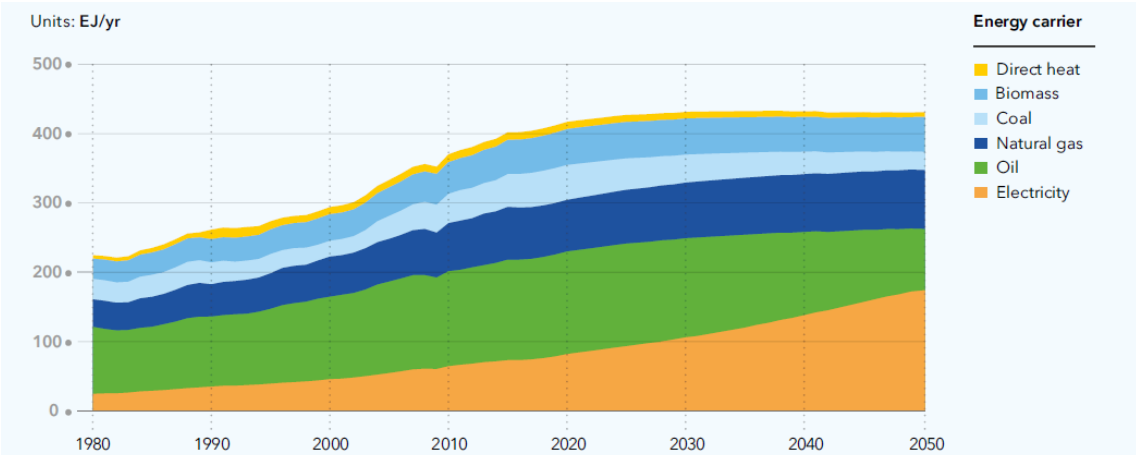

Figure 1.2: Forecast of the world's final energy demand by energy carrier. Figure is taken from [2].

The key to reducing the GHG emissions from the electricity sector will lie in the successful implementation of renewable energy technologies. Among these, photovoltaic solar cells has been one of the most successful technologies so far, and it is expected to grow exponentially in the next few decades. The predictions in the

DNV GL report [2], shown in figures 1.3 and 1.4, indicates that photovoltaic solar cells will become the biggest source of electricity before 2035. Furthermore, in 2050 it will be by far the biggest electricity source and it will only be beaten by oil and gas as a supplier of primary energy. If these predictions prove to be correct, then photovoltaic solar cells will play a huge role in ensuring the supply of clean energy and in mitigating climate change.

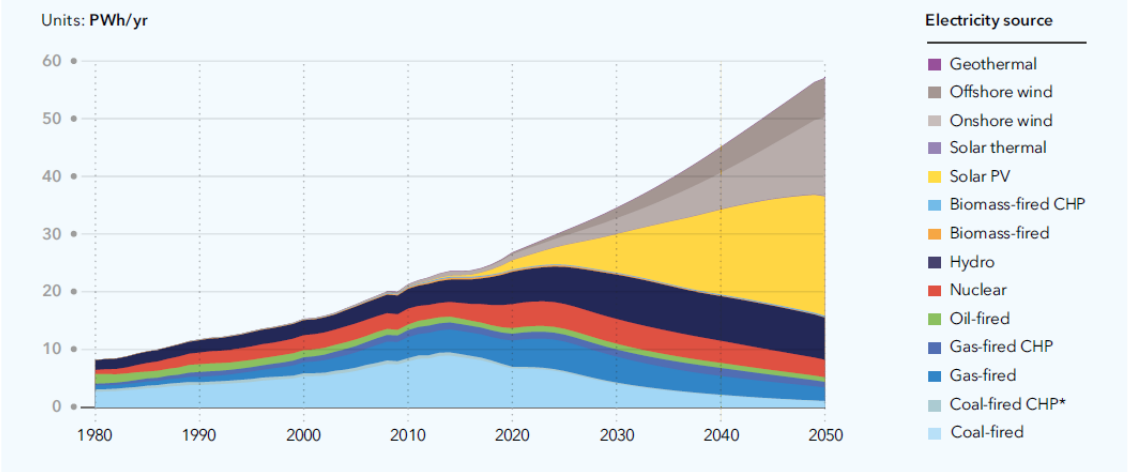

Figure 1.3: Forecast of the world's electricity generation by source. Figure is taken from [2].

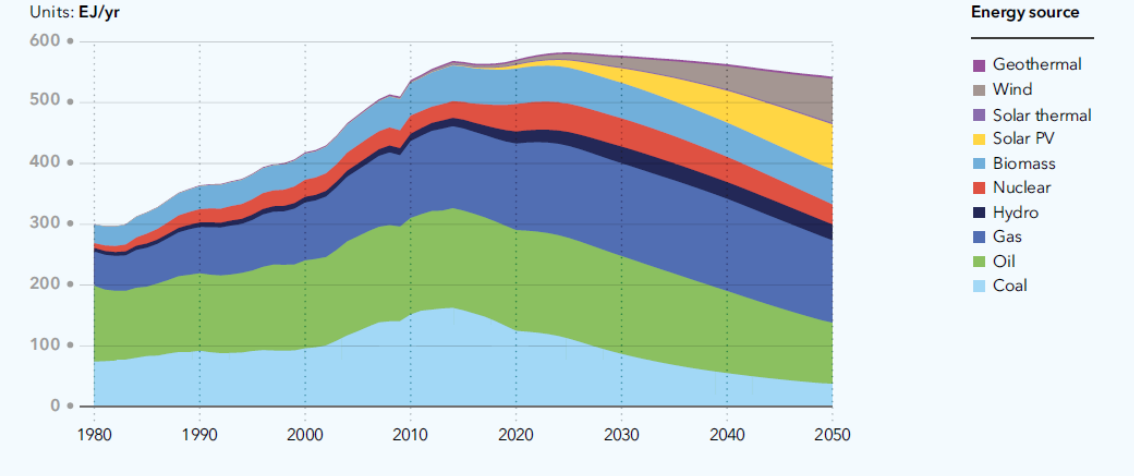

Figure 1.4: Forecast of the world's primary energy supply by source. Figure is taken from [2].

Photovoltaic solar cells have had a lot of success already, but they still supply only a very small fraction of the world's electricity. The power conversion efficiency of this technology has risen and the cost has gone down substantially, particularly in the new millennium. However, further progress is needed if this energy technology is going to fulfill the predictions of the DNV GL report [2] and others. Efficiency needs to increase even further and costs must go down even further, but there are other factors as well that could accelerate the implementation of photovoltaic technologies. This includes lowering weight while increasing flexibility

and transparency so that photovoltaic solar cells can be integrated into buildings (walls, windows, roofs), electric cars and other modes of transportation, and personal electronic equipment. One of the most promising photovoltaic technologies in that regard is perovskite photovoltaic solar cells. The research concentrated on these solar cells started less than a decade ago, but already these solar cells are showing power conversion efficiencies that are rivaling other thin film photovoltaic technologies and fast approaching that of crystalline photovoltaic solar panels [7]. Perovskite photovoltaic solar cells also possess other advantages, like a cheap and easy manufacturing process, but there are still several challenges that need to be solved before this technology can be commercialized. These include problems with degradation, the presence of toxic lead, hysteresis effects that causes measurements of the current-voltage curve to yield different results depending on the scanning direction, scanning rate and order of scanning directions, as well as the challenge of scaling up to large area devices. This is discussed in more detail in chapter 3.

There has been intense research activity related to perovskite solar cells over the past few years, and one of the focus areas has been the integration of metal nanoparticles to increase the power conversion efficiency of these solar cells [18, 21, 22, 23, 24]. This is done to enhance the absorptance, and consequently the electricity generation. There exists a large number of research publications where positive effects have been seen, both in simulations and experiments. This will be the main theme of this thesis. By using the computer software Lumerical FDTD Solutions, simulations will be performed to investigate the effect of metal nanoparticles on the optical absorptance of perovskite solar cells. The shape, size, position and material of the nanoparticles will be varied in between simulations to investigate the effect of these variables. The difference between solid and core-shell nanoparticles will also be simulated. This should result in an extensive overview of the effect of nanoparticles on the optical absorptance in perovskite solar cells, which can be used as supportive material in further experimental work to optimize the power conversion efficiency of these solar cells in the near future.

1.2 Thesis Objectives

The objectives in this thesis are:

- Simulate the effect of metal nanoparticles on the optical absorptance of perovskite solar cells using Lumerical FDTD Solutions
- Evaluate the results of the simulations and compare them to each other and relevant research published in scientific literature so that a conclusion can be made regarding the effect of nanoparticles on the absorptance in perovskite solar cells

1.3 Methods and Tools

Books, published scientific articles, technical reports, as well as a few websites have been used as sources for the descriptive sections of the thesis. Research articles were also used as sources for the material data needed for the simulations. All simulations were done using the Lumerical FDTD Solutions software [16]. The datasets

from each simulation was imported into MATLAB [25] where scripts were written to create plots that display the simulation results in the desired way. These plots are included in chapter 6 of the thesis. The datasets from the simulations were also imported into Microsoft Excel [26] where a spreadsheet was created that integrates the datapoints across the whole simulation wavelength interval to calculate the total reflectance and transmittance of each simulation. The spreadsheet then uses the reflectance and transmittance values to calculate the total absorptance of each simulation. All MATLAB scripts and Excel spreadsheets were written by the author of this thesis. The thesis was written and compiled using LaTeX [27]. The plots used for comparison in section 6.1 was imported using the shareware Datathief [28].

1.4 Thesis Outline

Chapter 2 gives a general description of photovoltaic solar cell technologies, including the working principle, characteristics and various types of photovoltaic technologies. Chapter 3 gives a more thorough description of perovskite photovoltaic solar cells, including materials, architecture, working principle and challenges. Chapter 4 describes the use of nanoparticles in photovoltaic solar cells, i.e. plasmonic solar cells, both in general and specifically for perovskite solar cells, including a discussion of the research state of the art in plasmonic perovskite solar cells. Chapter 5 gives a description of Lumercial FDTD Solutions and the simulation settings used in this thesis. Chapter 6 is the main chapter and it goes through and evaluates the results of the simulations, while chapter 7 gives a summary and provides a conclusion for the thesis.

1.5 Definitions

An important expression in this thesis is *absorptance*. As mentioned in the thesis objectives, this thesis will investigate the effect that metal nanoparticles have on the optical *absorptance* of perovskite solar cells. Absorptance is defined as the ratio of absorbed incident radiation in a given part of the spectrum to the total incident radiation in that same part of the spectrum [29]. In other words, it tells us how much of the incident radiation that is absorbed by the structure that we are investigating. It is a dimensionless number and it is always less than 1. Similarly, *transmittance* gives us the ratio of transmitted radiation to total radiation, and *reflectance* gives us the ratio of reflected radiation to total radiation. Absorptance, transmittance and reflectance always add up to 1 (100%). As an example, if an object has an absorptance of 0.55, a transmittance of 0.25 and a reflectance of 0.20, this means that the object absorbs 55% of the incident radiation, while 25% of the incident radiation is transmitted through the object and 20% of the incident radiation is reflected away by the object. So the difference between *absorption* and *absorptance* is that *absorption* refers to the act of absorbing in general, and it can be given as a value with a unit, while *absorptance* is *only* the ratio described above, and it is *only* given as a dimensionless number less than (or equal to) 1. It is mostly absorptance that is used in this thesis.

Chapter 2

Photovoltaic Solar Cells

This chapter will go through the most important and relevant parts of photovoltaic solar cell technology. It starts with a brief history of the development of photovoltaic technologies in section 2.1. A description of the general working principle of photovoltaic solar cells is then given in section 2.2. The important pn junction is described in section 2.3, followed by the most vital characteristics of the photovoltaic solar cell in section 2.4. Finally, an overview of the different types of photovoltaic solar cells is given in section 2.5.

2.1 History

The photovoltaic effect is the generation of electricity from light and it was discovered almost 180 years ago by the French physicist Edmond Becquerel. He published a paper in 1839 in which he describes his own experiments with a wet cell battery, and he states that the battery voltage increased when the silver plates of the battery was exposed to sunlight [30]. Willoughby Smith then discovered the photoconductivity of selenium in 1873 [31] and this led to the first report of the photovoltaic effect in a solid substance by Adams and Day in 1877 [30]. The two scientists were working at Cambridge University when they observed and described the variations in the electrical properties of selenium when exposed to light.

The first solar cell construction that was quite similar to the typical silicon solar cells seen today was patented by Charles Edgar Fritts in 1883. Fritts was an electrician in New York and he used a thin selenium wafer in his solar cell. He put a grid of very thin gold wires over the selenium wafer and a protective sheet of glass on top and the result was a fully functioning photovoltaic solar cell. However, the power conversion efficiency (PCE) of his device was extremely limited and converted less than 1% of the incoming sunlight into electricity [30]. The PCE of the selenium solar cell was increased up to about 1% in 1914 [31], but this was still much to low to allow for any widespread practical use.

It was not until the middle of the twentieth century that significant advances were seen in photovoltaic solar cell technology. The development of the first solid state devices started in the late 1940s [32] and this paved the way for a breakthrough at the Bell Telephone Laboratories (Bell Labs) in New Jersey, USA in 1954 [31]. The effects of light on semiconductor materials was one of the focus areas of the research at Bell Labs, and this led to the development of the first modern solar cell by a team of scientists including Darryl Chapin, Calvin Fuller and Gerald

Pearson. They used the semiconductor material silicon, the same one used in the majority of modern solar cells, and building on the previous work by other scientists at Bell Labs they managed to produce a silicon solar cell with a 6% PCE [30]. They demonstrated the practical use of this solar cell, but the costs were much too high to allow any widespread use at this point. Nevertheless, Western Electric began selling commercial licenses for silicon photovoltaic technologies in 1955, and the PCE of silicon solar cells reached 14% by 1958 [31]. In the same year, silicon solar cells were used to power the radio transmitter on the US space satellite Vanguard I [30]. Since then, photovoltaic solar cells has been a common power source in space applications.

The last decade has seen enormous growth in the field of photovoltaic technology. After developing and growing steadily but slowly during the last four decades of the twentieth century, the new millennium has seen a virtual explosion in the use of photovoltaic technologies for electricity generation, particularly during the last 10-15 years. The installed capacity in 2005 was 5.1 GW and this had grown to 227 GW in 2015 [3] (figure 2.1), giving an increase of approximately 4 350% in just one decade. This grew by more than 75 GW in 2016, resulting in a total installed capacity of at least 303 GW at the start of 2017 [33]. However, this still amounts to only 0.35% of the world's total energy consumption. The rapid growth is expected to continue though, and DNV GL predicts that photovoltaic power generation will increase by one order of magnitude from 2015 to 2024 and by another order of magnitude from 2024 to 2050. This will result in photovoltaic systems supplying 36% of the world's electricity (figure 2.2) and 13% of the world's total energy [2]. All in all, there exists a broad agreement that photovoltaic systems will be a big and very important part of the world's future energy supply.

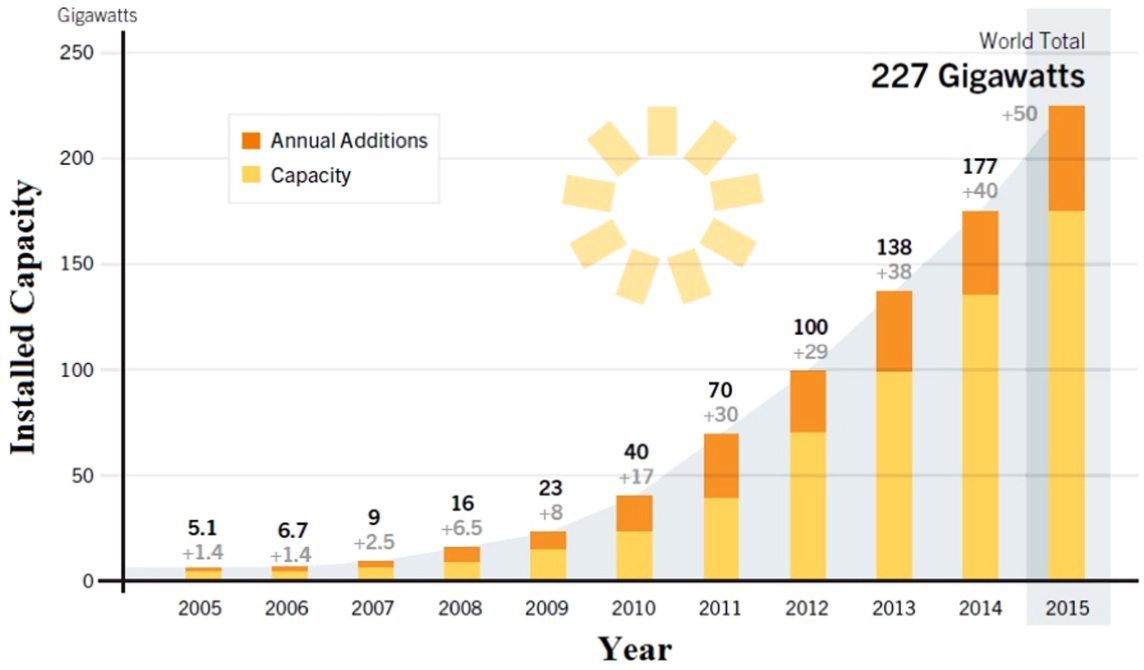

Figure 2.1: Global installed photovoltaic power capacity [3].

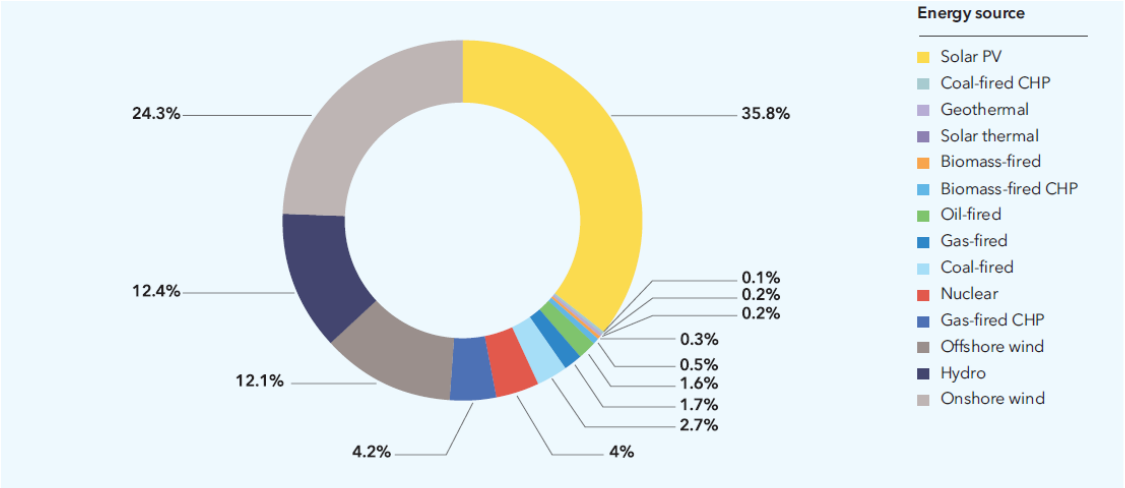

Figure 2.2: Predicted global electricity production in 2050 [2].

2.2 Working Principle

The general working principle of modern photovoltaic solar cells, hereinafter referred to as PV cells, will be described in this section. A PV cell utilizes electromagnetic radiation in the form of photons to generate electrical energy through the photovoltaic effect. This is done by arranging a semiconductor material in a junction and combining it with an external circuit. The majority of PV cells use a pn junction [4], so this junction will be described in section 2.3.

The basic steps that must take place in a PV cell is, firstly, that the incoming photon must transfer some of its energy to an electron in the absorbing semiconductor material. This will excite the electron and create a negatively charged carrier and a positively charged carrier, often referred to as an electron-hole pair, where the electron is the negative charge and the missing electron (hole) is the positive charge. The electron-hole pair will then move in different directions due to a built-in asymmetry (electric field) in the PV cell that drives the electron towards the cathode contact and the hole towards the anode contact. The electron arriving at the cathode will then travel through an external electric circuit where it transfers its energy to an external load, before combining with the arriving positive charge (hole) at the anode [34].

A semiconductor material is a material with specific electrical characteristics. Its electrical resistance is higher than the electrical resistance in metals, but lower than it is in insulator materials. This is the source of its name since it is in between a conductor (metal) and an insulator, hence *semi*conductor. The electrical conductivity of a semiconductor can be altered significantly by introducing small amounts of other substances in the semiconductor, often referred to as doping. One can either introduce a substance that causes a surplus of free electrons in the semiconductor, referred to as n-doping, or one can introduce a substance that causes a surplus of holes (deficit of free electrons) in the semiconductor, referred to as p-doping. By combining a n-doped layer with a p-doped layer, the abovementioned built-in asymmetry is achieved. This creates the electric field that causes the separation of the electron-hole pair. Another important aspect of a semiconductor is the band gap. This is the energy gap that exists between the valence band and the conduction band in the semiconductor. This is of great importance since the

incoming photon must have an energy amount greater than or equal to the band gap in order to be able to excite the electron from the valence band and into the conduction band of the semiconductor. The band gap is often used as a means of separating semiconductors from insulators, where it is common to refer to a material as a semiconductor if the band gap is below approximately 3 eV and an insulator if the band gap is above this value [5]. The most commonly used semiconductor in PV cells is silicon (Si) and a cross-section of a basic silicon PV cell is shown in figure 2.3.

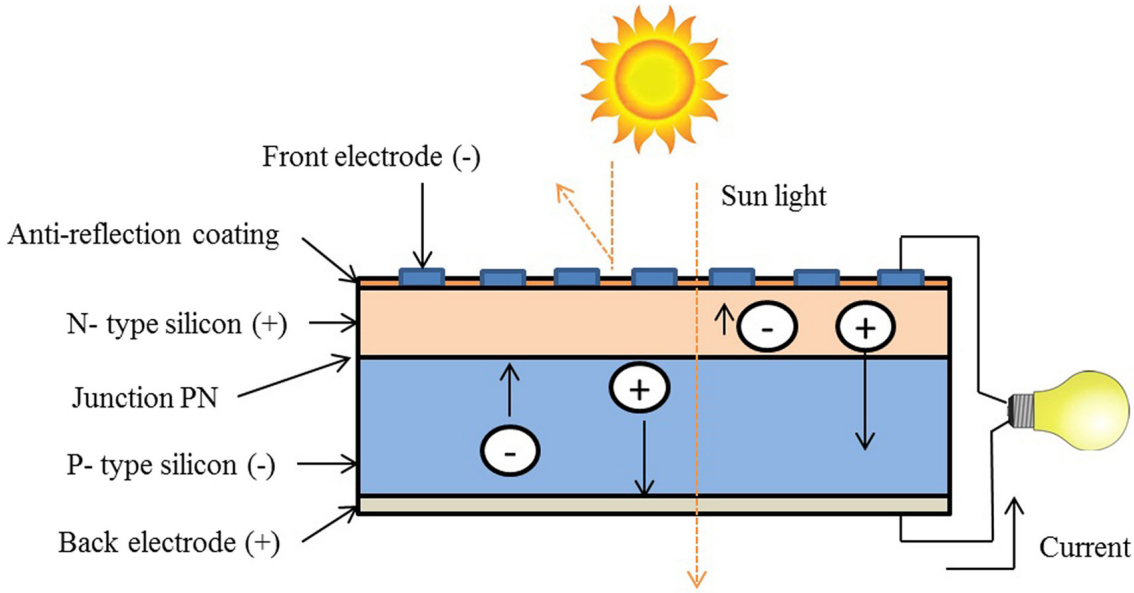

Figure 2.3: Cross-section of a basic silicon PV cell [4].

2.3 The pn Junction

A pn junction is the junction between a p-type semiconductor and a n-type semiconductor. This junction is usually created by starting with a pure (intrinsic) semiconductor and then adding small amounts of impurities to it so that it ends up with either a surplus of free electrons (n-type) or a surplus of holes (p-type). In the case of silicon PV cells, the n-type silicon can be created by doping the silicon with trace amounts of phosphorus (P). Phosphorus has five valence electrons while silicon has only four, and this results in a surplus of free electrons in the silicon that is doped with phosphorus. To create the p-type silicon, boron (B) can be used as the doping substance. Boron has only three valence electrons, so introducing boron in a piece of silicon will cause a surplus of holes [30].

Once the doping process is complete, the n-type layer and p-type layer can be joined to create a pn junction. When the two types are joined, some of the free electrons close to the junction on the n-side will diffuse into the p-side to combine with holes and some of the holes close to the junction on the p-side will diffuse into the n-side to combine with electrons. The result of this diffusion of free electrons and holes is that the region close to the pn junction on the p-side will be negatively charged because of the free electrons that came across the junction, and likewise will the region close to the pn junction on the n-side be positively charged

because of the holes that came across the junction. This asymmetry in electric charge creates an internal electric field in the direction from the positively charged n-side to the negatively charged p-side. It also means that these two regions close to the pn junction will be depleted of mobile charge carriers in the form of free electrons and holes since these are used up to create ions. These two regions combined are therefore commonly referred to as the depletion region or depletion layer.

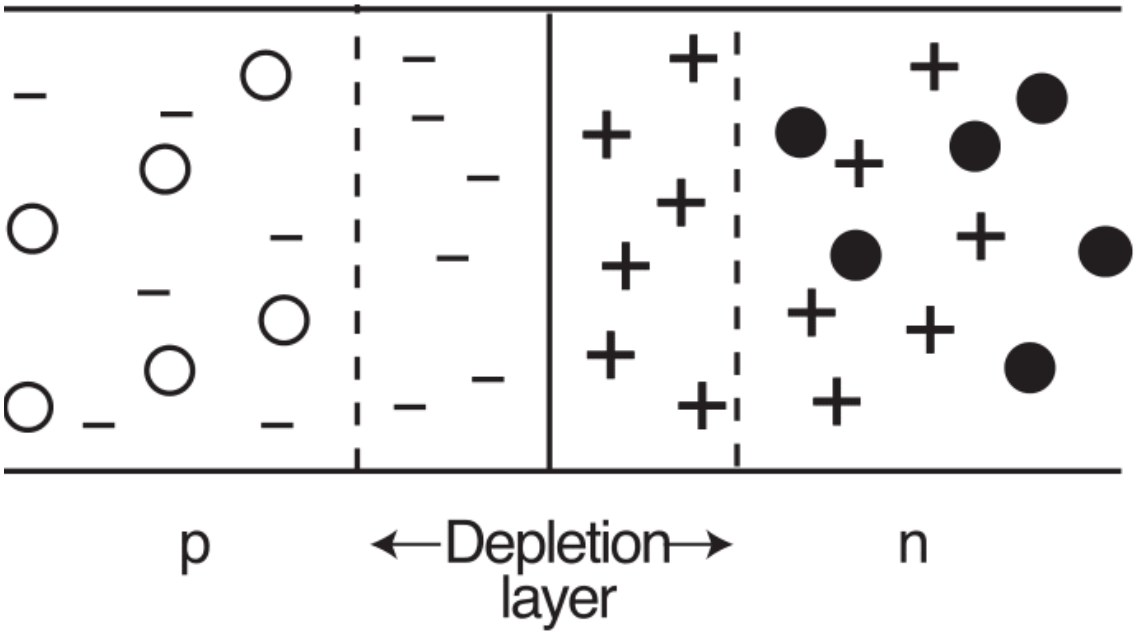

Figure 2.4: The pn junction after the n-type and p-type semiconductor layers have been combined. The full black circles and empty black circles are the free electrons and holes, respectively. The plus signs and minus signs are the positively and negatively charged ions, respectively. The depletion layer is shown in the middle and the electric field will be from the right to the left in the figure. The figure is taken from [5].

When an electron is excited into the conduction band by an incoming photon with an energy greater than or equal to the band gap of the semiconductor material, the internal electric field will pull the electron towards the positively charged n-side and drive the hole towards the negatively charged p-side, as seen in figure 2.3. As mentioned in the previous section, the excited electron can then move out of the semiconductor through the metal electrode (cathode), flow through an external circuit where it transfers electric energy to a load, before it finally combines with a hole at the opposite electrode (anode).

2.4 Characteristics of PV Cells

A PV cell has four quantities which constitute the key performance characteristics of the given PV cell, and they are: the short circuit current density, J_{sc}, the open circuit voltage, V_{oc}, the fill factor, *FF*, and the power conversion efficiency (PCE), η [6]. The current density and voltage are often used together to create the *J*-*V* curve, as seen in figure 2.5. The short circuit current density, J_{sc}, and the the open circuit voltage, V_{oc}, are the two extremes. J_{sc} occurs when the voltage between the

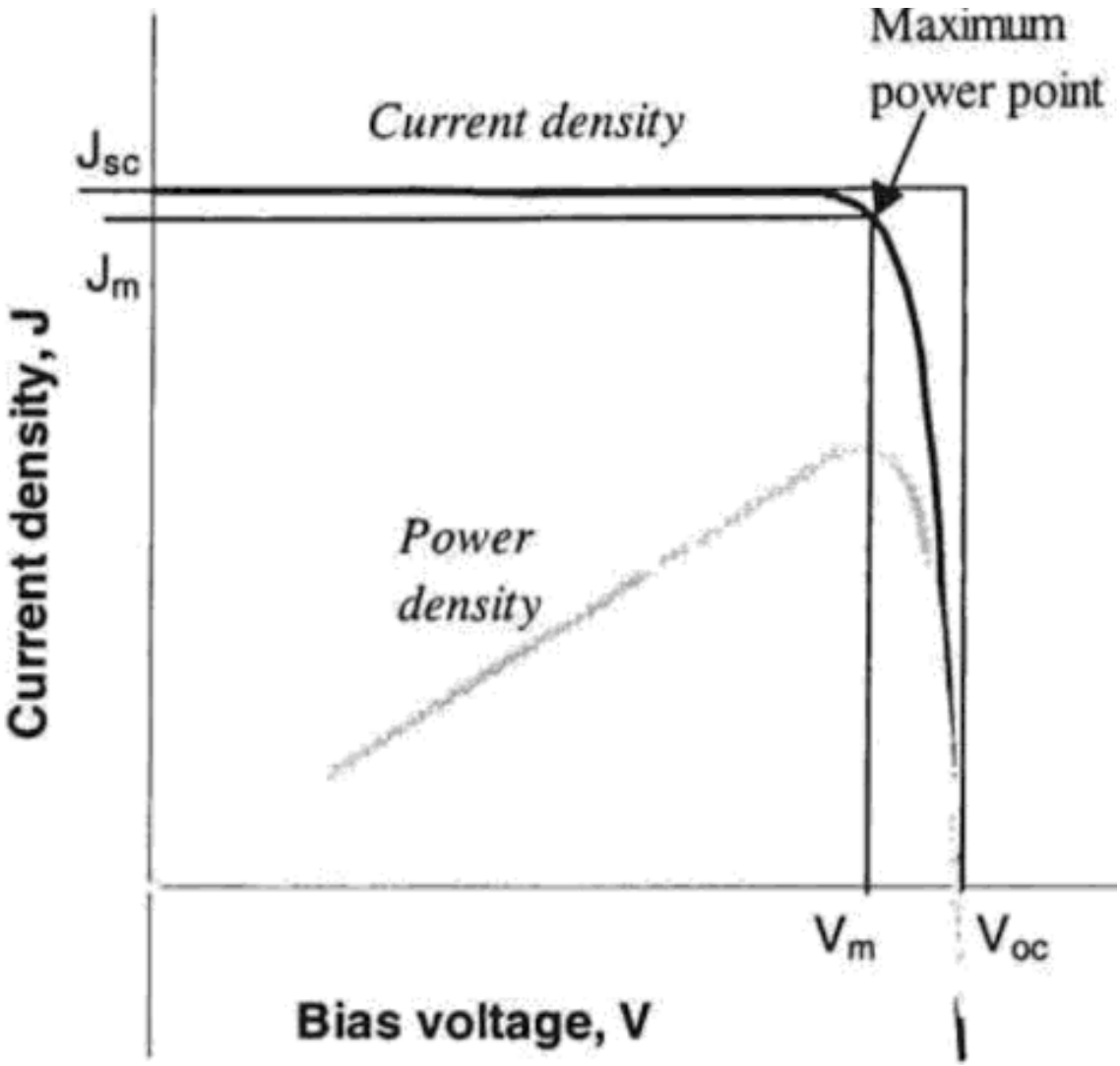

Figure 2.5: A typical J-V curve for a PV cell. The short circuit current density, J_{sc}, and the open circuit voltage, V_{oc}, is shown along with the maximum power point and the corresponding current, J_{m}, and voltage, V_{m}. The gray curve is the power density, and the peak of this curve has the voltage value V_{m}. See the text in section 2.4 for further details. The figure is taken from [6].

anode and the cathode is equal to zero, and likewise V_{oc} occurs when the current between the anode and the cathode is equal to zero. The power density of the solar cell at any point on the J-V curve is given by

$$P_{\mathrm{out}} = JV \tag{2.1}$$

and it is equal to the area of the rectangle constructed by drawing straight lines parallel to the x and y axes from the given point on the curve, and out to the x and y axes. The maximum power of any solar cell is therefore at the point on the J-V curve where the area of the abovementioned rectangle is maximized, as shown in figure 2.5. The power of an ideal PV cell would be equal to the product of J_{sc} and V_{oc}, which is equal to the area of the outer triangle seen in the figure. The relationship between the maximum power and the ideal power gives us the third key characteristic. This is called the fill factor, FF, which is always less than or equal

to 1, and given by

$$FF = \frac{J_m V_m}{J_{sc} V_{oc}} \tag{2.2}$$

This means that as the shape of the J-V curve approaches the shape of a rectangle, the area of the inner rectangle in figure 2.5 approaches the area of the outer rectangle, which is equivalent to the fill factor of the PV cell increasing, which means that the maximum power of the PV cell also increases and gets closer to the ideal value.

The fourth key characteristic of a PV cell is the power conversion efficiency (PCE), η. This is a measure of how much of the incident light power density (sunlight) that the PV cell actually converts to electric energy and it is given by

$$\eta = \frac{J_m V_m}{P_{in}} \tag{2.3}$$

η must be less than or equal to 1, and in real PV cells it is always much less than 1. It is common to multiply this value by 100% to get the PCE in %. Silicon PV modules have achieved PCE around 25% in lab conditions, but for the typical commercial modules the PCE is closer to 15% [35]. More advanced multi-junction type cells composed by stacking different semiconductor layers on top of each other can capture more of the incoming sunlight and have reached PCE up to 46% [7] in lab conditions, but these are still much too expensive to be commercialized. A chart showing the PCE development of the different PV technologies up until November of 2017 is shown in figure 2.6. This chart was made by the National Renewable Energy Laboratory (NREL) in USA, and it also includes perovskite PV cells, which are the PV cells that this thesis will focus on in the following chapters.

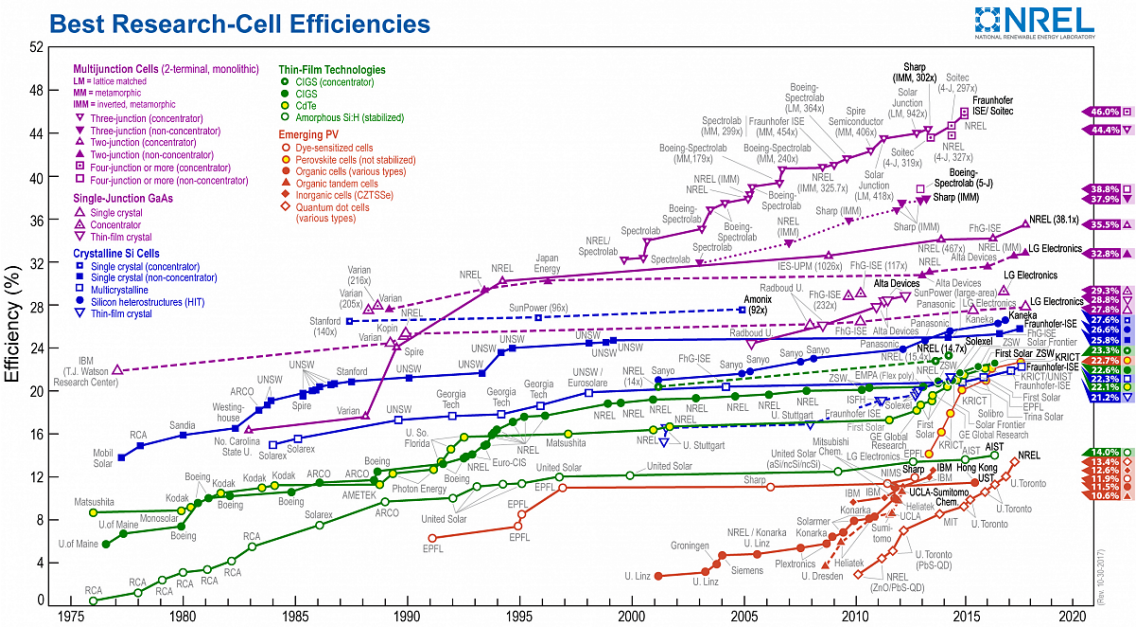

Figure 2.6: PCE development of different PV technologies [7].

The PCE, which is found by measuring the current and voltage characteristics, is commonly used to compare different PV cells and PV technologies to each other. Therefore, it is very important to have a set of standard test conditions for PV cells to ensure that all PV cells are tested under the same conditions. The Standard Test Conditions (STC) used for PV cells is to test the cells when illuminated

by an Air Mass 1.5 Global spectrum (AM1.5G) and at a temperature of 25°C [30]. The AM1.5G spectrum gives the solar irradiance as a function of wavelength, and integrated across all wavelengths it results in 1000 W/m^2, which is meant to represent a typical surface level irradiance, including both direct and diffuse light [34]. The Air Mass concept is based on the fact that the irradiance at any location on the surface of the earth will be reduced from the value that it has if measured above the atmosphere of the earth. The irradiance measured above the atmosphere, often referred to as the solar constant, is given by Air Mass 0 (AM0) and integrated across all wavelengths it is approximately 1365 W/m^2 [30]. As the sunlight passes through the atmosphere, the various molecules in the atmosphere attenuate the solar irradiance. The distance that the light (photons) has to travel through the atmosphere is affected by the angle of the sun relative to zenith, and the attenuation of the solar irradiance increases as the distance increases. The Air Mass 1.5 Direct (AM1.5D) spectrum corresponds to the sun having an angle of approximately 48 degrees relative to zenith [30], and integrated across all wavelengths it gives 888 W/m^2 [34]. By adding diffuse light to this spectrum, we arrive at the AM1.5G spectrum used in PV cell tests. Figure 2.7 [8] shows the three abovementioned solar spectra in the same plot.

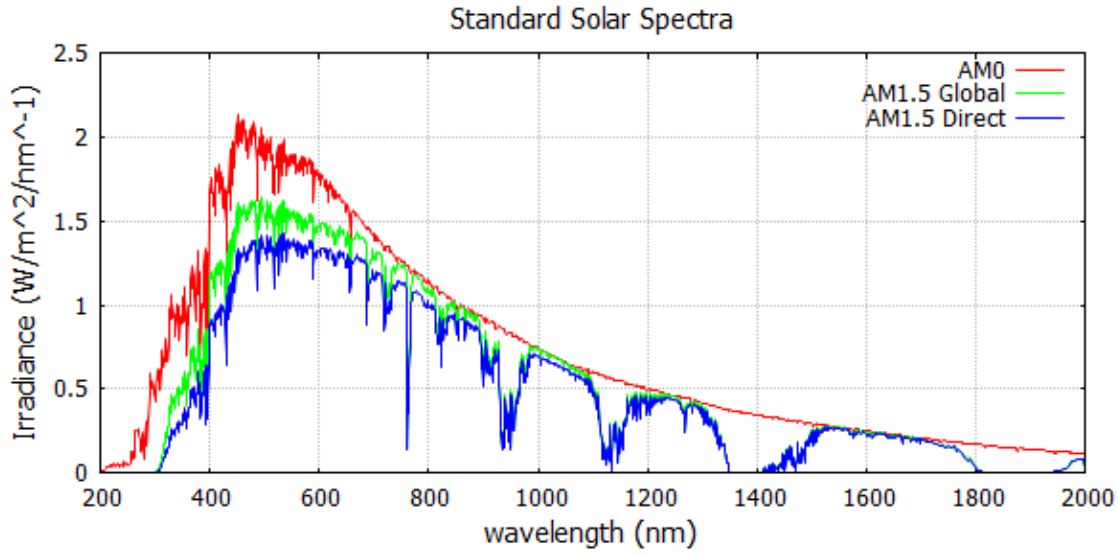

Figure 2.7: The standard solar spectra. AM0 is the irradiance above the atmosphere (solar constant), AM1.5 Direct is the irradiance at the earth surface with the sun at an angle of 48 degrees with only direct light, and AM1.5 Global is AM1.5 Direct plus the irradiance from diffuse light. AM1.5 Global is the spectrum that is used as Standard Test Condition (STC) for PV cells. Plot is taken from [8].

In real-world conditions, the actual irradiance that hits a PV cell at any given location on Earth will of course also depend on other variables, like time of day, season, latitude and cloud cover. In general, many of the locations with the highest irradiance values are quite close to the equator. Figure 2.8 [9] shows the long term average irradiance for a big part of the Earth surface.

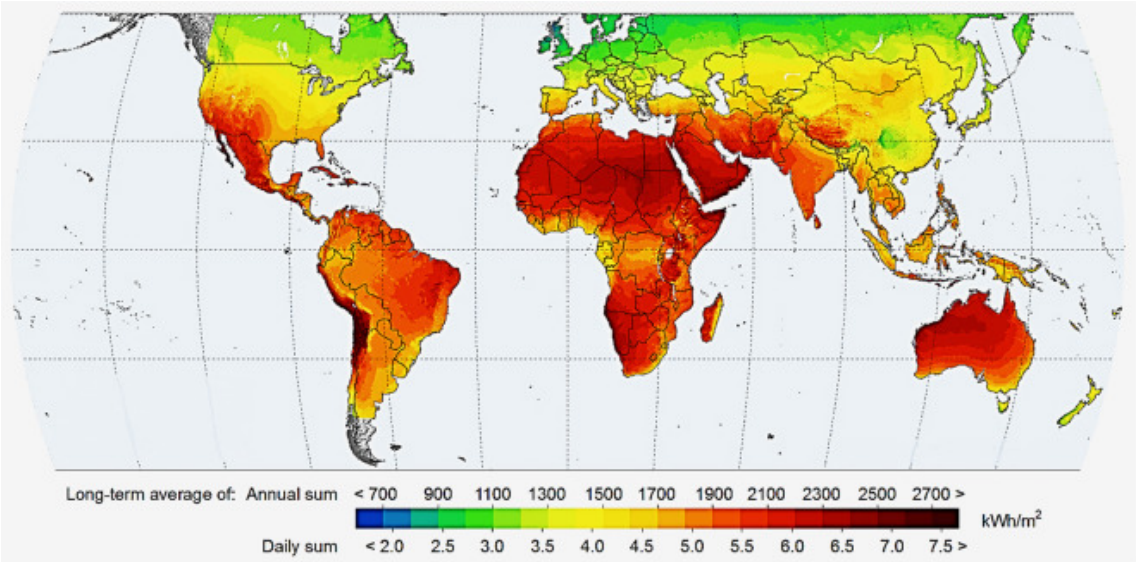

Figure 2.8: Map of global irradiance [9].

2.5 Types of PV cells

This section will give a short description of various types of PV cells. Perovskite PV cells, the main focus of this thesis, is included in this section, but will also be treated in much greater detail in the chapter 3.

2.5.1 Three Generations of PV cells

PV cells are traditionally divided into three generations according to [4]:

- First generation PV cells are considered fully commercialized and consist of PV cells made from crystalline silicon (c-Si). This includes both monocrystalline and polycrystalline silicon.
- Second generation PV cells are thin film PV cells. The three main types are: amorphous or micro amorphous silicon (a-Si), cadmium telluride (CdTe), and finally copper indium diselenide (CIS) or copper indium gallium diselenide (CIGS).
- Third generation PV cells are the most commercially immature of the three generations. This includes organic PV technologies and other concepts still in development. Perovskite PV cells belong to the third generation.

2.5.2 Crystalline Silicon (c-Si)

Crystalline silicon PV cells are by far the most common type of PV cells, and they dominate the commercial market with a global market share of about 90% [4, 36]. There are several reasons for this, including the fact that silicon is the second most abundant element on Earth, so supply is not a problem. Furthermore, the band gap of silicon is 1.12 eV [4] and this fits very well with the energy of the incident photons in sunlight. Silicon is also a generally stable and non-toxic substance. The highest reported PCE of a crystalline silicon PV cell at standard test conditions (STC) is

currently 25.8% [7], but the PCE of most commercially available PV cells are lower than this. The two common types of crystalline silicon PV cells are monocrystalline and polycrystalline. Monocrystalline cells are made from a single silicon crystal, and this is the oldest and most efficient of the two types. However, monocrystalline cells are more costly to produce due to a high energy demand in the production process and because the silicon material needs to be very pure. Therefore, some producers prefer to manufacture polycrystalline PV cells. As the name implies, this silicon PV cell consists of multiple smaller silicon crystals instead of just one. These PV cells are less costly to produce, the energy demand in the production process is lower and the silicon material does not need to be as pure as the monocrystalline. Monocrystalline PV cells are produced by growing cylindrical ingots of silicon through the use of the Czochralski process and then slicing the ingot into thin wafers. The wafers then go through chemical etching, anti-reflection coating and metal contacts are added. Polycrystalline PV cells are produced by melting silicon, then solidifying it to orient the crystals in a fixed direction in a square ingot. The ingot is then first sliced into blocks before the blocks are sliced into thin wafers. The PCE of commercial silicon PV cells are in the range 15-20% for monocrystalline silicon and 13-16% for polycrystalline silicon [31].

2.5.3 Gallium Arsenide (GaAs)

These PV cells use a compound semiconductor consisting of gallium (Ga) and arsenic (As). It has a similar structure to silicon PV cells, but it has different properties that gives it some advantages, as well as disadvantages, compared to silicon PV cells. GaAs PV cells generally have a higher PCE and lower weight than silicon PV cells. The increased PCE is due to the alloying of the GaAs layers with materials like aluminum (Al), antimony (Sb), Indium (In) and phosphorus (P). When these layers are stacked, the result is a multi-junction PV cell which has a higher PCE. The band gap for GaAs is 1.43 eV [35], which is suitable for a PV cell. The GaAs PV cells also have a high heat resistance, which makes them well suited for concentrator PV modules and space applications. The main disadvantage of these PV cells is that they are much more expensive to produce than silicon PV cells. As seen in figure 2.6, the record PCE of a single-junction GaAs PV cell is 27.8% [7]. The multi-junction versions have reached PCE as high as 46%, but these are much too expensive to be commercialized.

2.5.4 Amorphous Silicon (*a*-Si)

Amorphous silicon PV cells are the most mature and most used of the thin film PV technologies. The silicon atoms in *a*-Si are randomly oriented relative to each other, which causes this material to have a higher band gap (1.7 eV [32]) than crystalline silicon. Thin film PV technologies use up to 99% less material than crystalline PV technologies [31] and the production costs of the thin film technologies are therefore much lower. *a*-Si PV cells are produced by continuous deposition techniques, e.g. on a glass surface. Another advantage with thin film PV cells are that they are much easier to integrate into buildings, windows and curved surfaces due to their flexibility, low weight and semi-transparency. The main drawback of thin film PV cells are their relatively low PCE. The record PCE of a single junction *a*-Si PV cell in

laboratory conditions is 14% [7]. However, in real-world conditions a light-induced degradation effect known as the Staebler-Wronski effect cause the PCE to drop. This drop is usually in the range of 15-35% [31] before the PV cell stabilizes. Actual PCE of single junction *a*-Si PV cells is therefore usually in the range 4-8% [31]. To reduce the PCE degradation, multi-junction *a*-Si PV cells have been developed, and these usually have a slightly higher PCE than the single junction type.

2.5.5 Cadmium Telluride (CdTe)

CdTe PV cells are composed of cadmium (Cd), which is a by-product of zinc mining, and tellurium (Te), which is a by-product of copper processing. This is a popular thin film PV technology because it has both a lower production cost and a higher PCE than *a*-Si PV cells. The main reason for the higher PCE is that CdTe PV cells have an ideal band gap of 1.45 eV [31]. The record PCE of a CdTe PV cell is currently 22.1% [7]. The PCE in real-world conditions is not as high as this, but it can still be above 15% [31]. The main problem with CdTe PV cells is the fact that cadmium is a toxic material, which raises environmental concerns, and the fact that tellurium is a very scarce material, which could cause problems with raw material supply.

2.5.6 Copper Indium Gallium Selenide (CIGS) and Copper Indium Selenide (CIS)

CIGS and CIS are among the fastest developing and most popular thin film PV technologies. They consist of copper, indium and selenide, with CIGS also containing gallium which increases the band gap [32]. The band gap of these cells can vary depending on the composition, and it can be as high as 1.68 eV [35]. The record PCE of a CIGS PV cell is 22.6% [7], but the commercial PCE is in the range 7-16% [31]. An advantage with CIGS and CIS PV cells is that they experience only 10% of the degradation compared to other thin film PV technologies [31, 35]. The main challenges related to CIGS and CIS PV cells are a lack of understanding of technical issues related to grain boundaries, junction activation treatment and back contacts, as well as the fact that indium is a very scarce material which can cause supply problems.

2.5.7 Organic PV cells

Organic PV cells are still in the development phase and have quite low PCE, but they have attracted interest among researchers due to advantages like mechanical flexibility, low weight, low cost of both material and production process (easy production requiring neither high temperature nor vacuum), non-toxicity and disposability, as well as semi-transparency [31, 32]. These PV cells are thin film PV cells made from organic semiconductors such as polymers and compounds like pentacene, polyphenylene vinylene, copper phthalocyanine and carbon-based nanostructures (nanotubes, graphene, fullerenes). Due to the abovementioned advantages organic PV cells are particularly interesting as building integrated PV cells, but the low PCE and lack of long-term stability and reliability so far prevents their commercialization. The record PCE of an organic PV cell is currently 11.5% [7], increased from 1% in just 15

years [31]. One of the reasons for the limited PCE of organic PV cells is the fact that most polymers have a band gap of more than 2.0 eV, and this limits the absorption of photons by around 30% [4]. The challenge related to long-term stability is caused by oxygen and water penetrating the PV cell layers and causing degradation.

2.5.8 Dye-Sensitized Solar Cells (DSSC)

Dye-sensitized solar cells is another thin film PV technology in the development phase. These PV cells have many of the same advantages as organic PV cells, i.e. low production cost, simple production process and transparency. But just like organic PV cells, DSSC also has a very limited PCE. The record PCE is currently 11.9% [7], and the PCE of a DSSC is usually in the range 7-11% [4]. DSSC consists of a dye-sensitized photo-anode, a counter electrode and a redox electrolyte [31]. Titanium dioxide (TiO_2) nanoparticles are placed in a dye solution and left overnight to allow the dye molecules to attach themselves to the surface of the TiO_2 nanoparticles. This is called sensitization, hence the name *dye-sensitized* solar cells. The working principle of a DSSC is that the incident photon excites an electron in the dye molecule, thereby transferring it to the TiO_2 and leaving a hole in the dye molecule. The redox electrolyte acts as a mediator and fills the hole with one of its own electrons, while the excited electron travels through an external circuit and delivers electric energy to an external load [31]. The main challenge with DSSC, apart from the low PCE, is the fact that the electrolyte of the most efficient types of DSSC contains volatile solvents that deteriorate the seals of the PV cell, causing environmental concerns.

2.5.9 Perovskite

In recent years, perovskite solar cells has emerged as arguably the most promising of all thin film PV technologies. In just a few years of research since 2011, the PCE of these PV cells have risen very rapidly. The record PCE is currently 22.7% [7], already rivaling the PCE of the established thin film PV technologies (CdTe and CIGS) and rapidly approaching crystalline silicon PV cells. Perovskite is actually a whole group of materials with the general formula ABX_3, where A is an organic cation, B is an inorganic cation, and X is a halide anion [36]. This means that these materials can have several different band gaps, e.g. 1.6 eV if pure iodide (I^-) is used as the halide and 3.2 eV if pure chloride (Cl^-) is used as the halide anion [36]. Several different band gaps in between these two values can also be achieved through a combination of different materials in the halide. Generally, the types with the lower band gaps achieve the highest PCE. Advantages with perovskite PV cells include long carrier diffusion lengths, low recombination losses, low material costs, as well as the very promising PCE, while challenges include parasitic absorption in the hole-transporting material, high sensitivity to moisture, cell instability, as well as the use of toxic lead (Pb) [36]. A much more thorough and detailed description of perovskite PV cells is given in chapter 3.

2.5.10 Quantum Dots (QD)

Quantum dot PV cell materials are semiconductor compounds that consists of different material groups on the nanoscale that are combined in a variety of different

forms [32, 35]. This makes it possible to adjust the band gap of these materials to achieve desired characteristics. By increasing the band gap the voltage output will increase, while decreasing the band gap will result in increased current output. Another interesting opportunity with QD PV cells is that they have the ability to generate multiple electron-hole pairs per individual photon [31], and combined with the tunable band gap this could, in theory, allow for significantly higher PCE than the PV cells of today. QD PV cells are still in the development phase though, and research is focused on trying to improve the PCE. The record PCE of a QD PV cell is currently 13.4% [7]. Materials that have been used for QD PV cells include GaAs, silicon-silicon dioxide (Si-SiO_2), silicon-silicon carbide (Si-SiC) and silicon-silicon nitrite (Si-Si_3N_4) [32]. However, the best QD PV cells to date has been made using PbS or PbSe quantum dots as the active layer [36].

Chapter 3

Perovskite PV Cells

This chapter will give a detailed description of perovskite PV cells. Section 3.1 will go through the short history of perovskite PV cells in a chronological manner. Then the materials and structure of these PV cells will be described in section 3.2, followed by a description of the working principle in section 3.3. Finally, section 3.4 will discuss the current status and future possibilities for perovskite PV cells.

3.1 History

Perovskite PV cells is one of the most recently "discovered" PV technologies, but it has seen the fastest rise in PCE of any PV technology in history. Perovskite as a material for PV cells was first reported in 2006 when Miyasaka and co-workers constructed a $CH_3NH_3PbBr_3$ cell with a PCE of 2.2% [37]. In 2009, they replaced bromide (Br^-) with iodide (I^-) and consequently achieved a PCE of 3.8% [37, 11, 10, 12, 38, 39]. Park and co-workers then used $CH_3NH_3PbI_3$ nanoparticles deposited on a nanocrystalline TiO_2 surface and achieved a PCE of 6.5% in 2011 [37, 11, 10, 38, 39]. One of the challenges at this point was that the perovskite nanoparticles dissolved in the electrolyte, which rapidly degraded the performance of the PV cell. Park, Grätzel and co-workers therefore focused on this and replaced the electrolyte with a solid state hole-transporting material (HTM) called spiro-OMeTAD, and consequently achieved improved stability and a PCE of 9.7% [37, 11, 10, 38, 39]. In 2012, Snaith and Lee used a mixed halide anion to form $CH_3NH_3PbI_{3-x}Cl_x$ that exhibited better stability and carrier transport, resulting in a PCE of 10.9% [37, 11, 10, 38, 39]. Seok, Grätzel and co-workers experimented with two perovskite layers, one solid perovskite and the other nanoporous TiO_2 infiltrated by perovskite, as well as different HTMs, and achieved a PCE of 12.0% in 2013 [37, 38, 39]. Later that same year they used a mixed halide anion to form $CH_3NH_3PbI_{3-x}Br_x$ and reported a 12.3% PCE [37, 38, 39]. The development was rapid in 2013 and continued with both Grätzel's group and Snaith's group reporting PCE values above 15% [37, 38, 39]. The two groups used different methods, with Grätzel's group sticking to the two perovskite layers mentioned above, and Snaith's group sticking to just one perovskite layer with a mixed halide anion to form $CH_3NH_3PbI_{3-x}Cl_x$. Seok's group used a mixed halide anion to form $CH_3NH_3PbI_{3-x}Br_x$ with 10-15% bromine (Br) and a poly-triarylamine HTM instead of spiro-OMeTAD to achieve a PCE of 16.2% towards the end of 2013 [37, 38, 39]. The same group managed to achieve a PCE of 17.9% in the beginning of 2014 [37, 38]. Zhou and co-workers adjusted the band

alignment of the HTM and electron-transporting material (ETM) relative to the perovskite layer and achieved a PCE of 19.3% in 2014 [38]. The 20% PCE limit was broken in 2015 when researchers from the Korean Research Institute of Chemical Technology (KRICT) achieved a PCE of 20.1% [38]. In 2017, Shin and co-workers prepared and used an electrode of lanthanum (La)-doped $BaSnO_3$ (LBSO) instead of the usual TiO_2 and achieved a PCE of 21.2%, and this PV cell maintained 93% of its initial performance after 1000 hours of full sun illumination [38]. At the end of 2017, KRICT took back the world record when they reported a PCE of 22.7% [7], which is currently the highest achieved PCE.

A number of different materials and structures have been used in experiments since the first perovskite PV cell in 2006. Particularly since 2012, there has been a lot of activity and rapid progress made in the field. However, perovskite PV cells have still not been commercialized and the abovementioned PCEs have been achieved in lab experiments where the PV cells are usually approximately the size of a stamp.

3.2 Materials and Architecture

Perovskite materials are a whole class of materials named after Russian mineralogist L. A. Perovski, some of which are used in perovskite PV cells. These are usually metal-halide perovskites, particularly organic-inorganic hybrid compounds which are crystallized from organic halide and metal halide salts. The general structure of these materials is ABX_3, where A is an organic cation, B is a metal cation and X is the halide anion [40].

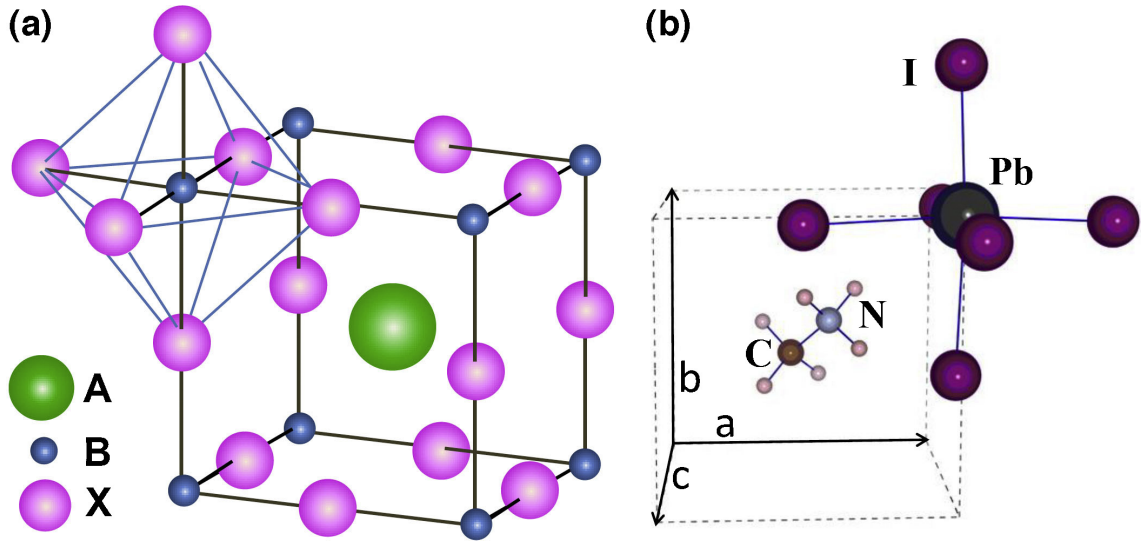

Figure 3.1: a) The ABX_3 perovskite crystal structure, also showing a BX_6 octahedral. b) The unit cell of one of the most common perovskite materials in PV cells. Methylammonium ($CH_3NH_3^+$) is the organic cation (A), lead (Pb^{2+}) is the metal cation (B) and iodide (I^-) is the halide anion (X), resulting in $CH_3NH_3PbI_3$. Figure taken from [10].

There are several different types of perovskite materials that have been used in PV cells so far. $CH_3NH_3PbI_3$ shown in figure 3.1 is perhaps the most common

one, but other versions of perovskite have also been used. The various materials have been used in several different architectures in combination with various other materials that function as HTM, ETM, anode and cathode. The various materials, architectures and layers will be described in the following subsections.

3.2.1 The Organic Cation (A)

The organic cation (A) has no direct influence on the electronic properties of the perovskite, but the size of it can affect the amount of contortion, which in turn can affect the electronic properties [11]. The most common materials used as organic cations in perovskite PV cells are methylammonium (MA), formamidinium (FA), cesium (Cs), as well as mixtures of different substances.

Methylammonium (MA)

MA ($CH_3NH_3^+$) is the most common of all the organic cations in perovskite PV cells. The band gap of $MAPbI_3$ is 1.51-1.55 eV [11], a little bit above the ideal band gap of 1.4 eV. The MA ion is a very small ion, so researchers have experimented with replacing MA with bigger ions to increase the symmetry and decrease the band gap. Ethylammonium (EA or $CH_3CH_2NH_3^+$), which is much bigger than MA, have been tried, but this resulted in a band gap of 2.2 eV [11], even further from the ideal band gap.

Formamidinium (FA)

FA ($HC(NH_2)_2^+$) has been tried instead of MA in numerous experiments. The size of the FA ion is bigger than MA, but smaller than EA. The band gap of $FAPbI_3$ is 1.43-1.48 eV [11], which is closer to the ideal band gap compared to MA. Therefore, there have been expectations that FA will give a better result than MA as the organic cation in perovskite PV cells. However, experiments has found that the formation of a non-perovskite polymorph of $FAPbI_3$ has resulted in reduced PCE when using FA as the organic cation. If this polymorph state can be eliminated, it is quite possible that the PCE of FA-based PV cells could exceed the PCE seen in MA-based PV cells.

Cesium (Cs)

Cesium was first used as the organic cation in a perovskite PV cell by Scaife and co-workers [11]. The perovskite they used also consisted of tin (Sn^{2+}) and iodide (I^-), and $CsSnI_3$ was found to exhibit strong photoluminescence at ambient temperature for the near-infrared domain of the spectrum. Cs is even smaller in size than MA, which ultimately results in a larger band gap of 1.73 eV [11], which is further away from the ideal band gap compared to MA.

Mixed Organic Cations

The idea behind using mixed organic cations is to try to combine the strengths of each individual component into one cation. Pellet and co-workers used a mixture of MA and FA to form $MA_xFA_{1-x}PbI_3$ and managed to achieve a PCE of 14.9% [11], which was higher than when only MA was used. The increased PCE was due

to a higher absorptance in the red portion of the spectrum compared to the MA-based version. Mei and co-workers mixed 5-aminovaleric acid (5-AVA) with MA to form $(5\text{-AVA})_x\text{MA}_{1-x}\text{PbI}_3$ and managed to achieve a PCE of 12.8% [11] along with advantages like extended exciton life span and enhanced resistance in normal ambience and light compared to the MA-based device.

3.2.2 The Metal Cation (B)

The metal cation (B) in PV cell perovskites is usually a metal from group IVA in a +2 oxidation state (Pb^{2+}, Sn^{2+}, Ge^{2+}) [11]. The most used of these has so far been lead (Pb) because the performance and stability has been better compared to tin (Sn). However, because Pb is a toxic material, there has also been some focus on creating perovskite PV cells with Sn instead of Pb. Germanium (Ge) is very unstable in its +2 oxidation state so it has rarely been used. A lack of stability has also been the main obstacle for the use of Sn up to this point. In theory, a MASnX_3 perovskite with its band gap of 1.2-1.4 eV would be a better choice for a PV cell than a MAPbX_3 perovskite with its band gap of 1.6-1.8 eV [11], but in practice this has not been the case so far. The main problem is that Sn oxidize rapidly to Sn^{4+} in air, and in turn this results in the volatile compound SnI_4. Perovskite PV cells using Sn as the metal cation has been constructed successfully by several researchers, but the PCE of these PV cells has so far been below the PCE of PV cells where Pb is used. Nevertheless, if the unstable nature of Sn^{2+} can be overcome, it has the potential to create PV cells with a higher short circuit current density than the Pb-based version. The most promising route is perhaps to use a mixture of Pb and Sn, resulting in a perovskite of the form $\text{MASn}_{1-x}\text{Pb}_x\text{I}_3$. A lot of progress has been made with this approach, where finding the right balance between Pb and Sn can result in increased absorptivity of photons and a decrease in the band gap compared to a perovskite where only Pb is used [11]. This is illustrated in figure 3.2.

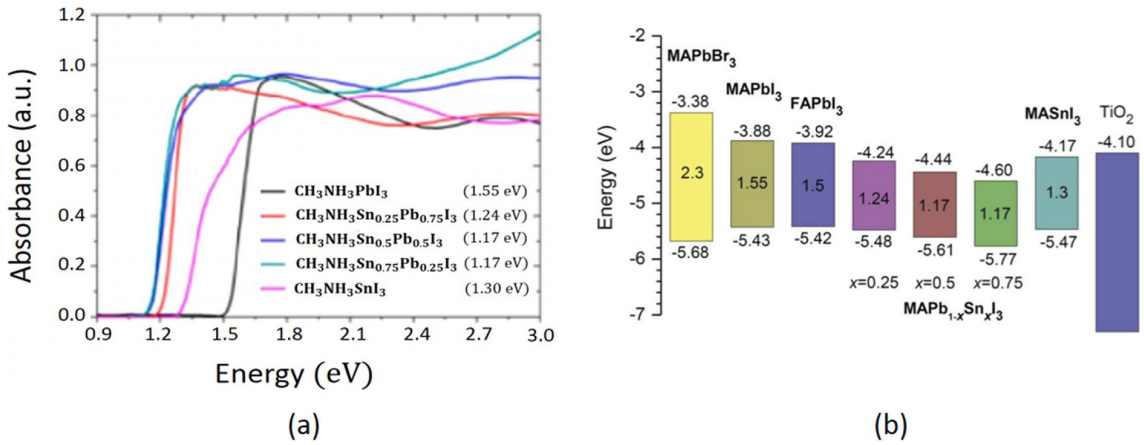

Figure 3.2: The absorbance and band gap of some of the different perovskite materials. a) Absorbance of perovskite with different metal cations (pure Pb, pure Sn and mixtures of both. b) Band gap for various perovskite materials. Figure taken from [11].

3.2.3 The Halide Anion (X)

The most effective way to change the performance of a perovskite PV cell is to make changes to the halide anion (X) in the perovskite. The anions used in this position come from the VIIA group in the periodic table, and they are: iodide (I^-), bromide (Br^-), chloride (Cl^-), fluoride (F^-), or a mixture of these [11]. Generally, when going downwards in the periodic table from fluoride to iodide, the atoms get larger, the absorption spectra shifts to longer wavelengths and energy decreases [11].

Iodide

The iodine anion is called iodide (I^-), and so far this is the most used halide anion in perovskite PV cells, having achieved PCEs above 20%. The electronegativity of iodide is quite close to that of the lead cation (Pb^{2+}), which results in a mixed bonding character that gives the most stable perovskite structure [11]. The main challenge with iodide is that it becomes unstable when exposed to humidity, which means that more research is needed to either overcome this or replace iodide with another anion.

Bromide

The bromine anion is called bromide (Br^-), and it has been used in several experiments on perovskite PV cells. Some have used only bromide in a $MAPbBr_3$ perovskite, but the most successful results have come from mixed halide anions in perovskites of the form $MAPbI_xBr_{3-x}$. These perovskites have exhibited enhanced PCEs and stability, and this has been achieved through chemical combinations that make it possible to adjust the band gap. Eperon and co-workers showed that by varying the ratio between bromide and iodide, the band gap can be adjusted in the range 1.48-2.23 eV [11]. They observed that by increasing the bromide content, V_{oc} increased and J_{sc} decreased.

Chloride

The chlorine anion is called chloride (Cl^-). In planar configurations (see section 3.2.5), chloride has been shown to enhance diffusion lengths and carrier lifetimes, which results in enhanced PCE [11]. Both pure chloride resulting in $MAPbCl_3$, and a mixture of chloride and iodide resulting in $MAPbI_{3-x}Cl_x$, has been used in experiments. It has been suggested that chloride incorporation controls the morphological evolution of the perovskite film, consequently affecting the material characteristics and PCE [11].

Fluoride

The fluorine anion is called fluoride (F^-). The superior electron withdrawing characteristic and potential for stronger hydrogen bond formation compared to the other halide anions, would suggest that fluoride is well suited for perovskite PV cells. However, due to the very small size of fluoride it has an unwanted tolerance factor and a large amount of lattice strain [11]. This reduces the light absorbing capacity and conductivity of the material, making it less suited for use in perovskite PV cells.

Complex Halide Anions

Nagane and co-workers recently experimented with a new type of halide anion by combining boron (B) with fluorine (F) in the molecular ion BF_4^- to form the perovskite material $MAPbI_{3-x}(BF_4)_x$ [11]. This material exhibited improved electrical conductivity at lower frequencies and enhanced response of photons under AM1.5 illumination compared to the $MAPbI_3$ type.

3.2.4 The Mesoporous Scaffold Architecture

The mesoporous scaffold architecture is the most common architecture for perovskite PV cells [11, 12]. It is based on the typical architecture of a solid state DSSC. The material most commonly used in the mesoporous layer is TiO_2 due to its high band gap (3.2 eV [12]), high chemical and thermal stabilities, photostability, non-toxicity and low cost [12]. Nanoparticles are sintered on the TiO_2 layer to make it porous, and this is done by spin coating a commercial TiO_2 paste before washing and sintering at 500°C. Then, the perovskite infiltrates the interstices in the mesoporous TiO_2. After this, the perovskite film is coated on top of the mesoporous layer. The general architecture (as shown in figure 3.3) of the completed PV cell will be, from bottom to top: metal anode (usually gold), HTM (usually spiro-OMeTAD), perovskite film, mesoporous layer, ETM (usually TiO_2), transparent cathode, and finally a glass cover.

The mesoporous layer assists the electron transfer between the perovskite layer and the fluorine-doped tin oxide (FTO) layer which functions as the transparent cathode. However, the mesoporous scaffold architecture exhibits a lower V_{oc} and lower light absorbance at wavelengths higher than 700 nm compared to some other architecture types [12]. It is also necessary to avoid contact between the mesoporous layer and HTM, as this frequently results in short circuiting.

3.2.5 The Planar Architecture

Liu and co-workers demonstrated that high PCEs can be achieved in perovskite PV cells without using the complex nanostructuring applied in the mesoporous scaffold architecture [11]. They showed that a much simpler planar architecture, similar to silicon PV cells, could also result in PCE values above 15%. The planar architecture is constructed using the vapor deposition technique developed by Snaith and co-workers [11]. In this technique, CH_3NH_3I and $PbCl_2$ is co-evaporated from two different pots at 120°C and 350°C, respectively. This is done in a box filled with N_2 gas. The evaporated substances accumulates on a c-TiO_2 laminated FTO glass under a vacuum level of 10^{-5} mbar and a molar ratio of 4:1 is the result. Finally, the crystalline structure of the perovskite is obtained by annealing [11]. This technique results in a highly uniform perovskite film.

Depending on the order of the layers, the PV cells are classified as conservative (n-i-p) or inverted (p-i-n). The conservative order is metal anode, HTM, perovskite, ETM, FTO, glass, whereas the inverted order is metal anode, ETM, perovskite, HTM, FTO, glass. In other words, the difference between conservative and inverted is that HTM and ETM switch places. Typical layer thicknesses are 30 nm (metal anode), 100-300 nm (HTM), 200-500 nm (perovskite), 10-80 nm (ETM),

420 nm (FTO) and 2 mm (glass) [41, 42]. Taghavi and co-workers performed simulations and found the optimum thickness of the perovskite layer to be around 300 nm [43]. The planar architecture generally exhibits a higher J_{sc} and V_{oc} than the mesoporous scaffold architecture, but it suffers more from J-V hysteresis (see section 3.4).

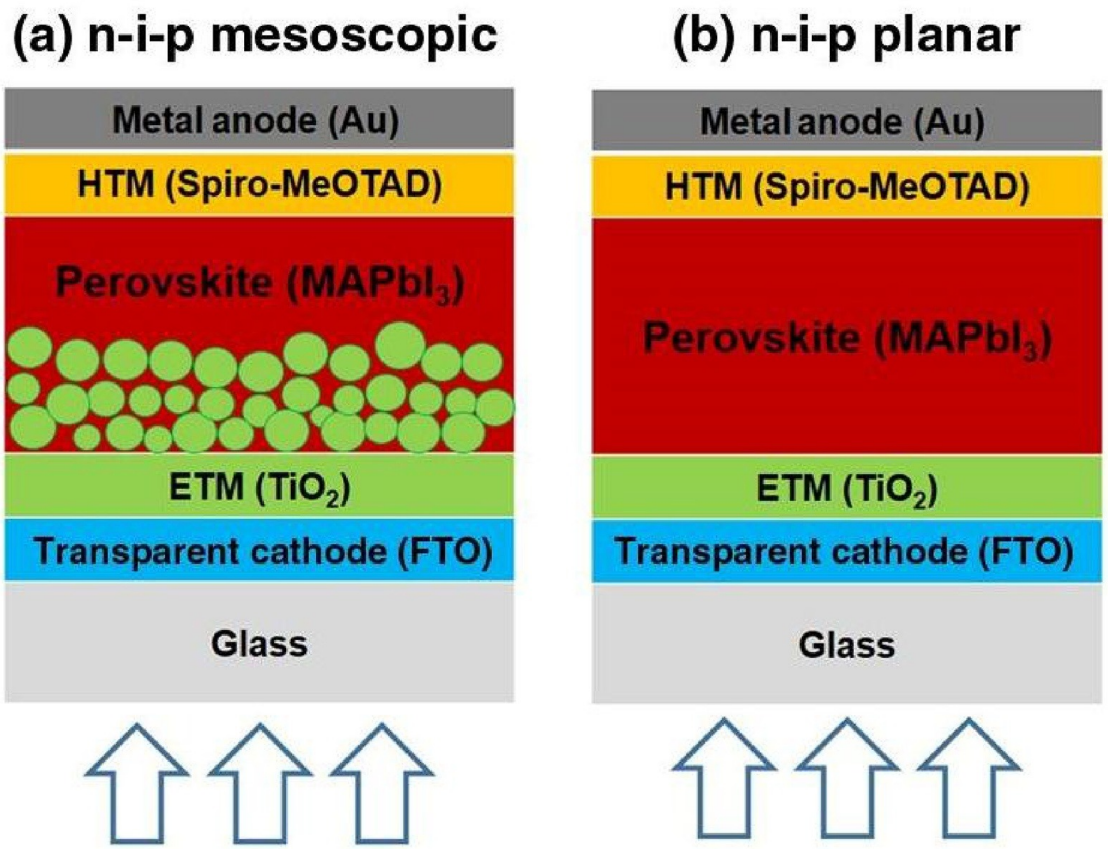

Figure 3.3: Two different architectures for perovskite PV cells. The arrows symbolize incident sunlight. a) Mesoporous/mesoscopic scaffold architecture, b) planar architecture. Figure taken from [11].

3.3 Working principle

The perovskite layer is the light absorbing material in a perovskite PV cell. It is this layer that produces charge separation that drives electrons to the n-i junction between the ETM (n-type material) and the perovskite and the holes to the i-p junction between the perovskite and the HTM (p-type material). The band alignment of the perovskite material with the ETM and HTM is very important to the efficiency of the charge extraction. The main rules are: the conduction band edge of the ETM must be lower than the perovskite conduction band, and the valence band edge of the HTM must be higher than the perovskite valence band [12] (see figure 3.4).

The step-by-step working principle of a typical perovskite PV cell is as follows [12]: As the perovskite layer absorbs a photon from the incident sunlight, an

electron-hole pair is created according to

$$\text{perovskite} + h\nu \rightarrow \text{e}^- + \text{h}^+ \tag{3.1}$$

Following this the electrons are driven to the ETM and the holes are driven to the HTM according to

$$\text{e}^- + \text{h}^+ \rightarrow \text{e}^-_{\text{cb}}(\text{TiO}_2) + \text{h}^+(\text{HTM}) \tag{3.2}$$

The driving force behind the separation of the charges are the built-in electric field caused by the p-n junctions. A space-charge region appears at the interfaces (n-i junction and i-p junction) and band-bending is observed (see figure 3.4). The excited electron then goes through the external circuit via the cathode (FTO) and ends up at the metal anode, while the hole is transported through the HTM and ends up at the same metal anode. Finally, the electron and hole recombines at the HTM/anode interface.

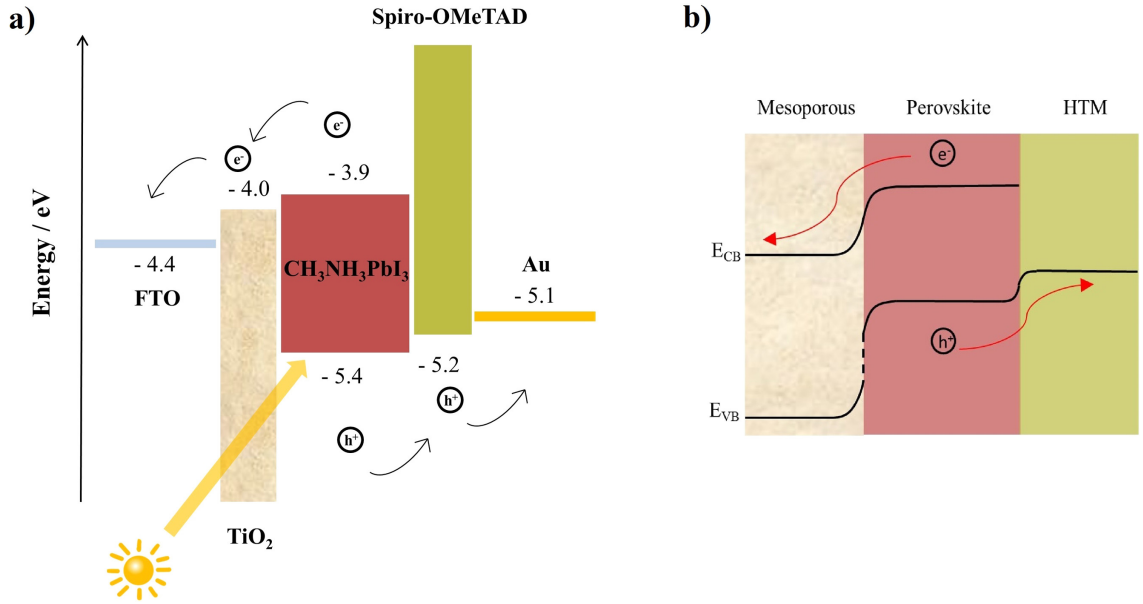

Figure 3.4: a) Energy diagram for a typical perovskite PV cell, also showing movements of electrons and holes. b) Band bending of energy levels during separation of charges. Figure taken from [12].

There are also undesired reactions that take place in perovskite PV cells. These reactions compete with the extraction of the charge carriers, thereby reducing the PCE of the PV cell. The main undesired reactions are [12]: exciton annihilation by photoluminescence according to

$$\text{e}^- + \text{h}^+ \rightarrow h\nu \tag{3.3}$$

non-radiative recombination according to

$$\text{e}^- + \text{h}^+ \rightarrow \nabla \tag{3.4}$$

recombination of charge carriers with consequent heat release at ETM/perovskite interface according to

$$\text{e}^-_{\text{cb}}(\text{TiO}_2) + \text{h}^+(\text{perovskite}) \rightarrow \nabla \tag{3.5}$$

recombination of charge carriers with consequent heat release at HTM/perovskite interface according to

$$h^+(\text{HTM}) + e^-(\text{perovskite}) \rightarrow \nabla \tag{3.6}$$

and finally recombination of charge carriers with consequent heat release at HTM/ETM interface according to

$$e^-_{cb}(TiO_2) + h^+(\text{HTM}) \rightarrow \nabla \tag{3.7}$$

3.4 Challenges and future possibilities

Perovskite PV cells have shown very promising research results with PCEs on the same level as the leading commercial thin film PV technologies and approaching the level of crystalline silicon PV cells. However, perovskite PV cells are still in the development phase and all results have been achieved in lab experiments, not using full-size modules in real-world conditions. There are still some challenges that need to be solved before perovskite PV cells can become fully commercialized, and the four main challenges are: stability, hysteresis, environmental concerns, and scaling up to large area devices [13]. This section will give a short description of these challenges, followed by a short summary of future possibilities.

Stability

Stability is perhaps the biggest challenge related to perovskite PV cells. The stability will be affected by temperature, illumination and exposure to oxygen and moisture. Degradation can occur in the perovskite layer, but also in the HTM, ETM and electrodes. Many reports have found negative and irreversible effects on $MAPbI_3$ perovskite when temperatures exceed 100°C, 85°C, and even as low as 50°C [13]. It seems that the exposure to oxygen without moisture is not very critical to perovskite PV cells, but the effect can become very destructive when the moisture level rises. Demonstrations have shown that the degradation is very rapid in conditions with high humidity [13]. The exposure to illumination will also speed up the degradation process. So it seems that increasing illumination, rising temperatures and rising humidity will all have a very negative effect on the stability of perovskite PV cells, causing degradation and decreasing PCE. Figure 3.5 shows the decrease in PCE in two different perovskite PV cells under two different sets of conditions.

There is a lot of effort directed towards improving the stability of perovskite PV cells, and many different experiments have already been performed. However, many of the experiments did not expose the PV cells to multiple stressors (humidity, illumination, elevated temperature) at the same time, so it is difficult to judge how relevant the results are for real-world conditions. It has been shown that $MAPbBr_3$ is more stable than both $MAPbI_3$ and versions where a mixed halide anion (iodide and bromide) was used [13], so altering the components of the perovskite material can improve stability. The deposition process can also have an effect on the stability, for example through the resulting crystallinity and grain sizes. Many other factors can also affect the long-term stability of perovskite PV cells, including HTM material, ETM material, electrode material and encapsulation method [13]. Numerous experiments have been performed with the aim of gaining increased understanding

of the processes that affect the long-term stability of these PV cells and to ultimately improve it, but the vast majority of research on perovskite PV cells still focus on improving the PCE, not the stability [12]. If perovskite PV cells are going to be commercialized, a lot more research on the stability challenge will be required. Most of all, rigorous long-term testing with PV cells exposed to all the stressors of real-world conditions is needed, particularly outside testing which has been very scarce so far [13].

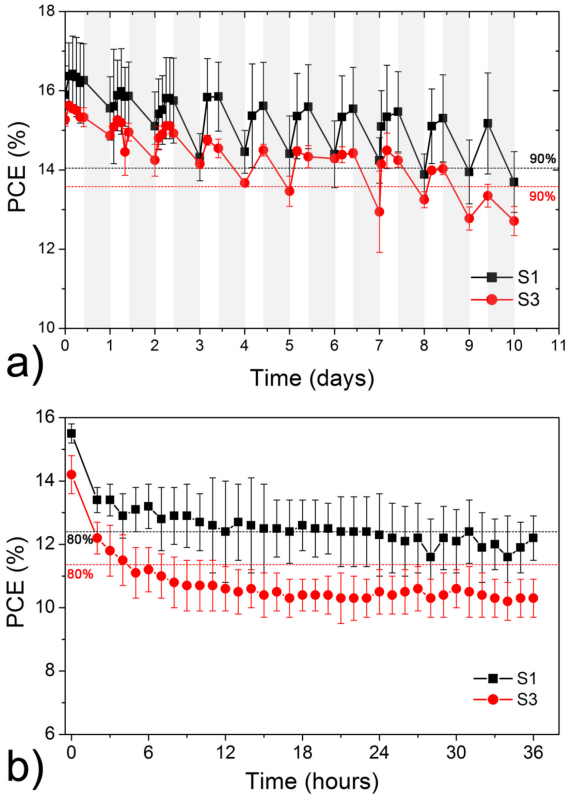

Figure 3.5: Average PCE for perovskite PV cells with (S1) and without (S2) excess PbI_2 in ambient air at 60% relative humidity (RH) as a function of time with a) alternating simulated sunlight in 10 hour dark/14 hour sunlight cycles at room temperature, and b) at 85°C and under constant simulated illumination. Figure taken from [13].

Hysteresis

Hysteresis describes how the state of a system depends on the history of that same system and there are numerous examples of this phenomenon in many different fields (e.g. magnets, deformed rubber bands). Hysteresis have been shown to have negative effects on the PCE and stability of perovskite PV cells and the general trend is that it is worse in planar architecture than mesoporous architecture, it is worse with metal oxide charge transport materials (HTM, ETM) than with organic charge transport materials, and it can be reduced by using mixed halide anions (bromide-iodide) [13]. The hysteresis effect shows itself when measuring the current-voltage (I-V) curve in the way that different scan direction and scan rates will result in different I-V curves, and it also depends on which scan (forward or reverse) is

performed first [12]. Figure 3.6 shows the hysteresis effect in a typical perovskite PV cell.

There exists many theories on the physical origins of hysteresis effects in perovskite PV cells including trapping of electron carriers at the perovskite interfaces, ferroelectric effects, ionic displacement, or combinations of several of these at once [12]. Van Reenen and co-workers concluded that the combined effect of the trapping of charge carriers at perovskite interfaces and ion migration through the perovskite was responsible for hysteresis, while Meloni and co-workers concluded that the migration of the halide species was the cause of hysteresis [12]. Possible remedies that have been suggested include achieving large grain sizes in the perovskite film, and passivation and interface engineering to reduce the charge trapping at the perovskite interfaces [13]. Yoon and co-workers managed to construct a perovskite PV cell with a PCE of 19% that did not show hysteresis by using C_{60} as ETM deposited in a room-temperature vacuum process [12]. A better understanding of the mechanisms behind hysteresis in perovskite PV cells is needed in order to eliminate the problem, which would give a more correct characterization of the PV cells and improve long-term stability. Properly standardized characterization techniques is also needed so that different PV cells can be evaluated fairly against each other. This could include measuring with both forward and reverse scanning direction, as well as measuring over time until steady-state is achieved [13]. Christians and co-workers [44] suggested a standard characterization method for perovskite PV cells that included calibration of illumination source, determine steady-state J_{sc} and V_{oc}, recording forward and reverse J-V curves at various scan rates, measuring steady-state photocurrent at several voltages near the maximum power output, and more.

Environmental Concerns

The environmental concerns with perovskite PV cells are mainly related to the presence of the toxic heavy metal lead (Pb). This is also related to the stability of perovskite PV cells, since increased degradation of the devices will increase the chance of Pb leaking into the environment. This means that strict standards for end-of-life disposal and/or recycling will most likely be required if perovskite PV cells are commercialized [13]. However, the presence of Pb might not be as much of a problem as one might think, and at the same time there may be other environmental concerns that are not as clear. To get a better understanding of all environmental concerns related to perovskite PV cells, comprehensive life cycle assessments (LCA) are needed and several researchers have performed a LCA on perovskite PV cells and found important results. For example, toxic organic solvents that are miscible with water are present in the fabrication process and could pose a greater threat than Pb [13]. Furthermore, it has also been found that since the amount of Pb in the PV cells is so small, a leakage would most likely not have any catastrophic effects and proper encapsulation and end-of-life disposal could limit the negative effect of Pb even more [13]. Even so, the presence of Pb is still a major concern to some, so a lot of effort has been put into finding replacements for Pb in perovskite PV cells. As mentioned in section 3.2.2, tin (Sn) is the most common replacement, either pure Sn or mixed with Pb. The main challenge with Sn-based perovskite PV cells is that the PCE is usually well below 10% [13], which is well below the PCE of Pb-based versions. Other metals have also been tried as replacements for Pb, includ-

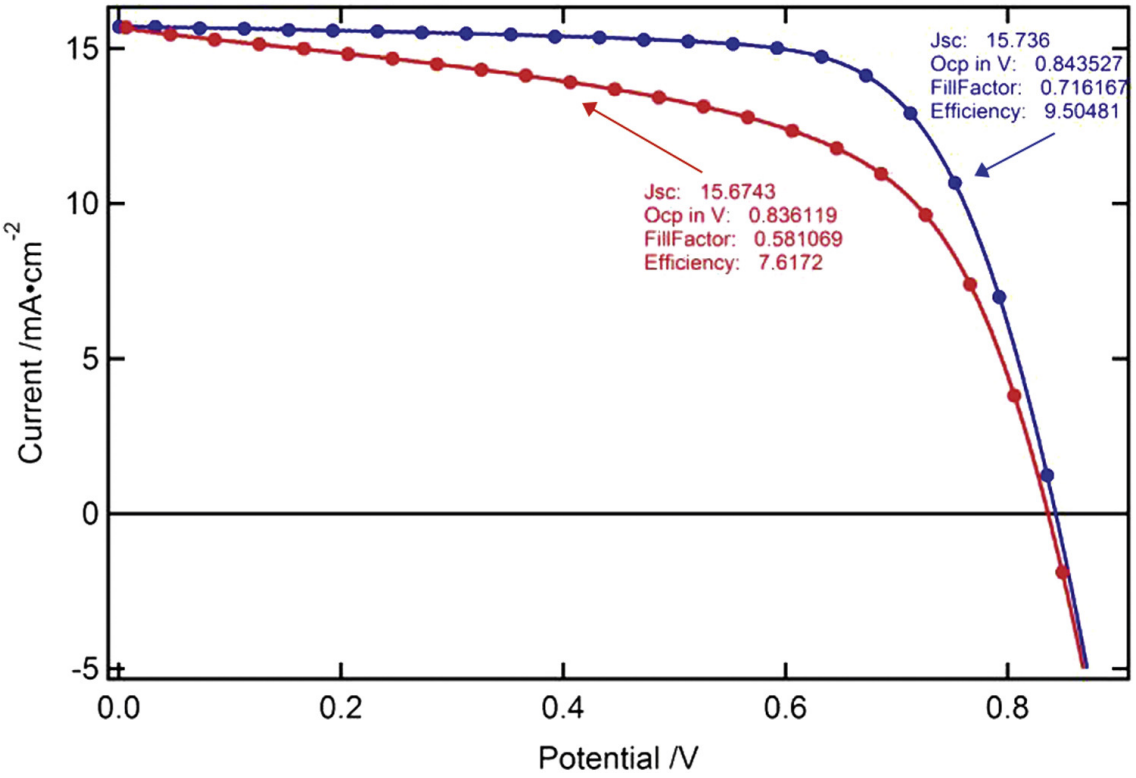

Figure 3.6: *I-V* curve of a standard perovskite PV cell showing hysteresis. The blue dots show the reverse scan and the red dots show the forward scan. Figure taken from [12].

ing caesium (Cs), bismuth (Bi) and copper (Cu), but these attempts have resulted in extremely low PCEs, often below 1% [13]. Ibn-Mohammed and co-workers [45] performed LCAs on two different perovskite PV cells, and their conclusion includes: the environmental impact of Pb is negligible, more research related to the operation phase and end-of-life scenarios is needed since these phases could show a large environmental impact, the use of gold in the cathode gives a large environmental impact and replacing the gold with copper reduces the impact considerably, energy consumption during fabrication could result in large environmental impact, and the lifetime of the perovskite PV cells need to be improved. These conclusions are supported by other assessments, with many focusing on avoiding the use of gold and silver, avoiding the use of toxic solvents during fabrication, extending the lifetime of the devices, reducing energy consumption during fabrication, and implementing sufficient disposal and recycling standards [13]. Regarding the environmental concern that gets the most attention, namely the use of Pb, the effect of this seems to be tolerable based on the performed LCAs, and it is also the only viable choice based on present technology.

Scaling Up to Large Area Devices

If perovskite PV cells are going to be commercialized, techniques for producing large-scale, flexible modules need to be developed further if the production costs are going to be competitive with other PV technologies. The main challenges related to this is uniformity of the perovskite layer, contact resistance of the electrode, and the

suitability of the manufacturing techniques for large area devices [13]. To make full-scale flexible perovskite PV cells with roll-to-roll printing, it must be ensured that all the device layers can be prepared in low-temperature printing processes. It is more challenging to scale up the production of flexible perovskite PV cells than rigid PV cells, and it is more challenging if TiO_2 is used as the ETM compared to an organic material [13]. A possible solution for the challenge of electrode conductivity is to use metal grids, similar to other PV technologies. There is a lot of research related to producing full-scale flexible perovskite PV cells, but still more is needed to reach commercialization. However, the challenges seems to be solvable with continued effort. Thus, it will probably be a question of when the production costs are low enough to make perovskite PV cells economically viable.

Future Possibilities

There are many future possibilities for perovskites, both as PV cells and for other applications. For perovskite PV cells, the possibilities seem almost unlimited *if* the present challenges can be overcome. Thin, lightweight and flexible perovskite PV cells is more and more looking like the most promising of all PV technologies when it comes to building-integrated PV cells (walls, windows, etc.), PV cells on cars and other transport modes, personal electronics, and any other application where light weight and flexibility is vital. Perovskite PV cells can also be tuned to different colors to make them more aesthetically pleasing [46]. With the PCE rising rapidly, perovskite PV cells could also challenge the much heavier and rigid crystalline silicon PV cells for large-scale power applications. Another possibility is to apply a perovskite layer on top of a crystalline silicon PV cell to make a tandem cell, and simulations related to this have shown that a PCE above 30% [13] could be possible. Schneider and co-workers [47] used a perovskite-on-silicon tandem cell to achieve an absolute PCE gain of 2-4%, and they state that this method can result in PV cells with PCEs approaching 35%. It is in tandem cell applications like this that many researchers expect perovskite PV technology to make its first appearance in the commercial market. Applications outside of PV cells that are suggested include photodetectors, image sensors, phototransistors, light emitting devices, batteries, super capacitors, thermoelectric systems, and many more [13]. Thus, it seems very possible that perovskite materials could play a significant role in the future of technology, both in PV technologies and elsewhere.

Chapter 4

Plasmonic PV Cells

This chapter will go through the use of nanoparticles in PV cells, often referred to as plasmonic solar cells or plasmonic PV cells. The main motivation for the use of nanoparticles in PV cells is to increase the PCE by taking advantage of the plasmonic effects that occur due to the integrated nanoparticles. This has been done in numerous ways with various particles in many different PV cells. Section 4.1 will go through the general working principle by describing the plasmonic effects, and section 4.2 will look specifically at the use of nanoparticles in perovskite PV cells, including the research state of the art in this field.

4.1 Working Principle

Nearly 60 years have passed since surface plasmons were first defined [15], but it is during the last 10-12 years that the field of plasmonic PV cells have developed the most, as seen in figure 4.1 where the number of research publications related to this subject during this period is shown.

Surface plasmons are the collective oscillations of free electrons in a conductor/metal at the interface between the conductor and the surrounding dielectric medium [15, 48, 49]. There are two main classes of surface plasmons, namely surface plasmon polaritons (SPP) and localized surface plasmon resonance (LSPR). SPPs are propagating, dispersive electromagnetic waves which are coupled to the free electrons of the conductor, while LSPRs are non-propagating oscillations of the free electrons of the conductor which are coupled to the electromagnetic field [48], and both of these phenomena can exist in plasmonic PV cells. There are three main mechanisms that are utilized in plasmonic PV cells: light scattering, near-field enhancement, and plasmon-induced energy transfer [15, 49]. One mechanism will often dominate for a given PV cell configuration, but there will always be more than just one mechanism at work and this can sometimes make it difficult to interpret experimental results [15]. Four different PV cell configurations are shown in figure 4.2. Configurations a) and c_1) are setups where light scattering will usually dominate [14]. The following sections will give a description of each of the three main plasmonic mechanisms.

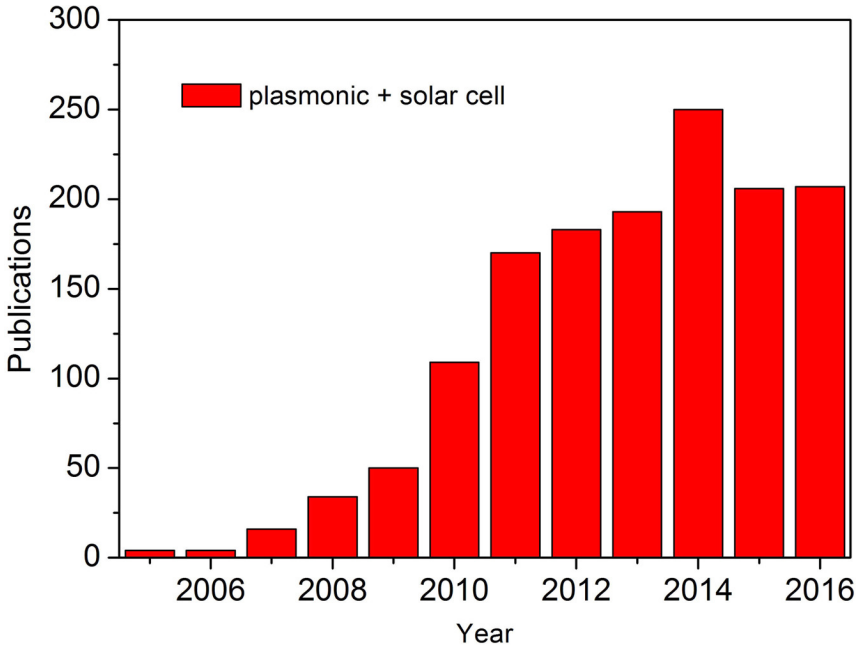

Figure 4.1: Number of scientific publications reported in the Scopus database by searching for "plasmonic solar cells". Figure taken from [14].

4.1.1 Light Scattering

Metal nanoparticles can be used to scatter incident photons, and this can be a quite effective tool to increase the PCE of a PV cell. This light scattering mechanism is often referred to as "light-trapping" or "far-field effect" [15]. If metal nanoparticles are placed at the front surface of a PV cell, they will scatter some of the incident photons and consequently give the photons a longer way to travel through the active layer of the PV cell [15], as shown in figure 4.2 a). Since the photons have to travel a longer distance through the active layer, it increases the probability that each photon will be absorbed by the active layer and consequently contribute to the generation of electricity. If metal nanoparticles are placed at the interface between the active layer and the back metal electrode, they will scatter some of the photons that did not get absorbed by the active layer back through that layer and consequently give the photons another "chance" to get absorbed in the active layer, as shown in figure 4.2 c_1). It is known that metal nanoparticles with relatively smaller sizes will result in the majority of scattering going in the forward direction, while the use of metal nanoparticles with relatively larger sizes will result in the majority of scattering going in the backward direction [15]. Therefore, it makes sense to place relatively small particles at the front of the PV cell and relatively large nanoparticles at the active layer/back contact interface to increase the absorptance and consequently the PCE of the PV cell. The mechanism of light scattering is particularly important for thin film PV technologies since the thickness of the active layer is so small in these PV cells.

When different nanoparticles are evaluated by their transmittance, one has to be aware of the fact that a drop in transmittance can be caused by scattering, but also by absorption. Since photons that are absorbed by the metal nanoparticle does not contribute to the generation of electricity, it is important to make sure that the scattering is as large as possible and the absorption as small as possible. Cath-

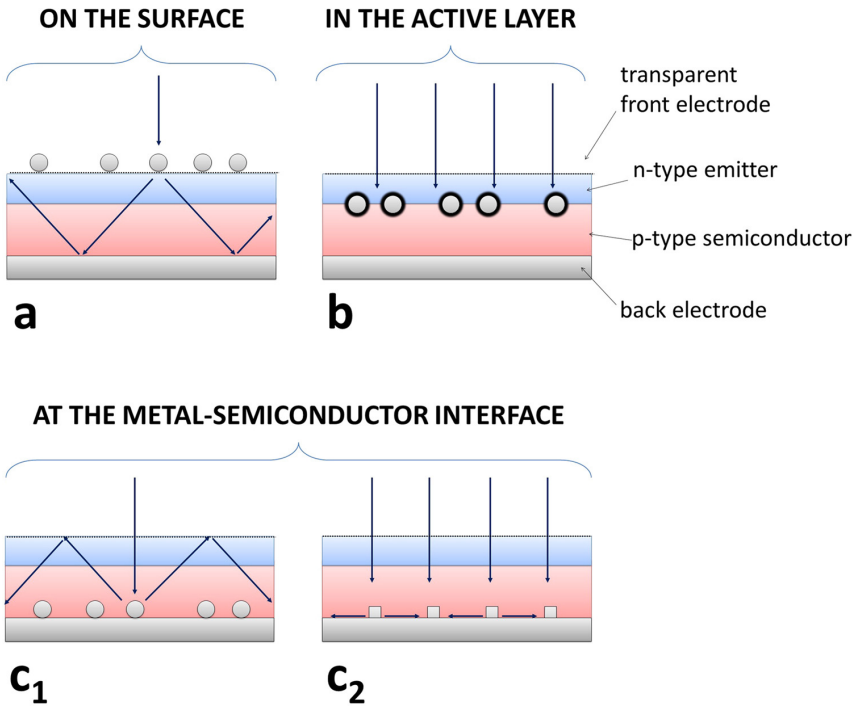

Figure 4.2: Different plasmonic light trapping configurations for thin film PV cells. a) Metal nanoparticles on the surface of the PV cell. b) Metal nanoparticles embedded in the active layer of the PV cell. c_1) Metal nanoparticles at the interface between the metal electrode and the active layer. c_2) Metal arrays at the interface between the metal electrode and the active layer. Figure taken from [14].

pole and co-workers described the basic mechanism of light scattering in plasmonic PV cells in 2008 [49], and they stated that if the diameter of the nanoparticle is well below the wavelength (λ) of the incident light, then the scattering (C_{scat}) and absorption (C_{abs}) cross sections can be calculated by

$$C_{\text{scat}} = \frac{1}{6\pi}\left(\frac{2\pi}{\lambda}\right)^4 |\alpha|^2 \tag{4.1}$$

$$C_{\text{abs}} = \frac{2\pi}{\lambda}\,\text{Im}[\alpha] \tag{4.2}$$

where α is the polarizability of the nanoparticle and it is given by

$$\alpha = 3V\left[\frac{\epsilon_{\text{p}}/\epsilon_{\text{m}} - 1}{\epsilon_{\text{p}}/\epsilon_{\text{m}} + 2}\right] \tag{4.3}$$

where V is the volume of the nanoparticle, ϵ_{p} is the dielectric function of the nanoparticle, and ϵ_{m} is the dielectric function of the surrounding medium. When $\epsilon_{\text{p}} = -2\epsilon_{\text{m}}$, the polarizability of the particle becomes very large, and this is the condition under which the LSPR is induced [49].

4.1.2 Near-Field Enhancement

Near-field enhancement can increase the PCE in a PV cell by increasing the absorptance of the active layer. The near-field is an electromagnetic field that is confined

at the surface of the metal nanoparticle. These fields decay exponentially and only extend a few tens of nanometers from the surface, which means that the active layer of the PV cell needs to be within this distance to utilize the near-field enhancement [15]. Near-fields can arise due to both SPP and LSPR [15, 50].

Near-Field Enhancement by SPP

Collective oscillations of free electrons on a metal film can create a strong, oscillating electric field that propagates along the surface of the metal film as seen in figure 4.3 A), and the resulting propagating electromagnetic waves are the SPP [15]. This near-field extends into both the metal and the surrounding dielectric, and it is the dielectric part that is responsible for the enhanced absorptance. SPP modes can be excited quite efficiently by implementing three-dimensional structures on the metal surface, e.g. grooves, holes or islands [15]. This works due to the mismatch between the SPP momentum and the momentum of light, as shown in figure 4.3 C). In a plasmonic PV cell there will usually be both scattering effects and near-field effects at work simultaneously to increase the absorptance, and to understand these mechanisms it can be useful to perform optical simulations to separate the contributions from scattering and the contributions from near-field from each other [15].

Near-Field Enhancement by LSPR

While SPPs occur on planar surfaces, LSPR only occur at curved or kinked surfaces (e.g. spheres, cubes) of metal nanoparticles [15]. This type of surface plasmons are confined within the nanoparticle and therefore they cannot propagate like SPPs do. They still oscillate though, and the result is a highly energetic near-field at the surface of the nanoparticle, as shown in figure 4.3 B). The LSPR near-field is highly dependent on the size and shape of the nanoparticle and this can make it very complicated to study. A spherical nanoparticle will result in one fundamental LSPR mode, while a cylindrical nanorod will exhibit both transverse and longitudinal modes, where the transverse mode is excited at a shorter wavelength with higher energy. Changing the aspect ratio and cross-sectional symmetry of anisotropic nanoparticles will also greatly affect the LSPR mode. By using a multitude of randomly shaped nanoparticles in the same PV cell, a broadband improvement can be achieved. The near-field can also be amplified greatly by placing two nanoparticles close together to generate a hot spot in between them, and the intensity of the field can be regulated by adjusting the gap between the two particles [15].

4.1.3 Plasmon-Induced Energy Transfer

Energy can also be transferred from an excited plasmon to a semiconductor in a PV cell in a non-radiative manner, either in the form of energetic hot charge carriers or as resonant energy from the oscillations and dephasing of the plasmons [15].

Hot Carrier Generation and Transfer

Electrons in metal nanostructures can be excited to a higher energy level by intense near-fields and thereby create hot charge carriers, often just referred to as hot carri-

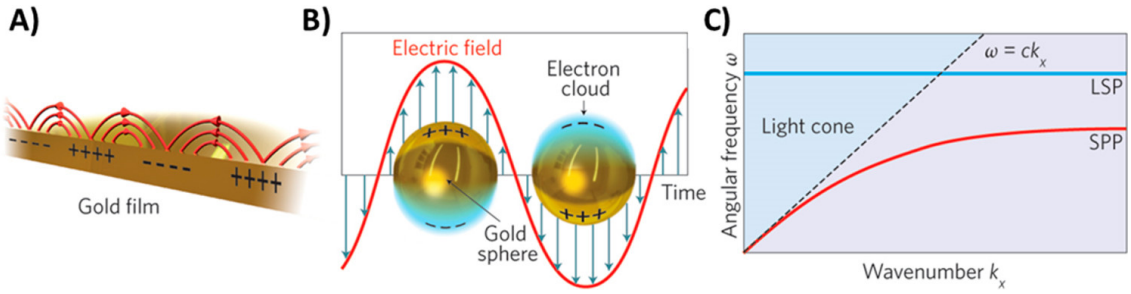

Figure 4.3: A) SPP near-field on a gold film. B) LSPR near-field on gold spheres. C) The dispersion plot of LSPR (LSP) and SPP together with light. Figure is taken from [15].

ers. This can happen either via intraband transitions (within the conduction band) or interband transitions (from d-band to sp-band). It has been observed that this is much more likely to happen in a hot spot between two nanoparticles [15]. When there is a connection between the metal and a semiconductor, the hot carriers can be injected directly into the conduction band edge of the semiconductor. This direct electron transfer can take place together with near-field enhancement. Hot electron generation is a topic of research in the Bergen Nanophysics group [51].

Resonant Energy Transfer

Plasmonic resonant energy transfer (PRET) in a PV cell takes place when a plasmonic nanostructure acts as a donor and transfers resonant energy to the active layer, which acts as the acceptor. This is in effect a transferred LSPR dipole, which in turn will create electron-hole pairs inside the active layer of the PV cell. The conditions for PRET to take place is that the active layer is located within the field of the plasmonic nanostructure and that their absorption spectrums overlap. The main advantage of this mechanism is that it can utilize photons with energy below the band gap of the active layer to create electron-hole pairs. However, there is very little proof and analysis of this mechanism in PV cells so far [15].

4.2 Plasmonic Perovskite PV Cells

Various nanoparticles have been utilized to achieve plasmonic effects in perovskite PV cells and achieve an increase in the PCE. Many different experiments and/or simulations have been performed by researchers in all parts of the world, and the general trend is that the use of nanoparticles usually show an increase in total absorptance for the PV cell, J_{sc}, PCE, or all of them [15]. The working principle behind the plasmonic effect in perovskite PV cells is the same as it is for all PV cells as described in section 4.1, but the effects are often particularly positive in thin film PV technologies like perovskite PV cells. It has been shown that the radiative decay of excitons can be increased by highly polarizable nanoparticles with a silver (Ag) core and TiO_2 shell, and this radiation can then be absorbed by the perovskite layer to increase the PCE [15]. These kinds of core-shell particles are usually written as "core material@shell material" in research publications, making the example just mentioned a Ag@TiO_2 nanoparticle. This convention will be used for all core-shell nanoparticles throughout the remainder of this thesis. It has also

been shown that placing a thin TiO_x-Au-TiO_x layer below the perovskite layer can significantly improve the charge extraction properties of the TiO_x layer through plasmon-induced hot carrier injection from the Au nanoparticles to TiO_x [15]. The presence of Au nanoparticles has also been shown to increase the absorptance in computer simulations [18, 19], and Au-embedded TiO_2 nanofibers has been used to enable plasmon-enhanced charge generation. The latter showed significant control over the optical field, improved absorptance, reduction in charge recombination in Au@TiO_2 nanofiber electrodes, as well as increased current density. This was due not only to light scattering and near-field enhancement by LSPR, but also to LSPR-induced direct transfer of hot electrons from the nanostructures to the conduction band of TiO_2, resulting in a photocurrent density of 21.63 mA/cm^2 and a PCE of 14.92% [15, 21]. Other researchers have shown increased broadband absorptance and efficient photon-generated charge transfer through the use of Au-Ag alloy popcorn-shaped nanoparticles [52], and increased J_{sc} and a 11.4% increase in PCE through the use of Au@SiO_2 nanoparticles [53]. Shalan and co-workers [54] used Au nanoislands at the interface between the perovskite layer and the ETM on an inverted perovskite PV cell and achieved a doubling in PCE compared to the PV cell without nanoislands, although the PCE was still a modest 5.1%. Carretero-Palacios and co-workers [19] achieved a 10% absorptance enhancement in 200 nm perovskite films and a 6% absorptance enhancement in 300 nm films by using Au nanospheres, and by using two nanospheres close together they achieved a 12% absorptance enhancement. They also showed enhanced absorptance with the use of Ag and aluminum (Al) nanospheres, Au@SiO_2 and Ag@SiO_2 core-shell nanospheres and nanorods, Au nanostars, as well as Ag nanocubes [18]. Tavakoli and co-workers [55] used a nanocone array antireflection film attached to the glass surface to increase the PCE of a perovskite PV cell from 12.06 to 13.14%, and it also showed excellent flexibility and superhydrophobicity. Xie and co-workers [56] simulated nanotextures in the form of an array of indentations shaped like cones or cylinders in perovskite PV cells and reported a 42-84% increase in PCE for the cylinder shape and a 52-63% increase for the cone shape. Yue and co-workers [24] simulated the effect of an array of closely spaced Ag nanospheres in a perovskite PV cell and reported a 58.2% increase in absorptance in the infrared region. Cai and co-workers [23] also simulated the effect of Ag nanospheres, as well as "lumpy" Ag nanospheres, on perovskite PV cells and found that the photocurrent increased. Nourolahi and co-workers [57] experimented with Ag nanospheres in a HTM-free mesoporous perovskite PV cell and reported a 30% enhancement in PCE. Kim and co-workers [58] constructed semi-transparent perovskite PV cells with Ag nanocubes and reported a 28% increase in the visual transparency index and a 6% increase in PCE. Mohebpour and co-workers [59] simulated the effect of platinum (Pt) nanospheres, nanocubes and nanopyramids on mixed halide perovskite PV cells and found that the current density can be enhanced as much as 22%. Yu and co-workers [60] constructed a mesoporous perovskite PV cell with a collaborative scaffold of Ag@SiO_2 nanowires and orchid-like TiO_2 nanowires and they reported a PCE of 15.09%, which was a 24% increase compared to a version with only TiO_2 nanowires. Fu and co-workers [61] constructed several perovskite PV cells with Au@Ag nanocuboids and reported a 20-60% enhancement in photon-to-electron conversion efficiency (IPCE) in the range 550-750 nm, a PCE enhancement of 20.8%, average PCE of 17.83% and peak PCE of 18.31%. Tang and co-workers [22] constructed $CH_3NH_3PbI_3$ perovskite PV

cells with Au@SiO_2 core-shell nanorods and managed to increase the maximum external quantum efficiency (EQE) by 16.1% and the maximum J_{sc} by 13.5%. This is a selection of the available research on plasmonic perovskite PV cells, summarized in table 4.1. More exists and more is likely to come in the near future since this is a very popular research field in many countries. The general trend that can be seen in the abovementioned research results is that the inclusion of metal nanoparticles of various shapes and materials will in many cases improve the characteristics of perovskite PV cells. This can be seen in enhanced absorptance, J_{sc}, IPCE, EQE, and consequently enhanced PCE.

Researchers	Nanoparticle	Effect
Mali et al. [21]	TiO_2 nanofibers with embedded Au nanoparticles	Improved absorptance, reduced charge recombination, increased current density
Lu et al. [52]	Au-Ag alloy shaped like popcorn	Increased absorptance
Zhang et al. [53]	Au@SiO_2 nanospheres	11.4% increase in PCE, increased J_{sc}
Shalan et al. [54]	Au nanoislands at perovskite/ETM interface on inverted PV cell	Doubling of PCE relative to PV cell without nanoislands
Carretero-Palacios et al. [19]	Au nanospheres	10% absorptance enhancement in 200 nm perovskite film, 6% absorptance enhancement in 300 nm perovskite film
Carretero-Palacios et al. [19]	Two and two Au nanospheres with small gap in between	12% absorptance enhancement
Carretero-Palacios et al. [18]	Ag nanospheres, Al nanospheres, Au@SiO_2 nanospheres and nanorods, Ag@SiO_2 nanospheres and nanorods, Au nanostars, Ag nanocubes	Increased absorptance in all cases
Tavakoli et al. [55]	Polydimethylsiloxan nanocone array	PCE increased from 12.06% to 13.14%
Xie et al. [56]	Array of nanoscale indentations in the $CH_3NH_3PbI_3$ surface	42-84% increase in PCE for cylinder-shaped indentation and 52-63% increase for cone-shaped
Yue et al. [24]	Ag nanospheres	58.2% increased absorptance in the infrared region
Cai et al. [23]	Ag nanospheres, both smooth and lumpy	Increased photocurrent
Nourolahi et al. [57]	Ag nanospheres	30% increase in PCE
Kim et al. [58]	Ag nanocubes	28% increase in visual transparency index, 6% increase in PCE
Mohebpour et al. [59]	Pt nanospheres, nanocubes and nanopyramids	Up to 22% increase in current density
Yu et al. [60]	Ag@SiO_2 nanowires	24% increase in PCE
Fu et al. [61]	Au@Ag nanocuboids	20-60% increase in IPCE in the range 550-750 nm, 20.8% increase in PCE
Tang et al. [22]	Au@SiO_2 nanorods	16.1% increase in EQE, 13.5% increase in J_{sc}

Table 4.1: Summary of published research articles investigating the effect of nanoparticles in perovskite PV cells. All percentage increases are relative to the same PV cell without the given nanoparticles.

Chapter 5

Computer Simulation Model

This chapter will describe the computer model used to perform the simulations in this thesis. The software used in these simulations is Lumerical FDTD Solutions [16] and section 5.1 will describe the physics behind this software package, followed by a description of the simulation settings used for the work in this thesis in section 5.2.

5.1 Lumerical FDTD Solutions

All simulations in this thesis were done using the Lumerical FDTD Solutions software package, release 2017b, version 8.18.1332. This software solves Maxwell's equations in the time domain by using the finite-difference time-domain (FDTD) method [16]. The equations are solved numerically on a discrete grid in both space and time and the derivatives are handled with finite differences. The results are highly accurate due to the fact that the software does not make any approximations or assumptions about the system it is simulating, and it solves for all vector components of the electric and magnetic fields.

Maxwell's equations are four partial differential equations that form much of the foundation for classical electromagnetism, classical optics and electric circuits. Since PV cell materials obviously are made of matter, Maxwell's equations in matter are used in the simulations. The first equation is called Gauss's law and it gives the divergence of the electric displacement field in a volume according to

$$\vec{\nabla} \cdot \vec{D} = \rho \tag{5.1}$$

where ρ is the free charge density inside the volume and the electric displacement field $\vec{D}$ is given by

$$\vec{D} = \epsilon_0 \vec{E} + \vec{P} \tag{5.2}$$

where ϵ_0 is the permittivity of free space, $\vec{E}$ is the electric field and $\vec{P}$ is the polarization [62]. Gauss's law for magnetism is the second equation and it tells us that the divergence of the magnetic flux density $\vec{B}$ is equal to zero according to

$$\vec{\nabla} \cdot \vec{B} = 0 \tag{5.3}$$

Faraday's law is the third equation and the essence of this equation is that a changing magnetic flux density induces an electric field [62] according to

$$\vec{\nabla} \times \vec{E} = -\frac{\partial \vec{B}}{\partial t} \tag{5.4}$$

Ampere's law is the fourth and final of Maxwell's equations and it is given by

$$\vec{\nabla} \times \vec{H} = \vec{J} + \frac{\partial \vec{D}}{\partial t} \tag{5.5}$$

where $\vec{J}$ is the free current density and $\vec{H}$ is given by

$$\vec{H} = \frac{1}{\mu_0}\vec{B} - \vec{M} \tag{5.6}$$

where μ_0 is the permeability of free space and $\vec{M}$ is the magnetization [62].

In Lumerical FDTD Solutions, the electric and magnetic field components are distributed in space over a unit cell called the Yee cell, as shown in figure 5.1. The simulation space is divided into many Yee cells, and the more cells used in a given simulation space, the more accurate the results of that simulation will be [16]. Both the electric and magnetic fields are typically zero at the start of each simulation, and the software starts the simulation at time zero with the electric field given by

$$\vec{E}^{-\frac{1}{2}} = 0 \tag{5.7}$$

and the magnetic field given by

$$\vec{H}^0 = 0 \tag{5.8}$$

Lumerical then proceeds to calculate the electric field at time (n+1/2), where n is the time step. This electric field is a function of the electric field at the previous time step plus a term that is proportional to the curl of the magnetic field at time n [16], as given by

$$\vec{E}^{n+\frac{1}{2}} = \vec{E}^{n-\frac{1}{2}} + \frac{\Delta t}{\epsilon}\vec{\nabla} \times \vec{H}^n \tag{5.9}$$

where Δt is the length of the time interval and ϵ is the permittivity of the material. Once the electric field is updated, Lumerical proceeds to calculate the magnetic field at time (n+1). This is a function of the magnetic field at the previous time step minus a term that is proportional to the curl of the electric field at time (n+1/2) [16], as given by

$$\vec{H}^{n+1} = \vec{H}^n - \frac{\Delta t}{\mu}\vec{\nabla} \times \vec{E}^{n+\frac{1}{2}} \tag{5.10}$$

where μ is the permeability of the material. Lumerical can then continue this process and calculate the electric field and magnetic field at each time step by using the value from the previous time step in the manner

$$\vec{H}^0 \rightarrow \vec{E}^{\frac{1}{2}} \rightarrow \vec{H}^1 \rightarrow \vec{E}^{\frac{3}{2}} \rightarrow \vec{H}^2 \rightarrow \vec{E}^{\frac{5}{2}} \rightarrow \vec{H}^3 \rightarrow ... \tag{5.11}$$

Lumerical will continue this process for as long as the simulation requires it before it stops to finish the simulation. At the stopping point, the value of the electric field will be interpolated to the final time step. This is due to the fact that the electric field is always offset from the magnetic field by one half time step [16], as seen in equations 5.7-5.11.

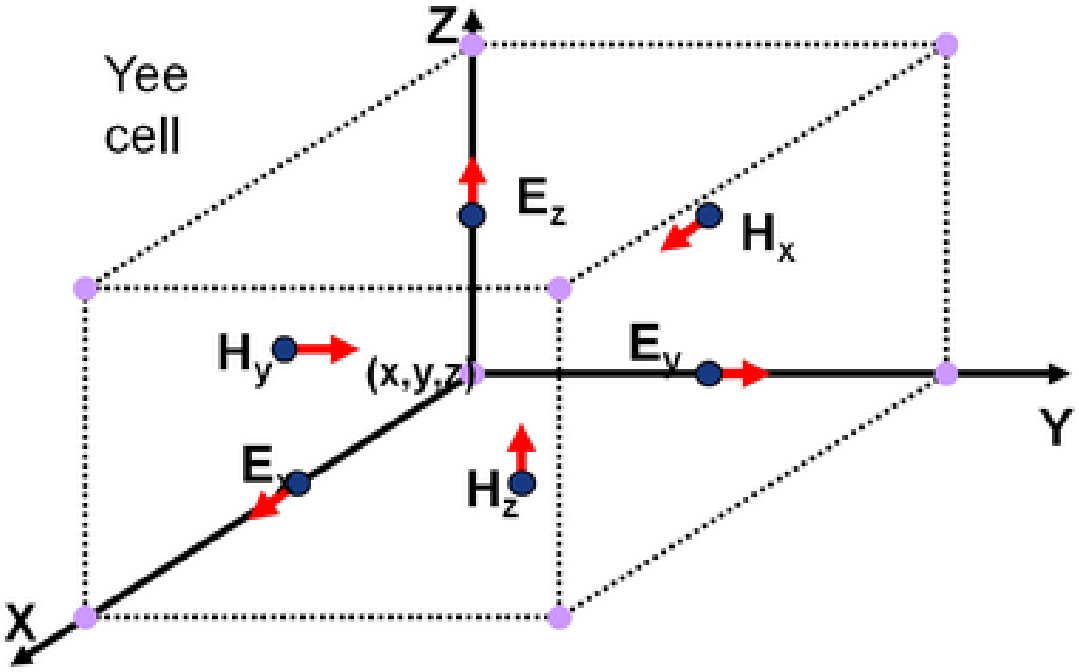

Figure 5.1: The Yee cell with the different components of the electric and magnetic fields. The simulation space in Lumerical is divided into numerous Yee cells. Figure taken from [16].

5.2 Simulation Settings

There is a multitude of possible simulation settings in Lumerical FDTD Solutions and it is vital to optimize these settings to get the most realistic and accurate results from the simulations. This section will go through the simulation settings and structural setup used in this thesis, as well as the reasons for using them.

The first thing that was needed for the simulations in this thesis was to import material data for the PV cell materials that were going to be used in the simulations. The Lumerical software package has a list of materials in the default materials database and this list included all the necessary materials for the nanostructures (Au, Ag, Al, Pt, SiO_2). Some of these materials have several different versions, and the version that is the best fit for each given simulation must be chosen. In some cases, the settings also need to be altered to make the material fit better. The versions used in this thesis was: "Au (Gold) - Johnson and Christy" (standard), "Ag (Silver) - Palik (0-2 μm)" (with max coefficients set to 5), "Al (Aluminum) - Palik" (standard), "Pt (Platinum) - Palik" (standard), and "SiO_2 (Glass) - Palik" (with fit tolerance set to 0, max coefficients set to 2, and imaginary weight set to 0). The "max coefficients" and "fit tolerance" are settings that can be adjusted up and down to visually check that the complex refractive index of the material model for the chosen material fits well with the experimental data for the same material in the chosen wavelength. The "imaginary weight" set to 0 tells Lumerical to ignore the imaginary part of the complex refractive index, and this can be done in cases where the imaginary part is close to 0 throughout the chosen wavelength interval and where the material model does not agree with this.

The material choices mentioned above resulted in good fits for the simulations in this thesis. However, the Lumerical materials database did not include any of the materials needed for the various perovskite PV cell layers (see section 3.2). Therefore, it was necessary to import data for these materials from published research articles. This can be done in several ways, but one of the most accurate methods is to import a dataset that gives values for the complex refractive index (both real and imaginary part) of the material versus the wavelength of incident light. The wavelength interval of the dataset must include the wavelength interval that will be used in the simulations. The most common wavelength interval for PV cell simulations is approximately 300-900 nm, because this is the interval that generates most of the electricity output from the PV cells. Therefore, this interval will be used in the simulations in this thesis.

The perovskite material chosen for the simulations was methylammonium lead iodide ($CH_3NH_3PbI_3$), simply because it is the most common perovskite material in PV cells at the current time. The experimental work by Löper and co-workers [17] were chosen as the source for the perovskite layer. They have used spectroscopic ellipsometry and spectrophotometry to determine the complex refractive index of $CH_3NH_3PbI_3$ across the wavelength interval 300-2000 nm, which includes the interval used in the simulations in this thesis.

The most common materials were also chosen for the HTM and ETM, namely spiro-OMeTAD for the HTM and TiO_2 for the ETM. The experimental work by Ball and co-workers [41] was chosen as the source for these materials. They give the complex refractive index of both materials across a wavelength interval of 300-900 nm, which matches exactly the interval used in the simulations in this thesis. The data for the complex refractive index of the various materials in the FTO layer were also imported from the same article, but ultimately these were not used in the simulations in this thesis. The reason for this is due to limited computing capacity on the laptop computer used for the work in this thesis. A typical complete perovskite PV cell includes a glass cover with a thickness of 2 mm [41], which is very thick compared to the other layers which usually have a thickness of maximum 500 nm. So by including the glass cover in the simulations, the simulation time became enormous for each simulation, making it impossible to include a 2 mm glass cover in the simulations. A method of letting the simulation region end within the glass to simulate a semi-infinite glass cover was attempted, but this also gave a simulation time of several hours for each simulation and the results did not look realistic. A decision was therefore made to simplify the PV structure, so that the simulation time would be manageable and the results as realistic as possible. Since the objective of this thesis is to investigate the effect of nanoparticles on the optical absorptance of the PV cell, it was decided to only include the layers closest to the nanoparticles. The nanoparticles are placed either within the perovskite layer, or at the interfaces between the perovskite layer and the HTM or ETM. Therefore, the simulation structure (not including nanoparticles) will only include the perovskite layer (middle), spiro-OMeTAD as HTM (bottom) and TiO_2 as ETM (top), as seen in figure 5.2. This is also the type of simplified structure used in the simulations by Carretero-Palacios and co-workers [19]. Since the generation of charge carriers takes place in the perovskite layer, this simplified structure still contains the most vital regions for absorptance. A minor drawback with not having all the layers of a complete PV cell is that the actual PCE of the PV cell cannot be calculated,

since this would also be affected by the presence of the other layers. However, the simulations still make it possible to calculate the absorptance in the simulated structure and compare the absorptance of the structure *without* nanoparticles to the structure *with* various nanoparticles present. Consequently, the relative change in absorptance between the various simulations can be studied, and this will give a strong indication of the change in actual PCE of a complete PV cell. This can be seen in the formula for the ultimate efficiency η of a PV cell [63, 64, 65] (equation 5.12), where it is obvious that an increase in the absorptance $A(\lambda)$ will result in an increase in efficiency if the other variables remain constant.

$$\eta = \frac{\int_0^{\lambda_g} I(\lambda)A(\lambda)\frac{\lambda}{\lambda_g}d\lambda}{\int_0^{\infty} I(\lambda)d\lambda} \tag{5.12}$$

where $I(\lambda)$ is the solar intensity per wavelength interval, λ is the wavelength and λ_g is the wavelength corresponding to the band gap of the PV cell. Consequently, if the PV cell is exposed to the same illumination and the band gap remains constant, an increased absorptance will result in an increase in the ultimate efficiency. However, it is important to be aware of the fact that equation 5.12 gives the *ultimate* efficiency, i.e. the maximum efficiency that is possible to achieve with the given solar irradiance, material band gap and absorptance. A real PV cell will not be able to achieve a PCE that is as high as this ultimate efficiency, due to various losses. One of the losses that is most relevant to the work in this thesis is the loss that is caused by photons being absorbed by the metal nanoparticle instead of the perovskite material. Since only photons absorbed by the perovskite material generate electricity, all photons absorbed by the metal nanoparticle that is integrated in the perovskite material will constitute a loss and consequent decrease in the actual PCE of the PV cell. Therefore, the absorptance of the integrated nanoparticles should be as low as possible, since the absorptance of these particles will "steal" a part of the total absorptance of the PV cell used in equation 5.12 and consequently lower the actual PCE of the PV cell compared to the ultimate efficiency of the same PV cell. This issue is also mentioned in chapter 4.1.1, which discusses light scattering. Similarly, photons absorbed by the ETM or HTM would also "steal" a part of the total absorptance of the PV cell and lower the actual PCE. In this thesis, it is the total absorptance of the whole PV cell structure that is simulated. It will not be investigated how much of this total absorptance belongs to the perovskite material and how much of it belongs to the metal nanoparticles, ETM and HTM. Therefore, as future work it would be very interesting to perform simulations and experiments to find out how much of the total absorptance is in the perovskite layer and how much is lost to the metal nanoparticles, ETM and HTM. An important part of an optimization process would be to find ways to minimize the absorptance of the metal nanoparticles, ETM and HTM without decreasing the total absorptance, so that the actual PCE of the PV cell can get as close to the ultimate efficiency as possible. Nevertheless, if the simulation results in this thesis show that the total absorptance increases, it is likely that the actual PCE of the PV cell would also increase. Some of the increase in total absorptance is most likely lost to absorptance in the integrated metal nanoparticle, but some of the increase will also be in the perovskite material, e.g. due to scattering from the metal nanoparticle (chapter 4.1.1). Therefore, it is highly likely that increased total absorptance also mean increased actual PCE, but further simulations and/or experiments would be necessary to quantify the increase

in PCE.

With all the materials imported, the simulation can be set up. As shown in figure 5.2, the perovskite layer is placed in the middle, with the TiO_2 directly above and spiro-OMeTAD directly below. A simulation region must then be chosen. This is the orange box seen in figure 5.2 and everything inside this box is included in the simulation. There are numerous options that must be chosen for the simulation region. A three-dimensional region was chosen to give realistic results, along with a standard simulation temperature of 300 K.

The span of the simulation region in the x and y directions were chosen to be 300 nm. The layers of the PV cell extends all the way through the boundaries of the simulation region in the x and y directions, and the boundaries in these directions are periodic. This means that the software simulates a semi-infinite extension of the structure in a periodic fashion in the x and y directions. So as an example: if a gold cube with a side distance of 100 nm is placed in the middle of the perovskite layer, the distances from the cube to the x and y boundaries are 100 nm, and that means that Lumerical will simulate a semi-infinite PV cell with gold cubes in the x and y directions where the distance between each cube is 200 nm. So larger particles will result in a shorter distance to the x and y boundaries, and consequently a shorter distance between each particle. Since the maximum span in the x and y directions for the particles in this thesis is chosen to be 250 nm (most are much smaller), 300 nm will be sufficient for the span in the x and y directions for the simulation region. As mentioned, the x and y boundaries are periodic, but the actual settings are anti-symmetric in the x direction and symmetric in the y direction. This is done to take advantage of the symmetry in the simulated structures. By using these boundary settings, Lumerical will only use 1/4 of the simulation region when the simulation is run. The region with positive x and y axes is used in the simulation, and then Lumerical expands the results from this region to give the results for the whole simulation region [16]. This drastically reduces the simulation time and gives the exact same results, as long as the structure has the required symmetry. Test simulations were performed both with and without this setting for the various structure types, and all tests confirmed that the results were the same with and without the setting activated. The simulation time saved by using these boundary conditions can then be used to increase the accuracy in other settings if desired.

The boundaries in the z direction is chosen to be the perfectly matched layer (PML) absorbing boundaries. These boundaries are the most common type to use in simulations, and they attempt to absorb all incident fields without creating any back reflection. To get higher accuracy results with fields from all angles, the stretched coordinate PML type with the steep angle profile is chosen. The rule of thumb with PML boundaries is that the simulation space must consist of the same material for a specific distance from the PML boundary, and this distance is given by the maximum wavelength used in the simulation, divided by two [16]. This is because the PML boundaries can reflect evanescent fields, so the distance from the structure to the boundaries must be large enough so that the structure does not interact with the evanescent fields [16, 66]. Therefore, since the maximum wavelength used in this thesis is 900 nm, there should be a distance of 450 nm from the top and bottom of the simulation structure and out to the PML boundaries (z direction). By basing the setup on the simulations with the thickest PV structure, the simulation region must extend 1000 nm in the negative z direction and 780 nm

in the positive z direction.

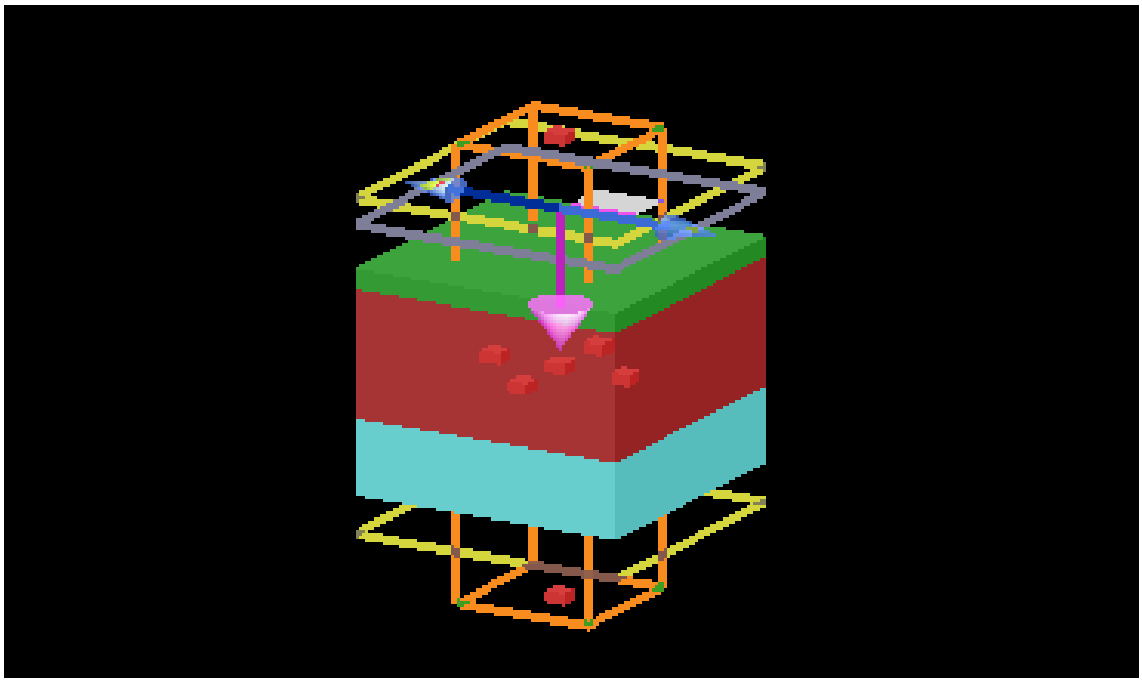

Figure 5.2: The basic structure used in the simulations in this thesis. The red layer is perovskite (active layer), the green layer is TiO_2 (ETM) and the blue layer is spiro-OMeTAD (HTM). The purple arrow indicates the direction of the incident light, which is perpendicular to the surface of the structure. Everything inside the orange box is the simulation region, the yellow square at the top is a monitor that records reflectance and the yellow square at the bottom is a monitor that records transmittance.

The mesh type is set to the standard auto non-uniform with mesh accuracy 5, which gives high accuracy. It is possible to increase the mesh accuracy up to 8 to get even higher accuracy, but this increases the simulation time drastically. However, in many cases this is not necessary, and test simulations performed with higher mesh accuracy than 5 gave almost identical results. Therefore, a mesh accuracy of 5 is deemed sufficient for this thesis.

The plane wave source was chosen as the light source, since this is the most common light source in PV cell simulations. The plane wave type is bloch/periodic, the injection axis is set to the z axis and the direction is set to backwards. This means that the light will propagate along the z axis in the negative direction, as shown by the purple arrow in figure 5.2. The light source must be set to extend at least as far as the simulation region in the x and y directions, and it is placed at 500 nm along the positive z axis so that the light wave starts above the PV structure. The wavelength interval is set to 300-900 nm. The number of measuring points on this interval must also be selected. In this thesis, it was chosen to have one measurement/datapoint for every nm in the wavelength interval length. Since this length is 600 nm in this case, a total of 601 datapoints was chosen. This can be set by accessing global properties under the monitors banner, and then entering the desired number in the frequency points box.

The absorptance is usually calculated by using the fact that all incident

light is either absorbed, reflected or transmitted. Consequently, the absorbed part $A(\lambda)$ can be found by subtracting the reflected part $R(\lambda)$ and the transmitted part $T(\lambda)$ from the total incident light (which is set to 1) [19], according to

$$A(\lambda) = 1 - R(\lambda) - T(\lambda) \tag{5.13}$$

This means that two monitors are needed to get the desired data from the simulations, one for reflectance and one for transmittance. The frequency-domain field and power monitor is used in both cases because these are best suited for these measurements. This monitor is basically a screen that measures the amount of light that crosses it. That means that the monitor that is going to measure reflectance must be placed above the light source, so that the only light that crosses this monitor is light that is reflected back by the PV structure. Using the same logic, the transmittance monitor must be placed below the PV structure, so that the only light that crosses this monitor is light that has been transmitted through the PV structure. Consequently, by subtracting these two amounts from 1, only the fraction of light that is neither reflected nor transmitted remains, namely the absorptance. The monitor type is set to 2D Z-normal, which means that the measuring screen is normal to the z axis. Just like the light source, the span in the x and y directions needs to be set so that the monitor extends at least as far as the simulation region. The reflectance monitor is placed at 600 nm along the positive z axis, and the transmittance monitor is placed at 700 nm along the negative z axis. The data to record is set to only output power. This is the only quantity needed for reflectance and transmittance, and the simulation time is reduced by un-checking the electric and magnetic field components. The other monitor options are left in their standard settings. The yellow square at the top of figure 5.2 is the reflectance monitor and the yellow square at the bottom of figure 5.2 is the transmittance monitor.

To include nanoparticles in the simulations, the desired particle shape is placed at the desired location within the PV structure. The dimensions and the material for the nanoparticle must be set. It is also important to check the material explorer before simulations to make sure that the data for the chosen material is good for the chosen wavelength interval. When placing an object within another object, it is important to use the override mesh order option and assign the correct mesh order to each object. Higher mesh order gives higher priority. So if a gold sphere is placed inside the PV structure, the gold sphere must have a higher mesh order than the perovskite. Otherwise the gold sphere will just disappear inside the perovskite. Similarly, if a core-shell particle is placed inside the perovskite, the core must have the highest mesh order, the shell must have the second highest, and the perovskite must have the lowest.

Finally, a simulation mesh should be added when nanoparticles are included in the simulation. The simulation mesh is a region where the mesh dimensions can be decreased to give higher accuracy results. This is highly recommended to use when structures with curves or sharp corners are included in the simulation. This is most easily done by choosing the geometry to be based on a structure and then enter the name of the structure that the mesh should surround. A buffer region around the structure can also be set, and a buffer of 10% of the diameter (or side length) of the nanostructure was chosen in this thesis to increase the accuracy of the results. The mesh dimensions in the x, y and z directions must be set manually. Smaller dimensions give more accurate results, but smaller dimensions also drastically in-

crease the simulation time. The dimensions chosen for all simulations in this thesis is 2.5 nm in all directions. This gives high accuracy results with a tolerable simulation time for the simulations in this thesis. Test simulations with smaller mesh dimensions were also performed, giving almost exactly the same results while the simulation time was drastically increased. Therefore, the chosen mesh dimensions should be sufficient for the simulations in this thesis. The simulation settings are summarized in table 5.1.

When the simulation has been set up correctly and the material fits have been checked, the simulation can be performed. Once it is complete, the resulting reflectance and transmittance data can be accessed. These can be plotted directly in Lumerical, but the data can also be exported to MATLAB [25] to create more advanced plots. The method used in this thesis is to do all the simulations in Lumerical, export the datasets to MATLAB to create plots, and export the datasets to a spreadsheet in Microsoft Excel [26] to calculate the total reflectance, transmittance and absorptance. This method is described in more detail in Appendix A.

Layers included	Perovskite, ETM and HTM
Simulation region span	x=y=300 nm, z=1780 nm
Simulation temperature	300 K
x boundary	Anti-symmetric
y boundary	Symmetric
z boundary	PML, stretched coordinate type with steep angle profile
Mesh accuracy	5
Light source	Plane wave, bloch/periodic type, injection axis is z, backwards direction
Light source location	z=500 nm
Wavelength interval	300-900 nm
Monitors for reflectance and transmittance	Frequency-domain field and power, 2D Z-normal, record only output power
Reflectance monitor location	z=600 nm
Transmittance monitor location	z=-700 nm
Mesh override region	Based on nanoparticle structure + 10% of particle diameter as buffer
Mesh override dimensions	dx=dy=dz=2.5 nm

Table 5.1: Summary of simulation settings used in Lumerical FDTD Solutions.

Chapter 6

Simulation Results

This chapter will go through the main work of this thesis, namely the computer simulations that were performed to find the effect of various nanoparticles on the optical absorptance of perovskite PV cells. Section 6.1 will compare the simulation model used in this thesis with existing work published in scientific literature. The subsequent sections will go through the results of the various simulations in this thesis. The total number of simulations is 391, not counting the various test simulations that were performed to fine-tune the simulation settings to get the best possible results and the simulations that were performed to compare the simulation model with existing work. Section 6.2 will go through the simulations of the perovskite, spiro-OMeTAD and TiO_2 PV structure *without* any nanoparticles, and the subsequent sections will each go through the PV structure with one nanostructure and material type (e.g. gold spheres) included within the PV structure. Wavelength in these simulations refer to the wavelength of the incident light.

6.1 Comparison with Existing Work

A significant amount of research articles focused on plasmonic perovskite PV cells have been published in the last few years, as summarized in section 4.2. This section will describe a few simulations that were performed to compare the simulation model used in this thesis to the results from existing work. However, there is a multitude of different materials and architectures used in perovskite PV cell research, and any variation in material properties and PV cell architecture will affect the final result. This means that even if the setup in two different simulations/experiments is the same, the results will most likely be different if the materials or PV cell architecture is different. The shareware Datathief [28] was used to extract data from the plots in published articles.

The first comparison is the one where the best result fit is expected. As described in section 5.2, the material data for the chosen perovskite material in this thesis was imported from the article by Löper and co-workers [17]. This dataset listed several values for the complex refractive index of the perovskite material in the range 300-2000 nm. A simulation was performed for this wavelength range to test that the material data import was successful. Löper and co-workers used a perovskite film with a thickness of 305.68 nm deposited on a glass substrate. They measured the reflectance and transmittance of this structure experimentally, and they used the Forouhi-Bloomer formulation to calculate the reflectance and transmittance [17].

Both the experimental and the calculated results are shown in figure 6.1b. The same setup with the perovskite film deposited on a glass substrate was simulated in this thesis using Lumerical FDTD Solutions. Datathief were not able to extract the data from the plot in figure 6.1b (due to the circles being mixed with the lines), so the result from the simulation in this thesis is shown in figure 6.1a. However, even if the results are not in the same plot, it is quite clear to the naked eye that the result fit is very good. Both the reflectance and the transmittance graphs are very similar in the two plots. The general shape of the graphs are very similar, the peaks and troughs have very similar locations, and the reflectance and transmittance values are very similar for the whole interval. The only noticeable difference is that the transmittance peak at approximately 800 nm seems to be a bit higher in [17] than in this thesis, but overall the simulation of the perovskite material shows a very good fit with the source material [17].

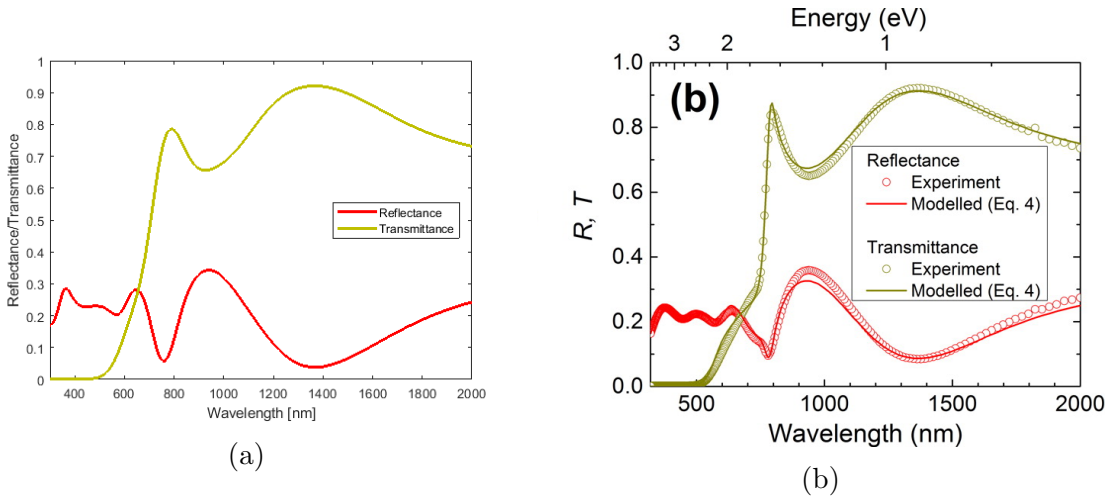

(a) (b)

Figure 6.1: The reflectance and transmittance for the perovskite material deposited on a glass substrate. The thickness of the perovskite film is 305.68 nm. (a) Simulation from this thesis, using Lumerical. (b) Experimental and modeled results from [17].

Simulations were also performed to compare the simulation model in this thesis to the results in the two articles by Carretero-Palacios and co-workers [18, 19]. These articles are relevant because they used a PV cell structure that resembles the one used in this thesis. However, there are also important differences. Firstly, the perovskite material data was acquired from a different source than the one used in this thesis, and as shown in the supporting information to [18], the source of the perovskite material data will affect the resulting absorptance. Secondly, [18, 19] used glass instead of TiO_2 and a generic HTM instead of spiro-OMeTAD. For both the glass and the HTM, [18, 19] used a constant refractive index for the whole simulation region (400-800 nm), while this thesis used data for both TiO_2 and spiro-OMeTAD that gave the complex refractive index as a function of wavelength, as described in section 5.2. These differences naturally resulted in differences in the simulation results between this thesis and [18, 19]. However, the results show similarities despite these differences.

Figure 6.2a shows the absorptance of a PV cell structure where the perovskite layer has a thickness of 300 nm, both simulated in [18] and in this thesis.

Figure 6.2b shows the absorptance of a PV cell structure where the perovskite layer has a thickness of 300 nm and a gold sphere with a diameter of 240 nm is included in the structure, both simulated in [18] and in this thesis. Figure 6.2c shows the absorptance of a PV cell structure where the perovskite layer has a thickness of 300 nm and an aluminum sphere with a diameter of 240 nm is included in the structure, both simulated in [18] and in this thesis. Figure 6.2d shows the absorptance of a PV cell structure where the perovskite layer has a thickness of 600 nm and two gold spheres with diameters of 180 nm and with a gap of 10 nm between the spheres is included in the structure, both simulated in [19] and in this thesis.

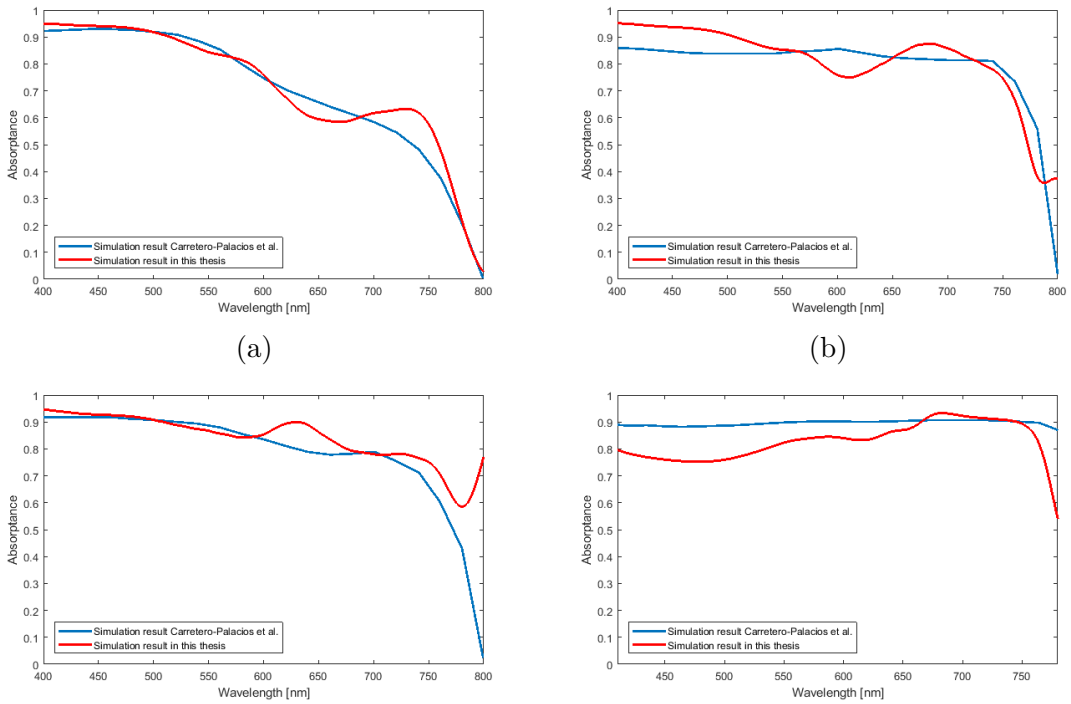

Figure 6.2: The absorptance of a perovskite PV cell, both simulated in [18, 19] and in this thesis. (a) Perovskite with thickness 300 nm, no nanoparticle. (b) Perovskite with thickness 300 nm, gold sphere with diameter 240 nm. (c) Perovskite with thickness 300 nm, aluminum sphere with diameter 240 nm. (d) Perovskite with thickness 600 nm, two gold spheres with diameter 180 nm and 10 nm gap between spheres.

The very good fit seen between the simulation result in this thesis and the simulation and experimental results in [17] (figures 6.1a and 6.1b), and the reasonably good fit (considering the differences in material properties) between the simulation results in this thesis and the simulation results in [18, 19] (figures 6.2a, 6.2b, 6.2c and 6.2d), indicates that the simulation model described in chapter 5 is a valid model that will yield reasonable results. This simulation model, with variations in layer thicknesses and nanoparticles, is therefore used in all subsequent simulations in this thesis.

6.2 Perovskite Without Nanoparticles

The first set of simulations were performed with only the basic PV structure consisting of perovskite layer, TiO_2 layer (ETM) and spiro-OMeTAD layer (HTM) as shown in figure 5.2. The first reason for doing this was to acquire reference data that the PV structures *with* nanoparticles can be compared to and thereby calculate the relative change in absorptance. The other reason was to compare the absorptance of PV structures with different layer thicknesses to each other. The thickness of the ETM and HTM is adjusted along with the thickness of the perovskite layer, according to the layer thickness constraints given in [42]. Seven different simulations were done, each with different layer thicknesses, and the resulting absorptance is shown in figure 6.3. The general trend in this plot is that the absorptance is relatively high up until a sharp drop in the region 775-800 nm, which corresponds very well with the approximate band gap of $CH_3NH_3PbI_3$, which is in the same region [11, 36, 19, 17]. After this drop, the absorptance starts to rise again. These results fit well with the results in the material data sources [41, 17]. The thicknesses of all the layers are given in table 6.2 and the total absorptance, reflectance and transmittance across the chosen wavelength interval is given in table 6.1. The latter table also includes the absorptance per nm of active layer (perovskite) to give an indication of how effectively each structure absorbs light compared to the thickness of the active layer. The trend seen in the values in table 6.1 shows that while the total reflectance and transmittance can vary both up and down, the total absorptance increases with increasing perovskite thickness. However, the relative increase is greatest from the thinnest perovskite layer to the second thinnest where it is 11.1%. From here it goes down with each simulation, and the relative increase from the second thickest layer to the thickest layer is only 1.36%. The right column also shows that the absorptance per nm of active layer decreases as the layer thickness increases.

For the simulations throughout the rest of this chapter, various types of nanoparticles will be included in the PV structure. Due to the amount of variations in nanoparticles (shape, size, material, solid vs. core-shell), there is simply not enough time to include all of the seven different PV structures for every variation of nanoparticle. Furthermore, it is the effect of the various nanoparticles on a PV structure relative to the same structure without nanoparticles that will be most interesting, so it is more important to include many different nanoparticles than many different PV structures. However, two different PV structures will be included so that it can be seen whether or not the trend is the same for different PV cell thicknesses. The two structures chosen for the remaining simulations are the thinnest and the thickest PV structures, i.e. the one with a 200 nm perovskite layer and the one with a 500 nm perovskite layer. The thinnest is chosen because it shows the highest absorptance per nm of perovskite thickness, and the thickest is chosen because it shows the highest total absorptance. These PV cells will henceforth in the subsequent simulations be referred to as the 310 nm PV cell and the 880 nm PV cell, which refers to the total thickness (ETM+perovskite+HTM) of each PV cell structure.

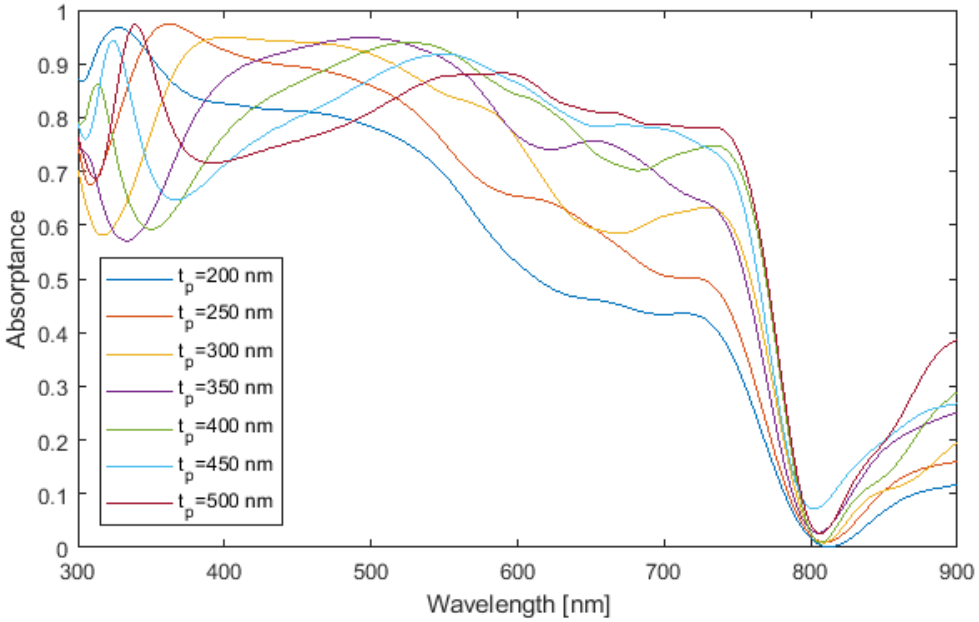

Figure 6.3: Absorptance for perovskite PV cell without nanoparticles. Seven different simulations are shown with various layer thicknesses. t_p is the thickness of the perovskite layer. The thicknesses of the TiO_2 layer (ETM) and spiro-OMeTAD layer (HTM) is given in table 6.2

.

Perovskite thickness [nm]	Reflectance	Transmittance	Absorptance	Absorptance per thickness [nm^{-1}]
200	0.189	0.280	0.531	0.00266
250	0.147	0.263	0.590	0.00236
300	0.152	0.225	0.623	0.00208
350	0.145	0.213	0.642	0.00183
400	0.165	0.181	0.654	0.00164
450	0.146	0.192	0.662	0.00147
500	0.145	0.184	0.671	0.00134

Table 6.1: Total reflectance, transmittance and absorptance for the seven different PV cells without nanoparticles. The values in the right column gives the total absorptance divided by the thickness of the active layer (perovskite). As shown, the absorptance per nanometer decreases as the thickness of the active layer increases.

Layer	Thickness [nm]
Perovskite (dark blue graph)	200
TiO_2 (dark blue graph)	10
Spiro-OMeTAD (dark blue graph)	100
Perovskite (orange graph)	250
TiO_2 (orange graph)	22
Spiro-OMeTAD (orange graph)	133
Perovskite (yellow graph)	300
TiO_2 (yellow graph)	33
Spiro-OMeTAD (yellow graph)	167
Perovskite (purple graph)	350
TiO_2 (purple graph)	45
Spiro-OMeTAD (purple graph)	200
Perovskite (green graph)	400
TiO_2 (green graph)	57
Spiro-OMeTAD (green graph)	233
Perovskite (light blue graph)	450
TiO_2 (light blue graph)	68
Spiro-OMeTAD (light blue graph)	267
Perovskite (red graph)	500
TiO_2 (red graph)	80
Spiro-OMeTAD (red graph)	300

Table 6.2: Thicknesses of the various layers for the simulations of the PV cell without nanoparticles. Perovskite is the active layer, TiO_2 is the ETM and spiro-OMeTAD is the HTM.

6.3 Solid Gold Spheres

This simulation group consists of thirteen simulations where one solid gold (Au) sphere is placed at the center of the perovskite layer in the PV cell structure shown in figure 5.2. Seven simulations use the 310 nm PV cell with the sphere diameter in the range 20-150 nm, and the other six simulations use the 880 nm PV cell with the sphere diameter in the range 20-250 nm.

The absorptance from the seven simulations using the 310 nm PV cell compared to the reference PV cell (without nanoparticles) is shown in figure 6.4. As expected, all structures with nanoparticles show enhanced absorptance. Furthermore, the absorptance increases with increasing nanosphere diameter.

The absorptance from the six simulations using the 880 nm PV cell compared to the reference PV cell (without nanoparticles) is shown in figure 6.5. The simulations with this PV cell show the same general trend as the simulations with the 310 nm PV cell, i.e. the absorptance of the PV cell increases when nanoparticles are included, and it also increases with increasing nanosphere diameter. It can also be seen for both the 310 and 880 nm PV cell that the absorptance for all sphere diameters is almost equal to both each other and the reference PV cell without nanoparticles in the wavelength range 300-500 nm, and shortly after 500 nm the absorptance of the PV cells with Au nanospheres becomes larger than the absorptance

of the reference PV cell and it stays larger for the rest of the simulation region. In the region after the band gap wavelength, which is after approximately 800 nm, the PV cells with relatively big nanospheres show a much larger absorptance than the reference cell, while the PV cells with the relatively small nanospheres show an absorptance much closer to the reference cell. The total reflectance, transmittance and absorptance of all the PV cells, including reference cells, are shown in tables 6.3 and 6.4. Furthermore, the percentage increase in absorptance for all PV cells relative to the reference cell is also shown is these tables, and these values are calculated by the standard formula

$$\%\Delta A = \frac{A_{\text{np}} - A_{\text{ref}}}{A_{\text{ref}}} \times 100\% \tag{6.1}$$

where $\%\Delta A$ is the relative percentage increase in absorptance, A_{np} is the total absorptance of the PV cell *with* nanoparticle, and A_{ref} is the total absorptance of the PV cell *without* nanoparticle. This same formula will be used to calculate the relative percentage increase in absorptance for all subsequent simulations.

Nanosphere diameter [nm]	Reflectance	Transmittance	Absorptance	Absorptance increase $\%\Delta A$
-	0.189	0.280	0.531	-
20	0.188	0.279	0.533	0.377%
30	0.187	0.276	0.537	1.13%
50	0.182	0.261	0.557	4.90%
75	0.177	0.219	0.604	13.7%
100	0.191	0.169	0.640	20.5%
125	0.209	0.121	0.670	26.2%
150	0.211	0.083	0.706	33.0%

Table 6.3: Total reflectance, transmittance and absorptance for the 310 nm PV cell with Au nanospheres with various diameters, as well as the percentage increase in absorptance ($\%\Delta A$) relative to the reference cell. The first row is the reference PV cell without nanosphere.

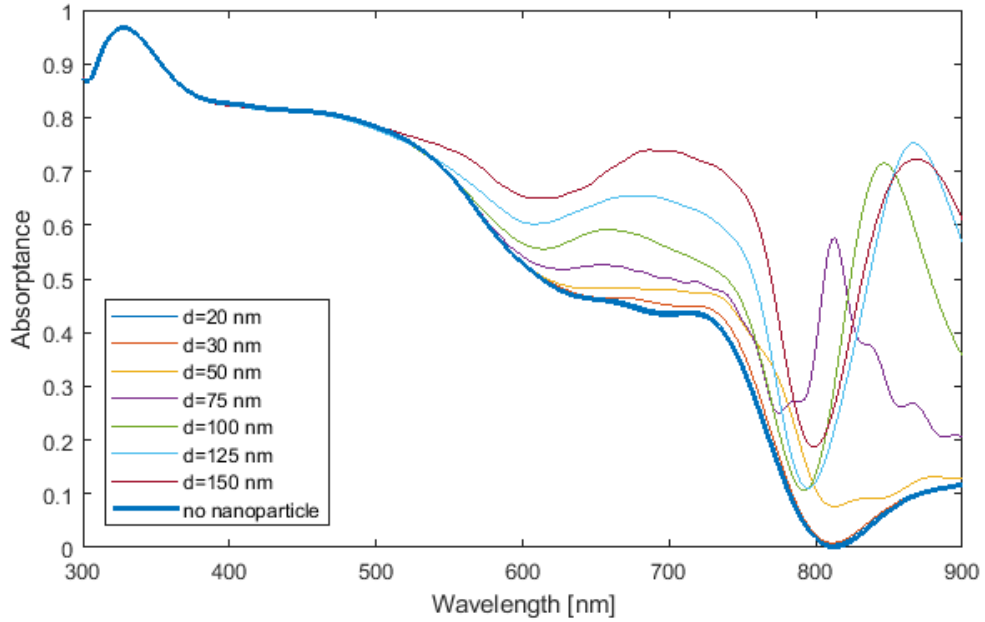

Figure 6.4: Absorptance for the 310 nm PV cell with solid Au nanospheres of various diameters included. The thick blue line is the absorptance of the reference PV cell without nanoparticles.

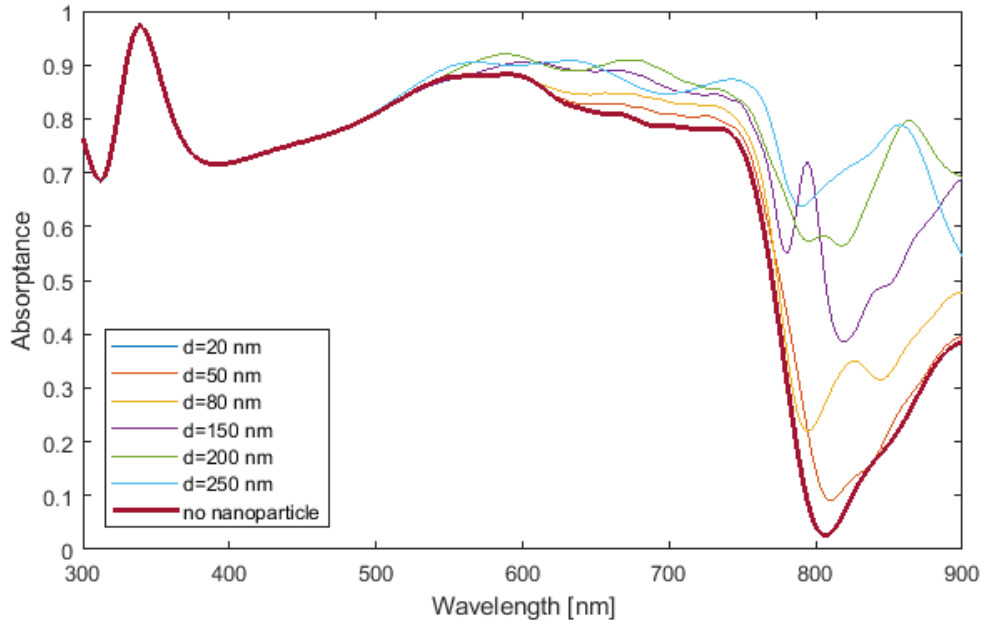

Figure 6.5: Absorptance for the 880 nm PV cell with solid Au nanospheres of various diameters included. The thick red line is the absorptance of the reference PV cell without nanoparticles.

Nanosphere diameter [nm]	Reflectance	Transmittance	Absorptance	Absorptance increase $\%\Delta A$
-	0.145	0.184	0.671	-
20	0.145	0.183	0.672	0.149%
50	0.143	0.170	0.687	2.38%
80	0.158	0.128	0.714	6.41%
150	0.188	0.045	0.767	14.3%
200	0.143	0.059	0.798	18.9%
250	0.169	0.028	0.803	19.7%

Table 6.4: Total reflectance, transmittance and absorptance for the 880 nm PV cell with Au nanospheres with various diameters, as well as the percentage increase in absorptance ($\%\Delta A$) relative to the reference cell. The first row is the reference PV cell without nanosphere.

6.4 Solid Silver Spheres

This simulation group consists of thirteen simulations where one solid silver (Ag) sphere is placed at the center of the perovskite layer in the PV cell structure shown in figure 5.2. Seven simulations use the 310 nm PV cell with the sphere diameter in the range 20-150 nm, and the other six simulations use the 880 nm PV cell with the sphere diameter in the range 20-250 nm.

The absorptance from the seven simulations using the 310 nm PV cell compared to the reference PV cell (without nanoparticles) is shown in figure 6.6, and the same is shown in figure 6.7 for the six simulations using the 880 nm PV cell. The total reflectance, transmittance, absorptance and absorptance increase are shown in tables 6.5 and 6.6 for all PV cells. The results are almost the same as they were when Au nanospheres were used, as described in section 6.3. Therefore, judging from the simulations performed in this thesis, both Au and Ag nanospheres have approximately the same positive effect on the PV cells.

Nanosphere diameter [nm]	Reflectance	Transmittance	Absorptance	Absorptance increase $\%\Delta A$
-	0.189	0.280	0.531	-
20	0.188	0.279	0.533	0.377%
30	0.188	0.276	0.536	0.942%
50	0.182	0.262	0.556	4.71%
75	0.176	0.220	0.604	13.7%
100	0.190	0.170	0.640	20.5%
125	0.210	0.121	0.669	26.0%
150	0.211	0.082	0.707	33.1%

Table 6.5: Total reflectance, transmittance and absorptance for the 310 nm PV cell with Ag nanospheres with various diameters, as well as the percentage increase in absorptance ($\%\Delta A$) relative to the reference cell. The first row is the reference PV cell without nanosphere.

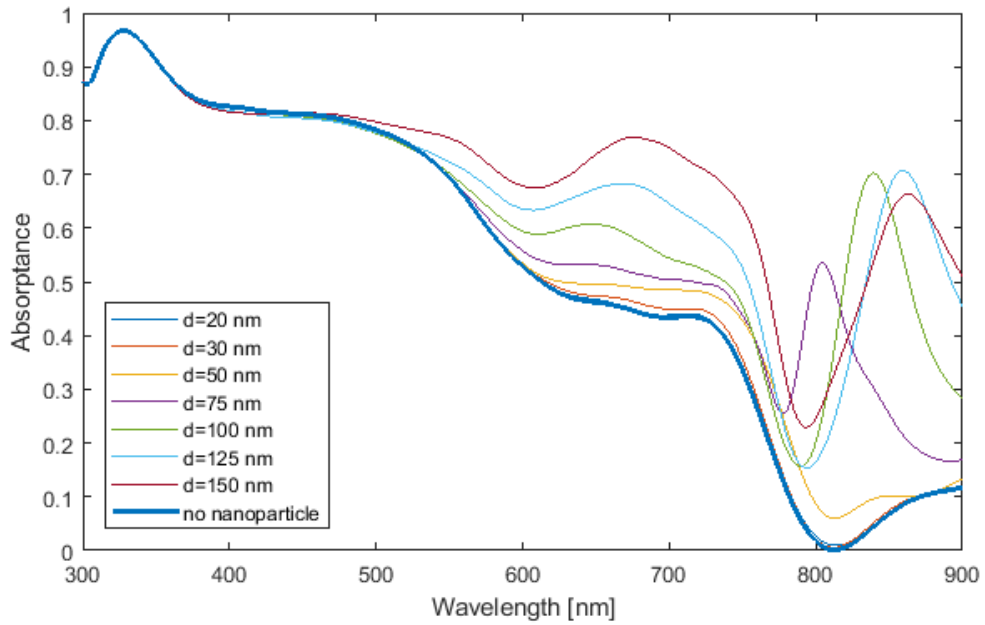

Figure 6.6: Absorptance for the 310 nm PV cell with solid Ag nanospheres of various diameters included. The thick blue line is the absorptance of the reference PV cell without nanoparticles.

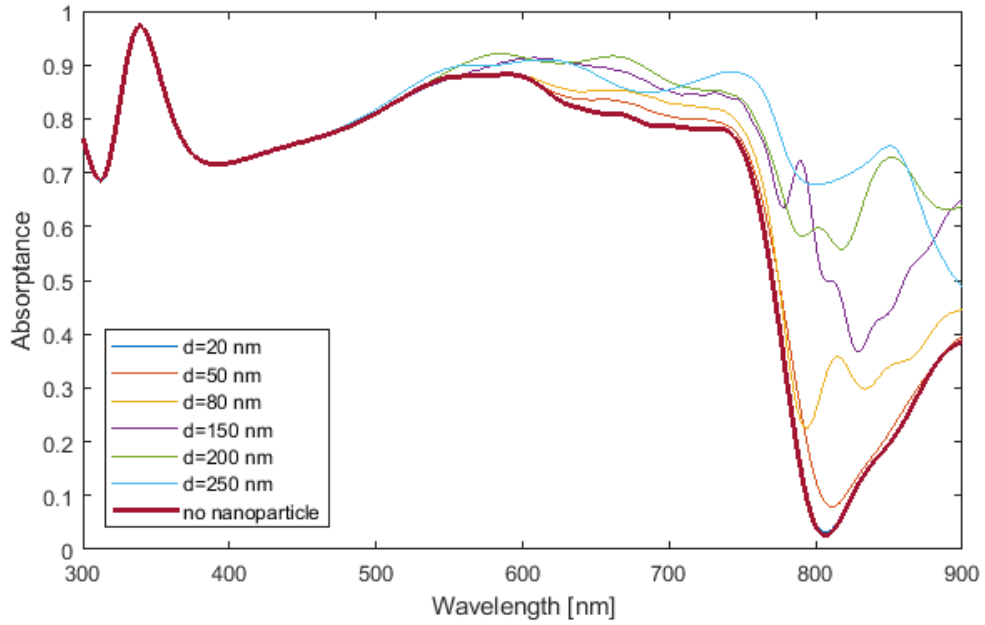

Figure 6.7: Absorptance for the 880 nm PV cell with solid Ag nanospheres of various diameters included. The thick red line is the absorptance of the reference PV cell without nanoparticles.

Nanosphere diameter [nm]	Reflectance	Transmittance	Absorptance	Absorptance increase $\%\Delta A$
-	0.145	0.184	0.671	-
20	0.145	0.183	0.672	0.149%
50	0.143	0.172	0.685	2.09%
80	0.156	0.131	0.713	6.26%
150	0.191	0.044	0.765	14.0%
200	0.145	0.063	0.792	18.0%
250	0.167	0.033	0.800	19.2%

Table 6.6: Total reflectance, transmittance and absorptance for the 880 nm PV cell with Ag nanospheres with various diameters, as well as the percentage increase in absorptance ($\%\Delta A$) relative to the reference cell. The first row is the reference PV cell without nanosphere.

6.5 Solid Aluminum Spheres

This simulation group consists of thirteen simulations where one solid aluminum (Al) sphere is placed at the center of the perovskite layer in the PV cell structure shown in figure 5.2. Seven simulations use the 310 nm PV cell with the sphere diameter in the range 20-150 nm, and the other six simulations use the 880 nm PV cell with the sphere diameter in the range 20-250 nm.

The absorptance from the seven simulations using the 310 nm PV cell compared to the reference PV cell (without nanoparticles) is shown in figure 6.8, and the same is shown in figure 6.9 for the six simulations using the 880 nm PV cell. The total reflectance, transmittance, absorptance and absorptance increase are shown in tables 6.7 and 6.8 for all PV cells. The results show the same general trend as they did when Au nanospheres were used, as described in section 6.3, but there are some differences in the total absorptance that is worth noting. For most of the simulations, the Au nanospheres give a higher total absorptance than their Al counterparts. However, something happens when the nanospheres get larger. For the two largest nanospheres in each PV cell (d=125 nm and d=150 nm for the 310 nm PV cell, and d=200 nm and d=250 nm for the 880 nm PV cell), the total absorptance is notably higher when using Al compared to Au. Therefore, judging from the simulations in this thesis, Au nanospheres is more successful in increasing total absorptance for small to medium nanosphere diameters, but Al actually results in a higher total absorptance for large nanosphere diameters.

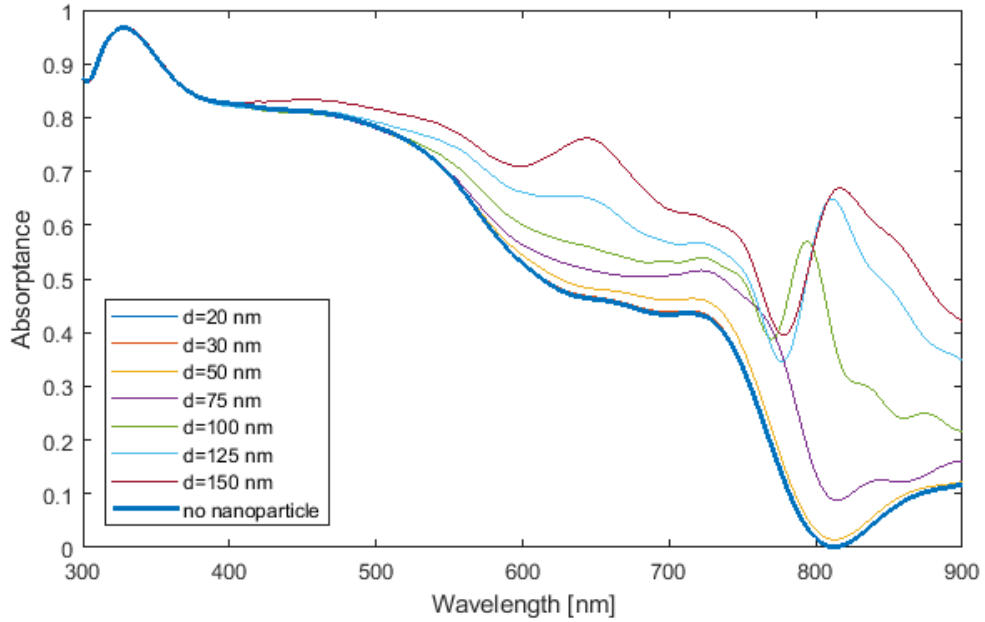

Figure 6.8: Absorptance for the 310 nm PV cell with solid Al nanospheres of various diameters included. The thick blue line is the absorptance of the reference PV cell without nanoparticles.

Nanosphere diameter [nm]	Reflectance	Transmittance	Absorptance	Absorptance increase $\%\Delta A$
-	0.189	0.280	0.531	-
20	0.189	0.280	0.531	0.00%
30	0.188	0.279	0.533	0.377%
50	0.183	0.275	0.542	2.07%
75	0.172	0.254	0.574	8.10%
100	0.162	0.213	0.625	17.7%
125	0.160	0.166	0.674	26.9%
150	0.157	0.125	0.718	35.2%

Table 6.7: Total reflectance, transmittance and absorptance for the 310 nm PV cell with Al nanospheres with various diameters, as well as the percentage increase in absorptance ($\%\Delta A$) relative to the reference cell. The first row is the reference PV cell without nanosphere.

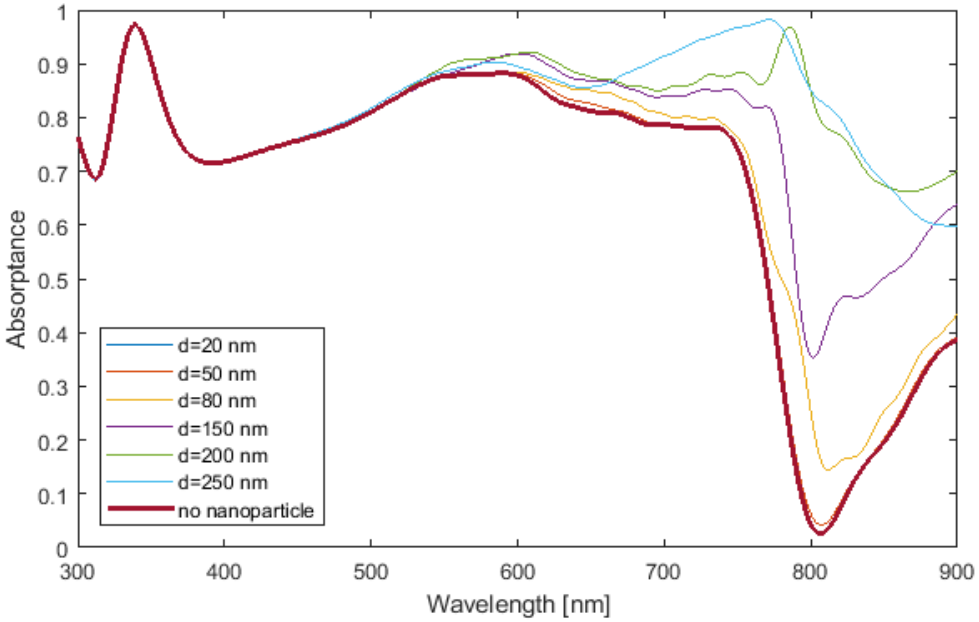

Figure 6.9: Absorptance for the 880 nm PV cell with solid Al nanospheres of various diameters included. The thick red line is the absorptance of the reference PV cell without nanoparticles.

Nanosphere diameter [nm]	Reflectance	Transmittance	Absorptance	Absorptance increase $\%\Delta A$
-	0.145	0.184	0.671	-
20	0.145	0.184	0.671	0.00%
50	0.144	0.181	0.685	0.596%
80	0.142	0.158	0.700	4.32%
150	0.171	0.066	0.763	13.7%
200	0.135	0.047	0.818	21.9%
250	0.146	0.029	0.825	23.0%

Table 6.8: Total reflectance, transmittance and absorptance for the 880 nm PV cell with Al nanospheres with various diameters, as well as the percentage increase in absorptance ($\%\Delta A$) relative to the reference cell. The first row is the reference PV cell without nanosphere.

6.6 Solid Platinum Spheres

This simulation group consists of thirteen simulations where one solid platinum (Pt) sphere is placed at the center of the perovskite layer in the PV cell structure shown in figure 5.2. Seven simulations use the 310 nm PV cell with the sphere diameter in the range 20-150 nm, and the other six simulations use the 880 nm PV cell with the sphere diameter in the range 20-250 nm.

The absorptance from the seven simulations using the 310 nm PV cell compared to the reference PV cell (without nanoparticles) is shown in figure 6.10, and the same is shown in figure 6.11 for the six simulations using the 880 nm PV

cell. The total reflectance, transmittance, absorptance and absorptance increase are shown in tables 6.9 and 6.10 for all PV cells. The results show the same general trend as they did when Al nanospheres were used, as described in section 6.5, but the total absorptance with large nanosphere diameters is even higher when Pt is used. Of the four metals (Au, Ag, Al, Pt) used as material for the centered solid nanospheres in this thesis, Au shows the highest total absorptance for small and medium nanosphere diameters, while Pt shows the highest total absorptance for large nanosphere diameters.

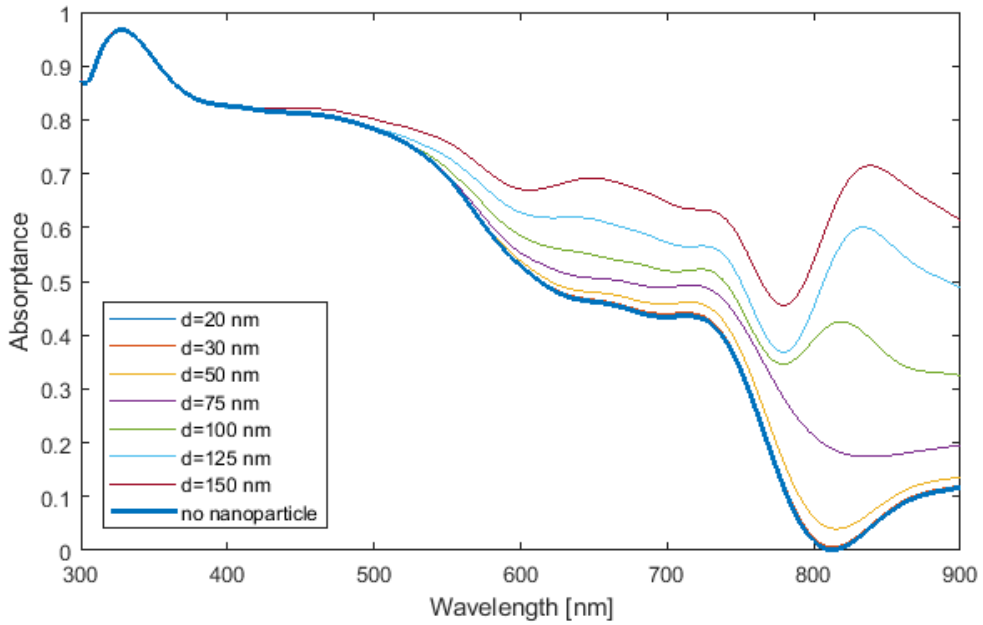

Figure 6.10: Absorptance for the 310 nm PV cell with solid Pt nanospheres of various diameters included. The thick blue line is the absorptance of the reference PV cell without nanoparticles.

Nanosphere diameter [nm]	Reflectance	Transmittance	Absorptance	Absorptance increase $\%\Delta A$
-	0.189	0.280	0.531	-
20	0.189	0.279	0.532	0.188%
30	0.188	0.278	0.534	0.565%
50	0.184	0.271	0.545	2.64%
75	0.176	0.246	0.578	8.85%
100	0.167	0.207	0.626	17.9%
125	0.161	0.164	0.675	27.1%
150	0.154	0.120	0.726	36.7%

Table 6.9: Total reflectance, transmittance and absorptance for the 310 nm PV cell with Pt nanospheres with various diameters, as well as the percentage increase in absorptance ($\%\Delta A$) relative to the reference cell. The first row is the reference PV cell without nanosphere.

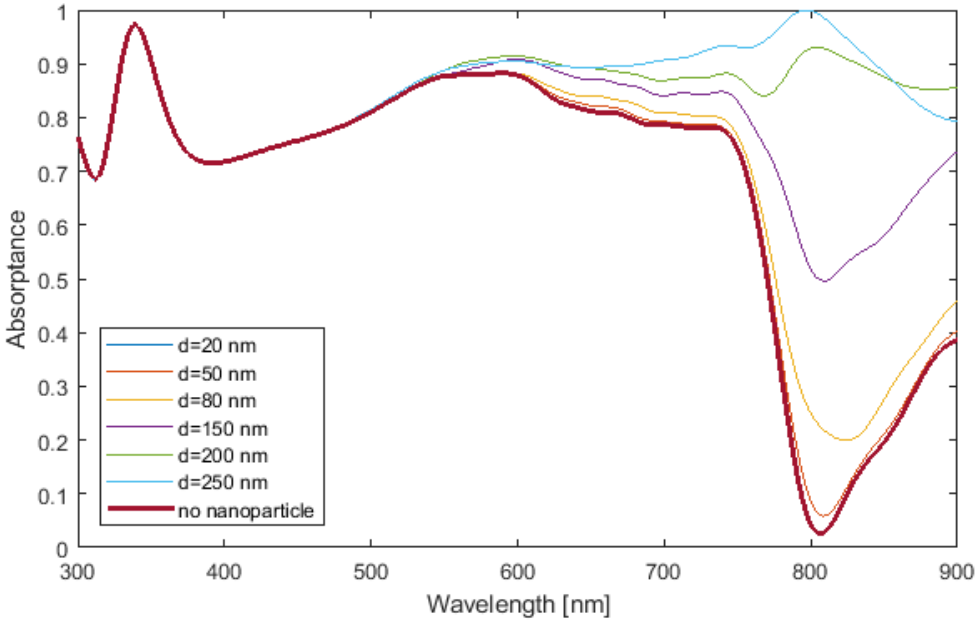

Figure 6.11: Absorptance for the 880 nm PV cell with solid Pt nanospheres of various diameters included. The thick red line is the absorptance of the reference PV cell without nanoparticles.

Nanosphere diameter [nm]	Reflectance	Transmittance	Absorptance	Absorptance increase $\%\Delta A$
-	0.145	0.184	0.671	-
20	0.145	0.183	0.672	0.149%
50	0.144	0.178	0.678	1.04%
80	0.145	0.153	0.702	4.62%
150	0.155	0.068	0.777	15.8%
200	0.131	0.023	0.846	26.1%
250	0.134	0.006	0.860	28.2%

Table 6.10: Total reflectance, transmittance and absorptance for the 880 nm PV cell with Pt nanospheres with various diameters, as well as the percentage increase in absorptance ($\%\Delta A$) relative to the reference cell. The first row is the reference PV cell without nanosphere.

6.7 Solid Gold Cubes

This simulation group consists of thirteen simulations where one solid Au cube is placed at the center of the perovskite layer in the PV cell structure shown in figure 5.2. Seven simulations use the 310 nm PV cell with the cube side length in the range 20-150 nm, and the other six simulations use the 880 nm PV cell with the cube side length in the range 20-250 nm.

The absorptance from the seven simulations using the 310 nm PV cell compared to the reference PV cell (without nanoparticles) is shown in figure 6.12, and the same is shown in figure 6.13 for the six simulations using the 880 nm PV

cell. The total reflectance, transmittance, absorptance and absorptance increase are shown in tables 6.11 and 6.12 for all PV cells.

The results for the 310 nm PV cell shows that the total absorptance increases with increasing cube size, just like it did when spheres were used. The total absorptance is higher for the nanocubes than it was for the nanospheres, but this could be due to the fact that a cube with a given side length has a volume that is approximately 1.9 times as big as a sphere with diameter equal to the side length of the cube. So the increased volumes of the cubes compared to the spheres could be the cause of the increased absorptance.

The results for the 880 nm PV cell show a different trend than the simulations where nanospheres were used. The absorptance increases with increasing cube size for the four smallest cubes, but then it drops noticeably from the fourth cube to the fifth and it drops again from the fifth to the sixth. The two largest cubes show a much lower absorptance than the cube with side length 150 nm, and in fact the largest cube (s=250 nm) even has a lower absorptance than the cube with side length 50 nm. This drop in absorptance for the two largest cubes is caused by a very high reflectance. The periodic boundaries described in section 5.2 will simulate cubes in the x and y directions, and since the side length for the biggest cube is 250 nm, that means there will only be a gap of 50 nm between each cube. For the second biggest cube the gap would be 100 nm. So the cause of the increased reflectance in the case of the two biggest cubes is simply that the cubes, which have plane top surfaces, are getting so close together that they are starting to resemble a plane surface, and a plane metal surface will naturally result in high reflectance. Therefore, judging by the simulations in this thesis, Au nanocubes cannot have longer side lengths than 150 nm in the 880 nm PV cell before the reflectance increases drastically, which results in decreased absorptance.

Nanocube side length [nm]	Reflectance	Transmittance	Absorptance	Absorptance increase $\%\Delta A$
-	0.189	0.280	0.531	-
20	0.188	0.278	0.534	0.565%
30	0.185	0.268	0.547	3.01%
50	0.184	0.234	0.582	9.60%
75	0.200	0.179	0.621	16.9%
100	0.186	0.163	0.651	22.6%
125	0.132	0.167	0.701	32.0%
150	0.131	0.116	0.753	41.8%

Table 6.11: Total reflectance, transmittance and absorptance for the 310 nm PV cell with Au nanocubes with various side lengths, as well as the percentage increase in absorptance ($\%\Delta A$) relative to the reference cell. The first row is the reference PV cell without nanocube.

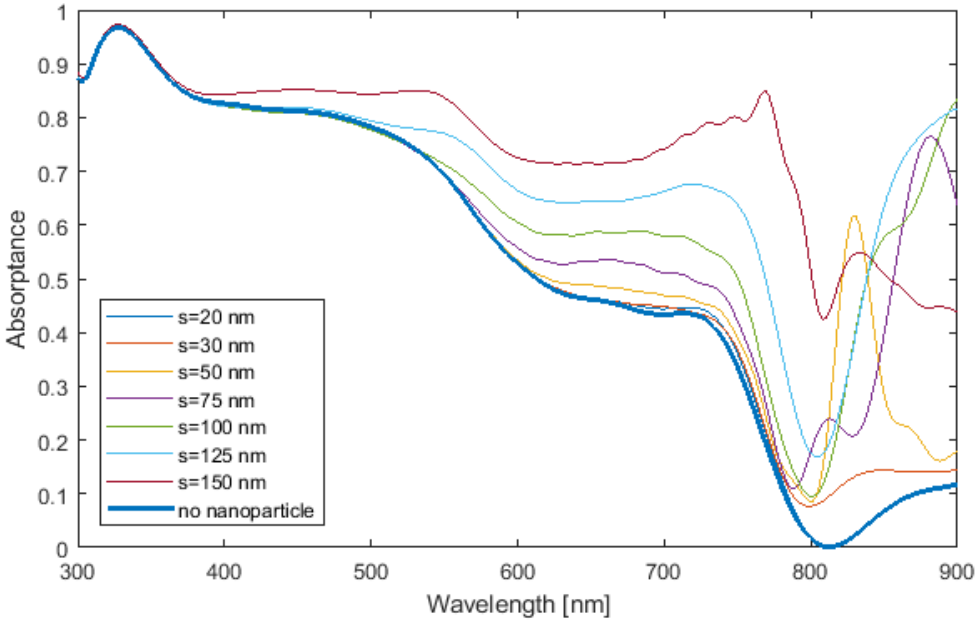

Figure 6.12: Absorptance for the 310 nm PV cell with solid Au nanocubes with various side lengths included (s is side length). The thick blue line is the absorptance of the reference PV cell without nanoparticles.

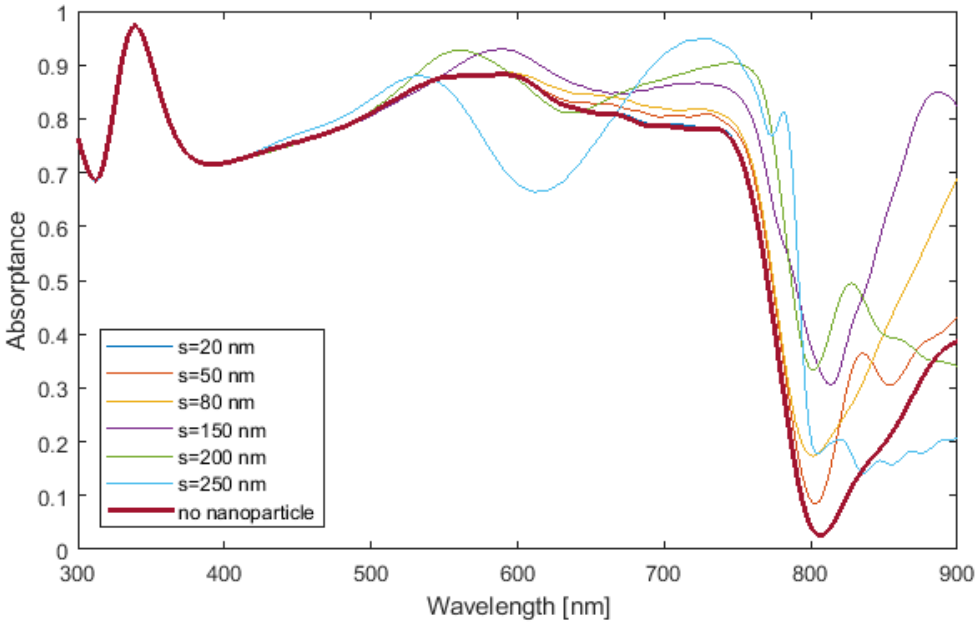

Figure 6.13: Absorptance for the 880 nm PV cell with solid Au nanocubes with various side lengths included (s is side length). The thick red line is the absorptance of the reference PV cell without nanoparticles.

Nanocube side length [nm]	Reflectance	Transmittance	Absorptance	Absorptance increase $\%\Delta A$
-	0.145	0.184	0.671	-
20	0.145	0.183	0.672	0.149%
50	0.158	0.145	0.697	3.87%
80	0.155	0.126	0.719	7.15%
150	0.148	0.078	0.774	15.4%
200	0.253	0.004	0.743	10.7%
250	0.307	0.001	0.692	3.13%

Table 6.12: Total reflectance, transmittance and absorptance for the 880 nm PV cell with Au nanocubes with various side lengths, as well as the percentage increase in absorptance ($\%\Delta A$) relative to the reference cell. The first row is the reference PV cell without nanocube.

6.8 Solid Silver Cubes

This simulation group consists of thirteen simulations where one solid Ag cube is placed at the center of the perovskite layer in the PV cell structure shown in figure 5.2. Seven simulations use the 310 nm PV cell with the cube side length in the range 20-150 nm, and the other six simulations use the 880 nm PV cell with the cube side length in the range 20-250 nm.

The absorptance from the seven simulations using the 310 nm PV cell compared to the reference PV cell (without nanoparticles) is shown in figure 6.14, and the same is shown in figure 6.15 for the six simulations using the 880 nm PV cell. The total reflectance, transmittance, absorptance and absorptance increase are shown in tables 6.13 and 6.14 for all PV cells. The general trend in the results is the same as it was when Au nanocubes were used, as described in section 6.7. The values for total absorptance are also approximately the same for Au and Ag nanocubes. Therefore, judging from the simulations performed in this thesis, both Au and Ag nanocubes have approximately the same positive effect on the PV cells.

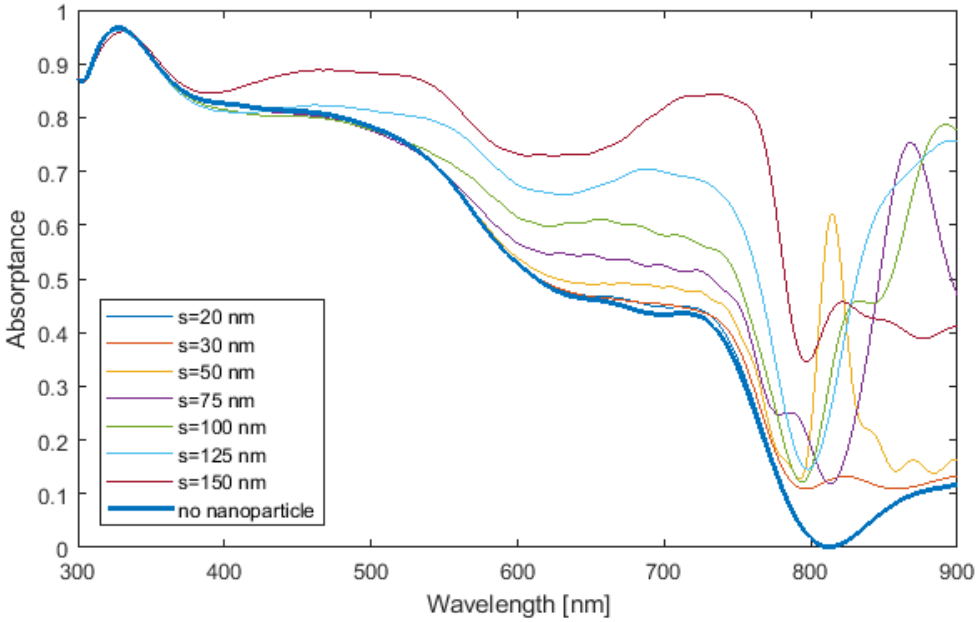

Figure 6.14: Absorptance for the 310 nm PV cell with solid Ag nanocubes with various side lengths included (s is side length). The thick blue line is the absorptance of the reference PV cell without nanoparticles.

Nanocube side length [nm]	Reflectance	Transmittance	Absorptance	Absorptance increase $\%\Delta A$
-	0.189	0.280	0.531	-
20	0.188	0.278	0.534	0.565%
30	0.185	0.267	0.548	3.20%
50	0.185	0.235	0.580	9.23%
75	0.202	0.170	0.628	18.3%
100	0.194	0.148	0.658	23.9%
125	0.129	0.166	0.705	32.8%
150	0.133	0.119	0.748	40.9%

Table 6.13: Total reflectance, transmittance and absorptance for the 310 nm PV cell with Ag nanocubes with various side lengths, as well as the percentage increase in absorptance ($\%\Delta A$) relative to the reference cell. The first row is the reference PV cell without nanocube.

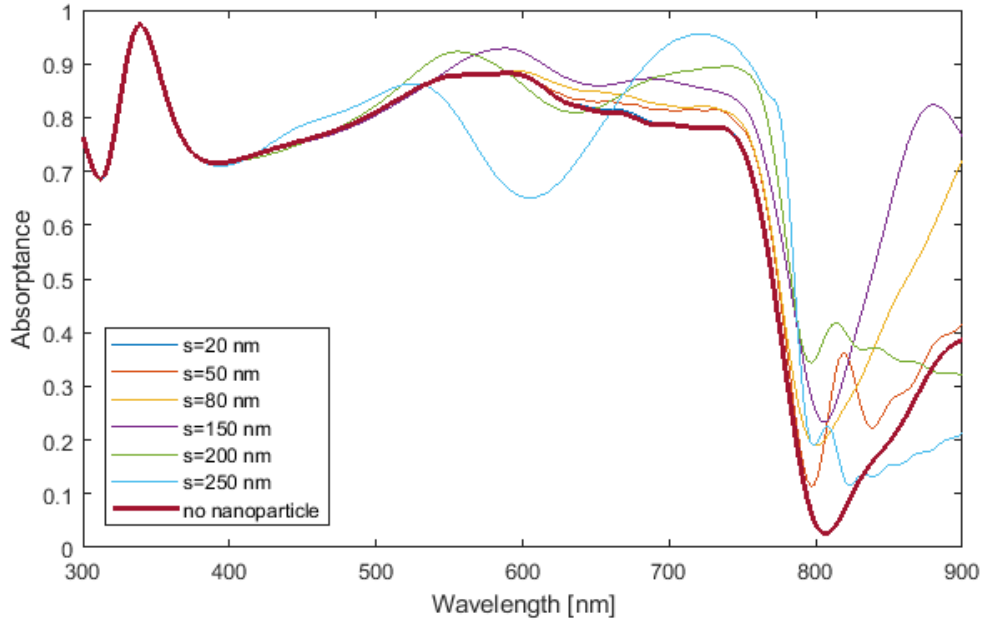

Figure 6.15: Absorptance for the 880 nm PV cell with solid Ag nanocubes with various side lengths included (s is side length). The thick red line is the absorptance of the reference PV cell without nanoparticles.

Nanocube side length [nm]	Reflectance	Transmittance	Absorptance	Absorptance increase $\%\Delta A$
-	0.145	0.184	0.671	-
20	0.145	0.183	0.672	0.149%
50	0.155	0.147	0.698	4.02%
80	0.157	0.117	0.726	8.20%
150	0.150	0.083	0.767	14.3%
200	0.264	0.003	0.733	9.24%
250	0.315	0.001	0.684	1.94%

Table 6.14: Total reflectance, transmittance and absorptance for the 880 nm PV cell with Ag nanocubes with various side lengths, as well as the percentage increase in absorptance ($\%\Delta A$) relative to the reference cell. The first row is the reference PV cell without nanocube.

6.9 Solid Aluminum Cubes

This simulation group consists of thirteen simulations where one solid Al cube is placed at the center of the perovskite layer in the PV cell structure shown in figure 5.2. Seven simulations use the 310 nm PV cell with the cube side length in the range 20-150 nm, and the other six simulations use the 880 nm PV cell with the cube side length in the range 20-250 nm.

The absorptance from the seven simulations using the 310 nm PV cell compared to the reference PV cell (without nanoparticles) is shown in figure 6.16,

and the same is shown in figure 6.17 for the six simulations using the 880 nm PV cell. The total reflectance, transmittance, absorptance and absorptance increase are shown in tables 6.15 and 6.16 for all PV cells. The general trend in the results is the same as is was when Au nanocubes were used, as described in section 6.7. However, the values for total absorptance are not the same as they were for Au nanocubes. For the smaller sized cubes, the total absorptance is a little lower for Al compared to Au, but this shifts as the nanocubes increase in size. Somewhere between s=50 nm and s=75 nm for the 310 nm PV cell, and between s=50 nm and s=80 nm for the 880 nm PV cell, the total absorptance becomes higher for Al nanocubes than it is for Au nanocubes. For the three largest nanocubes, both for the 310 and the 880 nm PV cells, the total absorptance is significantly higher when using Al compared to Au. This is similar to what was seen when the Au and Al nanospheres were compared, but the shift seems to take place a little sooner for the nanocubes than for the nanospheres. The reason why it shifts sooner for cubes than for spheres could be related to the fact that nanocubes have approximately 1.9 times the volume of a nanosphere if the side length of the cube is equal to the diameter of the sphere, as mentioned in section 6.7. Judging from the simulations in this thesis, Au nanocubes is more successful in increasing total absorptance for relatively small cube sizes, but Al actually results in a much higher total absorptance for relatively large cube sizes.

Nanocube side length [nm]	Reflectance	Transmittance	Absorptance	Absorptance increase $\%\Delta A$
-	0.189	0.280	0.531	-
20	0.188	0.280	0.532	0.188%
30	0.186	0.277	0.537	1.13%
50	0.177	0.261	0.562	5.84%
75	0.162	0.202	0.636	19.8%
100	0.157	0.131	0.712	34.1%
125	0.140	0.084	0.776	46.1%
150	0.163	0.053	0.784	47.6%

Table 6.15: Total reflectance, transmittance and absorptance for the 310 nm PV cell with Al nanocubes with various side lengths, as well as the percentage increase in absorptance ($\%\Delta A$) relative to the reference cell. The first row is the reference PV cell without nanocube.

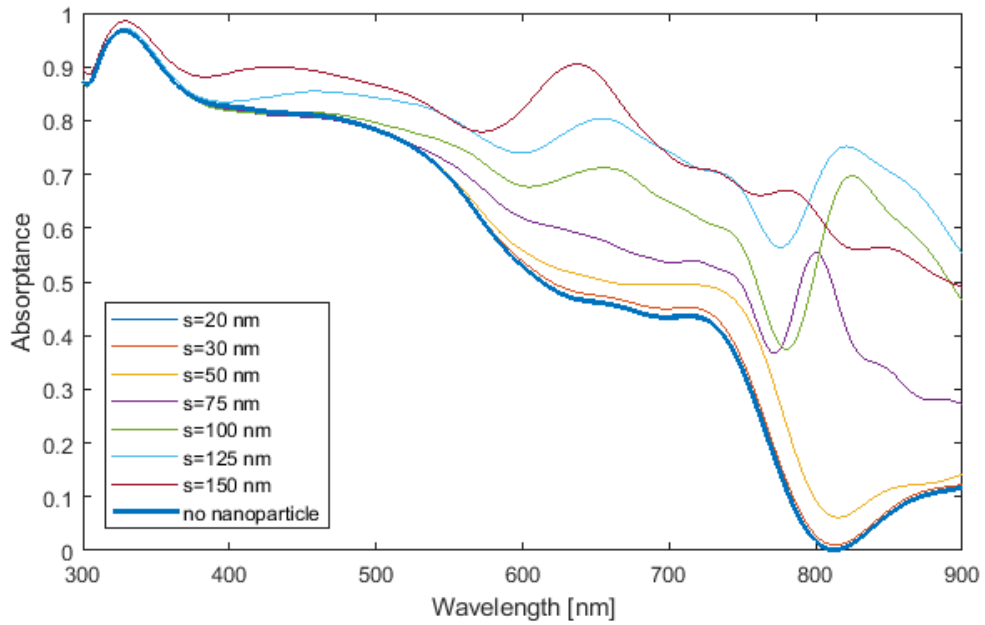

Figure 6.16: Absorptance for the 310 nm PV cell with solid Al nanocubes with various side lengths included (s is side length). The thick blue line is the absorptance of the reference PV cell without nanoparticles.

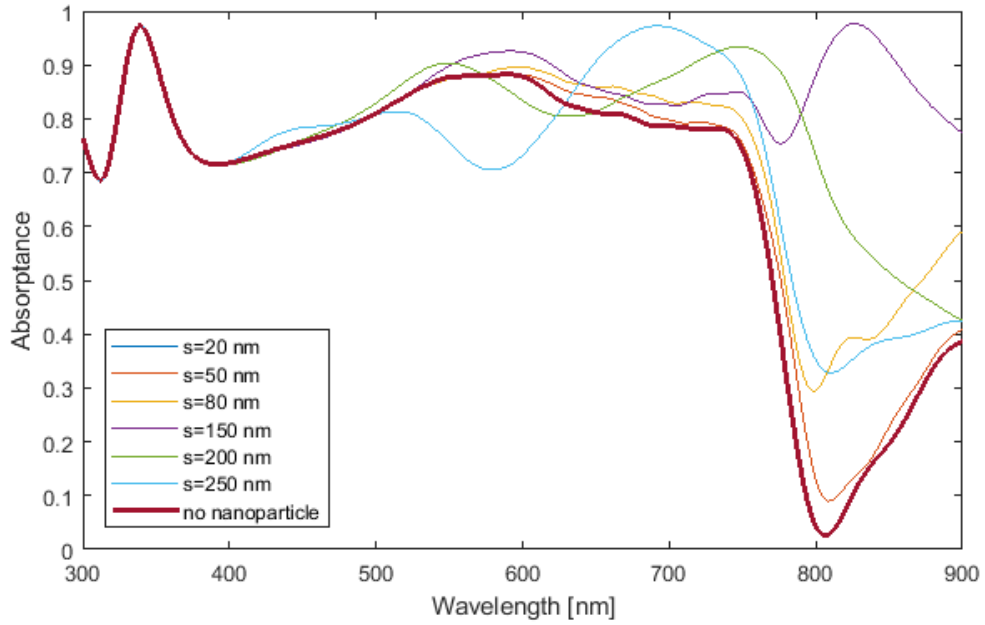

Figure 6.17: Absorptance for the 880 nm PV cell with solid Al nanocubes with various side lengths included (s is side length). The thick red line is the absorptance of the reference PV cell without nanoparticles.

Nanocube side length [nm]	Reflectance	Transmittance	Absorptance	Absorptance increase $\%\Delta A$
-	0.145	0.184	0.671	-
20	0.145	0.184	0.671	0.00%
50	0.142	0.171	0.687	2.38%
80	0.160	0.105	0.735	9.54%
150	0.139	0.025	0.836	24.6%
200	0.215	0.005	0.780	16.2%
250	0.271	0.001	0.728	8.49%

Table 6.16: Total reflectance, transmittance and absorptance for the 880 nm PV cell with Al nanocubes with various side lengths, as well as the percentage increase in absorptance ($\%\Delta A$) relative to the reference cell. The first row is the reference PV cell without nanocube.

6.10 Solid Platinum Cubes

This simulation group consists of thirteen simulations where one solid Pt cube is placed at the center of the perovskite layer in the PV cell structure shown in figure 5.2. Seven simulations use the 310 nm PV cell with the cube side length in the range 20-150 nm, and the other six simulations use the 880 nm PV cell with the cube side length in the range 20-250 nm.

The absorptance from the seven simulations using the 310 nm PV cell compared to the reference PV cell (without nanoparticles) is shown in figure 6.18, and the same is shown in figure 6.19 for the six simulations using the 880 nm PV cell. The total reflectance, transmittance, absorptance and absorptance increase are shown in tables 6.17 and 6.18 for all PV cells. The results are quite similar to the results for Al nanocubes, as described in section 6.9, but there are some differences in the absorptance values. In most of the simulations, the total absorptance is higher for Al nanocubes than it is for Pt nanocubes. However, for the largest cube size in the 310 nm PV cell and the three largest cube sizes in the 880 nm PV cell, the total absorptance is significantly higher for Pt cubes than for Al cubes. The Pt cube with side length 150 nm shows a 52.9% increase in total absorptance relative to the 310 nm reference PV cell, which is the largest increase seen so far in this thesis. The drop in total absorptance for the two largest nanocubes in the 880 nm PV cell that was observed when using Au, Ag and Al nanocubes is also seen when using Pt nanocubes. However, the drop is much smaller than it is for the three other metals, so Pt has by far the highest absorptance for those two cube sizes. Of the four metals (Au, Ag, Al, Pt) used as material for the centered solid nanocubes in this thesis, Au shows the highest total absorptance for small cube sizes, while Al and Pt shows higher total absorptance for medium and large cube sizes. For the largest cube sizes, Pt is even better than Al.

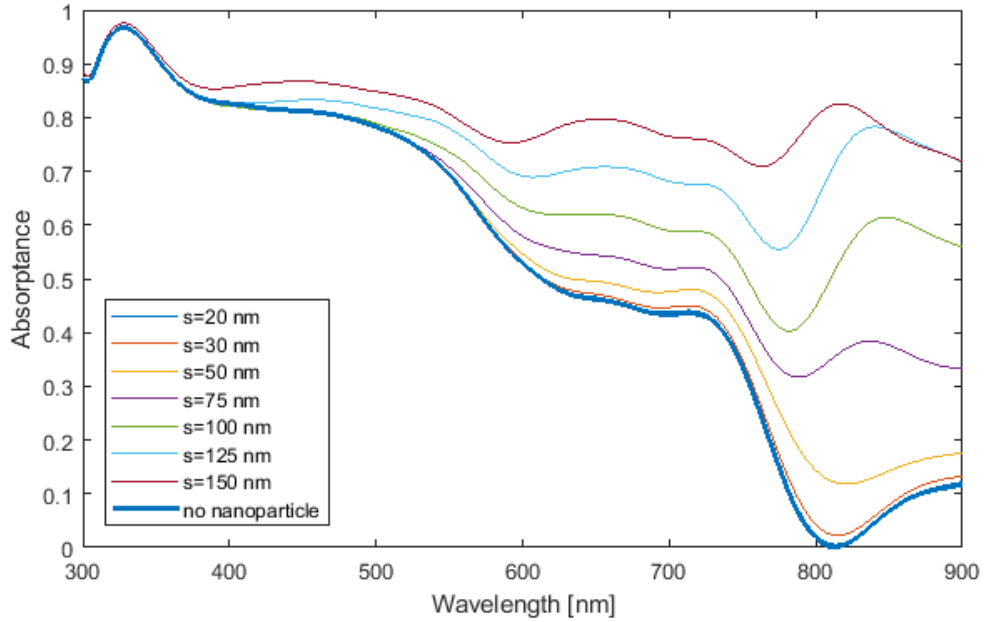

Figure 6.18: Absorptance for the 310 nm PV cell with solid Pt nanocubes with various side lengths included (s is side length). The thick blue line is the absorptance of the reference PV cell without nanoparticles.

Nanocube side length [nm]	Reflectance	Transmittance	Absorptance	Absorptance increase $\%\Delta A$
-	0.189	0.280	0.531	-
20	0.188	0.279	0.533	0.377%
30	0.187	0.275	0.538	1.32%
50	0.180	0.257	0.563	6.03%
75	0.169	0.211	0.620	16.8%
100	0.159	0.155	0.686	29.2%
125	0.141	0.099	0.760	43.1%
150	0.138	0.050	0.812	52.9%

Table 6.17: Total reflectance, transmittance and absorptance for the 310 nm PV cell with Pt nanocubes with various side lengths, as well as the percentage increase in absorptance ($\%\Delta A$) relative to the reference cell. The first row is the reference PV cell without nanocube.

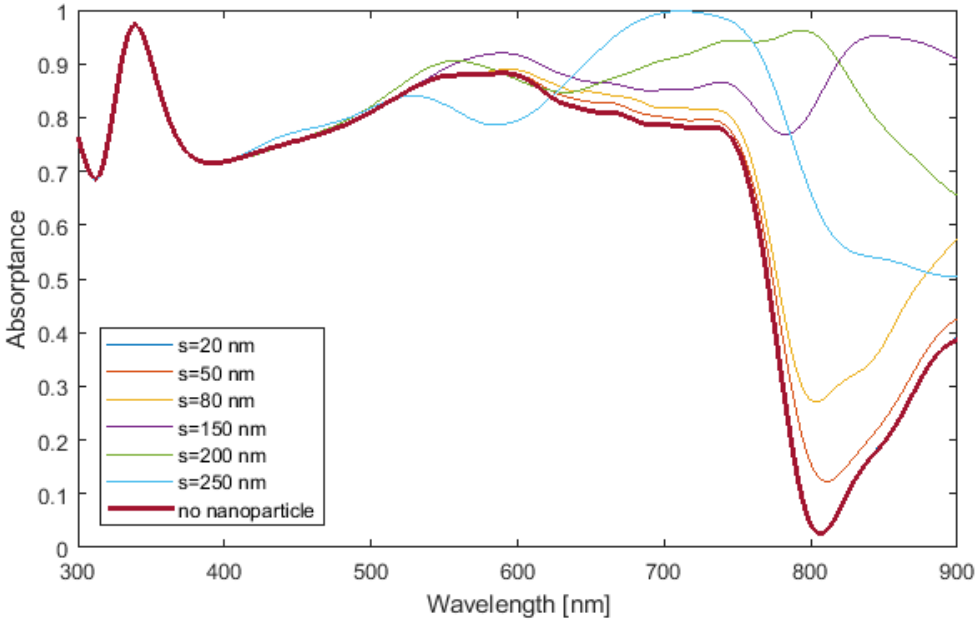

Figure 6.19: Absorptance for the 880 nm PV cell with solid Pt nanocubes with various side lengths included (s is side length). The thick red line is the absorptance of the reference PV cell without nanoparticles.

Nanocube side length [nm]	Reflectance	Transmittance	Absorptance	Absorptance increase $\%\Delta A$
-	0.145	0.184	0.671	-
20	0.145	0.183	0.672	0.149%
50	0.145	0.166	0.689	2.68%
80	0.151	0.126	0.723	7.75%
150	0.129	0.028	0.843	25.6%
200	0.158	0.003	0.839	25.0%
250	0.209	0.001	0.790	17.7%

Table 6.18: Total reflectance, transmittance and absorptance for the 880 nm PV cell with Pt nanocubes with various side lengths, as well as the percentage increase in absorptance ($\%\Delta A$) relative to the reference cell. The first row is the reference PV cell without nanocube.

6.11 Solid Gold Rods

This simulation group consists of ten simulations where one solid Au rod (cylinder) is placed at the center of the perovskite layer in the PV cell structure shown in figure 5.2. Five simulations use the 310 nm PV cell with the rod diameter in the range 20-60 nm, and the other five simulations use the 880 nm PV cell with the rod diameter in the range 20-160 nm. The length of all rods is equal to three times the diameter of that same rod (e.g. d=20 nm and L=60 nm). This means that the aspect ratio, i.e. the ratio between length and diameter given by L/d, for all the

rods is equal to 3, which was found to be the most beneficial aspect ratio by Tang and co-workers [22].

The absorptance from the simulations using the 310 nm PV cell compared to the reference PV cell (without nanoparticles) is shown in figure 6.20, and the same is shown in figure 6.21 for the simulations using the 880 nm PV cell. The total reflectance, transmittance, absorptance and absorptance increase are shown in tables 6.19 and 6.20 for all PV cells.

The results for the 310 nm PV cell shows that the total absorptance increases with increasing rod size, just like it did when spheres and cubes were used. The total absorptance is lower for the nanorods than it was for both nanospheres and nanocubes, but this is most likely due to the fact that the volume of the rods is smaller relative to both the spheres and the cubes.

The results for the 880 nm PV cell show a trend similar to the simulations where nanocubes were used, as described in section 6.7. The absorptance increases with increasing cube size for the three smallest cubes, but then it drops from the third rod to the fourth and it drops again from the fourth to the fifth. However, the drop is much smaller than it was in the case of nanocubes. The total absorptance decreases from 0.791 for the third rod to 0.772 for the fifth rod, so it could be argued that this more resembles a flattening out than a clear drop. Nonetheless, judging by the simulations in this thesis, Au nanorods seem to result in maximum absorptance around a rod size of d=80 nm and L=240 nm for the 880 nm PV cell, and a further increase in the size of the nanorod will slightly reduce the absorptance instead of increase it.

Nanorod dimensions [nm]	Reflectance	Transmittance	Absorptance	Absorptance increase $\%\Delta A$
-	0.189	0.280	0.531	-
d=20, L=60	0.187	0.277	0.536	0.942%
d=30, L=90	0.185	0.269	0.546	2.82%
d=40, L=120	0.182	0.248	0.570	7.34%
d=50, L=150	0.182	0.214	0.604	13.7%
d=60, L=180	0.190	0.178	0.632	19.0%

Table 6.19: Total reflectance, transmittance and absorptance for the 310 nm PV cell with Au nanorods with various diameters and lengths, as well as the percentage increase in absorptance ($\%\Delta A$) relative to the reference cell. The first row is the reference PV cell without nanorod.

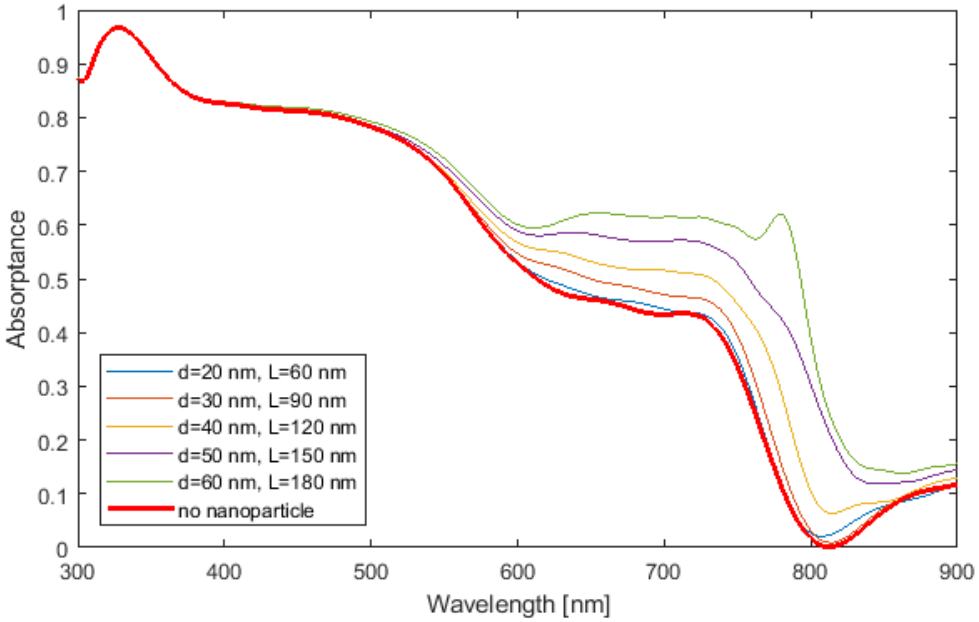

Figure 6.20: Absorptance for the 310 nm PV cell with solid Au nanorods with various diameters and lengths included (d is diameter, L is length). The thick red line is the absorptance of the reference PV cell without nanoparticles.

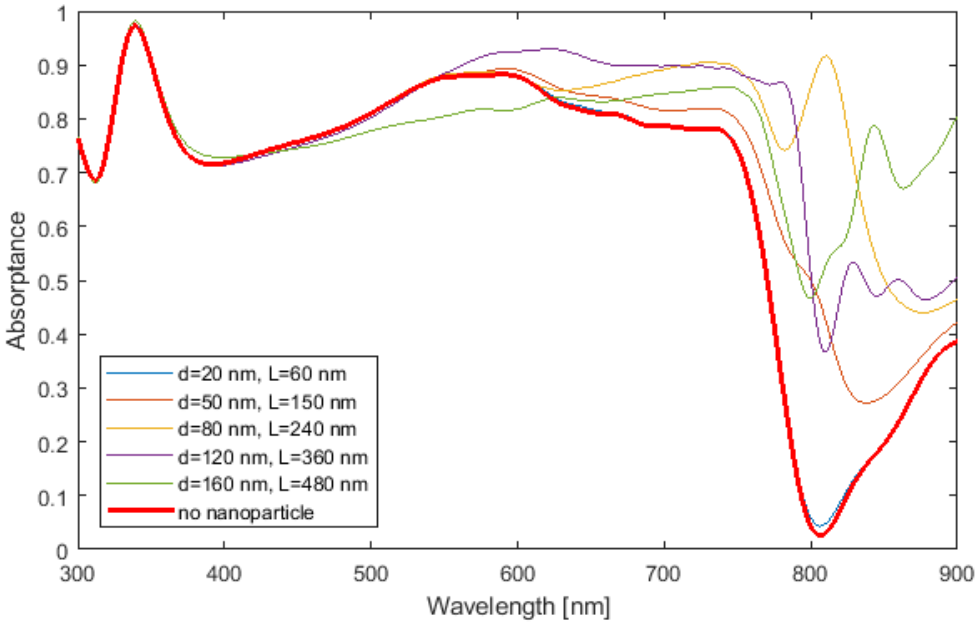

Figure 6.21: Absorptance for the 880 nm PV cell with solid Au nanorods with various diameters and lengths included (d is diameter, L is length). The thick red line is the absorptance of the reference PV cell without nanoparticles.

Nanorod dimensions [nm]	Reflectance	Transmittance	Absorptance	Absorptance increase $\%\Delta A$
-	0.145	0.184	0.671	-
d=20, L=60	0.145	0.182	0.673	0.298%
d=50, L=150	0.142	0.135	0.723	7.75%
d=80, L=240	0.159	0.051	0.790	17.7%
d=120, L=360	0.183	0.040	0.777	15.8%
d=160, L=480	0.191	0.037	0.772	15.1%

Table 6.20: Total reflectance, transmittance and absorptance for the 880 nm PV cell with Au nanorods with various diameters and lengths, as well as the percentage increase in absorptance ($\%\Delta A$) relative to the reference cell. The first row is the reference PV cell without nanorod.

6.12 Solid Silver Rods

This simulation group consists of ten simulations where one solid Ag rod (cylinder) is placed at the center of the perovskite layer in the PV cell structure shown in figure 5.2. Five simulations use the 310 nm PV cell with the rod diameter in the range 20-60 nm, and the other five simulations use the 880 nm PV cell with the rod diameter in the range 20-160 nm. The length of all rods is equal to three times the diameter of that same rod (e.g. d=20 nm and L=60 nm). This means that the aspect ratio, i.e. the ratio between length and diameter given by L/d, for all the rods is equal to 3, which was found to be the most beneficial aspect ratio by Tang and co-workers [22].

The absorptance from the simulations using the 310 nm PV cell compared to the reference PV cell (without nanoparticles) is shown in figure 6.22, and the same is shown in figure 6.23 for the simulations using the 880 nm PV cell. The total reflectance, transmittance, absorptance and absorptance increase are shown in tables 6.21 and 6.22 for all PV cells. The general trend in the results is the same as it was when Au nanorods were used, as described in section 6.11. The values for total absorptance are also approximately the same for Au and Ag nanorods, only slightly lower for Ag. Therefore, judging from the simulations performed in this thesis, both Au and Ag nanorods have approximately the same positive effect on the PV cells.

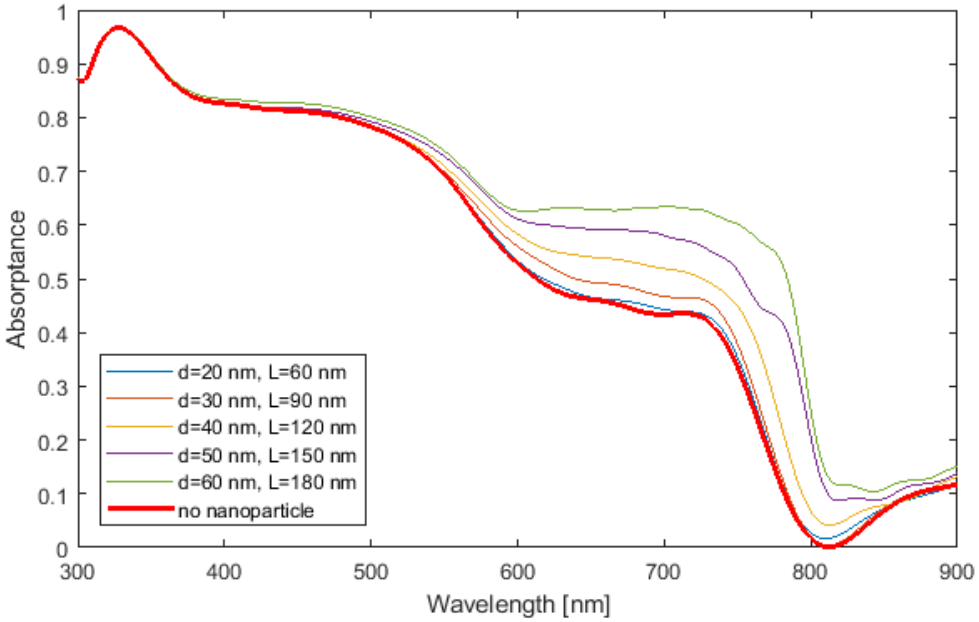

Figure 6.22: Absorptance for the 310 nm PV cell with solid Ag nanorods with various diameters and lengths included (d is diameter, L is length). The thick red line is the absorptance of the reference PV cell without nanoparticles.

Nanorod dimensions [nm]	Reflectance	Transmittance	Absorptance	Absorptance increase $\%\Delta A$
-	0.189	0.280	0.531	-
d=20, L=60	0.187	0.277	0.536	0.942%
d=30, L=90	0.185	0.271	0.544	2.45%
d=40, L=120	0.183	0.251	0.566	6.59%
d=50, L=150	0.183	0.217	0.600	13.0%
d=60, L=180	0.190	0.183	0.627	18.1%

Table 6.21: Total reflectance, transmittance and absorptance for the 310 nm PV cell with Ag nanorods with various diameters and lengths, as well as the percentage increase in absorptance ($\%\Delta A$) relative to the reference cell. The first row is the reference PV cell without nanorod.

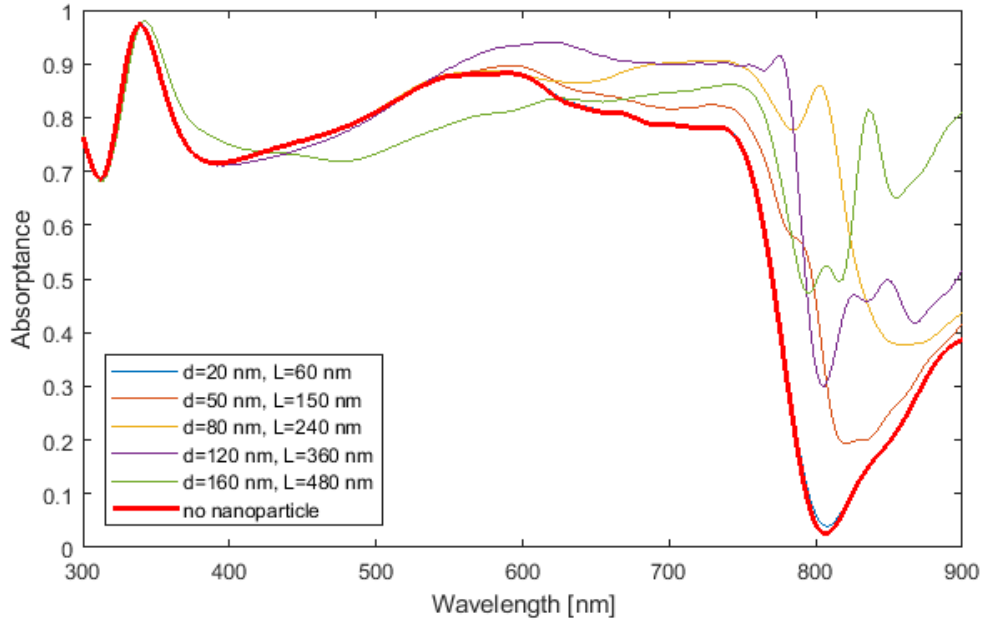

Figure 6.23: Absorptance for the 880 nm PV cell with solid Ag nanorods with various diameters and lengths included (d is diameter, L is length). The thick red line is the absorptance of the reference PV cell without nanoparticles.

Nanorod dimensions [nm]	Reflectance	Transmittance	Absorptance	Absorptance increase $\%\Delta A$
-	0.145	0.184	0.671	-
d=20, L=60	0.145	0.182	0.673	0.298%
d=50, L=150	0.144	0.142	0.714	6.41%
d=80, L=240	0.168	0.056	0.776	15.6%
d=120, L=360	0.191	0.039	0.770	14.8%
d=160, L=480	0.196	0.037	0.767	14.3%

Table 6.22: Total reflectance, transmittance and absorptance for the 880 nm PV cell with Ag nanorods with various diameters and lengths, as well as the percentage increase in absorptance ($\%\Delta A$) relative to the reference cell. The first row is the reference PV cell without nanorod.

6.13 Solid Aluminum Rods

This simulation group consists of ten simulations where one solid Al rod (cylinder) is placed at the center of the perovskite layer in the PV cell structure shown in figure 5.2. Five simulations use the 310 nm PV cell with the rod diameter in the range 20-60 nm, and the other five simulations use the 880 nm PV cell with the rod diameter in the range 20-160 nm. The length of all rods is equal to three times the diameter of that same rod (e.g. d=20 nm and L=60 nm). This means that the

aspect ratio, i.e. the ratio between length and diameter given by L/d, for all the rods is equal to 3, which was found to be the most beneficial aspect ratio by Tang and co-workers [22].

The absorptance from the simulations using the 310 nm PV cell compared to the reference PV cell (without nanoparticles) is shown in figure 6.24, and the same is shown in figure 6.25 for the simulations using the 880 nm PV cell. The total reflectance, transmittance, absorptance and absorptance increase are shown in tables 6.23 and 6.24 for all PV cells.

The general trend in the results for the 310 nm PV cell is the same as it was when Au nanorods were used, as described in section 6.11. However, the absorptance does not increase as much when Al is used compared to Au, so the total absorptance of the two largest rods is significantly lower for Al than it is for Au.

The results for the 880 nm PV cell with Al nanorods show some quite interesting differences compared to the results when Au and Ag is used. Both Au and Ag resulted in maximum absorptance for the PV cell with the third largest nanorod and then the absorptance decreased slightly for the two largest nanorods. When Al is used, the total absorptance increases with increasing size throughout all five simulations, resulting in a significantly higher absorptance for the two largest nanorods when Al is used compared to Au and Ag. Therefore, judging from the simulations in this thesis, Au results in higher total absorptance than Al for the 310 nm PV cell and for the three smallest nanorods in the 880 nm PV cell, but Al results in higher total absorptance for the two largest nanorods in the 880 nm PV cell.

Nanorod dimensions [nm]	Reflectance	Transmittance	Absorptance	Absorptance increase $\%\Delta A$
-	0.189	0.280	0.531	-
d=20, L=60	0.188	0.279	0.533	0.377%
d=30, L=90	0.185	0.278	0.537	1.13%
d=40, L=120	0.184	0.269	0.547	3.01%
d=50, L=150	0.186	0.250	0.564	6.21%
d=60, L=180	0.196	0.227	0.577	8.66%

Table 6.23: Total reflectance, transmittance and absorptance for the 310 nm PV cell with Al nanorods with various diameters and lengths, as well as the percentage increase in absorptance ($\%\Delta A$) relative to the reference cell. The first row is the reference PV cell without nanorod.

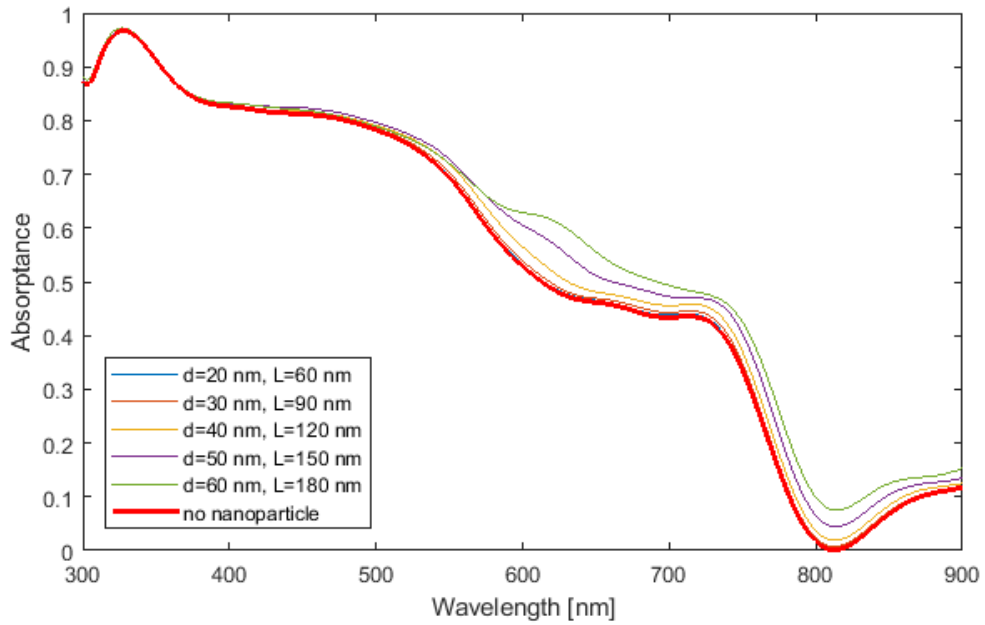

Figure 6.24: Absorptance for the 310 nm PV cell with solid Al nanorods with various diameters and lengths included (d is diameter, L is length). The thick red line is the absorptance of the reference PV cell without nanoparticles.

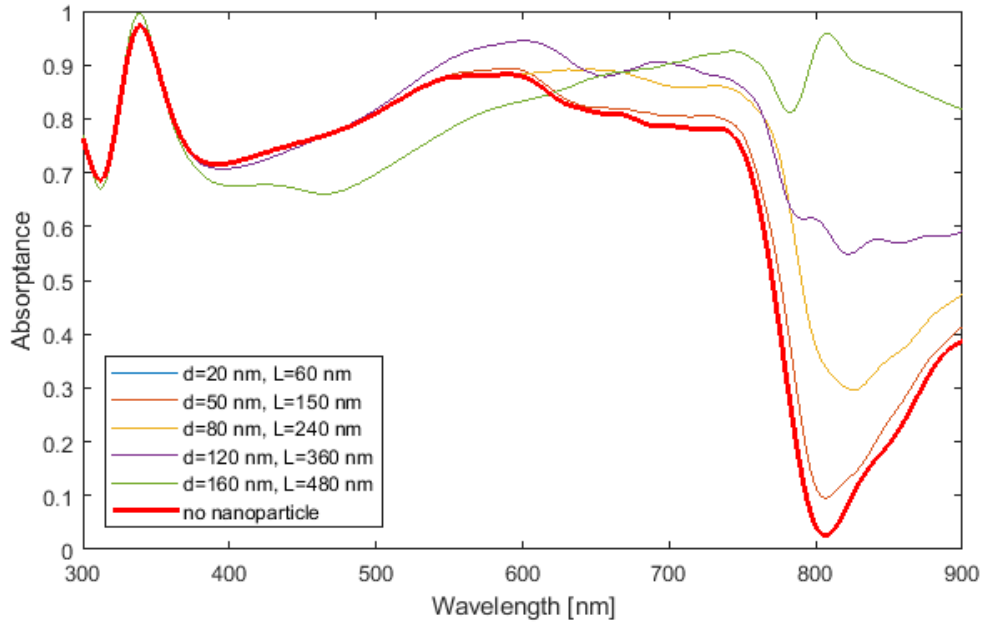

Figure 6.25: Absorptance for the 880 nm PV cell with solid Al nanorods with various diameters and lengths included (d is diameter, L is length). The thick red line is the absorptance of the reference PV cell without nanoparticles.

Nanorod dimensions [nm]	Reflectance	Transmittance	Absorptance	Absorptance increase $\%\Delta A$
-	0.145	0.184	0.671	-
d=20, L=60	0.145	0.183	0.672	0.149%
d=50, L=150	0.144	0.167	0.689	2.68%
d=80, L=240	0.153	0.108	0.739	10.1%
d=120, L=360	0.166	0.047	0.787	17.3%
d=160, L=480	0.157	0.030	0.813	21.2%

Table 6.24: Total reflectance, transmittance and absorptance for the 880 nm PV cell with Al nanorods with various diameters and lengths, as well as the percentage increase in absorptance ($\%\Delta A$) relative to the reference cell. The first row is the reference PV cell without nanorod.

6.14 Solid Platinum Rods

This simulation group consists of ten simulations where one solid Pt rod (cylinder) is placed at the center of the perovskite layer in the PV cell structure shown in figure 5.2. Five simulations use the 310 nm PV cell with the rod diameter in the range 20-60 nm, and the other five simulations use the 880 nm PV cell with the rod diameter in the range 20-160 nm. The length of all rods is equal to three times the diameter of that same rod (e.g. d=20 nm and L=60 nm). This means that the aspect ratio, i.e. the ratio between length and diameter given by L/d, for all the rods is equal to 3, which was found to be the most beneficial aspect ratio by Tang and co-workers [22].

The absorptance from the simulations using the 310 nm PV cell compared to the reference PV cell (without nanoparticles) is shown in figure 6.26, and the same is shown in figure 6.27 for the simulations using the 880 nm PV cell. The total reflectance, transmittance, absorptance and absorptance increase are shown in tables 6.25 and 6.26 for all PV cells. The general trend in the results is the same as it was when Al nanorods were used, as described in section 6.13. However, the total absorptance is higher when Pt is used compared to when Al is used. Of the four metals (Au, Ag, Al, Pt) used as material for the centered solid nanorods in this thesis, Au shows the highest total absorptance for all rod sizes, except for the two largest rods in the 880 nm PV cell. For those rods, Pt shows the highest absorptance.

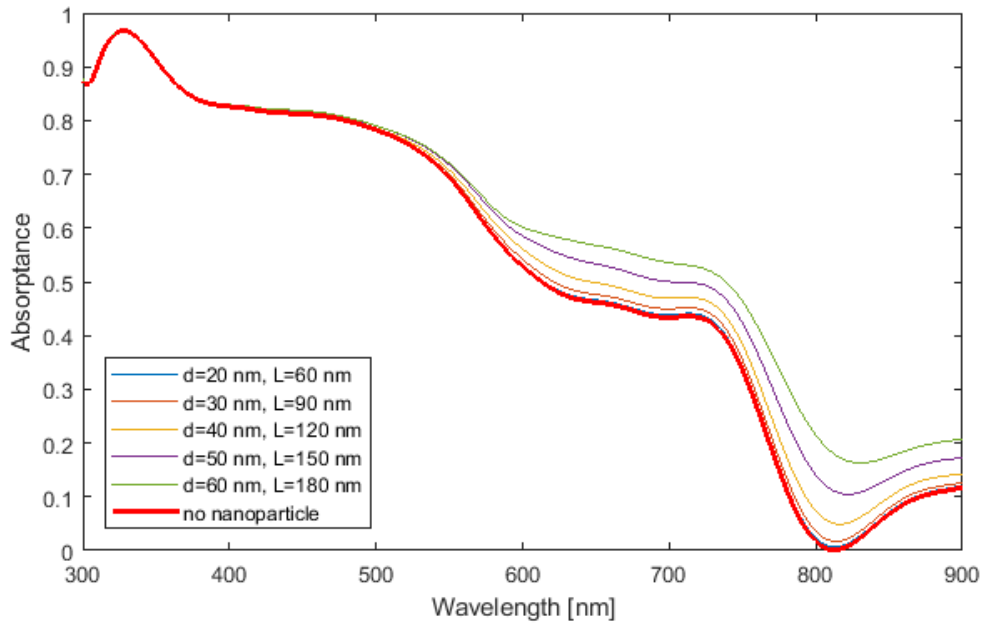

Figure 6.26: Absorptance for the 310 nm PV cell with solid Pt nanorods with various diameters and lengths included (d is diameter, L is length). The thick red line is the absorptance of the reference PV cell without nanoparticles.

Nanorod dimensions [nm]	Reflectance	Transmittance	Absorptance	Absorptance increase $\%\Delta A$
-	0.189	0.280	0.531	-
d=20, L=60	0.188	0.278	0.534	0.565%
d=30, L=90	0.186	0.274	0.540	1.69%
d=40, L=120	0.184	0.262	0.554	4.33%
d=50, L=150	0.184	0.240	0.576	8.47%
d=60, L=180	0.188	0.213	0.599	12.8%

Table 6.25: Total reflectance, transmittance and absorptance for the 310 nm PV cell with Pt nanorods with various diameters and lengths, as well as the percentage increase in absorptance ($\%\Delta A$) relative to the reference cell. The first row is the reference PV cell without nanorod.

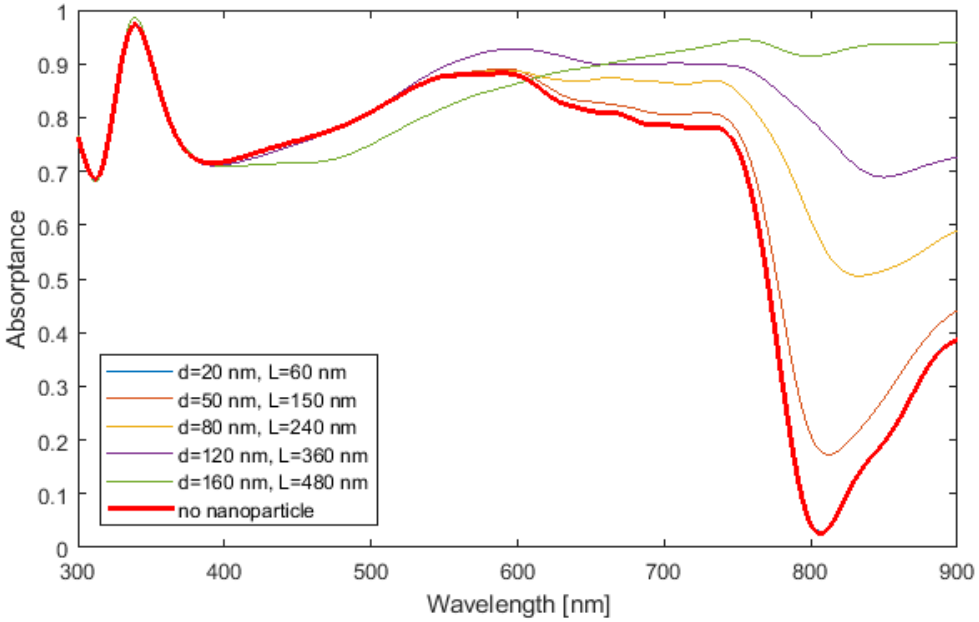

Figure 6.27: Absorptance for the 880 nm PV cell with solid Pt nanorods with various diameters and lengths included (d is diameter, L is length). The thick red line is the absorptance of the reference PV cell without nanoparticles.

Nanorod dimensions [nm]	Reflectance	Transmittance	Absorptance	Absorptance increase $\%\Delta A$
-	0.145	0.184	0.671	-
d=20, L=60	0.145	0.183	0.672	0.149%
d=50, L=150	0.143	0.157	0.700	4.32%
d=80, L=240	0.140	0.088	0.772	15.1%
d=120, L=360	0.153	0.025	0.822	22.5%
d=160, L=480	0.144	0.007	0.849	26.5%

Table 6.26: Total reflectance, transmittance and absorptance for the 880 nm PV cell with Pt nanorods with various diameters and lengths, as well as the percentage increase in absorptance ($\%\Delta A$) relative to the reference cell. The first row is the reference PV cell without nanorod.

6.15 Solid Gold Pyramids

This simulation group consists of twelve simulations where one solid Au pyramid is placed at the center of the perovskite layer in the PV cell structure shown in figure 5.2. Six simulations use the 310 nm PV cell with the side length and height in the range 20-150 nm, and the other six simulations use the 880 nm PV cell with the side length and height in the range 20-250 nm. The height h is equal to the side length s for all pyramids.

The absorptance from the simulations using the 310 nm PV cell compared to the reference PV cell (without nanoparticles) is shown in figure 6.28, and the same is shown in figure 6.29 for the simulations using the 880 nm PV cell. The total reflectance, transmittance, absorptance and absorptance increase are shown in tables 6.27 and 6.28 for all PV cells.

The general trend in the results is the same as it was when Au nanospheres were used, as described in section 6.3. The total absorptance of the PV cells increase with increasing pyramid size, both for the 310 and 880 nm PV cells. If the diameter of a sphere is equal to the side length and height of a pyramid, then the sphere will have a volume that is approximately 1.57 times higher than the volume of the pyramid. This is reflected in the fact that the total absorptance is higher for the Au spheres than it is for the Au pyramids when the diameter of the sphere is equal to the side length and the height of the pyramid. However, the two exceptions to this trend are the two largest pyramids in the 880 nm PV cell. Even though they have a smaller volume than the two largest spheres, the PV cells with pyramids show an absorptance that is higher than the absorptance of the PV cells with spheres. This indicates that it might be beneficial to use Au pyramids instead of Au spheres for the largest nanoparticles in the 880 nm PV cell.

Nanopyramid dimensions [nm]	Reflectance	Transmittance	Absorptance	Absorptance increase $\%\Delta A$
-	0.189	0.280	0.531	-
s=20, h=20	0.189	0.278	0.533	0.377%
s=30, h=30	0.189	0.277	0.534	0.565%
s=50, h=50	0.191	0.263	0.546	2.82%
s=75, h=75	0.197	0.241	0.562	5.84%
s=100, h=100	0.203	0.214	0.583	9.79%
s=150, h=150	0.207	0.144	0.649	22.2%

Table 6.27: Total reflectance, transmittance and absorptance for the 310 nm PV cell with Au nanopyramids with various side lengths and heights, as well as the percentage increase in absorptance ($\%\Delta A$) relative to the reference cell. The first row is the reference PV cell without nanopyramid.

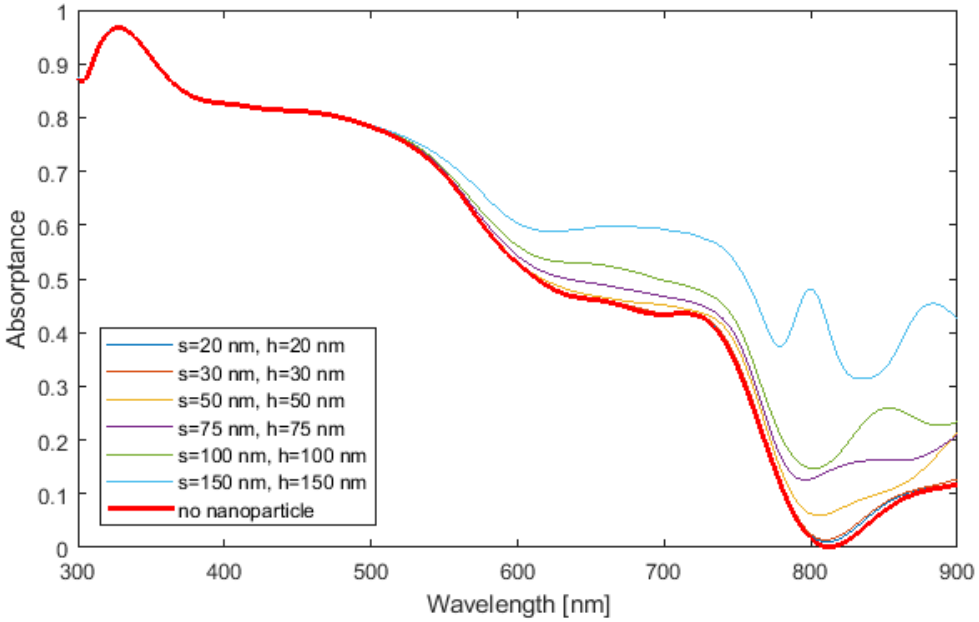

Figure 6.28: Absorptance for the 310 nm PV cell with solid Au nanopyramids with various side lengths and heights included (s is side length, h is height). The thick red line is the absorptance of the reference PV cell without nanoparticles.

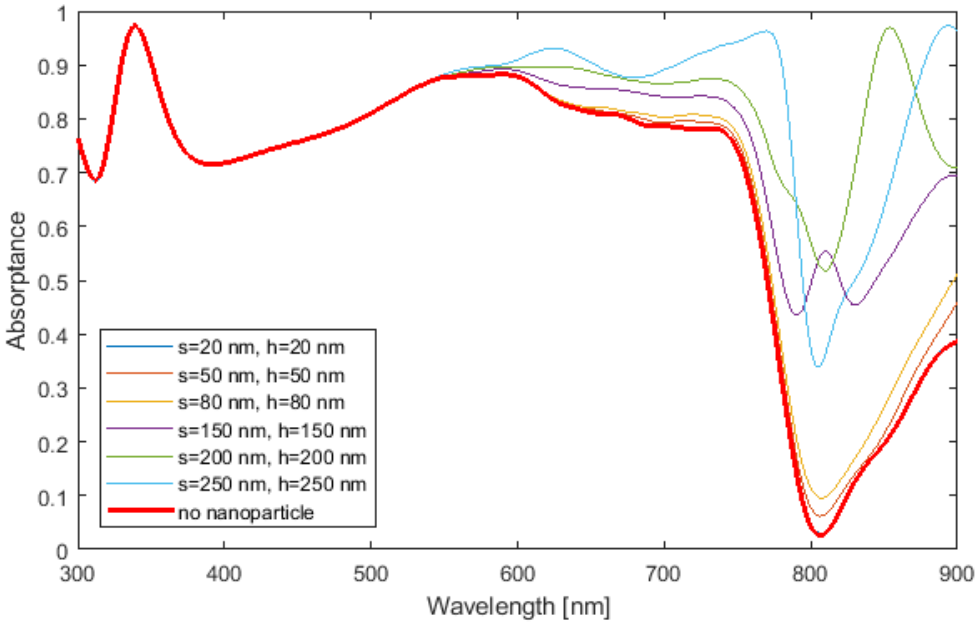

Figure 6.29: Absorptance for the 880 nm PV cell with solid Au nanopyramids with various side lengths and heights included (s is side length, h is height). The thick red line is the absorptance of the reference PV cell without nanoparticles.

Nanopyramid dimensions [nm]	Reflectance	Transmittance	Absorptance	Absorptance increase $\%\Delta A$
-	0.145	0.184	0.671	-
s=20, h=20	0.145	0.182	0.673	0.298%
s=50, h=50	0.147	0.173	0.680	1.34%
s=80, h=80	0.146	0.162	0.692	3.13%
s=150, h=150	0.138	0.101	0.761	13.4%
s=200, h=200	0.148	0.042	0.810	20.7%
s=250, h=250	0.181	0.008	0.811	20.9%

Table 6.28: Total reflectance, transmittance and absorptance for the 880 nm PV cell with Au nanopyramids with various side lengths and heights, as well as the percentage increase in absorptance ($\%\Delta A$) relative to the reference cell. The first row is the reference PV cell without nanopyramid.

6.16 Solid Silver Pyramids

This simulation group consists of twelve simulations where one solid Ag pyramid is placed at the center of the perovskite layer in the PV cell structure shown in figure 5.2. Six simulations use the 310 nm PV cell with the side length and height in the range 20-150 nm, and the other six simulations use the 880 nm PV cell with the side length and height in the range 20-250 nm. The height h is equal to the side length s for all pyramids.

The absorptance from the simulations using the 310 nm PV cell compared to the reference PV cell (without nanoparticles) is shown in figure 6.30, and the same is shown in figure 6.31 for the simulations using the 880 nm PV cell. The total reflectance, transmittance, absorptance and absorptance increase are shown in tables 6.29 and 6.30 for all PV cells. The general trend in the results is the same as it was when Au nanopyramids were used, as described in section 6.15. The values for total absorptance are also approximately the same for Au and Ag nanopyramids. Therefore, judging from the simulations performed in this thesis, both Au and Ag nanopyramids have approximately the same positive effect on the PV cells.

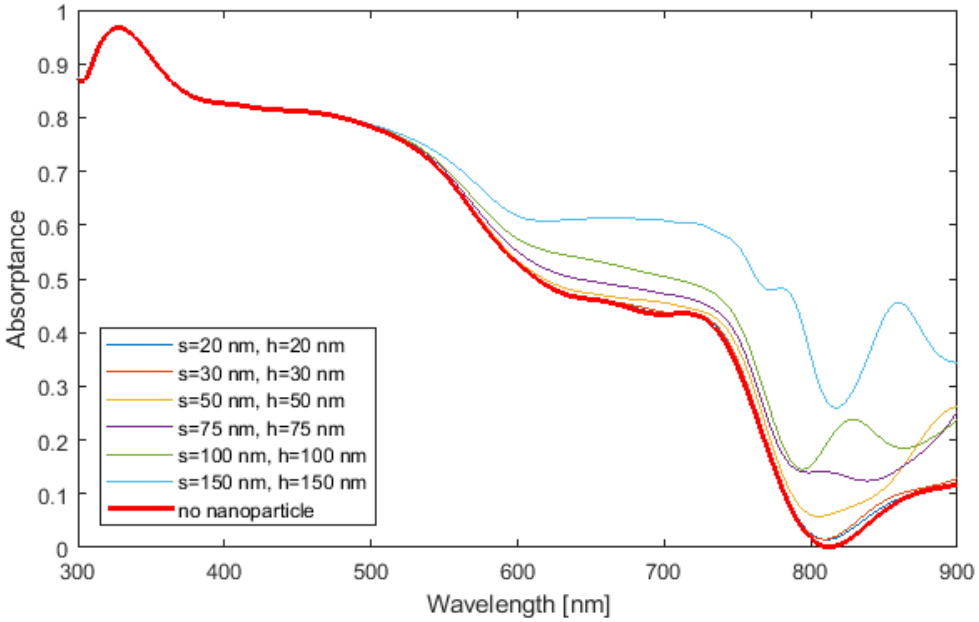

Figure 6.30: Absorptance for the 310 nm PV cell with solid Ag nanopyramids with various side lengths and heights included (s is side length, h is height). The thick red line is the absorptance of the reference PV cell without nanoparticles.

Nanopyramid dimensions [nm]	Reflectance	Transmittance	Absorptance	Absorptance increase $\%\Delta A$
-	0.189	0.280	0.531	-
s=20, h=20	0.189	0.278	0.533	0.377%
s=30, h=30	0.189	0.276	0.535	0.753%
s=50, h=50	0.191	0.258	0.551	3.77%
s=75, h=75	0.200	0.236	0.564	6.21%
s=100, h=100	0.206	0.210	0.584	9.98%
s=150, h=150	0.209	0.138	0.653	23.0%

Table 6.29: Total reflectance, transmittance and absorptance for the 310 nm PV cell with Ag nanopyramids with various side lengths and heights, as well as the percentage increase in absorptance ($\%\Delta A$) relative to the reference cell. The first row is the reference PV cell without nanopyramid.

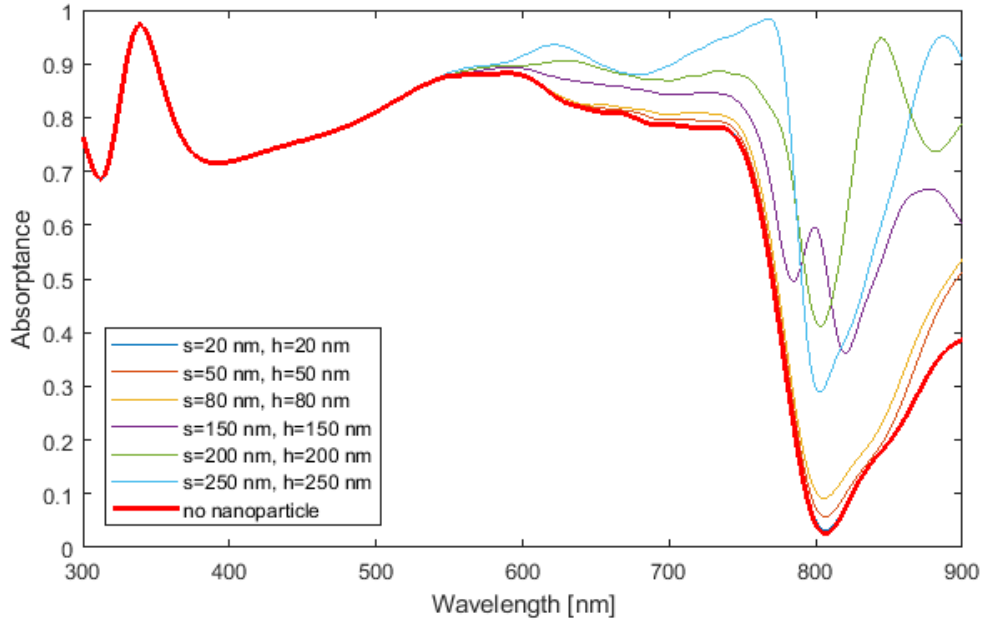

Figure 6.31: Absorptance for the 880 nm PV cell with solid Ag nanopyramids with various side lengths and heights included (s is side length, h is height). The thick red line is the absorptance of the reference PV cell without nanoparticles.

Nanopyramid dimensions [nm]	Reflectance	Transmittance	Absorptance	Absorptance increase $\%\Delta A$
-	0.145	0.184	0.671	-
s=20, h=20	0.145	0.182	0.673	0.298%
s=50, h=50	0.147	0.169	0.684	1.94%
s=80, h=80	0.147	0.159	0.694	3.43%
s=150, h=150	0.137	0.100	0.763	13.7%
s=200, h=200	0.155	0.036	0.809	20.6%
s=250, h=250	0.188	0.005	0.807	20.3%

Table 6.30: Total reflectance, transmittance and absorptance for the 880 nm PV cell with Ag nanopyramids with various side lengths and heights, as well as the percentage increase in absorptance ($\%\Delta A$) relative to the reference cell. The first row is the reference PV cell without nanopyramid.

6.17 Solid Aluminum Pyramids

This simulation group consists of twelve simulations where one solid Al pyramid is placed at the center of the perovskite layer in the PV cell structure shown in figure 5.2. Six simulations use the 310 nm PV cell with the side length and height in the range 20-150 nm, and the other six simulations use the 880 nm PV cell with the side length and height in the range 20-250 nm. The height h is equal to the side length s for all pyramids.

The absorptance from the simulations using the 310 nm PV cell compared to the reference PV cell (without nanoparticles) is shown in figure 6.32, and the same is shown in figure 6.33 for the simulations using the 880 nm PV cell. The total reflectance, transmittance, absorptance and absorptance increase are shown in tables 6.31 and 6.32 for all PV cells. The general trend in the results is the same as it was when Au nanopyramids were used, as described in section 6.15. However, in the majority of the simulations the values for total absorptance are higher when Al is used. This is particularly noticeable for the two largest nanopyramids in both the 310 and 880 nm PV cells, where the Al nanopyramids result in a significantly higher absorptance than the Au nanopyramids. Therefore, judging from the simulations performed in this thesis, Al is actually a better choice than Au and Ag for medium and large sized nanoparticles, if the nanoparticles are shaped like pyramids.

Nanopyramid dimensions [nm]	Reflectance	Transmittance	Absorptance	Absorptance increase $\%\Delta A$
-	0.189	0.280	0.531	-
s=20, h=20	0.189	0.279	0.532	0.188%
s=30, h=30	0.188	0.278	0.534	0.565%
s=50, h=50	0.185	0.267	0.548	3.20%
s=75, h=75	0.187	0.229	0.584	9.98%
s=100, h=100	0.208	0.175	0.617	16.2%
s=150, h=150	0.244	0.093	0.663	24.9%

Table 6.31: Total reflectance, transmittance and absorptance for the 310 nm PV cell with Al nanopyramids with various side lengths and heights, as well as the percentage increase in absorptance ($\%\Delta A$) relative to the reference cell. The first row is the reference PV cell without nanopyramid.

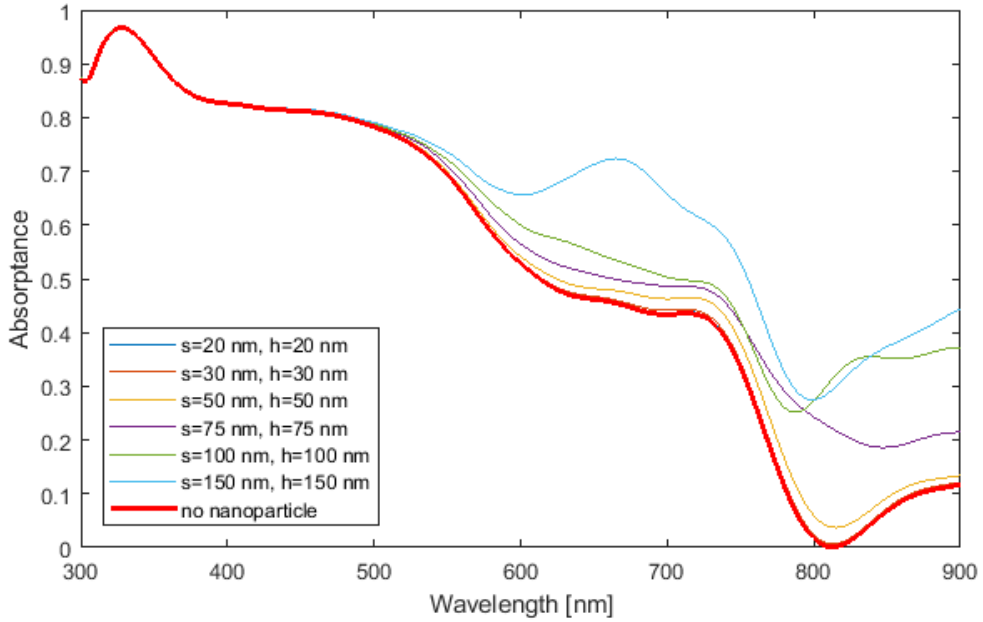

Figure 6.32: Absorptance for the 310 nm PV cell with solid Al nanopyramids with various side lengths and heights included (s is side length, h is height). The thick red line is the absorptance of the reference PV cell without nanoparticles.

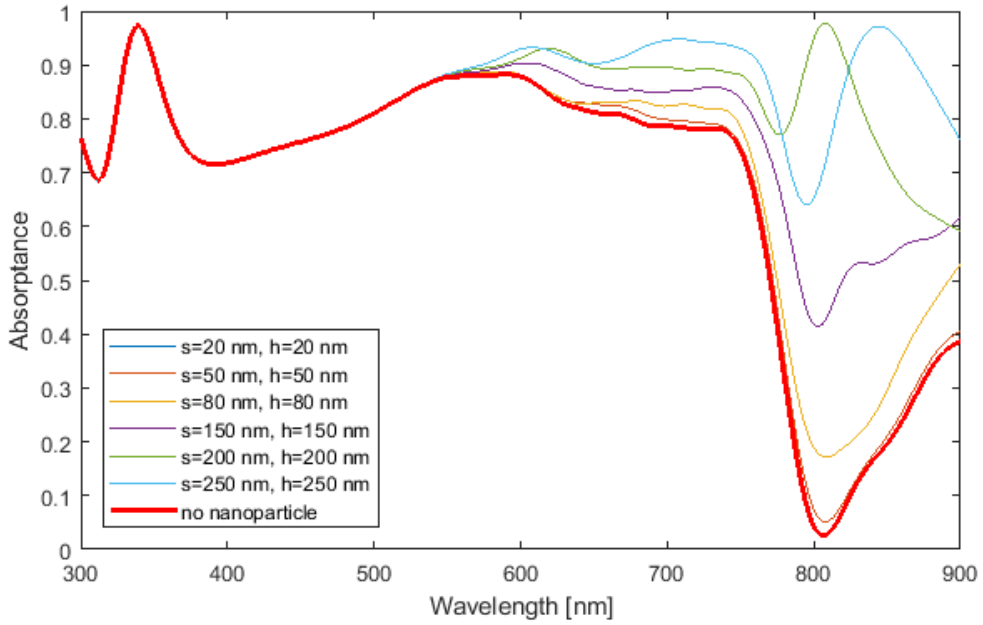

Figure 6.33: Absorptance for the 880 nm PV cell with solid Al nanopyramids with various side lengths and heights included (s is side length, h is height). The thick red line is the absorptance of the reference PV cell without nanoparticles.

Nanopyramid dimensions [nm]	Reflectance	Transmittance	Absorptance	Absorptance increase $\%\Delta A$
-	0.145	0.184	0.671	-
s=20, h=20	0.145	0.184	0.671	0.00%
s=50, h=50	0.146	0.175	0.679	1.19%
s=80, h=80	0.156	0.139	0.705	5.07%
s=150, h=150	0.166	0.070	0.764	13.9%
s=200, h=200	0.161	0.015	0.824	22.8%
s=250, h=250	0.147	0.005	0.848	26.4%

Table 6.32: Total reflectance, transmittance and absorptance for the 880 nm PV cell with Al nanopyramids with various side lengths and heights, as well as the percentage increase in absorptance ($\%\Delta A$) relative to the reference cell. The first row is the reference PV cell without nanopyramid.

6.18 Solid Platinum Pyramids

This simulation group consists of twelve simulations where one solid Pt pyramid is placed at the center of the perovskite layer in the PV cell structure shown in figure 5.2. Six simulations use the 310 nm PV cell with the side length and height in the range 20-150 nm, and the other six simulations use the 880 nm PV cell with the side length and height in the range 20-250 nm. The height h is equal to the side length s for all pyramids.

The absorptance from the simulations using the 310 nm PV cell compared to the reference PV cell (without nanoparticles) is shown in figure 6.34, and the same is shown in figure 6.35 for the simulations using the 880 nm PV cell. The total reflectance, transmittance, absorptance and absorptance increase are shown in tables 6.33 and 6.34 for all PV cells. The general trend in the results is the same as it was when Al nanopyramids were used, as described in section 6.17. The total absorptance is a bit lower in all simulations when Pt is used compared to Al, except for the two largest pyramids in the 880 nm PV cell. In these two simulations, Pt nanopyramids result in the highest absorptance. Of the four metals (Au, Ag, Al, Pt) used as material for the centered solid nanopyramids in this thesis, Al results in the highest absorptance for medium and large pyramid sizes (except for the two pyramids mentioned above where Pt is better), while all four metals yield similar results for small pyramid sizes.

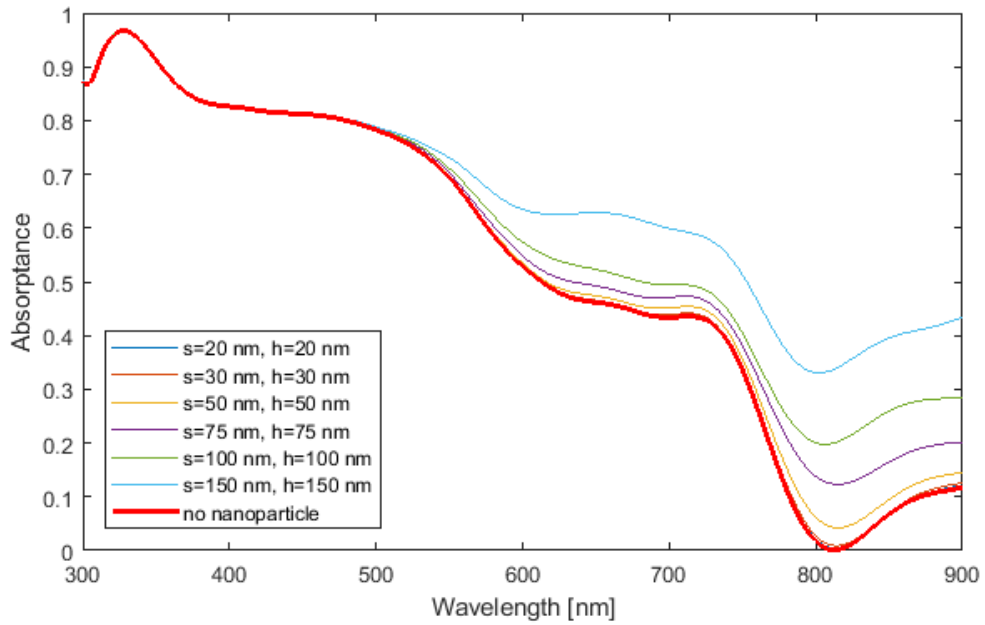

Figure 6.34: Absorptance for the 310 nm PV cell with solid Pt nanopyramids with various side lengths and heights included (s is side length, h is height). The thick red line is the absorptance of the reference PV cell without nanoparticles.

Nanopyramid dimensions [nm]	Reflectance	Transmittance	Absorptance	Absorptance increase $\%\Delta A$
-	0.189	0.280	0.531	-
s=20, h=20	0.189	0.279	0.532	0.188%
s=30, h=30	0.189	0.278	0.533	0.377%
s=50, h=50	0.187	0.269	0.544	2.45%
s=75, h=75	0.189	0.246	0.565	6.40%
s=100, h=100	0.197	0.212	0.591	11.3%
s=150, h=150	0.210	0.137	0.653	23.0%

Table 6.33: Total reflectance, transmittance and absorptance for the 310 nm PV cell with Pt nanopyramids with various side lengths and heights, as well as the percentage increase in absorptance ($\%\Delta A$) relative to the reference cell. The first row is the reference PV cell without nanopyramid.

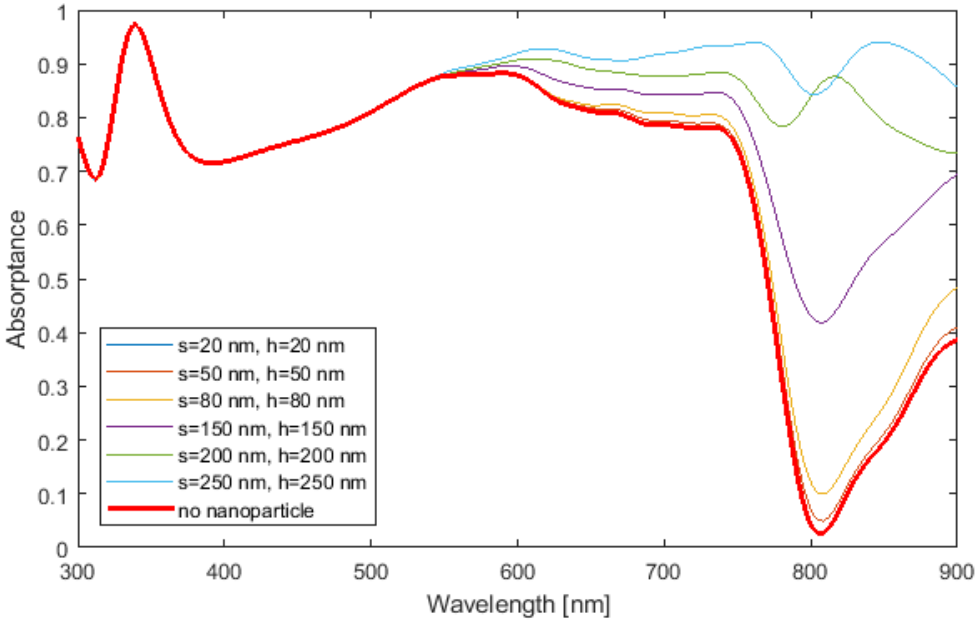

Figure 6.35: Absorptance for the 880 nm PV cell with solid Pt nanopyramids with various side lengths and heights included (s is side length, h is height). The thick red line is the absorptance of the reference PV cell without nanoparticles.

Nanopyramid dimensions [nm]	Reflectance	Transmittance	Absorptance	Absorptance increase $\%\Delta A$
-	0.145	0.184	0.671	-
s=20, h=20	0.145	0.184	0.671	0.00%
s=50, h=50	0.146	0.176	0.678	1.04%
s=80, h=80	0.149	0.158	0.693	3.28%
s=150, h=150	0.147	0.091	0.762	13.6%
s=200, h=200	0.140	0.032	0.828	23.4%
s=250, h=250	0.134	0.005	0.861	28.3%

Table 6.34: Total reflectance, transmittance and absorptance for the 880 nm PV cell with Pt nanopyramids with various side lengths and heights, as well as the percentage increase in absorptance ($\%\Delta A$) relative to the reference cell. The first row is the reference PV cell without nanopyramid.

6.19 Gold Sphere Variations

This simulation group consists of twelve simulations with Au nanospheres integrated in the PV cell structures. Different variations of spheres are used to compare the effect of these to the standard setup with a solid Au sphere at the center of the perovskite layer (section 6.3). The variations are:

- Au@SiO_2 core-shell nanosphere (Au core and SiO_2 shell). Two different sizes are used and compared to the regular solid Au nanospheres of the same sizes.

The thickness of the SiO_2 shell is set to 10% of the Au sphere diameter in both cases.

- A solid Au nanosphere at the interface between the perovskite layer and the spiro-OMeTAD (bottom), and a solid Au nanosphere at the interface between the perovskite layer and the TiO_2 layer (top). These are simulated separately and both are compared to the centered sphere of the same size.

- Two solid Au gold nanospheres in the same simulation. First, the two spheres are placed side by side in the middle of the perovskite layer. Then, the two spheres are placed one above the other (over/under), and the spheres are placed at equal distances from the center of the perovskite layer. The diameter of these two spheres is set so that the combined volume of the two spheres is equal to the volume of one of the centered spheres from section 6.3. Thus, the simulations with a double set of spheres can be combared to the simulation with a single sphere of equal total volume as the two spheres. The gap between the two spheres is set to 20% of the sphere diameter.

These variations are first simulated through six simulations using the 310 nm PV cell, and then the same variations are simulated through six simulations using the 880 nm PV cell. The absorptance from the simulations using the core-shell variations in the 310 nm PV cell compared to the PV cell with a standard setup Au sphere (from section 6.3) is shown in figure 6.36a, and the absorptance from the simulations using the top vs. bottom and double nanosphere variations in the 310 nm PV cell compared to the PV cell with a standard setup Au sphere (from section 6.3) is shown in figure 6.36b. The same absorptance plots from the simulations using the 880 nm PV cell is shown in figures 6.37a and 6.37b. The total reflectance, transmittance, absorptance and absorptance change are shown in tables 6.35 and 6.36 for all PV cells. The absorptance change for these simulations is given relative to the standard setup PV cell with a Au sphere at the center of the perovskite layer (section 6.3).

The simulation setup described above for this simulation group will be used for the next fifteen simulation groups as well. The only changes made will be the material (Au, Ag, Al, Pt) and the shape of the nanoparticle (sphere, cube, rod, pyramid). Therefore, a detailed description of the setup will not be given in the subsequent sections. Instead, the reader will be referred to the description above.

The simulation results in this group shows that the total absorptance of the PV cells with Au nanospheres decreases if the Au nanospheres are coated with a SiO_2 shell with a thickness of 10% of the sphere diameter, compared to the PV cell where the same Au nanosphere is used with no shell. This is the case for all four core-shell simulations, both in the 310 and 880 nm PV cells. This is mainly due to a large increase in transmittance when the core-shell configuration is used, which could indicate that the SiO_2 shell acts as a shield and cancels out some of the positive plasmonic effects of the Au nanospheres.

The results from the simulations where the position of the Au nanosphere is adjusted and from the simulations where a set of two Au nanospheres is used are different for the 310 and 880 nm PV cells. For the 310 nm PV cell, both the simulation with a Au nanosphere at the perovskite/HTM (bottom) interface and the simulation with a Au nanosphere at the perovskite/ETM (top) interface shows a slight decrease in total absorptance. The same PV cell shows a slight increase in

total absorptance when two nanospheres are placed side by side in the middle of the perovskite layer, and unchanged absorptance when two nanospheres are placed one above the other at equal distance from the middle of the perovskite layer. For the 880 nm PV cell, the simulation with a Au nanosphere at the perovskite/HTM (bottom) interface shows a slight decrease in absorptance, while the absorptance increased for the simulation with a Au nanosphere at the perovskite/ETM (top) interface. The same PV cell shows a slight decrease in total absorptance when two nanospheres are placed side by side in the middle of the perovskite layer, while the absorptance increased when two nanospheres are placed one above the other at equal distance from the middle of the perovskite layer.

Nanosphere properties	Reflectance	Transmittance	Absorptance	Absorptance change $\%\Delta A$
Au, center, d=150nm	0.210	0.083	0.707	-
Au@SiO_2, center, d=150nm, t=15nm	0.174	0.203	0.623	-11.9%
Au, center, d=75nm	0.177	0.219	0.604	-
Au@SiO_2, center, d=75nm, t=7.5nm	0.179	0.263	0.558	-7.62%
Au, bottom, d=75nm	0.208	0.211	0.581	-3.81%
Au, top, d=75nm	0.194	0.210	0.596	-1.32%
2xAu, side by side, d=59.52nm, g=11.90nm	0.183	0.206	0.611	+1.16%
2xAu, over/under, d=59.52nm, g=11.90nm	0.178	0.218	0.604	0.00%

Table 6.35: Total reflectance, transmittance and absorptance for the 310 nm PV cell with Au nanosphere with SiO_2 shell, Au nanosphere at perovskite/HTM interface, Au nanosphere at perovskite/ETM interface, two Au nanospheres side by side, two Au nanospheres over/under, as well as the two PV cells with standard setup Au nanosphere at center. The absorptance change for the various setups is given relative to the two PV cells with standard setup (from section 6.3). d is diameter, t is shell thickness and g is the gap between the two nanospheres.

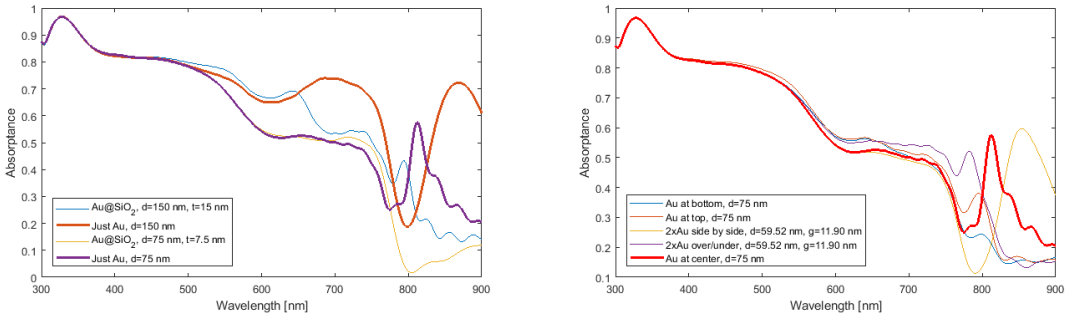

(a) (b)

Figure 6.36: Absorptance for various setups of the 310 nm PV cell. (a) Total absorptance of the Au@SiO_2 core-shell nanospheres (thin lines) compared to the Au sphere of the same size but without a SiO_2 shell (thick lines). d is the diameter of the Au sphere and t is the thickness of the SiO_2 shell. (b)Total absorptance for Au nanosphere at bottom interface, top interface, double nanospheres side by side, double nanospheres over/under, compared to the centered Au nanosphere of the same size (thick line) from section 6.3. d is the diameter of the sphere and g is the gap between the two spheres.

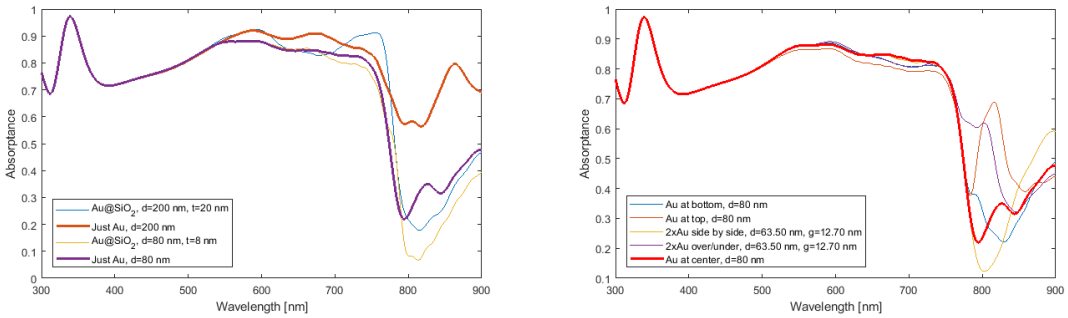

(a) (b)

Figure 6.37: Absorptance for various setups of the 880 nm PV cell. (a) Total absorptance of the Au@SiO_2 core-shell nanospheres (thin lines) compared to the Au sphere of the same size but without a SiO_2 shell (thick lines). d is the diameter of the Au sphere and t is the thickness of the SiO_2 shell. (b)Total absorptance for Au nanosphere at bottom interface, top interface, double nanospheres side by side, double nanospheres over/under, compared to the centered Au nanosphere of the same size (thick line) from section 6.3. d is the diameter of the sphere and g is the gap between the two spheres.

Nanosphere properties	Reflectance	Transmittance	Absorptance	Absorptance change $\%\Delta A$
Au, center, d=200nm	0.143	0.059	0.798	-
Au@SiO_2, center, d=200nm, t=20nm	0.162	0.115	0.723	-9.40%
Au, center, d=80nm	0.158	0.128	0.714	-
Au@SiO_2, center, d=80nm, t=8nm	0.141	0.172	0.687	-3.78%
Au, bottom, d=80nm	0.163	0.126	0.711	-0.420%
Au, top, d=80nm	0.134	0.135	0.731	+2.38%
2xAu, side by side, d=63.50nm, g=12.70nm	0.167	0.120	0.712	-0.280%
2xAu, over/under, d=63.50nm, g=12.70nm	0.141	0.124	0.735	+2.94%

Table 6.36: Total reflectance, transmittance and absorptance for the 880 nm PV cell with Au nanosphere with SiO_2 shell, Au nanosphere at perovskite/HTM interface, Au nanosphere at perovskite/ETM interface, two Au nanospheres side by side, two Au nanospheres over/under, as well as the two PV cells with standard setup Au nanosphere at center. The absorptance change for the various setups is given relative to the two PV cells with standard setup (from section 6.3). d is diameter, t is shell thickness and g is the gap between the two nanospheres.

6.20 Silver Sphere Variations

This simulation group consists of twelve simulations with Ag nanospheres integrated in the PV cell structures. Different variations of spheres are used to compare the effect of these to the standard setup with a solid Ag sphere at the center of the perovskite layer (section 6.4). The variations are the same as described for Au nanospheres in section 6.19. These variations are first simulated through six simulations using the 310 nm PV cell, and then the same variations are simulated through six simulations using the 880 nm PV cell. The absorptance from the simulations using the core-shell variations in the 310 nm PV cell compared to the PV cell with a standard setup Ag sphere (from section 6.4) is shown in figure 6.38a, and the absorptance from the simulations using the top vs. bottom and double nanosphere variations in the 310 nm PV cell compared to the PV cell with a standard setup Ag sphere (from section 6.4) is shown in figure 6.38b. The same absorptance plots from

the simulations using the 880 nm PV cell is shown in figures 6.39a and 6.39b. The total reflectance, transmittance, absorptance and absorptance change are shown in tables 6.37 and 6.38 for all PV cells. The absorptance change for these simulations is given relative to the standard setup PV cell with a Ag sphere at the center of the perovskite layer (section 6.4).

The simulation results shows that the total absorptance of the PV cells with Ag nanospheres decreases if the Ag nanospheres are coated with a SiO_2 shell with a thickness of 10% of the sphere diameter, compared to the PV cell where the same Ag nanosphere is used with no shell. This is the same effect as the one seen for Au@SiO_2 nanospheres in section 6.19.

The results from the simulations where the position of the Ag nanosphere is adjusted and from the simulations where a set of two Ag nanospheres is used are different for the 310 and 880 nm PV cells. For the 310 nm PV cell, both the simulation with a Ag nanosphere at the perovskite/HTM (bottom) interface and the simulation with a Ag nanosphere at the perovskite/ETM (top) interface shows a slight decrease in total absorptance. The same PV cell shows a slight increase in total absorptance when two nanospheres are placed side by side in the middle of the perovskite layer, and a slight decrease in absorptance when two nanospheres are placed one above the other at equal distance from the middle of the perovskite layer. For the 880 nm PV cell, the simulation with a Ag nanosphere at the perovskite/HTM (bottom) interface shows a slight decrease in absorptance, while the absorptance increased for the simulation with a Ag nanosphere at the perovskite/ETM (top) interface. The same PV cell shows a slight increase in total absorptance when two nanospheres are placed side by side in the middle of the perovskite layer and when two nanospheres are placed one above the other at equal distance from the middle of the perovskite layer.

Nanosphere properties	Reflectance	Transmittance	Absorptance	Absorptance change $\%\Delta A$
Ag, center, d=150nm	0.211	0.082	0.707	-
Ag@SiO_2, center, d=150nm, t=15nm	0.164	0.221	0.615	-13.0%
Ag, center, d=75nm	0.176	0.220	0.604	-
Ag@SiO_2, center, d=75nm, t=7.5nm	0.179	0.268	0.553	-8.44%
Ag, bottom, d=75nm	0.207	0.212	0.581	-3.81%
Ag, top, d=75nm	0.196	0.209	0.595	-1.49%
2xAg, side by side, d=59.52nm, g=11.90nm	0.182	0.203	0.615	+1.82%
2xAg, over/under, d=59.52nm, g=11.90nm	0.178	0.221	0.601	-0.497%

Table 6.37: Total reflectance, transmittance and absorptance for the 310 nm PV cell with Ag nanosphere with SiO_2 shell, Ag nanosphere at perovskite/HTM interface, Ag nanosphere at perovskite/ETM interface, two Ag nanospheres side by side, two Ag nanospheres over/under, as well as the two PV cells with standard setup Ag nanosphere at center. The absorptance change for the various setups is given relative to the two PV cells with standard setup (from section 6.4). d is diameter, t is shell thickness and g is the gap between the two nanospheres.

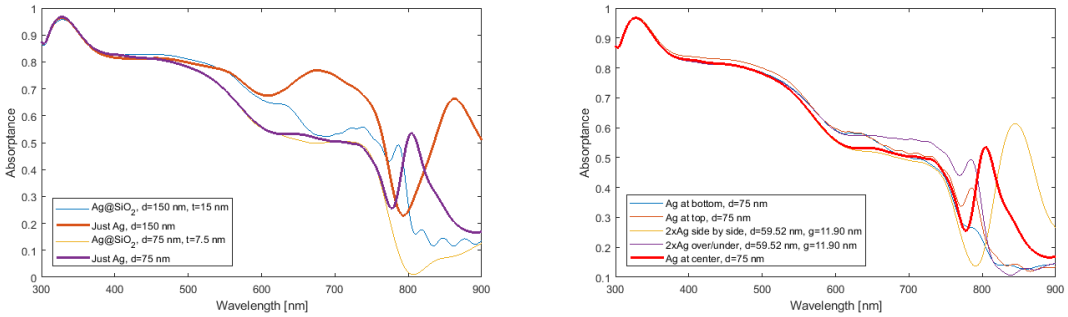

(a) (b)

Figure 6.38: Absorptance for various setups of the 310 nm PV cell. (a) Total absorptance of the Ag@SiO_2 core-shell nanospheres (thin lines) compared to the Ag sphere of the same size but without a SiO_2 shell (thick lines). d is the diameter of the Ag sphere and t is the thickness of the SiO_2 shell. (b)Total absorptance for Ag nanosphere at bottom interface, top interface, double nanospheres side by side, double nanospheres over/under, compared to the centered Ag nanosphere of the same size (thick line) from section 6.4. d is the diameter of the sphere and g is the gap between the two spheres.

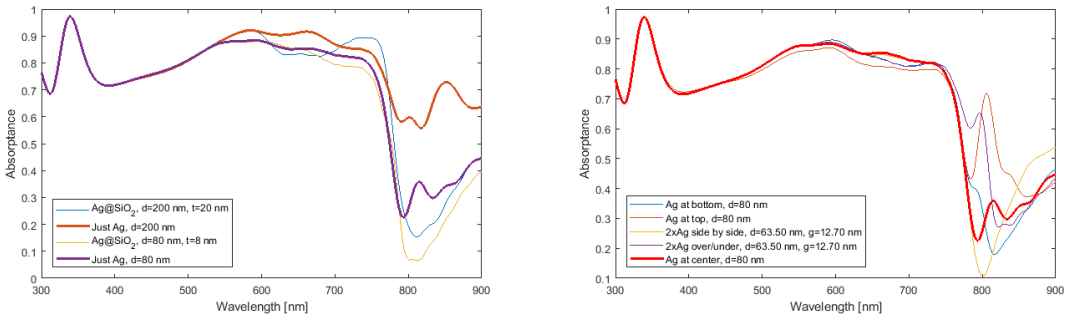

(a) (b)

Figure 6.39: Absorptance for various setups of the 880 nm PV cell. (a) Total absorptance of the Ag@SiO_2 core-shell nanospheres (thin lines) compared to the Ag sphere of the same size but without a SiO_2 shell (thick lines). d is the diameter of the Ag sphere and t is the thickness of the SiO_2 shell. (b)Total absorptance for Ag nanosphere at bottom interface, top interface, double nanospheres side by side, double nanospheres over/under, compared to the centered Ag nanosphere of the same size (thick line) from section 6.4. d is the diameter of the sphere and g is the gap between the two spheres.

Nanosphere properties	Reflectance	Transmittance	Absorptance	Absorptance change $\%\Delta A$
Ag, center, d=200nm	0.145	0.063	0.792	-
Ag@SiO_2, center, d=200nm, t=20nm	0.157	0.127	0.716	-9.60%
Ag, center, d=80nm	0.156	0.131	0.713	-
Ag@SiO_2, center, d=80nm, t=8nm	0.141	0.176	0.683	-4.21%
Ag, bottom, d=80nm	0.164	0.128	0.708	-0.701%
Ag, top, d=80nm	0.134	0.138	0.728	+2.10%
2xAg, side by side, d=63.50nm, g=12.70nm	0.168	0.118	0.714	+0.140%
2xAg, over/under, d=63.50nm, g=12.70nm	0.142	0.130	0.728	+2.10%

Table 6.38: Total reflectance, transmittance and absorptance for the 880 nm PV cell with Ag nanosphere with SiO_2 shell, Ag nanosphere at perovskite/HTM interface, Ag nanosphere at perovskite/ETM interface, two Ag nanospheres side by side, two Ag nanospheres over/under, as well as the two PV cells with standard setup Ag nanosphere at center. The absorptance change for the various setups is given relative to the two PV cells with standard setup (from section 6.4). d is diameter, t is shell thickness and g is the gap between the two nanospheres.

6.21 Aluminum Sphere Variations

This simulation group consists of twelve simulations with Al nanospheres integrated in the PV cell structures. Different variations of spheres are used to compare the effect of these to the standard setup with a solid Al sphere at the center of the perovskite layer (section 6.5). The variations are the same as described for Au nanospheres in section 6.19. These variations are first simulated through six simulations using the 310 nm PV cell, and then the same variations are simulated through six simulations using the 880 nm PV cell. The absorptance from the simulations using the core-shell variations in the 310 nm PV cell compared to the PV cell with a standard setup Al sphere (from section 6.5) is shown in figure 6.40a, and the absorptance from the simulations using the top vs. bottom and double nanosphere variations in the 310 nm PV cell compared to the PV cell with a standard setup Al sphere (from section 6.5) is shown in figure 6.40b. The same absorptance plots from

the simulations using the 880 nm PV cell is shown in figures 6.41a and 6.41b. The total reflectance, transmittance, absorptance and absorptance change are shown in tables 6.39 and 6.40 for all PV cells. The absorptance change for these simulations is given relative to the standard setup PV cell with a Al sphere at the center of the perovskite layer (section 6.5).

The simulation results shows that the total absorptance of the PV cells with Al nanospheres decreases if the Al nanospheres are coated with a SiO_2 shell with a thickness of 10% of the sphere diameter, compared to the PV cell where the same Al nanosphere is used with no shell. This is the same effect as the one seen for Au@SiO_2 nanospheres in section 6.19.

The results from the simulations where the position of the Al nanosphere is adjusted and from the simulations where a set of two Al nanospheres is used are quite similar for the 310 and 880 nm PV cells. For both PV cells, both the simulation with a Al nanosphere at the perovskite/HTM (bottom) interface and the simulation with a Al nanosphere at the perovskite/ETM (top) interface shows a slight decrease in total absorptance. Both PV cells also show a slight increase in total absorptance when two nanospheres are placed side by side in the middle of the perovskite layer, and a slight decrease in absorptance when two nanospheres are placed one above the other at equal distance from the middle of the perovskite layer.

Nanosphere properties	Reflectance	Transmittance	Absorptance	Absorptance change $\%\Delta A$
Al, center, d=150nm	0.157	0.125	0.718	-
Al@SiO_2, center, d=150nm, t=15nm	0.138	0.255	0.607	-15.5%
Al, center, d=75nm	0.172	0.254	0.574	-
Al@SiO_2, center, d=75nm, t=7.5nm	0.179	0.281	0.540	-5.92%
Al, bottom, d=75nm	0.198	0.241	0.561	-2.26%
Al, top, d=75nm	0.206	0.233	0.561	-2.26%
2xAl, side by side, d=59.52nm, g=11.90nm	0.170	0.239	0.591	+2.96%
2xAl, over/under, d=59.52nm, g=11.90nm	0.181	0.250	0.569	-0.871%

Table 6.39: Total reflectance, transmittance and absorptance for the 310 nm PV cell with Al nanosphere with SiO_2 shell, Al nanosphere at perovskite/HTM interface, Al nanosphere at perovskite/ETM interface, two Al nanospheres side by side, two Al nanospheres over/under, as well as the two PV cells with standard setup Al nanosphere at center. The absorptance change for the various setups is given relative to the two PV cells with standard setup (from section 6.5). d is diameter, t is shell thickness and g is the gap between the two nanospheres.

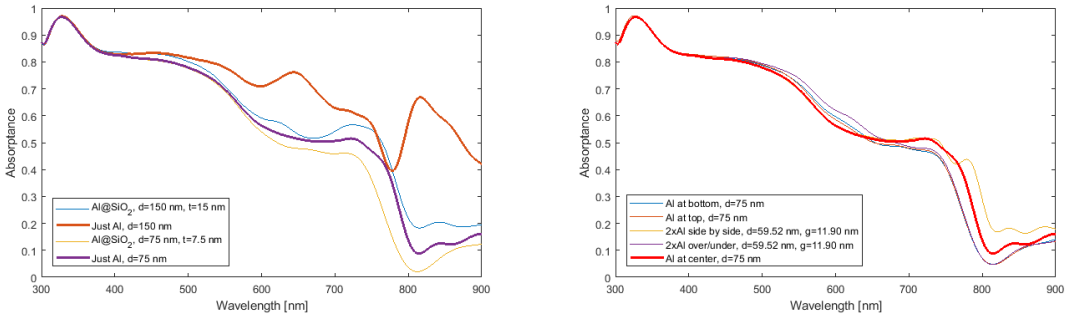

(a) (b)

Figure 6.40: Absorptance for various setups of the 310 nm PV cell. (a) Total absorptance of the Al@SiO_2 core-shell nanospheres (thin lines) compared to the Al sphere of the same size but without a SiO_2 shell (thick lines). d is the diameter of the Al sphere and t is the thickness of the SiO_2 shell. (b)Total absorptance for Al nanosphere at bottom interface, top interface, double nanospheres side by side, double nanospheres over/under, compared to the centered Al nanosphere of the same size (thick line) from section 6.5. d is the diameter of the sphere and g is the gap between the two spheres.

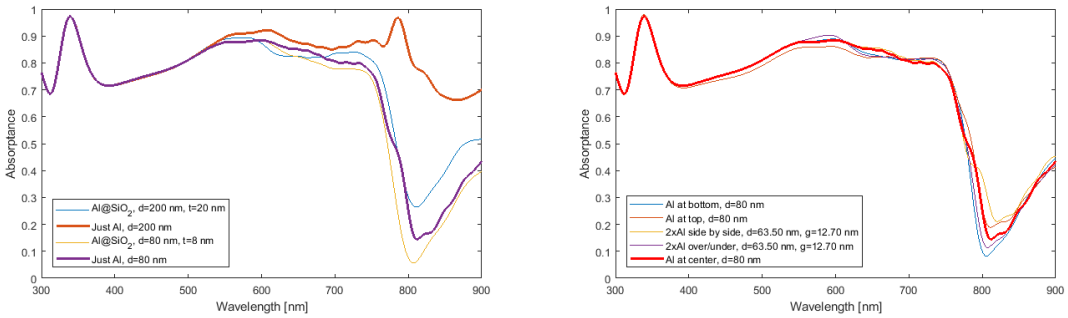

(a) (b)

Figure 6.41: Absorptance for various setups of the 880 nm PV cell. (a) Total absorptance of the Al@SiO_2 core-shell nanospheres (thin lines) compared to the Al sphere of the same size but without a SiO_2 shell (thick lines). d is the diameter of the Al sphere and t is the thickness of the SiO_2 shell. (b)Total absorptance for Al nanosphere at bottom interface, top interface, double nanospheres side by side, double nanospheres over/under, compared to the centered Al nanosphere of the same size (thick line) from section 6.5. d is the diameter of the sphere and g is the gap between the two spheres.

Nanosphere properties	Reflectance	Transmittance	Absorptance	Absorptance change $\%\Delta A$
Al, center, d=200nm	0.135	0.047	0.818	-
Al@SiO_2, center, d=200nm, t=20nm	0.137	0.136	0.727	-11.1%
Al, center, d=80nm	0.142	0.158	0.700	-
Al@SiO_2, center, d=80nm, t=8nm	0.142	0.181	0.677	-3.29%
Al, bottom, d=80nm	0.154	0.153	0.693	-1.00%
Al, top, d=80nm	0.138	0.165	0.697	-0.429%
2xAl, side by side, d=63.50nm, g=12.70nm	0.147	0.144	0.709	+1.29%
2xAl, over/under, d=63.50nm, g=12.70nm	0.144	0.161	0.695	-0.714%

Table 6.40: Total reflectance, transmittance and absorptance for the 880 nm PV cell with Al nanosphere with SiO_2 shell, Al nanosphere at perovskite/HTM interface, Al nanosphere at perovskite/ETM interface, two Al nanospheres side by side, two Al nanospheres over/under, as well as the two PV cells with standard setup Al nanosphere at center. The absorptance change for the various setups is given relative to the two PV cells with standard setup (from section 6.5). d is diameter, t is shell thickness and g is the gap between the two nanospheres.

6.22 Platinum Sphere Variations

This simulation group consists of twelve simulations with Pt nanospheres integrated in the PV cell structures. Different variations of spheres are used to compare the effect of these to the standard setup with a solid Pt sphere at the center of the perovskite layer (section 6.6). The variations are the same as described for Au nanospheres in section 6.19. These variations are first simulated through six simulations using the 310 nm PV cell, and then the same variations are simulated through six simulations using the 880 nm PV cell. The absorptance from the simulations using the core-shell variations in the 310 nm PV cell compared to the PV cell with a standard setup Pt sphere (from section 6.6) is shown in figure 6.42a, and the absorptance from the simulations using the top vs. bottom and double nanosphere variations in the 310 nm PV cell compared to the PV cell with a standard setup Pt sphere (from section 6.6) is shown in figure 6.42b. The same absorptance plots from the simulations using the 880 nm PV cell is shown in figures 6.43a and 6.43b. The

total reflectance, transmittance, absorptance and absorptance change are shown in tables 6.41 and 6.42 for all PV cells. The absorptance change for these simulations is given relative to the standard setup PV cell with a Pt sphere at the center of the perovskite layer (section 6.6).

The simulation results shows that the total absorptance of the PV cells with Pt nanospheres decreases if the Pt nanospheres are coated with a SiO_2 shell with a thickness of 10% of the sphere diameter, compared to the PV cell where the same Pt nanosphere is used with no shell. This is the same effect as the one seen for Au@SiO_2 nanospheres in section 6.19.

The results from the simulations where the position of the Pt nanosphere is adjusted and from the simulations where a set of two Pt nanospheres is used are different for the 310 and 880 nm PV cells. For the 310 nm PV cell, both the simulation with a Pt nanosphere at the perovskite/HTM (bottom) interface and the simulation with a Pt nanosphere at the perovskite/ETM (top) interface shows a slight decrease in total absorptance. The same PV cell shows a slight increase in total absorptance when two nanospheres are placed side by side in the middle of the perovskite layer, and a slight decrease in absorptance when two nanospheres are placed one above the other at equal distance from the middle of the perovskite layer. For the 880 nm PV cell, the simulation with a Pt nanosphere at the perovskite/HTM (bottom) interface shows a slight decrease in absorptance, while the absorptance increased for the simulation with a Pt nanosphere at the perovskite/ETM (top) interface. The same PV cell shows a slight increase in total absorptance when two nanospheres are placed side by side in the middle of the perovskite layer and when two nanospheres are placed one above the other at equal distance from the middle of the perovskite layer.

Nanosphere properties	Reflectance	Transmittance	Absorptance	Absorptance change $\%\Delta A$
Pt, center, d=150nm	0.154	0.120	0.726	-
Pt@SiO_2, center, d=150nm, t=15nm	0.144	0.210	0.646	-11.0%
Pt, center, d=75nm	0.176	0.246	0.578	-
Pt@SiO_2, center, d=75nm, t=7.5nm	0.181	0.269	0.550	-4.84%
Pt, bottom, d=75nm	0.197	0.238	0.565	-2.25%
Pt, top, d=75nm	0.194	0.236	0.570	-1.38%
2xPt, side by side, d=59.52nm, g=11.90nm	0.176	0.239	0.585	+1.21%
2xPt, over/under, d=59.52nm, g=11.90nm	0.181	0.244	0.575	-0.519%

Table 6.41: Total reflectance, transmittance and absorptance for the 310 nm PV cell with Pt nanosphere with SiO_2 shell, Pt nanosphere at perovskite/HTM interface, Pt nanosphere at perovskite/ETM interface, two Pt nanospheres side by side, two Pt nanospheres over/under, as well as the two PV cells with standard setup Pt nanosphere at center. The absorptance change for the various setups is given relative to the two PV cells with standard setup (from section 6.6). d is diameter, t is shell thickness and g is the gap between the two nanospheres.

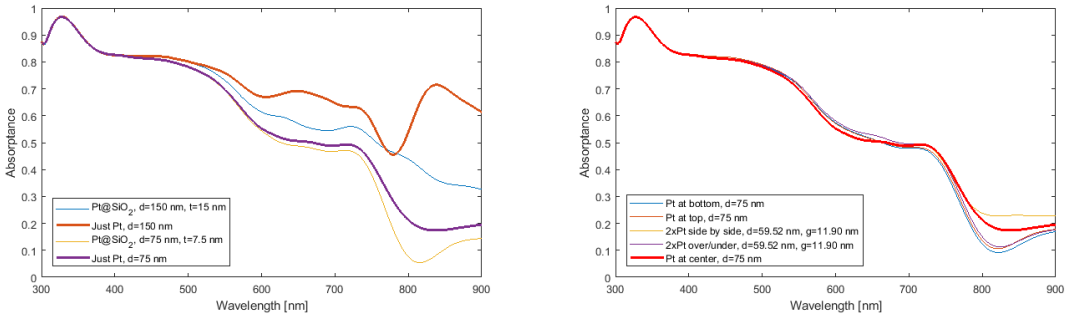

(a) (b)

Figure 6.42: Absorptance for various setups of the 310 nm PV cell. (a) Total absorptance of the Pt@SiO_2 core-shell nanospheres (thin lines) compared to the Pt sphere of the same size but without a SiO_2 shell (thick lines). d is the diameter of the Pt sphere and t is the thickness of the SiO_2 shell. (b)Total absorptance for Pt nanosphere at bottom interface, top interface, double nanospheres side by side, double nanospheres over/under, compared to the centered Pt nanosphere of the same size (thick line) from section 6.6. d is the diameter of the sphere and g is the gap between the two spheres.

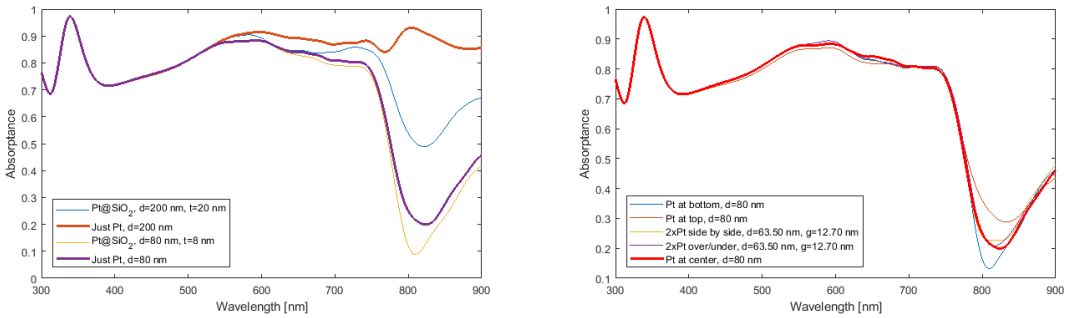

(a) (b)

Figure 6.43: Absorptance for various setups of the 880 nm PV cell. (a) Total absorptance of the Pt@SiO_2 core-shell nanospheres (thin lines) compared to the Pt sphere of the same size but without a SiO_2 shell (thick lines). d is the diameter of the Pt sphere and t is the thickness of the SiO_2 shell. (b)Total absorptance for Pt nanosphere at bottom interface, top interface, double nanospheres side by side, double nanospheres over/under, compared to the centered Pt nanosphere of the same size (thick line) from section 6.6. d is the diameter of the sphere and g is the gap between the two spheres.

Nanosphere properties	Reflectance	Transmittance	Absorptance	Absorptance change $\%\Delta A$
Pt, center, d=200nm	0.131	0.023	0.846	-
Pt@SiO_2, center, d=200nm, t=20nm	0.137	0.092	0.771	-8.87%
Pt, center, d=80nm	0.145	0.153	0.702	-
Pt@SiO_2, center, d=80nm, t=8nm	0.143	0.173	0.684	-2.56%
Pt, bottom, d=80nm	0.152	0.151	0.697	-0.712%
Pt, top, d=80nm	0.135	0.158	0.707	+0.712%
2xPt, side by side, d=63.50nm, g=12.70nm	0.148	0.147	0.705	+0.427%
2xPt, over/under, d=63.50nm, g=12.70nm	0.143	0.153	0.704	+0.285%

Table 6.42: Total reflectance, transmittance and absorptance for the 880 nm PV cell with Pt nanosphere with SiO_2 shell, Pt nanosphere at perovskite/HTM interface, Pt nanosphere at perovskite/ETM interface, two Pt nanospheres side by side, two Pt nanospheres over/under, as well as the two PV cells with standard setup Pt nanosphere at center. The absorptance change for the various setups is given relative to the two PV cells with standard setup (from section 6.6). d is diameter, t is shell thickness and g is the gap between the two nanospheres.

6.23 Gold Cube Variations

This simulation group consists of twelve simulations with Au nanocubes integrated in the PV cell structures. Different variations of cubes are used to compare the effect of these to the standard setup with a solid Au cube at the center of the perovskite layer (section 6.7). The variations are the same as described for Au nanospheres in section 6.19. These variations are first simulated through six simulations using the 310 nm PV cell, and then the same variations are simulated through six simulations using the 880 nm PV cell. The absorptance from the simulations using the core-shell variations in the 310 nm PV cell compared to the PV cell with a standard setup Au cube (from section 6.7) is shown in figure 6.44a, and the absorptance from the simulations using the top vs. bottom and double nanocube variations in the 310 nm PV cell compared to the PV cell with a standard setup Au cube (from section 6.7) is shown in figure 6.44b. The same absorptance plots from the simulations

using the 880 nm PV cell is shown in figures 6.45a and 6.45b. The total reflectance, transmittance, absorptance and absorptance change are shown in tables 6.43 and 6.44 for all PV cells. The absorptance change for these simulations is given relative to the standard setup PV cell with a Au cube at the center of the perovskite layer (section 6.7).

The simulation results shows that the total absorptance of the PV cells with Au nanocubes decreases if the Au nanocubes are coated with a SiO_2 shell with a thickness of 10% of the cube side length, compared to the PV cell where the same Au nanocube is used with no shell. This is the same effect as the one seen for Au@SiO_2 nanospheres in section 6.19, although the absorptance decreases less when cubes are used than when spheres are used.

The results from the simulations where the position of the Au nanocube is adjusted and from the simulations where a set of two Au nanocubes is used are different for the 310 and 880 nm PV cells. For the 310 nm PV cell, both the simulation with a Au nanocube at the perovskite/HTM (bottom) interface and the simulation with a Au nanocube at the perovskite/ETM (top) interface shows a decrease in total absorptance. The same PV cell also show decreased total absorptance when two nanocubes are placed side by side in the middle of the perovskite layer, but an increase in absorptance is seen when two nanocubes are placed one above the other at equal distance from the middle of the perovskite layer. For the 880 nm PV cell, both the simulation with a Au nanocube at the perovskite/HTM (bottom) interface and the simulation with a Au nanocube at the perovskite/ETM (top) interface shows increased absorptance. The same PV cell shows decreased total absorptance when two nanocubes are placed side by side in the middle of the perovskite layer, while the absorptance increases when two nanocubes are placed one above the other at equal distance from the middle of the perovskite layer.

Nanocube properties	Reflectance	Transmittance	Absorptance	Absorptance change $\%\Delta A$
Au, center, s=150nm	0.131	0.116	0.753	-
Au@SiO_2, center, s=150nm, t=15nm	0.125	0.157	0.718	-4.65%
Au, center, s=75nm	0.200	0.179	0.621	-
Au@SiO_2, center, s=75nm, t=7.5nm	0.181	0.226	0.593	-4.51%
Au, bottom, s=75nm	0.235	0.169	0.596	-4.03%
Au, top, s=75nm	0.195	0.186	0.619	-0.322%
2xAu, side by side, s=59.52nm, g=11.90nm	0.206	0.219	0.575	-7.41%
2xAu, over/under, s=59.52nm, g=11.90nm	0.163	0.188	0.649	+4.51%

Table 6.43: Total reflectance, transmittance and absorptance for the 310 nm PV cell with Au nanocube with SiO_2 shell, Au nanocube at perovskite/HTM interface, Au nanocube at perovskite/ETM interface, two Au nanocubes side by side, two Au nanocubes over/under, as well as the two PV cells with standard setup Au nanocube at center. The absorptance change for the various setups is given relative to the two PV cells with standard setup (from section 6.7). s is side length, t is shell thickness and g is the gap between the two nanocubes.

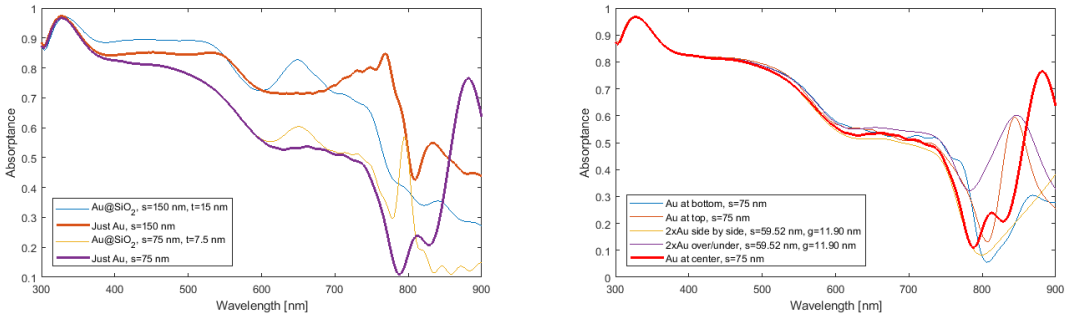

(a) (b)

Figure 6.44: Absorptance for various setups of the 310 nm PV cell. (a) Total absorptance of the Au@SiO_2 core-shell nanocubes (thin lines) compared to the Au cube of the same size but without a SiO_2 shell (thick lines). s is the side length of the Au cube and t is the thickness of the SiO_2 shell. (b)Total absorptance for Au nanocube at bottom interface, top interface, double nanocubes side by side, double nanocubes over/under, compared to the centered Au nanocube of the same size (thick line) from section 6.7. s is the side length of the cube and g is the gap between the two cubes.

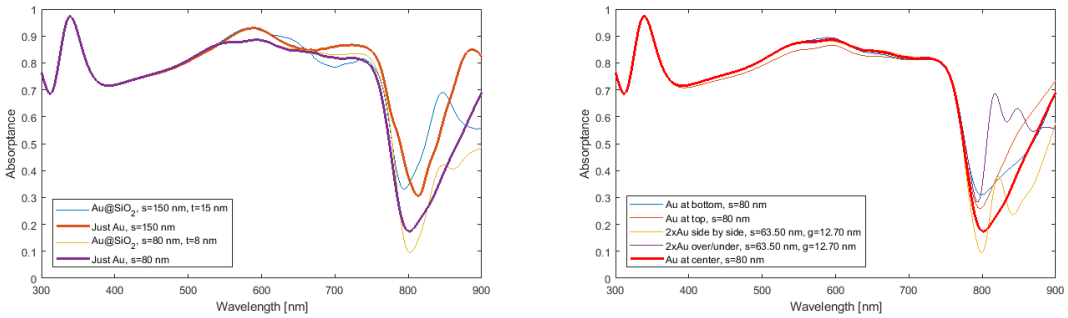

(a) (b)

Figure 6.45: Absorptance for various setups of the 880 nm PV cell. (a) Total absorptance of the Au@SiO_2 core-shell nanocubes (thin lines) compared to the Au cube of the same size but without a SiO_2 shell (thick lines). s is the side length of the Au cube and t is the thickness of the SiO_2 shell. (b)Total absorptance for Au nanocube at bottom interface, top interface, double nanocubes side by side, double nanocubes over/under, compared to the centered Au nanocube of the same size (thick line) from section 6.7. s is the side length of the cube and g is the gap between the two cubes.

Nanocube properties	Reflectance	Transmittance	Absorptance	Absorptance change $\%\Delta A$
Au, center, s=150nm	0.148	0.078	0.774	-
Au@SiO_2, center, s=150nm, t=15nm	0.144	0.102	0.754	-2.58%
Au, center, s=80nm	0.155	0.126	0.719	-
Au@SiO_2, center, s=80nm, t=8nm	0.177	0.109	0.714	-0.695%
Au, bottom, s=80nm	0.155	0.113	0.732	+1.81%
Au, top, s=80nm	0.150	0.118	0.732	+1.81%
2xAu, side by side, s=63.50nm, g=12.70nm	0.164	0.132	0.704	-2.09%
2xAu, over/under, s=63.50nm, g=12.70nm	0.143	0.105	0.752	+4.59%

Table 6.44: Total reflectance, transmittance and absorptance for the 880 nm PV cell with Au nanocube with SiO_2 shell, Au nanocube at perovskite/HTM interface, Au nanocube at perovskite/ETM interface, two Au nanocubes side by side, two Au nanocubes over/under, as well as the two PV cells with standard setup Au nanocube at center. The absorptance change for the various setups is given relative to the two PV cells with standard setup (from section 6.7). s is side length, t is shell thickness and g is the gap between the two nanocubes.

6.24 Silver Cube Variations

This simulation group consists of twelve simulations with Ag nanocubes integrated in the PV cell structures. Different variations of cubes are used to compare the effect of these to the standard setup with a solid Ag cube at the center of the perovskite layer (section 6.8). The variations are the same as described for Au nanospheres in section 6.19. These variations are first simulated through six simulations using the 310 nm PV cell, and then the same variations are simulated through six simulations using the 880 nm PV cell. The absorptance from the simulations using the core-shell variations in the 310 nm PV cell compared to the PV cell with a standard setup Ag cube (from section 6.8) is shown in figure 6.46a, and the absorptance from the simulations using the top vs. bottom and double nanocube variations in the 310 nm PV cell compared to the PV cell with a standard setup Ag cube (from section 6.8) is shown in figure 6.46b. The same absorptance plots from the simulations

using the 880 nm PV cell is shown in figures 6.47a and 6.47b. The total reflectance, transmittance, absorptance and absorptance change are shown in tables 6.45 and 6.46 for all PV cells. The absorptance change for these simulations is given relative to the standard setup PV cell with a Ag cube at the center of the perovskite layer (section 6.8).

The results in this group is very similar to the results for the group with variations of Au nanocubes in section 6.23. The results shows that the total absorptance of the PV cells with Ag nanocubes decreases if the Ag nanocubes are coated with a SiO_2 shell with a thickness of 10% of the cube side length, compared to the PV cell where the same Ag nanocube is used with no shell.

The results from the simulations where the position of the Ag nanocube is adjusted and from the simulations where a set of two Ag nanocubes is used are different for the 310 and 880 nm PV cells. For the 310 nm PV cell, both the simulation with a Ag nanocube at the perovskite/HTM (bottom) interface and the simulation with a Ag nanocube at the perovskite/ETM (top) interface shows a decrease in total absorptance. The same PV cell also show decreased total absorptance when two nanocubes are placed side by side in the middle of the perovskite layer, but an increase in absorptance is seen when two nanocubes are placed one above the other at equal distance from the middle of the perovskite layer. For the 880 nm PV cell, both the simulation with a Ag nanocube at the perovskite/HTM (bottom) interface and the simulation with a Ag nanocube at the perovskite/ETM (top) interface shows increased absorptance. The same PV cell shows decreased total absorptance when two nanocubes are placed side by side in the middle of the perovskite layer, while the absorptance increases when two nanocubes are placed one above the other at equal distance from the middle of the perovskite layer.

Nanocube properties	Reflectance	Transmittance	Absorptance	Absorptance change $\%\Delta A$
Ag, center, s=150nm	0.133	0.119	0.748	-
Ag@SiO_2, center, s=150nm, t=15nm	0.140	0.155	0.705	-5.75%
Ag, center, s=75nm	0.202	0.170	0.628	-
Ag@SiO_2, center, s=75nm, t=7.5nm	0.176	0.233	0.591	-5.89%
Ag, bottom, s=75nm	0.236	0.166	0.598	-4.78%
Ag, top, s=75nm	0.206	0.181	0.613	-2.39%
2xAg, side by side, s=59.52nm, g=11.90nm	0.209	0.210	0.581	-7.48%
2xAg, over/under, s=59.52nm, g=11.90nm	0.162	0.187	0.651	+3.66%

Table 6.45: Total reflectance, transmittance and absorptance for the 310 nm PV cell with Ag nanocube with SiO_2 shell, Ag nanocube at perovskite/HTM interface, Ag nanocube at perovskite/ETM interface, two Ag nanocubes side by side, two Ag nanocubes over/under, as well as the two PV cells with standard setup Ag nanocube at center. The absorptance change for the various setups is given relative to the two PV cells with standard setup (from section 6.8). s is side length, t is shell thickness and g is the gap between the two nanocubes.

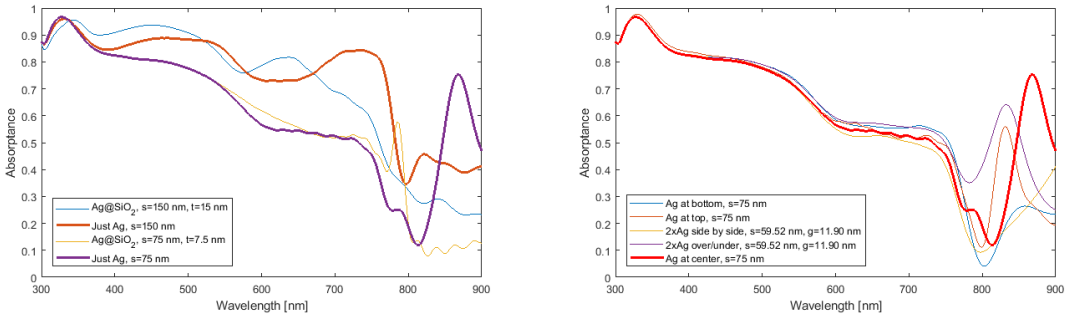

(a) (b)

Figure 6.46: Absorptance for various setups of the 310 nm PV cell. (a) Total absorptance of the Ag@SiO_2 core-shell nanocubes (thin lines) compared to the Ag cube of the same size but without a SiO_2 shell (thick lines). s is the side length of the Ag cube and t is the thickness of the SiO_2 shell. (b)Total absorptance for Ag nanocube at bottom interface, top interface, double nanocubes side by side, double nanocubes over/under, compared to the centered Ag nanocube of the same size (thick line) from section 6.8. s is the side length of the cube and g is the gap between the two cubes.

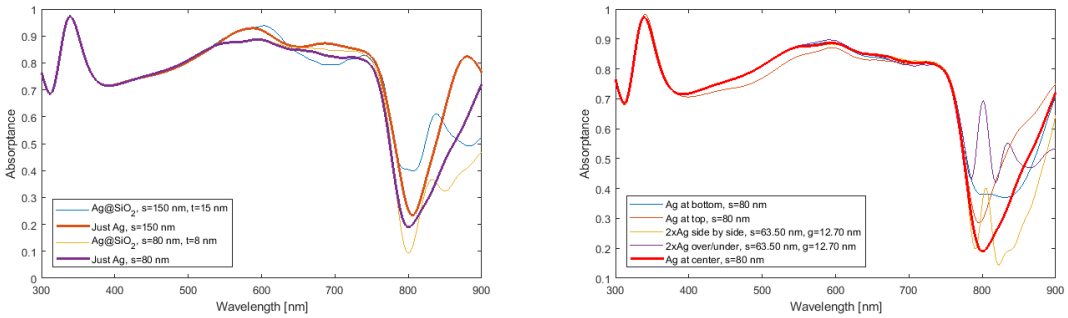

(a) (b)

Figure 6.47: Absorptance for various setups of the 880 nm PV cell. (a) Total absorptance of the Ag@SiO_2 core-shell nanocubes (thin lines) compared to the Ag cube of the same size but without a SiO_2 shell (thick lines). s is the side length of the Ag cube and t is the thickness of the SiO_2 shell. (b)Total absorptance for Ag nanocube at bottom interface, top interface, double nanocubes side by side, double nanocubes over/under, compared to the centered Ag nanocube of the same size (thick line) from section 6.8. s is the side length of the cube and g is the gap between the two cubes.

Nanocube properties	Reflectance	Transmittance	Absorptance	Absorptance change $\%\Delta A$
Ag, center, s=150nm	0.150	0.083	0.767	-
Ag@SiO_2, center, s=150nm, t=15nm	0.146	0.105	0.749	-2.35%
Ag, center, s=80nm	0.157	0.117	0.726	-
Ag@SiO_2, center, s=80nm, t=8nm	0.172	0.116	0.712	-1.93%
Ag, bottom, s=80nm	0.161	0.103	0.736	+1.38%
Ag, top, s=80nm	0.154	0.108	0.738	+1.65%
2xAg, side by side, s=63.50nm, g=12.70nm	0.171	0.121	0.708	-2.48%
2xAg, over/under, s=63.50nm, g=12.70nm	0.149	0.103	0.748	+3.03%

Table 6.46: Total reflectance, transmittance and absorptance for the 880 nm PV cell with Ag nanocube with SiO_2 shell, Ag nanocube at perovskite/HTM interface, Ag nanocube at perovskite/ETM interface, two Ag nanocubes side by side, two Ag nanocubes over/under, as well as the two PV cells with standard setup Ag nanocube at center. The absorptance change for the various setups is given relative to the two PV cells with standard setup (from section 6.8). s is side length, t is shell thickness and g is the gap between the two nanocubes.

6.25 Aluminum Cube Variations

This simulation group consists of twelve simulations with Al nanocubes integrated in the PV cell structures. Different variations of cubes are used to compare the effect of these to the standard setup with a solid Al cube at the center of the perovskite layer (section 6.9). The variations are the same as described for Au nanospheres in section 6.19. These variations are first simulated through six simulations using the 310 nm PV cell, and then the same variations are simulated through six simulations using the 880 nm PV cell. The absorptance from the simulations using the core-shell variations in the 310 nm PV cell compared to the PV cell with a standard setup Al cube (from section 6.9) is shown in figure 6.48a, and the absorptance from the simulations using the top vs. bottom and double nanocube variations in the 310 nm PV cell compared to the PV cell with a standard setup Al cube (from section 6.9) is shown in figure 6.48b. The same absorptance plots from the simulations

using the 880 nm PV cell is shown in figures 6.49a and 6.49b. The total reflectance, transmittance, absorptance and absorptance change are shown in tables 6.47 and 6.48 for all PV cells. The absorptance change for these simulations is given relative to the standard setup PV cell with a Al cube at the center of the perovskite layer (section 6.9).

The results shows that the total absorptance of the PV cells with Al nanocubes decreases if the Al nanocubes are coated with a SiO_2 shell with a thickness of 10% of the cube side length, compared to the PV cell where the same Al nanocube is used with no shell.

The results from the simulations where the position of the Al nanocube is adjusted and from the simulations where a set of two Al nanocubes is used are different for the 310 and 880 nm PV cells. For the 310 nm PV cell, both the simulation with a Al nanocube at the perovskite/HTM (bottom) interface and the simulation with a Al nanocube at the perovskite/ETM (top) interface shows a decrease in total absorptance. The same PV cell show increased total absorptance when two nanocubes are placed side by side in the middle of the perovskite layer, but a decrease in absorptance is seen when two nanocubes are placed one above the other at equal distance from the middle of the perovskite layer. For the 880 nm PV cell, the simulation with a Al nanocube at the perovskite/HTM (bottom) interface shows decreased absorptance, and the simulation with a Al nanocube at the perovskite/ETM (top) interface shows increased absorptance. The same PV cell shows decreased total absorptance when two nanocubes are placed side by side in the middle of the perovskite layer, while the absorptance increases when two nanocubes are placed one above the other at equal distance from the middle of the perovskite layer.

Nanocube properties	Reflectance	Transmittance	Absorptance	Absorptance change $\%\Delta A$
Al, center, s=150nm	0.163	0.053	0.784	-
Al@SiO_2, center, s=150nm, t=15nm	0.149	0.153	0.698	-11.0%
Al, center, s=75nm	0.162	0.202	0.636	-
Al@SiO_2, center, s=75nm, t=7.5nm	0.167	0.270	0.563	-11.5%
Al, bottom, s=75nm	0.212	0.195	0.593	-6.76%
Al, top, s=75nm	0.220	0.189	0.591	-7.08%
2xAl, side by side, s=59.52nm, g=11.90nm	0.181	0.164	0.655	+2.99%
2xAl, over/under, s=59.52nm, g=11.90nm	0.172	0.207	0.621	-2.36%

Table 6.47: Total reflectance, transmittance and absorptance for the 310 nm PV cell with Al nanocube with SiO_2 shell, Al nanocube at perovskite/HTM interface, Al nanocube at perovskite/ETM interface, two Al nanocubes side by side, two Al nanocubes over/under, as well as the two PV cells with standard setup Al nanocube at center. The absorptance change for the various setups is given relative to the two PV cells with standard setup (from section 6.9). s is side length, t is shell thickness and g is the gap between the two nanocubes.

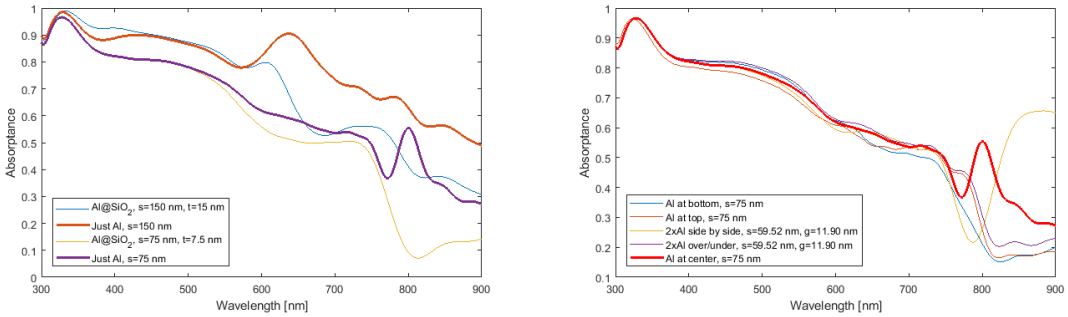

(a) (b)

Figure 6.48: Absorptance for various setups of the 310 nm PV cell. (a) Total absorptance of the Al@SiO_2 core-shell nanocubes (thin lines) compared to the Al cube of the same size but without a SiO_2 shell (thick lines). s is the side length of the Al cube and t is the thickness of the SiO_2 shell. (b)Total absorptance for Al nanocube at bottom interface, top interface, double nanocubes side by side, double nanocubes over/under, compared to the centered Al nanocube of the same size (thick line) from section 6.9. s is the side length of the cube and g is the gap between the two cubes.

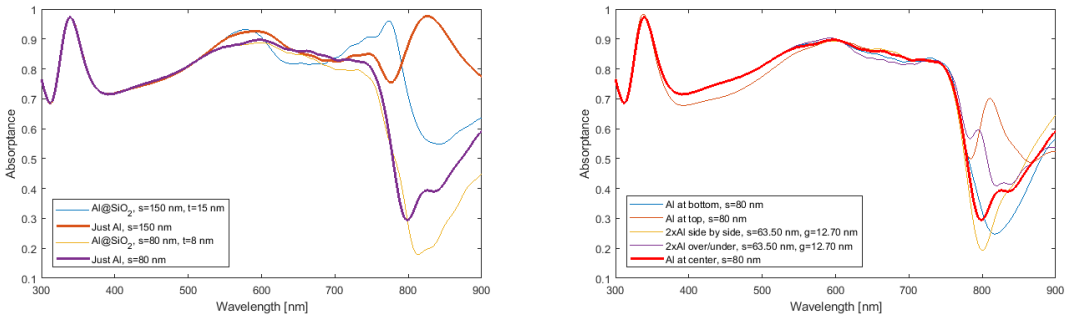

(a) (b)

Figure 6.49: Absorptance for various setups of the 880 nm PV cell. (a) Total absorptance of the Al@SiO_2 core-shell nanocubes (thin lines) compared to the Al cube of the same size but without a SiO_2 shell (thick lines). s is the side length of the Al cube and t is the thickness of the SiO_2 shell. (b)Total absorptance for Al nanocube at bottom interface, top interface, double nanocubes side by side, double nanocubes over/under, compared to the centered Al nanocube of the same size (thick line) from section 6.9. s is the side length of the cube and g is the gap between the two cubes.

Nanocube properties	Reflectance	Transmittance	Absorptance	Absorptance change $\%\Delta A$
Al, center, s=150nm	0.139	0.025	0.836	-
Al@SiO_2, center, s=150nm, t=15nm	0.136	0.074	0.790	-5.50%
Al, center, s=80nm	0.160	0.105	0.735	-
Al@SiO_2, center, s=80nm, t=8nm	0.142	0.154	0.704	-4.22%
Al, bottom, s=80nm	0.166	0.109	0.725	-1.36%
Al, top, s=80nm	0.136	0.114	0.750	+2.04%
2xAl, side by side, s=63.50nm, g=12.70nm	0.171	0.098	0.731	-0.544%
2xAl, over/under, s=63.50nm, g=12.70nm	0.137	0.117	0.746	+1.50%

Table 6.48: Total reflectance, transmittance and absorptance for the 880 nm PV cell with Al nanocube with SiO_2 shell, Al nanocube at perovskite/HTM interface, Al nanocube at perovskite/ETM interface, two Al nanocubes side by side, two Al nanocubes over/under, as well as the two PV cells with standard setup Al nanocube at center. The absorptance change for the various setups is given relative to the two PV cells with standard setup (from section 6.9). s is side length, t is shell thickness and g is the gap between the two nanocubes.

6.26 Platinum Cube Variations

This simulation group consists of twelve simulations with Pt nanocubes integrated in the PV cell structures. Different variations of cubes are used to compare the effect of these to the standard setup with a solid Pt cube at the center of the perovskite layer (section 6.10). The variations are the same as described for Au nanospheres in section 6.19. These variations are first simulated through six simulations using the 310 nm PV cell, and then the same variations are simulated through six simulations using the 880 nm PV cell. The absorptance from the simulations using the core-shell variations in the 310 nm PV cell compared to the PV cell with a standard setup Pt cube (from section 6.10) is shown in figure 6.50a, and the absorptance from the simulations using the top vs. bottom and double nanocube variations in the 310 nm PV cell compared to the PV cell with a standard setup Pt cube (from section 6.10) is shown in figure 6.50b. The same absorptance plots from the simulations using the 880 nm PV cell is shown in figures 6.51a and 6.51b. The total reflectance, transmittance, absorptance and absorptance change are shown in tables 6.49 and

6.50 for all PV cells. The absorptance change for these simulations is given relative to the standard setup PV cell with a Pt cube at the center of the perovskite layer (section 6.10).

The results shows that the total absorptance of the PV cells with Pt nanocubes decreases if the Pt nanocubes are coated with a SiO_2 shell with a thickness of 10% of the cube side length, compared to the PV cell where the same Pt nanocube is used with no shell.

The results from the simulations where the position of the Pt nanocube is adjusted and from the simulations where a set of two Pt nanocubes is used are different for the 310 and 880 nm PV cells. For the 310 nm PV cell, both the simulation with a Pt nanocube at the perovskite/HTM (bottom) interface and the simulation with a Pt nanocube at the perovskite/ETM (top) interface shows a decrease in total absorptance. The same PV cell also show decreased total absorptance when two nanocubes are placed side by side in the middle of the perovskite layer and when two nanocubes are placed one above the other at equal distance from the middle of the perovskite layer. For the 880 nm PV cell, the simulation with a Pt nanocube at the perovskite/HTM (bottom) interface shows decreased absorptance, and the simulation with a Pt nanocube at the perovskite/ETM (top) interface shows increased absorptance. The same PV cell shows decreased total absorptance when two nanocubes are placed side by side in the middle of the perovskite layer, while the absorptance increases when two nanocubes are placed one above the other at equal distance from the middle of the perovskite layer.

Nanocube properties	Reflectance	Transmittance	Absorptance	Absorptance change $\%\Delta A$
Pt, center, s=150nm	0.138	0.050	0.812	-
Pt@SiO_2, center, s=150nm, t=15nm	0.127	0.100	0.773	-4.80%
Pt, center, s=75nm	0.169	0.211	0.620	-
Pt@SiO_2, center, s=75nm, t=7.5nm	0.172	0.248	0.580	-6.45%
Pt, bottom, s=75nm	0.205	0.202	0.593	-4.35%
Pt, top, s=75nm	0.197	0.204	0.599	-3.39%
2xPt, side by side, s=59.52nm, g=11.90nm	0.179	0.205	0.616	-0.645%
2xPt, over/under, s=59.52nm, g=11.90nm	0.174	0.218	0.608	-1.94%

Table 6.49: Total reflectance, transmittance and absorptance for the 310 nm PV cell with Pt nanocube with SiO_2 shell, Pt nanocube at perovskite/HTM interface, Pt nanocube at perovskite/ETM interface, two Pt nanocubes side by side, two Pt nanocubes over/under, as well as the two PV cells with standard setup Pt nanocube at center. The absorptance change for the various setups is given relative to the two PV cells with standard setup (from section 6.10). s is side length, t is shell thickness and g is the gap between the two nanocubes.

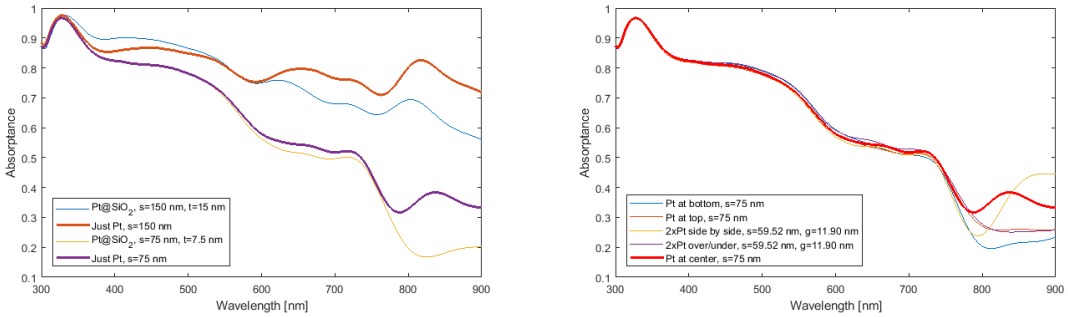

(a) (b)

Figure 6.50: Absorptance for various setups of the 310 nm PV cell. (a) Total absorptance of the Pt@SiO_2 core-shell nanocubes (thin lines) compared to the Pt cube of the same size but without a SiO_2 shell (thick lines). s is the side length of the Pt cube and t is the thickness of the SiO_2 shell. (b)Total absorptance for Pt nanocube at bottom interface, top interface, double nanocubes side by side, double nanocubes over/under, compared to the centered Pt nanocube of the same size (thick line) from section 6.10. s is the side length of the cube and g is the gap between the two cubes.

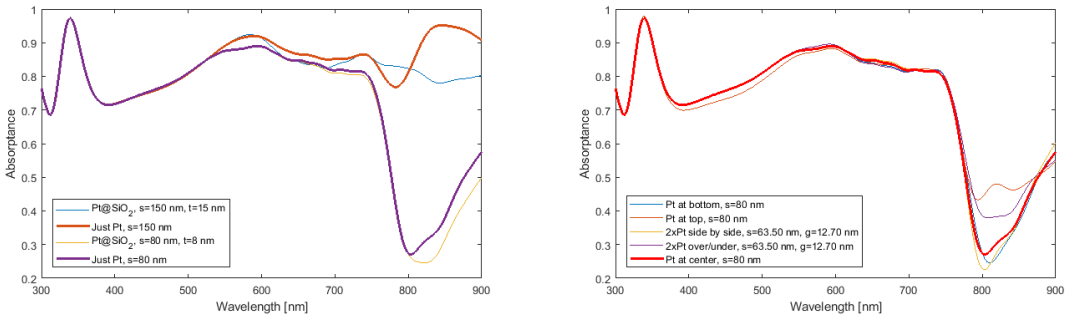

(a) (b)

Figure 6.51: Absorptance for various setups of the 880 nm PV cell. (a) Total absorptance of the Pt@SiO_2 core-shell nanocubes (thin lines) compared to the Pt cube of the same size but without a SiO_2 shell (thick lines). s is the side length of the Pt cube and t is the thickness of the SiO_2 shell. (b)Total absorptance for Pt nanocube at bottom interface, top interface, double nanocubes side by side, double nanocubes over/under, compared to the centered Pt nanocube of the same size (thick line) from section 6.10. s is the side length of the cube and g is the gap between the two cubes.

Nanocube properties	Reflectance	Transmittance	Absorptance	Absorptance change $\%\Delta A$
Pt, center, s=150nm	0.129	0.028	0.843	-
Pt@SiO_2, center, s=150nm, t=15nm	0.132	0.047	0.821	-2.61%
Pt, center, s=80nm	0.151	0.126	0.723	-
Pt@SiO_2, center, s=80nm, t=8nm	0.146	0.144	0.710	-1.80%
Pt, bottom, s=80nm	0.153	0.125	0.722	-0.138%
Pt, top, s=80nm	0.137	0.129	0.734	+1.52%
2xPt, side by side, s=63.50nm, g=12.70nm	0.156	0.123	0.721	-0.277%
2xPt, over/under, s=63.50nm, g=12.70nm	0.139	0.126	0.734	+1.52%

Table 6.50: Total reflectance, transmittance and absorptance for the 880 nm PV cell with Pt nanocube with SiO_2 shell, Pt nanocube at perovskite/HTM interface, Pt nanocube at perovskite/ETM interface, two Pt nanocubes side by side, two Pt nanocubes over/under, as well as the two PV cells with standard setup Pt nanocube at center. The absorptance change for the various setups is given relative to the two PV cells with standard setup (from section 6.10). s is side length, t is shell thickness and g is the gap between the two nanocubes.

6.27 Gold Rod Variations

This simulation group consists of twelve simulations with Au nanorods integrated in the PV cell structures. Different variations of rods are used to compare the effect of these to the standard setup with a solid Au rod at the center of the perovskite layer (section 6.11). The variations are the same as described for Au nanospheres in section 6.19. These variations are first simulated through six simulations using the 310 nm PV cell, and then the same variations are simulated through six simulations using the 880 nm PV cell. The absorptance from the simulations using the core-shell variations in the 310 nm PV cell compared to the PV cell with a standard setup Au rod (from section 6.11) is shown in figure 6.52a, and the absorptance from the simulations using the top vs. bottom and double nanorod variations in the 310 nm PV cell compared to the PV cell with a standard setup Au rod (from section 6.11) is shown in figure 6.52b. The same absorptance plots from the simulations

using the 880 nm PV cell is shown in figures 6.53a and 6.53b. The total reflectance, transmittance, absorptance and absorptance change are shown in tables 6.51 and 6.52 for all PV cells. The absorptance change for these simulations is given relative to the standard setup PV cell with a Au rod at the center of the perovskite layer (section 6.11).

The simulation results shows that the total absorptance of the PV cells with Au nanorods decreases if the Au nanorods are coated with a SiO_2 shell with a thickness of 10% of the rod diameter, compared to the PV cell where the same Au nanorod is used with no shell. This is the same effect as the one seen for Au@SiO_2 nanospheres and nanocubes in sections 6.19 and 6.23.

The results from the simulations where the position of the Au nanorod is adjusted and from the simulations where a set of two Au nanorods is used are quite similar for the 310 and 880 nm PV cells. For both PV cells, both the simulation with a Au nanorod at the perovskite/HTM (bottom) interface and the simulation with a Au nanorod at the perovskite/ETM (top) interface shows a decrease in total absorptance. Both PV cells show an increase in total absorptance when two nanorods are placed side by side in the middle of the perovskite layer, and a decrease in absorptance when two nanorods are placed one above the other at equal distance from the middle of the perovskite layer.

Nanorod properties	Reflectance	Transmittance	Absorptance	Absorptance change $\%\Delta A$
Au, center, d=60nm	0.190	0.178	0.632	-
Au@SiO_2, center, d=60nm, t=6nm	0.191	0.238	0.571	-9.65%
Au, center, d=30nm	0.185	0.269	0.546	-
Au@SiO_2, center, d=30nm, t=3nm	0.187	0.275	0.538	-1.47%
Au, bottom, d=30nm	0.189	0.268	0.543	-0.549%
Au, top, d=30nm	0.192	0.265	0.543	-0.549%
2xAu, side by side, d=23.81nm, g=4.76nm	0.182	0.257	0.561	+2.75%
2xAu, over/under, d=23.81nm, g=4.76nm	0.188	0.267	0.545	-0.183%

Table 6.51: Total reflectance, transmittance and absorptance for the 310 nm PV cell with Au nanorod with SiO_2 shell, Au nanorod at perovskite/HTM interface, Au nanorod at perovskite/ETM interface, two Au nanorods side by side, two Au nanorods over/under, as well as the two PV cells with standard setup Au nanorod at center. The absorptance change for the various setups is given relative to the two PV cells with standard setup (from section 6.11). d is diameter, t is shell thickness and g is the gap between the two nanorods. All rods in this thesis have a length that is equal to three times its diameter (aspect ratio is 3).

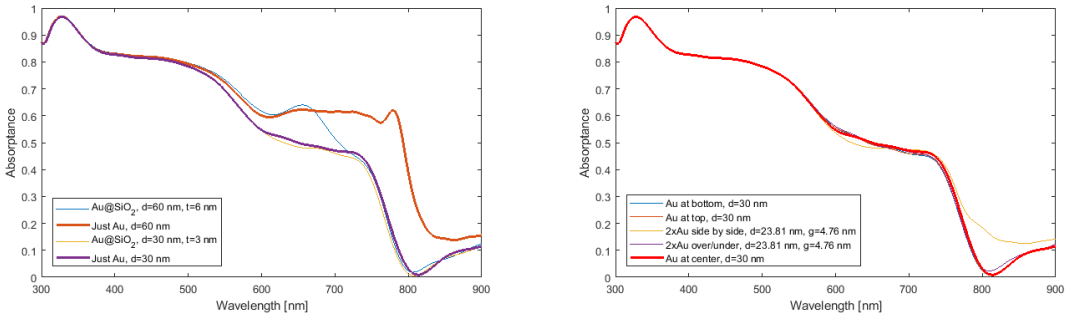

(a) (b)

Figure 6.52: Absorptance for various setups of the 310 nm PV cell. (a) Total absorptance of the Au@SiO_2 core-shell nanorods (thin lines) compared to the Au rod of the same size but without a SiO_2 shell (thick lines). d is the diameter of the Au rod and t is the thickness of the SiO_2 shell. (b)Total absorptance for Au nanorod at bottom interface, top interface, double nanorods side by side, double nanorods over/under, compared to the centered Au nanorod of the same size (thick line) from section 6.11. d is the diameter of the rod and g is the gap between the two rods. All rods in this thesis have a length that is equal to three times its diameter (aspect ratio is 3).

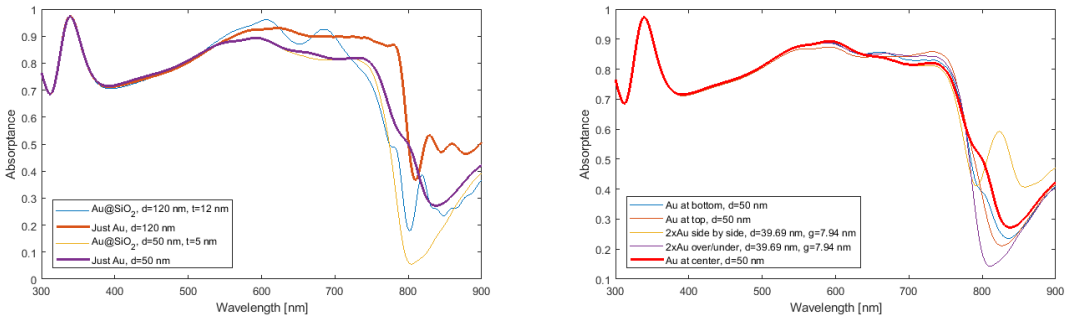

(a) (b)

Figure 6.53: Absorptance for various setups of the 880 nm PV cell. (a) Total absorptance of the Au@SiO_2 core-shell nanorods (thin lines) compared to the Au rod of the same size but without a SiO_2 shell (thick lines). d is the diameter of the Au rod and t is the thickness of the SiO_2 shell. (b)Total absorptance for Au nanorod at bottom interface, top interface, double nanorods side by side, double nanorods over/under, compared to the centered Au nanorod of the same size (thick line) from section 6.11. d is the diameter of the rod and g is the gap between the two rods. All rods in this thesis have a length that is equal to three times its diameter (aspect ratio is 3).

Nanorod properties	Reflectance	Transmittance	Absorptance	Absorptance change $\%\Delta A$
Au, center, d=120nm	0.183	0.040	0.777	-
Au@SiO_2, center, d=120nm, t=12nm	0.169	0.117	0.714	-8.11%
Au, center, d=50nm	0.142	0.135	0.723	-
Au@SiO_2, center, d=50nm, t=5nm	0.146	0.172	0.682	-5.67%
Au, bottom, d=50nm	0.141	0.142	0.717	-0.830%
Au, top, d=50nm	0.146	0.140	0.714	-1.24%
2xAu, side by side, d=39.69nm, g=7.94nm	0.142	0.120	0.738	+2.07%
2xAu, over/under, d=39.69nm, g=7.94nm	0.146	0.148	0.706	-2.35%

Table 6.52: Total reflectance, transmittance and absorptance for the 880 nm PV cell with Au nanorods with SiO_2 shell, Au nanorod at perovskite/HTM interface, Au nanorod at perovskite/ETM interface, two Au nanorods side by side, two Au nanorods over/under, as well as the two PV cells with standard setup Au nanorod at center. The absorptance change for the various setups is given relative to the two PV cells with standard setup (from section 6.11). d is diameter, t is shell thickness and g is the gap between the two nanorods. All rods in this thesis have a length that is equal to three times its diameter (aspect ratio is 3).

6.28 Silver Rod Variations

This simulation group consists of twelve simulations with Ag nanorods integrated in the PV cell structures. Different variations of rods are used to compare the effect of these to the standard setup with a solid Ag rod at the center of the perovskite layer (section 6.12). The variations are the same as described for Au nanospheres in section 6.19. These variations are first simulated through six simulations using the 310 nm PV cell, and then the same variations are simulated through six simulations using the 880 nm PV cell. The absorptance from the simulations using the core-shell variations in the 310 nm PV cell compared to the PV cell with a standard setup Ag rod (from section 6.12) is shown in figure 6.54a, and the absorptance from the simulations using the top vs. bottom and double nanorod variations in the 310 nm PV cell compared to the PV cell with a standard setup Ag rod (from section

6.12) is shown in figure 6.54b. The same absorptance plots from the simulations using the 880 nm PV cell is shown in figures 6.55a and 6.55b. The total reflectance, transmittance, absorptance and absorptance change are shown in tables 6.53 and 6.54 for all PV cells. The absorptance change for these simulations is given relative to the standard setup PV cell with a Ag rod at the center of the perovskite layer (section 6.12).

The simulation results shows that the total absorptance of the PV cells with Ag nanorods decreases if the Ag nanorods are coated with a SiO_2 shell with a thickness of 10% of the rod diameter, compared to the PV cell where the same Ag nanorod is used with no shell.

The results from the simulations where the position of the Ag nanorod is adjusted and from the simulations where a set of two Ag nanorods is used are different for the 310 and 880 nm PV cells. For the 310 nm PV cell, both the simulation with a Ag nanorod at the perovskite/HTM (bottom) interface and the simulation with a Ag nanorod at the perovskite/ETM (top) interface shows a decrease in total absorptance. The same PV cell show increased total absorptance when two nanorods are placed side by side in the middle of the perovskite layer and when two nanorods are placed one above the other at equal distance from the middle of the perovskite layer. For the 880 nm PV cell, both the simulation with a Ag nanorod at the perovskite/HTM (bottom) interface and the simulation with a Ag nanorod at the perovskite/ETM (top) interface shows decreased absorptance. The same PV cell shows increased total absorptance when two nanorods are placed side by side in the middle of the perovskite layer, while the absorptance decreases when two nanorods are placed one above the other at equal distance from the middle of the perovskite layer.

Nanorod properties	Reflectance	Transmittance	Absorptance	Absorptance change $\%\Delta A$
Ag, center, d=60nm	0.190	0.183	0.627	-
Ag@SiO_2, center, d=60nm, t=6nm	0.191	0.247	0.562	-10.4%
Ag, center, d=30nm	0.185	0.271	0.544	-
Ag@SiO_2, center, d=30nm, t=3nm	0.187	0.276	0.537	-1.29%
Ag, bottom, d=30nm	0.189	0.269	0.542	-0.368%
Ag, top, d=30nm	0.193	0.266	0.541	-0.551%
2xAg, side by side, d=23.81nm, g=4.76nm	0.182	0.258	0.560	+2.94%
2xAg, over/under, d=23.81nm, g=4.76nm	0.188	0.267	0.545	+0.184%

Table 6.53: Total reflectance, transmittance and absorptance for the 310 nm PV cell with Ag nanorod with SiO_2 shell, Ag nanorod at perovskite/HTM interface, Ag nanorod at perovskite/ETM interface, two Ag nanorods side by side, two Ag nanorods over/under, as well as the two PV cells with standard setup Ag nanorod at center. The absorptance change for the various setups is given relative to the two PV cells with standard setup (from section 6.12). d is diameter, t is shell thickness and g is the gap between the two nanorods. All rods in this thesis have a length that is equal to three times its diameter (aspect ratio is 3).

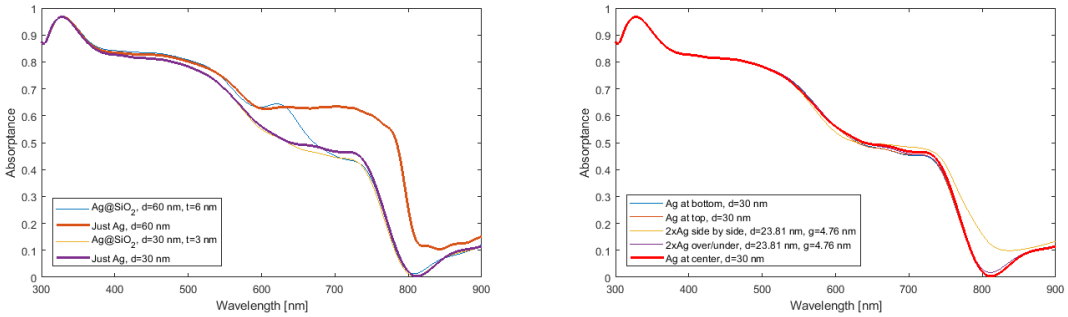

(a) (b)

Figure 6.54: Absorptance for various setups of the 310 nm PV cell. (a) Total absorptance of the Ag@SiO_2 core-shell nanorods (thin lines) compared to the Ag rod of the same size but without a SiO_2 shell (thick lines). d is the diameter of the Ag rod and t is the thickness of the SiO_2 shell. (b)Total absorptance for Ag nanorod at bottom interface, top interface, double nanorods side by side, double nanorods over/under, compared to the centered Ag nanorod of the same size (thick line) from section 6.12. d is the diameter of the rod and g is the gap between the two rods. All rods in this thesis have a length that is equal to three times its diameter (aspect ratio is 3).

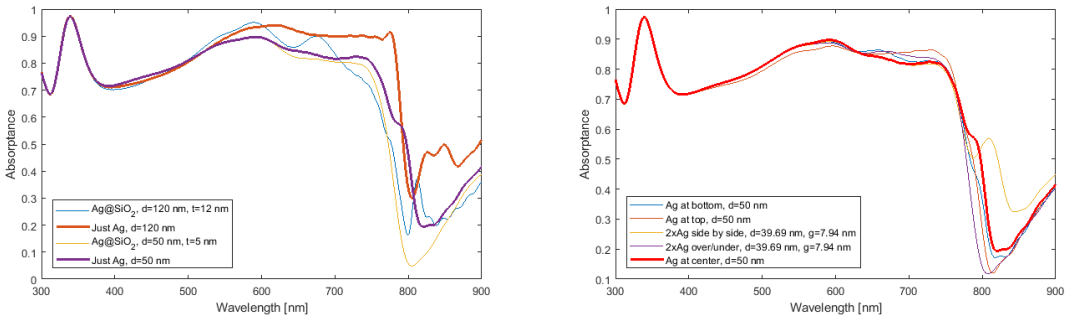

(a) (b)

Figure 6.55: Absorptance for various setups of the 880 nm PV cell. (a) Total absorptance of the Ag@SiO_2 core-shell nanorods (thin lines) compared to the Ag rod of the same size but without a SiO_2 shell (thick lines). d is the diameter of the Ag rod and t is the thickness of the SiO_2 shell. (b)Total absorptance for Ag nanorod at bottom interface, top interface, double nanorods side by side, double nanorods over/under, compared to the centered Ag nanorod of the same size (thick line) from section 6.12. d is the diameter of the rod and g is the gap between the two rods. All rods in this thesis have a length that is equal to three times its diameter (aspect ratio is 3).

Nanorod properties	Reflectance	Transmittance	Absorptance	Absorptance change $\%\Delta A$
Ag, center, d=120nm	0.191	0.039	0.770	-
Ag@SiO_2, center, d=120nm, t=12nm	0.166	0.133	0.701	-8.96%
Ag, center, d=50nm	0.144	0.142	0.714	-
Ag@SiO_2, center, d=50nm, t=5nm	0.146	0.176	0.678	-5.04%
Ag, bottom, d=50nm	0.142	0.149	0.709	-0.700%
Ag, top, d=50nm	0.148	0.147	0.705	-1.26%
2xAg, side by side, d=39.69nm, g=7.94nm	0.144	0.124	0.732	+2.52%
2xAg, over/under, d=39.69nm, g=7.94nm	0.147	0.154	0.699	-2.10%

Table 6.54: Total reflectance, transmittance and absorptance for the 880 nm PV cell with Ag nanorods with SiO_2 shell, Ag nanorod at perovskite/HTM interface, Ag nanorod at perovskite/ETM interface, two Ag nanorods side by side, two Ag nanorods over/under, as well as the two PV cells with standard setup Ag nanorod at center. The absorptance change for the various setups is given relative to the two PV cells with standard setup (from section 6.12). d is diameter, t is shell thickness and g is the gap between the two nanorods. All rods in this thesis have a length that is equal to three times its diameter (aspect ratio is 3).

6.29 Aluminum Rod Variations

This simulation group consists of twelve simulations with Al nanorods integrated in the PV cell structures. Different variations of rods are used to compare the effect of these to the standard setup with a solid Al rod at the center of the perovskite layer (section 6.13). The variations are the same as described for Au nanospheres in section 6.19. These variations are first simulated through six simulations using the 310 nm PV cell, and then the same variations are simulated through six simulations using the 880 nm PV cell. The absorptance from the simulations using the core-shell variations in the 310 nm PV cell compared to the PV cell with a standard setup Al rod (from section 6.13) is shown in figure 6.56a, and the absorptance from the simulations using the top vs. bottom and double nanorod variations in the 310 nm PV cell compared to the PV cell with a standard setup Al rod (from section

6.13) is shown in figure 6.56b. The same absorptance plots from the simulations using the 880 nm PV cell is shown in figures 6.57a and 6.57b. The total reflectance, transmittance, absorptance and absorptance change are shown in tables 6.55 and 6.56 for all PV cells. The absorptance change for these simulations is given relative to the standard setup PV cell with a Al rod at the center of the perovskite layer (section 6.13).

The simulation results shows that the total absorptance of the PV cells with Al nanorods decreases if the Al nanorods are coated with a SiO_2 shell with a thickness of 10% of the rod diameter, compared to the PV cell where the same Al nanorod is used with no shell.

The results from the simulations where the position of the Al nanorod is adjusted and from the simulations where a set of two Al nanorods is used are quite similar for the 310 and 880 nm PV cells. For both PV cells, both the simulation with a Al nanorod at the perovskite/HTM (bottom) interface and the simulation with a Al nanorod at the perovskite/ETM (top) interface shows a decrease in total absorptance. Both PV cells show an increase in total absorptance when two nanorods are placed side by side in the middle of the perovskite layer, and a decrease in absorptance when two nanorods are placed one above the other at equal distance from the middle of the perovskite layer.

Nanorod properties	Reflectance	Transmittance	Absorptance	Absorptance change $\%\Delta A$
Al, center, d=60nm	0.196	0.227	0.577	-
Al@SiO_2, center, d=60nm, t=6nm	0.196	0.270	0.534	-7.45%
Al, center, d=30nm	0.185	0.278	0.537	-
Al@SiO_2, center, d=30nm, t=3nm	0.187	0.280	0.533	-0.745%
Al, bottom, d=30nm	0.189	0.276	0.535	-0.372%
Al, top, d=30nm	0.194	0.274	0.532	-0.931%
2xAl, side by side, d=23.81nm, g=4.76nm	0.184	0.273	0.543	+1.12%
2xAl, over/under, d=23.81nm, g=4.76nm	0.189	0.275	0.536	-0.186%

Table 6.55: Total reflectance, transmittance and absorptance for the 310 nm PV cell with Al nanorod with SiO_2 shell, Al nanorod at perovskite/HTM interface, Al nanorod at perovskite/ETM interface, two Al nanorods side by side, two Al nanorods over/under, as well as the two PV cells with standard setup Al nanorod at center. The absorptance change for the various setups is given relative to the two PV cells with standard setup (from section 6.13). d is diameter, t is shell thickness and g is the gap between the two nanorods. All rods in this thesis have a length that is equal to three times its diameter (aspect ratio is 3).

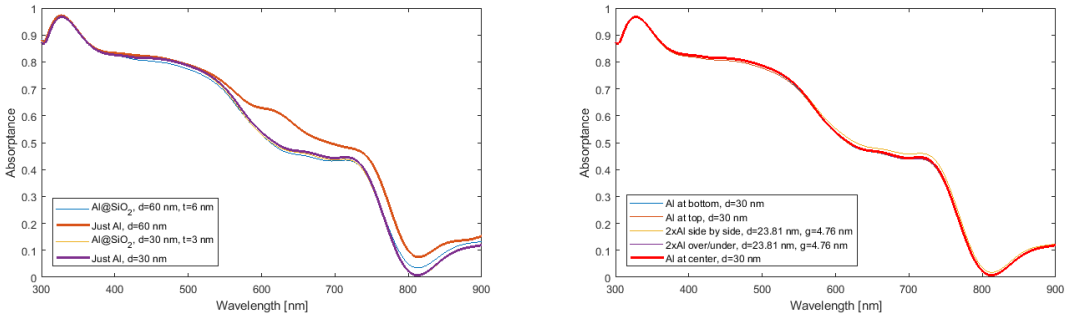

(a) (b)

Figure 6.56: Absorptance for various setups of the 310 nm PV cell. (a) Total absorptance of the Al@SiO_2 core-shell nanorods (thin lines) compared to the Al rod of the same size but without a SiO_2 shell (thick lines). d is the diameter of the Al rod and t is the thickness of the SiO_2 shell. (b)Total absorptance for Al nanorod at bottom interface, top interface, double nanorods side by side, double nanorods over/under, compared to the centered Al nanorod of the same size (thick line) from section 6.13. d is the diameter of the rod and g is the gap between the two rods. All rods in this thesis have a length that is equal to three times its diameter (aspect ratio is 3).

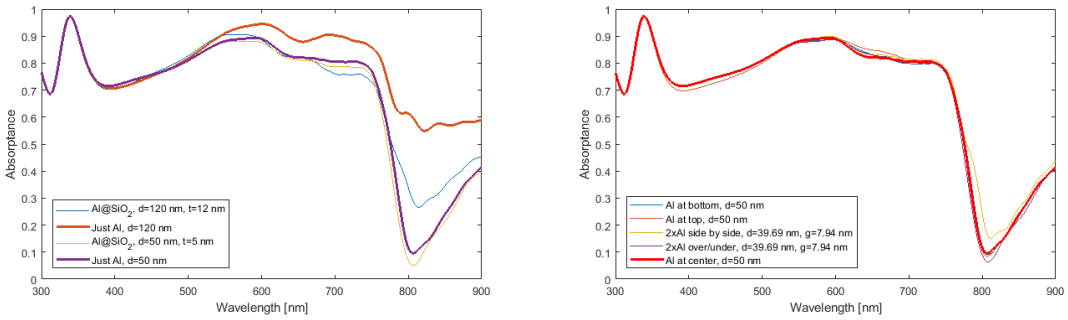

(a) (b)

Figure 6.57: Absorptance for various setups of the 880 nm PV cell. (a) Total absorptance of the Al@SiO_2 core-shell nanorods (thin lines) compared to the Al rod of the same size but without a SiO_2 shell (thick lines). d is the diameter of the Al rod and t is the thickness of the SiO_2 shell. (b)Total absorptance for Al nanorod at bottom interface, top interface, double nanorods side by side, double nanorods over/under, compared to the centered Al nanorod of the same size (thick line) from section 6.13. d is the diameter of the rod and g is the gap between the two rods. All rods in this thesis have a length that is equal to three times its diameter (aspect ratio is 3).

Nanorod properties	Reflectance	Transmittance	Absorptance	Absorptance change $\%\Delta A$
Al, center, d=120nm	0.166	0.047	0.787	-
Al@SiO_2, center, d=120nm, t=12nm	0.150	0.141	0.709	-9.91%
Al, center, d=50nm	0.144	0.167	0.689	-
Al@SiO_2, center, d=50nm, t=5nm	0.144	0.180	0.676	-1.89%
Al, bottom, d=50nm	0.143	0.170	0.687	-0.290%
Al, top, d=50nm	0.145	0.169	0.686	-0.435%
2xAl, side by side, d=39.69nm, g=7.94nm	0.142	0.156	0.702	+1.89%
2xAl, over/under, d=39.69nm, g=7.94nm	0.147	0.170	0.683	-0.871%

Table 6.56: Total reflectance, transmittance and absorptance for the 880 nm PV cell with Al nanorods with SiO_2 shell, Al nanorod at perovskite/HTM interface, Al nanorod at perovskite/ETM interface, two Al nanorods side by side, two Al nanorods over/under, as well as the two PV cells with standard setup Al nanorod at center. The absorptance change for the various setups is given relative to the two PV cells with standard setup (from section 6.13). d is diameter, t is shell thickness and g is the gap between the two nanorods. All rods in this thesis have a length that is equal to three times its diameter (aspect ratio is 3).

6.30 Platinum Rod Variations

This simulation group consists of twelve simulations with Pt nanorods integrated in the PV cell structures. Different variations of rods are used to compare the effect of these to the standard setup with a solid Pt rod at the center of the perovskite layer (section 6.14). The variations are the same as described for Au nanospheres in section 6.19. These variations are first simulated through six simulations using the 310 nm PV cell, and then the same variations are simulated through six simulations using the 880 nm PV cell. The absorptance from the simulations using the core-shell variations in the 310 nm PV cell compared to the PV cell with a standard setup Pt rod (from section 6.14) is shown in figure 6.58a, and the absorptance from the simulations using the top vs. bottom and double nanorod variations in the 310 nm PV cell compared to the PV cell with a standard setup Pt rod (from section 6.14) is shown in figure 6.58b. The same absorptance plots from the simulations

using the 880 nm PV cell is shown in figures 6.59a and 6.59b. The total reflectance, transmittance, absorptance and absorptance change are shown in tables 6.57 and 6.58 for all PV cells. The absorptance change for these simulations is given relative to the standard setup PV cell with a Pt rod at the center of the perovskite layer (section 6.14).

The simulation results shows that the total absorptance of the PV cells with Pt nanorods decreases if the Pt nanorods are coated with a SiO_2 shell with a thickness of 10% of the rod diameter, compared to the PV cell where the same Pt nanorod is used with no shell.

The results from the simulations where the position of the Pt nanorod is adjusted and from the simulations where a set of two Pt nanorods is used are quite similar for the 310 and 880 nm PV cells. For both PV cells, both the simulation with a Pt nanorod at the perovskite/HTM (bottom) interface and the simulation with a Pt nanorod at the perovskite/ETM (top) interface shows a decrease in total absorptance. Both PV cells show an increase in total absorptance when two nanorods are placed side by side in the middle of the perovskite layer, and a decrease in absorptance when two nanorods are placed one above the other at equal distance from the middle of the perovskite layer.

Nanorod properties	Reflectance	Transmittance	Absorptance	Absorptance change $\%\Delta A$
Pt, center, d=60nm	0.188	0.213	0.599	-
Pt@SiO_2, center, d=60nm, t=6nm	0.190	0.250	0.560	-6.51%
Pt, center, d=30nm	0.186	0.274	0.540	-
Pt@SiO_2, center, d=30nm, t=3nm	0.187	0.277	0.536	-0.741%
Pt, bottom, d=30nm	0.189	0.273	0.538	-0.370%
Pt, top, d=30nm	0.192	0.271	0.537	-0.556%
2xPt, side by side, d=23.81nm, g=4.76nm	0.184	0.270	0.546	+1.11%
2xPt, over/under, d=23.81nm, g=4.76nm	0.189	0.272	0.539	-0.185%

Table 6.57: Total reflectance, transmittance and absorptance for the 310 nm PV cell with Pt nanorod with SiO_2 shell, Pt nanorod at perovskite/HTM interface, Pt nanorod at perovskite/ETM interface, two Pt nanorods side by side, two Pt nanorods over/under, as well as the two PV cells with standard setup Pt nanorod at center. The absorptance change for the various setups is given relative to the two PV cells with standard setup (from section 6.14). d is diameter, t is shell thickness and g is the gap between the two nanorods. All rods in this thesis have a length that is equal to three times its diameter (aspect ratio is 3).

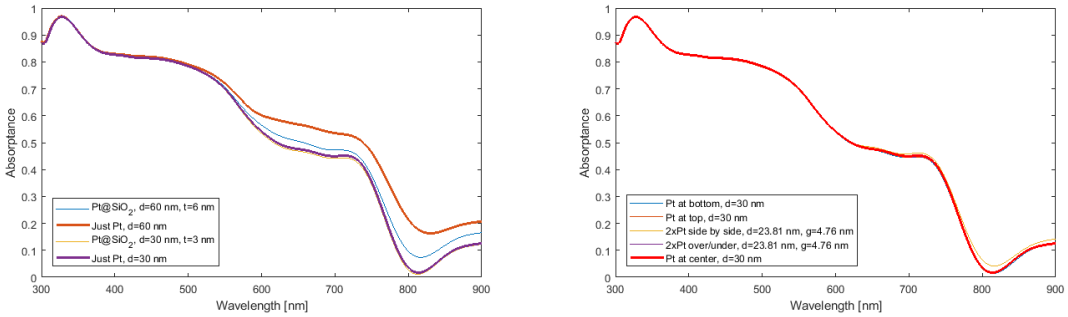

(a) (b)

Figure 6.58: Absorptance for various setups of the 310 nm PV cell. (a) Total absorptance of the Pt@SiO_2 core-shell nanorods (thin lines) compared to the Pt rod of the same size but without a SiO_2 shell (thick lines). d is the diameter of the Pt rod and t is the thickness of the SiO_2 shell. (b)Total absorptance for Pt nanorod at bottom interface, top interface, double nanorods side by side, double nanorods over/under, compared to the centered Pt nanorod of the same size (thick line) from section 6.14. d is the diameter of the rod and g is the gap between the two rods. All rods in this thesis have a length that is equal to three times its diameter (aspect ratio is 3).

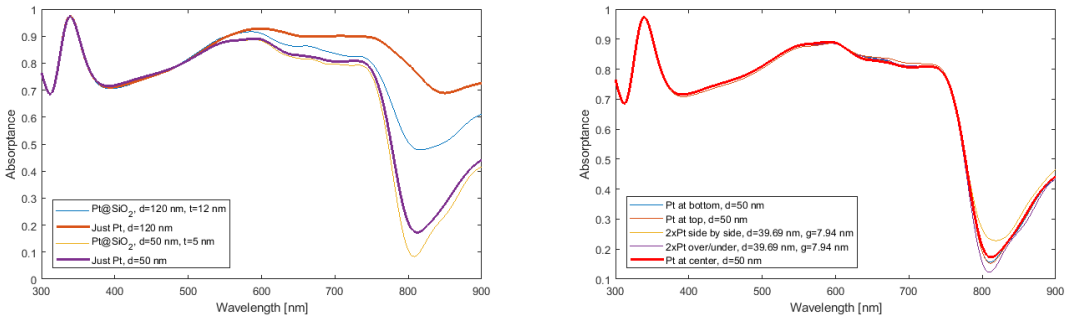

(a) (b)

Figure 6.59: Absorptance for various setups of the 880 nm PV cell. (a) Total absorptance of the Pt@SiO_2 core-shell nanorods (thin lines) compared to the Pt rod of the same size but without a SiO_2 shell (thick lines). d is the diameter of the Pt rod and t is the thickness of the SiO_2 shell. (b)Total absorptance for Pt nanorod at bottom interface, top interface, double nanorods side by side, double nanorods over/under, compared to the centered Pt nanorod of the same size (thick line) from section 6.14. d is the diameter of the rod and g is the gap between the two rods. All rods in this thesis have a length that is equal to three times its diameter (aspect ratio is 3).

Nanorod properties	Reflectance	Transmittance	Absorptance	Absorptance change $\%\Delta A$
Pt, center, d=120nm	0.153	0.025	0.822	-
Pt@SiO_2, center, d=120nm, t=12nm	0.148	0.091	0.761	-7.42%
Pt, center, d=50nm	0.143	0.157	0.700	-
Pt@SiO_2, center, d=50nm, t=5nm	0.144	0.172	0.684	-2.29%
Pt, bottom, d=50nm	0.143	0.159	0.698	-0.286%
Pt, top, d=50nm	0.143	0.159	0.698	-0.286%
2xPt, side by side, d=39.69nm, g=7.94nm	0.143	0.150	0.707	+1.00%
2xPt, over/under, d=39.69nm, g=7.94nm	0.145	0.160	0.695	-0.714%

Table 6.58: Total reflectance, transmittance and absorptance for the 880 nm PV cell with Pt nanorods with SiO_2 shell, Pt nanorod at perovskite/HTM interface, Pt nanorod at perovskite/ETM interface, two Pt nanorods side by side, two Pt nanorods over/under, as well as the two PV cells with standard setup Pt nanorod at center. The absorptance change for the various setups is given relative to the two PV cells with standard setup (from section 6.14). d is diameter, t is shell thickness and g is the gap between the two nanorods. All rods in this thesis have a length that is equal to three times its diameter (aspect ratio is 3).

6.31 Gold Pyramid Variations

This simulation group consists of twelve simulations with Au nanopyramids integrated in the PV cell structures. Different variations of pyramids are used to compare the effect of these to the standard setup with a solid Au pyramid at the center of the perovskite layer (section 6.15). The variations are the same as described for Au nanospheres in section 6.19. These variations are first simulated through six simulations using the 310 nm PV cell, and then the same variations are simulated through six simulations using the 880 nm PV cell. The absorptance from the simulations using the core-shell variations in the 310 nm PV cell compared to the PV cell with a standard setup Au pyramid (from section 6.15) is shown in figure 6.60a, and the absorptance from the simulations using the top vs. bottom and double nanopyramid variations in the 310 nm PV cell compared to the PV cell with a standard setup

Au pyramid (from section 6.15) is shown in figure 6.60b. The same absorptance plots from the simulations using the 880 nm PV cell is shown in figures 6.61a and 6.61b. The total reflectance, transmittance, absorptance and absorptance change are shown in tables 6.59 and 6.60 for all PV cells. The absorptance change for these simulations is given relative to the standard setup PV cell with a Au pyramid at the center of the perovskite layer (section 6.15).

The simulation results for the two largest (s=150 nm and s=200 nm) pyramids in both the 310 and 880 nm PV cell show that the total absorptance of the PV cells with these nanopyramids decreases if the Au nanopyramids are coated with a SiO_2 shell with a thickness of 10% of the pyramid side length, compared to the PV cell where the same Au nanopyramid is used with no shell. However, the results for the two smallest (s=75 nm and s=80 nm) pyramids in both the 310 and 880 nm PV cell show that the total absorptance of the PV cells with these nanopyramids increases slightly if the Au nanopyramids are coated with a SiO_2 shell. These are two of only four simulations where the SiO_2 shell increased the absorptance of the PV cell compared to the standard setup with no shell. The other two cases where this happened is in section 6.32 with Ag pyramids.

The results from the simulations where the position of the Au nanopyramid is adjusted and from the simulations where a set of two Au nanopyramids is used are quite similar for the 310 and 880 nm PV cells. For both PV cells, both the simulation with a Au nanopyramid at the perovskite/HTM (bottom) interface and the simulation with a Au nanopyramid at the perovskite/ETM (top) interface shows either a slight increase in total absorptance, or unchanged absorptance. Both PV cells show a decrease in total absorptance when two nanopyramids are placed side by side in the middle of the perovskite layer, and an increase in absorptance when two nanopyramids are placed one above the other at equal distance from the middle of the perovskite layer.

Nanopyramid properties	Reflectance	Transmittance	Absorptance	Absorptance change $\%\Delta A$
Au, center, s=150nm	0.207	0.144	0.649	-
Au@SiO_2, center, s=150nm, t=15nm	0.243	0.148	0.609	-6.16%
Au, center, s=75nm	0.197	0.241	0.562	-
Au@SiO_2, center, s=75nm, t=7.5nm	0.199	0.225	0.576	+2.49%
Au, bottom, s=75nm	0.191	0.237	0.572	+1.78%
Au, top, s=75nm	0.173	0.255	0.572	+1.78%
2xAu, side by side, s=59.52nm, g=11.90nm	0.198	0.246	0.556	-1.07%
2xAu, over/under, s=59.52nm, g=11.90nm	0.186	0.243	0.571	+1.60%

Table 6.59: Total reflectance, transmittance and absorptance for the 310 nm PV cell with Au nanopyramid with SiO_2 shell, Au nanopyramid at perovskite/HTM interface, Au nanopyramid at perovskite/ETM interface, two Au nanopyramids side by side, two Au nanopyramids over/under, as well as the two PV cells with standard setup Au nanopyramid at center. The absorptance change for the various setups is given relative to the two PV cells with standard setup (from section 6.15). s is side length, t is shell thickness and g is the gap between the two nanopyramids. All pyramids in this thesis have a height that is equal to its side length.

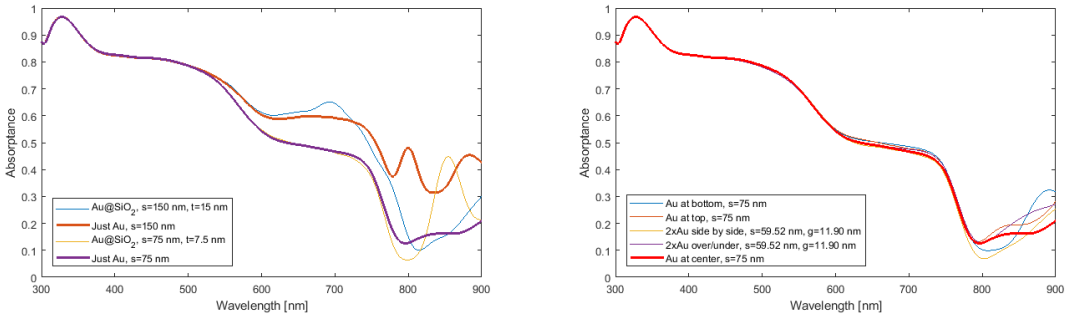

(a) (b)

Figure 6.60: Absorptance for various setups of the 310 nm PV cell. (a) Total absorptance of the Au@SiO_2 core-shell nanopyramids (thin lines) compared to the Au pyramid of the same size but without a SiO_2 shell (thick lines). s is the side length of the Au pyramid and t is the thickness of the SiO_2 shell. (b)Total absorptance for Au nanopyramid at bottom interface, top interface, double nanopyramids side by side, double nanopyramids over/under, compared to the centered Au nanopyramid of the same size (thick line) from section 6.15. s is the side length of the pyramid and g is the gap between the two pyramids. All pyramids in this thesis have a height that is equal to its side length.

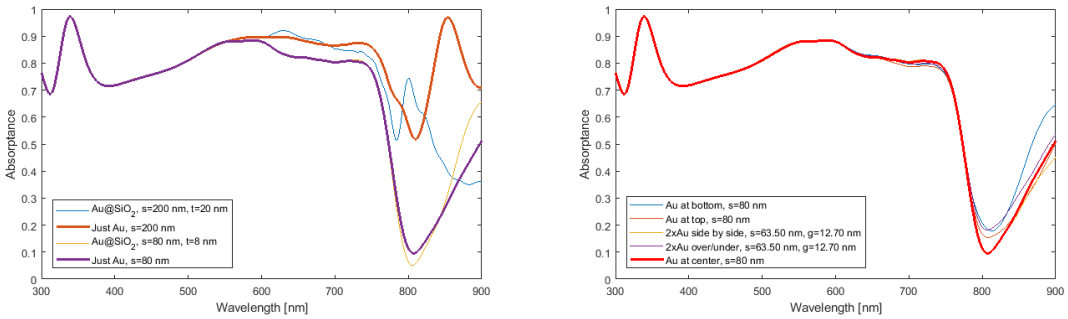

(a) (b)

Figure 6.61: Absorptance for various setups of the 880 nm PV cell. (a) Total absorptance of the Au@SiO_2 core-shell nanopyramids (thin lines) compared to the Au pyramid of the same size but without a SiO_2 shell (thick lines). s is the side length of the Au pyramid and t is the thickness of the SiO_2 shell. (b)Total absorptance for Au nanopyramid at bottom interface, top interface, double nanopyramids side by side, double nanopyramids over/under, compared to the centered Au nanopyramid of the same size (thick line) from section 6.15. s is the side length of the pyramid and g is the gap between the two pyramids. All pyramids in this thesis have a height that is equal to its side length.

Nanopyramid properties	Reflectance	Transmittance	Absorptance	Absorptance change $\%\Delta A$
Au, center, s=200nm	0.148	0.042	0.810	-
Au@SiO_2, center, s=200nm, t=20nm	0.205	0.039	0.756	-6.67%
Au, center, s=80nm	0.146	0.162	0.692	-
Au@SiO_2, center, s=80nm, t=8nm	0.155	0.147	0.698	+0.867%
Au, bottom, s=80nm	0.142	0.147	0.711	+2.75%
Au, top, s=80nm	0.151	0.157	0.692	0.00%
2xAu, side by side, s=63.50nm, g=12.70nm	0.147	0.164	0.689	-0.434%
2xAu, over/under, s=63.50nm, g=12.70nm	0.142	0.156	0.702	+1.45%

Table 6.60: Total reflectance, transmittance and absorptance for the 880 nm PV cell with Au nanopyramids with SiO_2 shell, Au nanopyramid at perovskite/HTM interface, Au nanopyramid at perovskite/ETM interface, two Au nanopyramids side by side, two Au nanopyramids over/under, as well as the two PV cells with standard setup Au nanopyramid at center. The absorptance change for the various setups is given relative to the two PV cells with standard setup (from section 6.15). s is side length, t is shell thickness and g is the gap between the two nanopyramids. All pyramids in this thesis have a height that is equal to its side length.

6.32 Silver Pyramid Variations

This simulation group consists of twelve simulations with Ag nanopyramids integrated in the PV cell structures. Different variations of pyramids are used to compare the effect of these to the standard setup with a solid Ag pyramid at the center of the perovskite layer (section 6.16). The variations are the same as described for Au nanospheres in section 6.19. These variations are first simulated through six simulations using the 310 nm PV cell, and then the same variations are simulated through six simulations using the 880 nm PV cell. The absorptance from the simulations using the core-shell variations in the 310 nm PV cell compared to the PV cell with a standard setup Ag pyramid (from section 6.16) is shown in figure 6.62a, and the absorptance from the simulations using the top vs. bottom and double nanopyramid variations in the 310 nm PV cell compared to the PV cell with a standard setup

Ag pyramid (from section 6.16) is shown in figure 6.62b. The same absorptance plots from the simulations using the 880 nm PV cell is shown in figures 6.63a and 6.63b. The total reflectance, transmittance, absorptance and absorptance change are shown in tables 6.61 and 6.62 for all PV cells. The absorptance change for these simulations is given relative to the standard setup PV cell with a Ag pyramid at the center of the perovskite layer (section 6.16).

The simulation results for the two largest (s=150 nm and s=200 nm) pyramids in both the 310 and 880 nm PV cell show that the total absorptance of the PV cells with these nanopyramids decreases if the Ag nanopyramids are coated with a SiO_2 shell with a thickness of 10% of the pyramid side length, compared to the PV cell where the same Ag nanopyramid is used with no shell. However, the results for the two smallest (s=75 nm and s=80 nm) pyramids in both the 310 and 880 nm PV cell show that the total absorptance of the PV cells with these nanopyramids increases slightly if the Ag nanopyramids are coated with a SiO_2 shell. These are two of only four simulations where the SiO_2 shell increased the absorptance of the PV cell compared to the standard setup with no shell. The other two cases where this happened is in section 6.31 with Au pyramids.

The results from the simulations where the position of the Ag nanopyramid is adjusted and from the simulations where a set of two Ag nanopyramids is used are different for the 310 and 880 nm PV cells. For the 310 nm PV cell, both the simulation with a Ag nanopyramid at the perovskite/HTM (bottom) interface and the simulation with a Ag nanopyramid at the perovskite/ETM (top) interface shows an increase in total absorptance. The same PV cell shows decreased total absorptance when two nanopyramids are placed side by side in the middle of the perovskite layer, and increased absorptance when two nanopyramids are placed one above the other at equal distance from the middle of the perovskite layer. For the 880 nm PV cell, the simulation with a Ag nanopyramid at the perovskite/HTM (bottom) interface shows increased absorptance, and the simulation with a Ag nanopyramid at the perovskite/ETM (top) interface shows decreased absorptance. The same PV cell shows decreased total absorptance when two nanopyramids are placed side by side in the middle of the perovskite layer, while the absorptance increases when two nanopyramids are placed one above the other at equal distance from the middle of the perovskite layer.

Nanopyramid properties	Reflectance	Transmittance	Absorptance	Absorptance change $\%\Delta A$
Ag, center, s=150nm	0.209	0.138	0.653	-
Ag@SiO_2, center, s=150nm, t=15nm	0.260	0.134	0.606	-7.20%
Ag, center, s=75nm	0.200	0.236	0.564	-
Ag@SiO_2, center, s=75nm, t=7.5nm	0.197	0.227	0.576	+2.13%
Ag, bottom, s=75nm	0.197	0.226	0.577	+2.30%
Ag, top, s=75nm	0.170	0.254	0.576	+2.13%
2xAg, side by side, s=59.52nm, g=11.90nm	0.199	0.241	0.560	-0.709%
2xAg, over/under, s=59.52nm, g=11.90nm	0.185	0.238	0.577	+2.30%

Table 6.61: Total reflectance, transmittance and absorptance for the 310 nm PV cell with Ag nanopyramid with SiO_2 shell, Ag nanopyramid at perovskite/HTM interface, Ag nanopyramid at perovskite/ETM interface, two Ag nanopyramids side by side, two Ag nanopyramids over/under, as well as the two PV cells with standard setup Ag nanopyramid at center. The absorptance change for the various setups is given relative to the two PV cells with standard setup (from section 6.16). s is side length, t is shell thickness and g is the gap between the two nanopyramids. All pyramids in this thesis have a height that is equal to its side length.

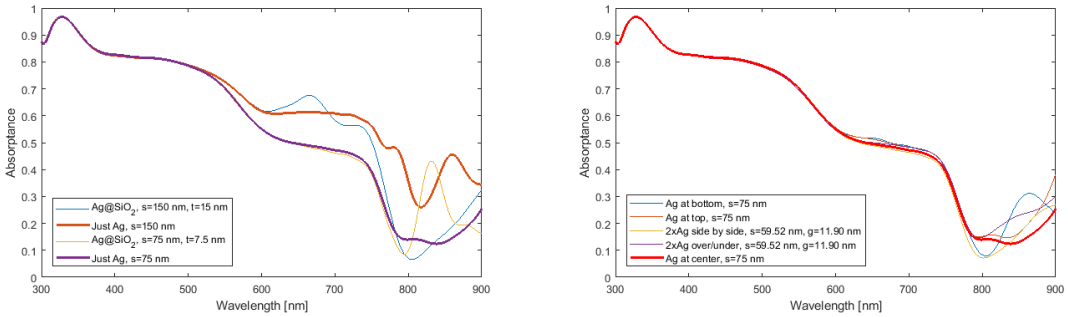

(a) (b)

Figure 6.62: Absorptance for various setups of the 310 nm PV cell. (a) Total absorptance of the Ag@SiO_2 core-shell nanopyramids (thin lines) compared to the Ag pyramid of the same size but without a SiO_2 shell (thick lines). s is the side length of the Ag pyramid and t is the thickness of the SiO_2 shell. (b)Total absorptance for Ag nanopyramid at bottom interface, top interface, double nanopyramids side by side, double nanopyramids over/under, compared to the centered Ag nanopyramid of the same size (thick line) from section 6.16. s is the side length of the pyramid and g is the gap between the two pyramids. All pyramids in this thesis have a height that is equal to its side length.

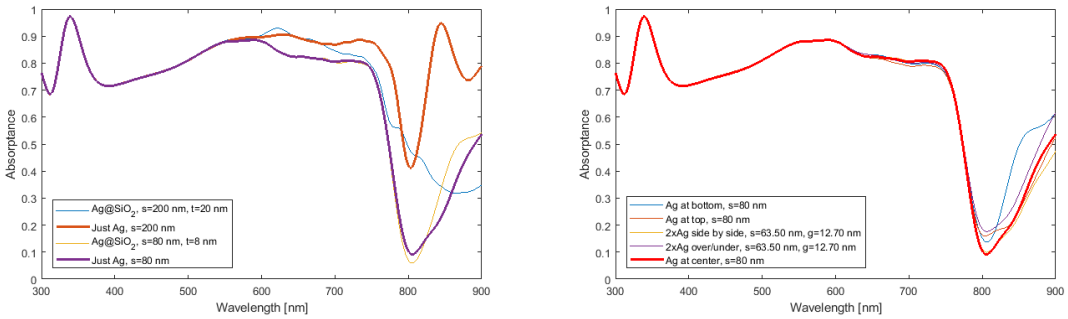

(a) (b)

Figure 6.63: Absorptance for various setups of the 880 nm PV cell. (a) Total absorptance of the Ag@SiO_2 core-shell nanopyramids (thin lines) compared to the Ag pyramid of the same size but without a SiO_2 shell (thick lines). s is the side length of the Ag pyramid and t is the thickness of the SiO_2 shell. (b)Total absorptance for Ag nanopyramid at bottom interface, top interface, double nanopyramids side by side, double nanopyramids over/under, compared to the centered Ag nanopyramid of the same size (thick line) from section 6.16. s is the side length of the pyramid and g is the gap between the two pyramids. All pyramids in this thesis have a height that is equal to its side length.

Nanopyramid properties	Reflectance	Transmittance	Absorptance	Absorptance change $\%\Delta A$
Ag, center, s=200nm	0.155	0.036	0.809	-
Ag@SiO_2, center, s=200nm, t=20nm	0.236	0.030	0.734	-9.27%
Ag, center, s=80nm	0.147	0.159	0.694	-
Ag@SiO_2, center, s=80nm, t=8nm	0.163	0.137	0.700	+0.865%
Ag, bottom, s=80nm	0.143	0.141	0.716	+3.17%
Ag, top, s=80nm	0.153	0.154	0.693	-0.144%
2xAg, side by side, s=63.50nm, g=12.70nm	0.148	0.163	0.689	-0.720%
2xAg, over/under, s=63.50nm, g=12.70nm	0.142	0.152	0.706	+1.73%

Table 6.62: Total reflectance, transmittance and absorptance for the 880 nm PV cell with Ag nanopyramids with SiO_2 shell, Ag nanopyramid at perovskite/HTM interface, Ag nanopyramid at perovskite/ETM interface, two Ag nanopyramids side by side, two Ag nanopyramids over/under, as well as the two PV cells with standard setup Ag nanopyramid at center. The absorptance change for the various setups is given relative to the two PV cells with standard setup (from section 6.16). s is side length, t is shell thickness and g is the gap between the two nanopyramids. All pyramids in this thesis have a height that is equal to its side length.

6.33 Aluminum Pyramid Variations

This simulation group consists of twelve simulations with Al nanopyramids integrated in the PV cell structures. Different variations of pyramids are used to compare the effect of these to the standard setup with a solid Al pyramid at the center of the perovskite layer (section 6.17). The variations are the same as described for Au nanospheres in section 6.19. These variations are first simulated through six simulations using the 310 nm PV cell, and then the same variations are simulated through six simulations using the 880 nm PV cell. The absorptance from the simulations using the core-shell variations in the 310 nm PV cell compared to the PV cell with a standard setup Al pyramid (from section 6.17) is shown in figure 6.64a, and the absorptance from the simulations using the top vs. bottom and double nanopyramid variations in the 310 nm PV cell compared to the PV cell with a standard setup

Al pyramid (from section 6.17) is shown in figure 6.64b. The same absorptance plots from the simulations using the 880 nm PV cell is shown in figures 6.65a and 6.65b. The total reflectance, transmittance, absorptance and absorptance change are shown in tables 6.63 and 6.64 for all PV cells. The absorptance change for these simulations is given relative to the standard setup PV cell with a Al pyramid at the center of the perovskite layer (section 6.17).

The simulation results shows that the total absorptance of the PV cells with Al nanopyramids decreases if the Al nanopyramids are coated with a SiO_2 shell with a thickness of 10% of the pyramid side length, compared to the PV cell where the same Al nanopyramid is used with no shell.

The results from the simulations where the position of the Al nanopyramid is adjusted and from the simulations where a set of two Al nanopyramids is used are quite similar for the 310 and 880 nm PV cells. For the 310 nm PV cell, the simulation with an Al nanopyramid at the perovskite/HTM (bottom) interface shows decreased absorptance, while the absorptance is unchanged in the same simulation for the 800 nm PV cell. The simulation with an Al nanopyramid at the perovskite/ETM (top) interface, the simulation where two Al nanopyramids are placed side by side in the middle of the perovskite layer, and the simulation where two Al nanopyramids are placed one above the other at equal distance from the middle of the perovskite layer all show slightly increased absorptance, both for the 310 and 880 nm PV cells.

Nanopyramid properties	Reflectance	Transmittance	Absorptance	Absorptance change $\%\Delta A$
Al, center, s=150nm	0.244	0.093	0.663	-
Al@SiO_2, center, s=150nm, t=15nm	0.236	0.126	0.638	-3.77%
Al, center, s=75nm	0.187	0.229	0.584	-
Al@SiO_2, center, s=75nm, t=7.5nm	0.183	0.260	0.557	-4.62%
Al, bottom, s=75nm	0.199	0.232	0.569	-2.57%
Al, top, s=75nm	0.170	0.231	0.599	+2.57%
2xAl, side by side, s=59.52nm, g=11.90nm	0.188	0.222	0.590	+1.03%
2xAl, over/under, s=59.52nm, g=11.90nm	0.181	0.232	0.587	+0.514%

Table 6.63: Total reflectance, transmittance and absorptance for the 310 nm PV cell with Al nanopyramid with SiO_2 shell, Al nanopyramid at perovskite/HTM interface, Al nanopyramid at perovskite/ETM interface, two Al nanopyramids side by side, two Al nanopyramids over/under, as well as the two PV cells with standard setup Al nanopyramid at center. The absorptance change for the various setups is given relative to the two PV cells with standard setup (from section 6.17). s is side length, t is shell thickness and g is the gap between the two nanopyramids. All pyramids in this thesis have a height that is equal to its side length.

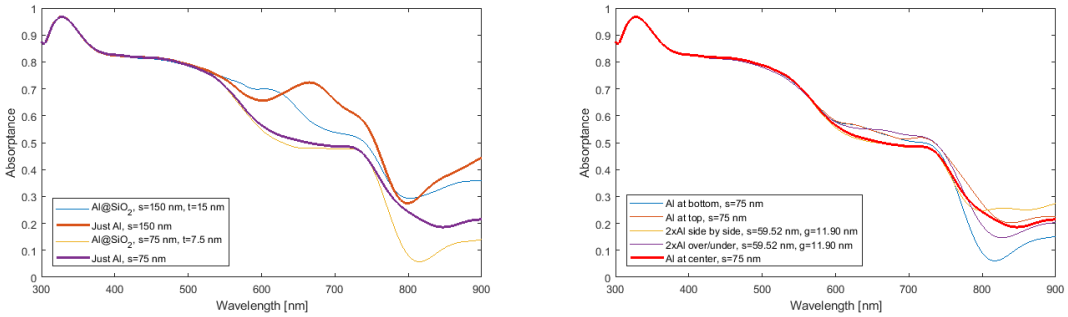

(a) (b)

Figure 6.64: Absorptance for various setups of the 310 nm PV cell. (a) Total absorptance of the Al@SiO_2 core-shell nanopyramids (thin lines) compared to the Al pyramid of the same size but without a SiO_2 shell (thick lines). s is the side length of the Al pyramid and t is the thickness of the SiO_2 shell. (b)Total absorptance for Al nanopyramid at bottom interface, top interface, double nanopyramids side by side, double nanopyramids over/under, compared to the centered Al nanopyramid of the same size (thick line) from section 6.17. s is the side length of the pyramid and g is the gap between the two pyramids. All pyramids in this thesis have a height that is equal to its side length.

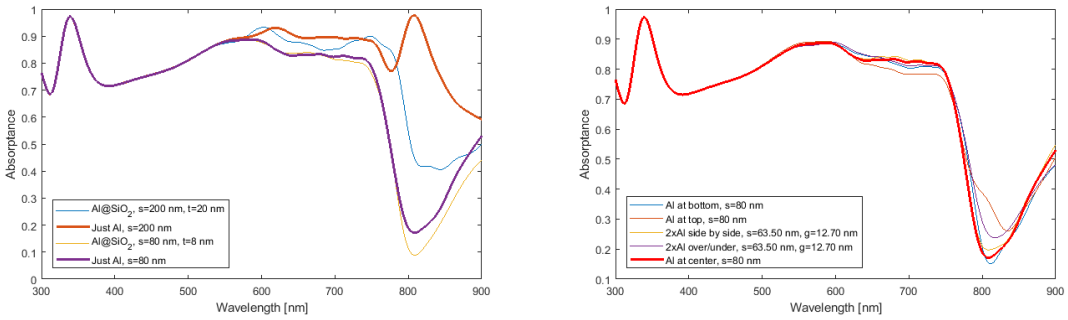

(a) (b)

Figure 6.65: Absorptance for various setups of the 880 nm PV cell. (a) Total absorptance of the Al@SiO_2 core-shell nanopyramids (thin lines) compared to the Al pyramid of the same size but without a SiO_2 shell (thick lines). s is the side length of the Al pyramid and t is the thickness of the SiO_2 shell. (b)Total absorptance for Al nanopyramid at bottom interface, top interface, double nanopyramids side by side, double nanopyramids over/under, compared to the centered Al nanopyramid of the same size (thick line) from section 6.17. s is the side length of the pyramid and g is the gap between the two pyramids. All pyramids in this thesis have a height that is equal to its side length.

Nanopyramid properties	Reflectance	Transmittance	Absorptance	Absorptance change $\%\Delta A$
Al, center, s=200nm	0.161	0.015	0.824	-
Al@SiO_2, center, s=200nm, t=20nm	0.205	0.031	0.764	-7.28%
Al, center, s=80nm	0.156	0.139	0.705	-
Al@SiO_2, center, s=80nm, t=8nm	0.150	0.161	0.689	-2.27%
Al, bottom, s=80nm	0.153	0.142	0.705	0.00%
Al, top, s=80nm	0.148	0.142	0.710	+0.709%
2xAl, side by side, s=63.50nm, g=12.70nm	0.158	0.133	0.709	+0.567%
2xAl, over/under, s=63.50nm, g=12.70nm	0.145	0.142	0.713	+1.13%

Table 6.64: Total reflectance, transmittance and absorptance for the 880 nm PV cell with Al nanopyramids with SiO_2 shell, Al nanopyramid at perovskite/HTM interface, Al nanopyramid at perovskite/ETM interface, two Al nanopyramids side by side, two Al nanopyramids over/under, as well as the two PV cells with standard setup Al nanopyramid at center. The absorptance change for the various setups is given relative to the two PV cells with standard setup (from section 6.17). s is side length, t is shell thickness and g is the gap between the two nanopyramids. All pyramids in this thesis have a height that is equal to its side length.

6.34 Platinum Pyramid Variations

This simulation group consists of twelve simulations with Pt nanopyramids integrated in the PV cell structures. Different variations of pyramids are used to compare the effect of these to the standard setup with a solid Pt pyramid at the center of the perovskite layer (section 6.18). The variations are the same as described for Au nanospheres in section 6.19. These variations are first simulated through six simulations using the 310 nm PV cell, and then the same variations are simulated through six simulations using the 880 nm PV cell. The absorptance from the simulations using the core-shell variations in the 310 nm PV cell compared to the PV cell with a standard setup Pt pyramid (from section 6.18) is shown in figure 6.66a, and the absorptance from the simulations using the top vs. bottom and double nanopyramid variations in the 310 nm PV cell compared to the PV cell with a standard setup Pt pyramid (from section 6.18) is shown in figure 6.66b. The same absorptance plots from the simulations using the 880 nm PV cell is shown in figures 6.67a and

6.67b. The total reflectance, transmittance, absorptance and absorptance change are shown in tables 6.65 and 6.66 for all PV cells. The absorptance change for these simulations is given relative to the standard setup PV cell with a Pt pyramid at the center of the perovskite layer (section 6.18).

The simulation results shows that the total absorptance of the PV cells with Pt nanopyramids decreases if the Pt nanopyramids are coated with a SiO_2 shell with a thickness of 10% of the pyramid side length, compared to the PV cell where the same Pt nanopyramid is used with no shell.

The results from the simulations where the position of the Pt nanopyramid is adjusted and from the simulations where a set of two Pt nanopyramids is used are different for the 310 and 880 nm PV cells. For the 310 nm PV cell, the simulation with a Pt nanopyramid at the perovskite/HTM (bottom) interface shows decreased total absorptance, while the simulation with a Pt nanopyramid at the perovskite/ETM (top) interface shows an increase in total absorptance. The same PV cell shows decreased total absorptance when two nanopyramids are placed side by side in the middle of the perovskite layer, and unchanged absorptance when two nanopyramids are placed one above the other at equal distance from the middle of the perovskite layer. For the 880 nm PV cell, both the simulation with a Pt nanopyramid at the perovskite/HTM (bottom) interface and the simulation with a Pt nanopyramid at the perovskite/ETM (top) interface shows increased total absorptance. The same PV cell also shows increased total absorptance when two nanopyramids are placed side by side in the middle of the perovskite layer, and when two nanopyramids are placed one above the other at equal distance from the middle of the perovskite layer.

Nanopyramid properties	Reflectance	Transmittance	Absorptance	Absorptance change $\%\Delta A$
Pt, center, s=150nm	0.210	0.137	0.653	-
Pt@SiO_2, center, s=150nm, t=15nm	0.212	0.154	0.634	-2.91%
Pt, center, s=75nm	0.189	0.246	0.565	-
Pt@SiO_2, center, s=75nm, t=7.5nm	0.187	0.255	0.558	-1.24%
Pt, bottom, s=75nm	0.194	0.245	0.561	-0.708%
Pt, top, s=75nm	0.175	0.251	0.574	+1.59%
2xPt, side by side, s=59.52nm, g=11.90nm	0.189	0.247	0.564	-0.177%
2xPt, over/under, s=59.52nm, g=11.90nm	0.185	0.250	0.565	0.00%

Table 6.65: Total reflectance, transmittance and absorptance for the 310 nm PV cell with Pt nanopyramid with SiO_2 shell, Pt nanopyramid at perovskite/HTM interface, Pt nanopyramid at perovskite/ETM interface, two Pt nanopyramids side by side, two Pt nanopyramids over/under, as well as the two PV cells with standard setup Pt nanopyramid at center. The absorptance change for the various setups is given relative to the two PV cells with standard setup (from section 6.18). s is side length, t is shell thickness and g is the gap between the two nanopyramids. All pyramids in this thesis have a height that is equal to its side length.

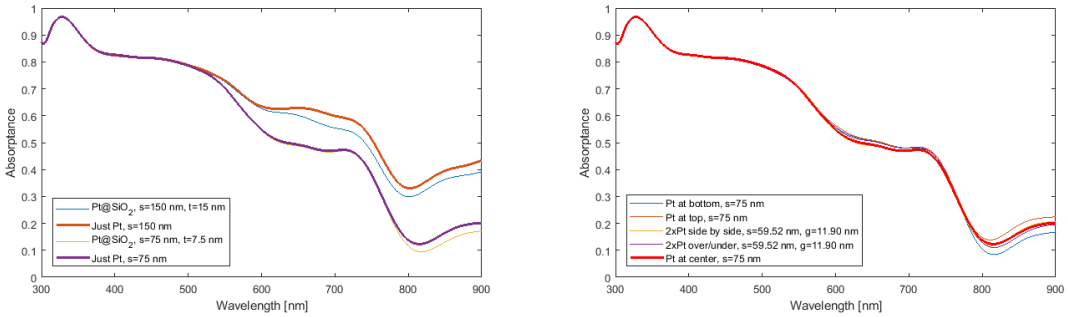

(a) (b)

Figure 6.66: Absorptance for various setups of the 310 nm PV cell. (a) Total absorptance of the Pt@SiO_2 core-shell nanopyramids (thin lines) compared to the Pt pyramid of the same size but without a SiO_2 shell (thick lines). s is the side length of the Pt pyramid and t is the thickness of the SiO_2 shell. (b)Total absorptance for Pt nanopyramid at bottom interface, top interface, double nanopyramids side by side, double nanopyramids over/under, compared to the centered Pt nanopyramid of the same size (thick line) from section 6.18. s is the side length of the pyramid and g is the gap between the two pyramids. All pyramids in this thesis have a height that is equal to its side length.

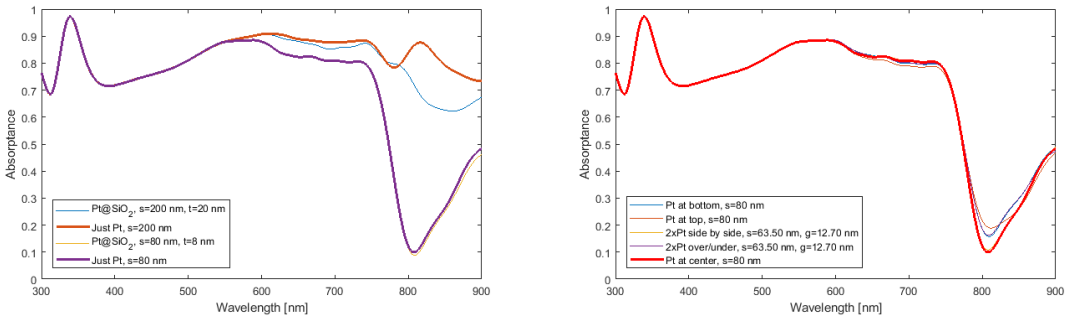

(a) (b)

Figure 6.67: Absorptance for various setups of the 880 nm PV cell. (a) Total absorptance of the Pt@SiO_2 core-shell nanopyramids (thin lines) compared to the Pt pyramid of the same size but without a SiO_2 shell (thick lines). s is the side length of the Pt pyramid and t is the thickness of the SiO_2 shell. (b)Total absorptance for Pt nanopyramid at bottom interface, top interface, double nanopyramids side by side, double nanopyramids over/under, compared to the centered Pt nanopyramid of the same size (thick line) from section 6.18. s is the side length of the pyramid and g is the gap between the two pyramids. All pyramids in this thesis have a height that is equal to its side length.

Nanopyramid properties	Reflectance	Transmittance	Absorptance	Absorptance change $\%\Delta A$
Pt, center, s=200nm	0.140	0.032	0.828	-
Pt@SiO_2, center, s=200nm, t=20nm	0.158	0.043	0.799	-3.50%
Pt, center, s=80nm	0.149	0.158	0.693	-
Pt@SiO_2, center, s=80nm, t=8nm	0.149	0.162	0.689	-0.577%
Pt, bottom, s=80nm	0.146	0.154	0.700	+1.01%
Pt, top, s=80nm	0.146	0.159	0.695	+0.289%
2xPt, side by side, s=63.50nm, g=12.70nm	0.150	0.156	0.694	+0.144%
2xPt, over/under, s=63.50nm, g=12.70nm	0.144	0.157	0.699	+0.866%

Table 6.66: Total reflectance, transmittance and absorptance for the 880 nm PV cell with Pt nanopyramids with SiO_2 shell, Pt nanopyramid at perovskite/HTM interface, Pt nanopyramid at perovskite/ETM interface, two Pt nanopyramids side by side, two Pt nanopyramids over/under, as well as the two PV cells with standard setup Pt nanopyramid at center. The absorptance change for the various setups is given relative to the two PV cells with standard setup (from section 6.18). s is side length, t is shell thickness and g is the gap between the two nanopyramids. All pyramids in this thesis have a height that is equal to its side length.

6.35 Results Summary

This section will summarize the results of all simulations performed in this thesis as a whole, to try to identify the best choices regarding material (Au, Ag, Al, Pt) and shape (sphere, cube, rod, pyramid) of the nanoparticles. This will be done for both the 310 and 880 nm PV cells to see if there are differences in the preferred materials and shapes for the two different PV cell thicknesses. All simulations result in increased absorptance relative to the reference cell without nanoparticles, except a few rare exceptions with the smallest particle size which result in unchanged absorptance. This is consistent with other available research results summarized in chapter 4.2 and table 4.1, which also show improved PV cell characteristics in all cases when metal nanoparticles are integrated into the PV cell structure. However, the majority of research articles in the field deal with only one metal at a time and

does not compare the different metals to each other. A rare exception to this is the article by Carretero-Palacios and co-workers [18] where Au, Ag and Al nanospheres are used in the simulations. Their results indicate that Ag is the most beneficial of these three metals in terms of increasing the absorptance of the PV cell. However, the thickness of their perovskite layer is 300 nm, they used normal glass instead of TiO_2, and they used a generic substrate with constant refractive index instead of spiro-OMeTAD. These differences could all have a significant effect on the results of the simulations, and therefore the results cannot be directly compared to the results in this thesis.

6.35.1 Maximum Absorptance

The general trend in the simulation results is that relatively large nanoparticles results in higher absorptance than relatively small nanoparticles. A rare exception to this trend is seen in the simulations using nanocubes in the 880 nm PV cell. In these simulations, the maximum absorptance and highest absorptance increase is seen in the third largest nanocube (medium sized), and then the absorptance actually drops for the two largest nanocubes. This drop is particularly significant for the Au, Ag and Al nanocubes, while it is less pronounced for the Pt nanocubes.

Another clear trend is that the simulations using the 880 nm PV cells result in higher total absorptance when compared to the simulations using the 310 nm PV cell with the same nanoparticle material and shape. However, the simulations using the 310 nm PV cell usually show a much higher relative absorptance increase. This could indicate that thinner PV cells could benefit even more from the plasmonic effects related to the use of nanoparticles than relatively thicker PV cells. This is consistent with other research results, among them Carretero-Palacios and co-workers [18] who found a 10% enhancement in absorptance for a perovskite film with a thickness of 200 nm, while the absorptance enhancement for a 300 nm film was found to be 6%.

The maximum total absorptance seen in the simulations was achieved by the Pt pyramid with side length and height equal to 250 nm, embedded at the center of the perovskite layer in the 880 nm PV cell. The total absorptance achieved with this setup was 0.861, which means that 86.1% of the incident light in the chosen wavelength interval (300-900 nm) was absorbed by the PV cell structure. A possible explanation for this nanoparticle resulting in the highest total absorptance could be that this is the particle that covers the largest area of the simulation region that is perpendicular to the incident light, but at the same time the pyramid shape means that the "plane surface effect" described in chapter 6.7 is not dominant in this case. This is both because it is only the base of the pyramid that is in close proximity to the pyramids around it, and also because Pt is the material in this thesis that suffers the least from this effect.

The maximum increase in absorptance relative to the reference PV cell without nanoparticles was achieved by the Pt cube with side lengths equal to 150 nm, embedded at the center of the perovskite layer in the 310 nm PV cell. This setup increased the total absorptance by 52.9% relative to the same PV cell without a Pt cube. The value for the total absorptance was 0.812 (81.2% of incident light absorbed), which was even higher than the total absorptance of many of the setups using the 880 nm PV cell. The explanation for this high absorptance is most likely

that the 150 nm nanocube covers the largest area of the simulation region that is perpendicular to the incident light, and at the same time there is enough space between the nanocubes to avoid the "plane surface effect" described in chapter 6.7.

These two maximum results indicate that Pt could be the most efficient material for nanoparticles when it comes to increasing the total absorptance of the type of perovskite PV cells used in this thesis.

6.35.2 Spheres

This section gives a summary of the results from the simulations using solid spheres as nanoparticles.

310 nm PV cell

In the simulations with small sphere sizes, all four metals result in approximately the same absorptance. Once the diameter of the sphere gets to 50 nm, Au and Ag start to result in higher absorptance than Al and Pt. This difference increases until the diameter of the sphere is 100 nm, at which point Au and Ag results in noticeably higher absorptance than Al and Pt. However, this shifts for the two largest sphere sizes. Particularly for the largest sphere with a diameter of 150 nm, Al and Pt result in noticably higher absorptance than Au and Ag. The Pt sphere with a diameter of 150 nm results in the highest total absorptance value of 0.726, which is a 36.7% increase in absorptance relative to the reference cell without nanoparticles. The results show that the size of the nanosphere will most likely affect which metal is best suited to increase the absorptance of the PV cell. The absorptance increase for all metals and sphere sizes relative to the reference PV cell without nanoparticles is shown in figure 6.68a.

880 nm PV cell

For the three smallest sphere sizes with diameters equal to 20, 50 and 80 nm, Au and Ag result in slightly higher absorptance than Al and Pt. When the diameter gets to 150 nm, Al is approximately equal to Au and Ag, while Pt now results in higher absorptance than the other three. For the two largest spheres with diameters of 200 and 250 nm, Al results in noticably higher absorptance than Au and Ag, but it is Pt that results in the highest absorptance by far. The Pt sphere with diameter 250 nm results in the highest total absorptance with a value of 0.860, which is a 28.2% increase in absorptance relative to the reference cell without nanoparticles. The results again show that the size of the nanosphere will most likely affect which metal is best suited to increase the absorptance of the PV cell. The absorptance increase for all metals and sphere sizes relative to the reference PV cell without nanoparticles is shown in figure 6.68b.

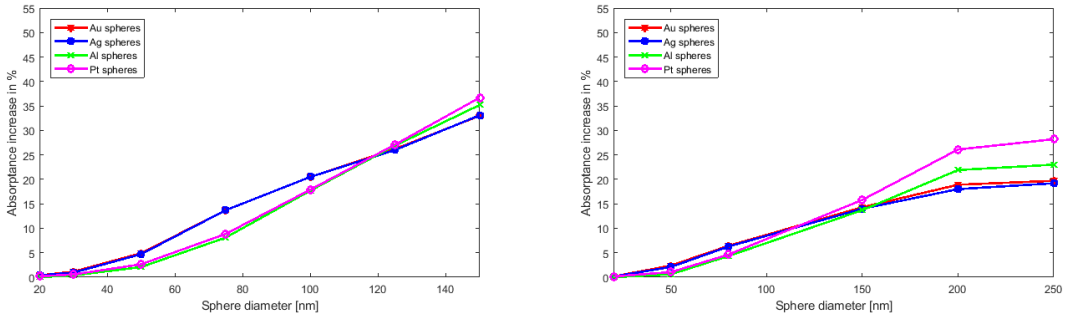

(a) (b)

Figure 6.68: Percentage increase in total absorptance for the PV cells with integrated nanospheres. (a) 310 nm PV cell. (b) 880 nm PV cell.

6.35.3 Cubes

This section gives a summary of the results from the simulations using solid cubes as nanoparticles.

310 nm PV cell

For the three smallest cubes with side lengths of 20, 30 and 50 nm, Au and Ag results in higher absorptance than Al and Pt. Once the side length of the cube gets to 75 nm, Pt is almost equal to Au and Ag while Al now results in the highest absorptance. For the three largest cubes with side lengths of 100, 125 and 150 nm, Al and Pt result in significantly higher absorptance than Au and Ag. Al results in even higher absorptance than Pt for side lengths of 100 and 125 nm, while Pt results in the highest absorptance for the largest cube size. The Pt cube with a side length of 150 nm results in the highest total absorptance value of 0.812, which is a 52.9% increase in absorptance relative to the reference cell without nanoparticles. This is the highest relative increase achieved in a simulation in this thesis. The results show that the size of the nanocube will most likely affect which metal is best suited to increase the absorptance of the PV cell. The absorptance increase for all metals and cube sizes relative to the reference PV cell without nanoparticles is shown in figure 6.69a.

880 nm PV cell

For the two smallest cube sizes with side lengths equal to 20 and 50 nm, Au and Ag result in slightly higher absorptance than Al and Pt. When the side length gets to 80 nm, Pt is approximately equal to Au and Ag, while Al now results in higher absorptance than the other three. For the three largest spheres with diameters of 150, 200 and 250 nm, Al results in noticeably higher absorptance than Au and Ag, but it is Pt that results in the highest absorptance by far. This is very similar to the results from the simulations using spheres, as described in section 6.35.2. A noticeable difference in the results from the simulations using cubes compared to the simulations using spheres is that the absorptance maximum is reached with the cube of side length 150 nm, and then the absorptance decreases for the two largest cubes. The magnitude of this absorptance drop for the two largest spheres is particularly

large for Au, Ag and Al cubes, while it is less significant for the Pt cubes. The Pt cube with side length 150 nm results in the highest total absorptance with a value of 0.843, which is a 25.6% increase in absorptance relative to the reference cell without nanoparticles. The results again show that the size of the nanocube will most likely affect which metal is best suited to increase the absorptance of the PV cell. The absorptance increase for all metals and cube sizes relative to the reference PV cell without nanoparticles is shown in figure 6.69b.

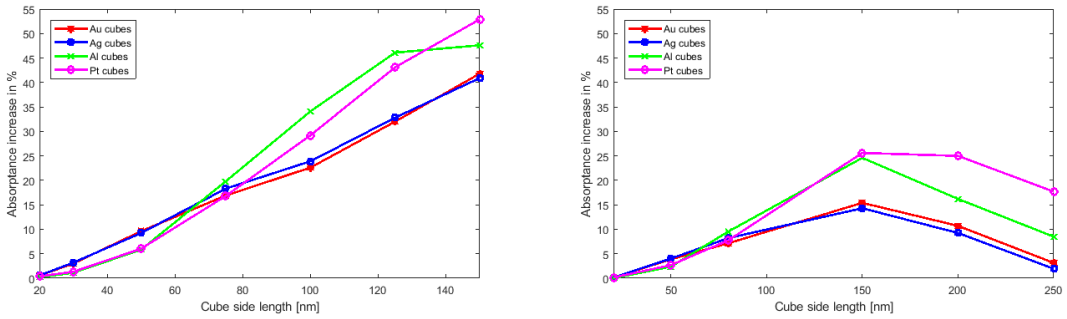

(a) (b)

Figure 6.69: Percentage increase in total absorptance for the PV cells with integrated nanocubes. (a) 310 nm PV cell. (b) 880 nm PV cell.

6.35.4 Rods

This section gives a summary of the results from the simulations using solid rods as nanoparticles.

310 nm PV cell

The results show a clear trend, which is that Au and Ag result in the highest absorptance for all rod sizes. The absorptance increases with increasing rod size for all metals, and the difference between the best metals (Au and Ag) and the worst metals (Al and Pt) also increases with increasing rod size. Pt results in higher absorptance than Al. The Au rod with a diameter of 60 nm and height of 180 nm results in the highest total absorptance value of 0.632, which is a 19.0% increase in absorptance relative to the reference cell without nanoparticles. The results show that the size of the nanorod will most likely not affect which metal is best suited to increase the absorptance of the PV cell. The absorptance increase for all metals and rod sizes relative to the reference PV cell without nanoparticles is shown in figure 6.70a.

880 nm PV cell

For the three smallest rod sizes, Au results in the highest total absorptance, followed by Ag, then Pt and finally Al. Ag results in only slightly lower absorptance than Au, while Pt and Al results in significantly lower absorptance. Al results in even lower absorptance than Pt. However, something very interesting happens for the two largest rods. For these rods, Au and Ag experiences a drop in absorptance similar to that described for cubes in section 6.7, while the absorptance continues to increase

for these rods for both Al and Pt. The absorptance drop experienced with Au and Ag nanorods is not as significant as the one seen for nanocubes, but the absorptance decreases nonetheless. Since the absorptance resulting from Al and Pt continues to rise, the total absorptance with these two metals goes from being significantly lower than Au and Ag for the three smallest rods to being significantly higher for the two largest rods. The Pt rod with a diameter of 160 nm and lenght of 480 nm results in the highest total absorptance with a value of 0.849, which is a 26.5% increase in absorptance relative to the reference cell without nanoparticles. The results show that the size of the nanorod will most likely affect which metal is best suited to increase the absorptance of the 880 nm PV cell. The absorptance increase for all metals and rod sizes relative to the reference PV cell without nanoparticles is shown in figure 6.70b.

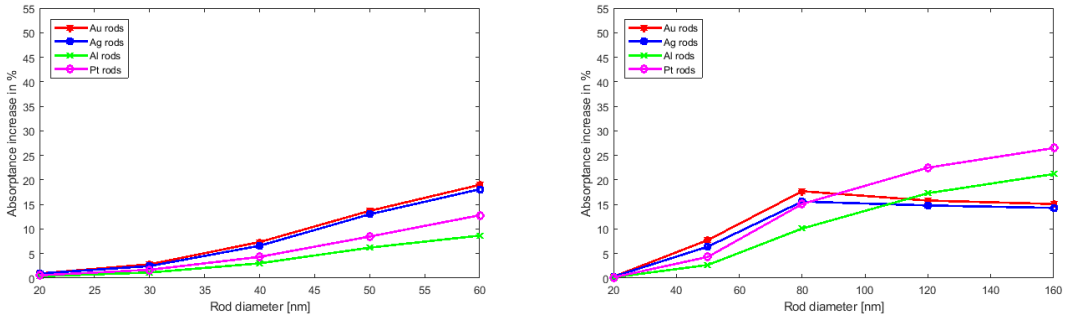

(a) (b)

Figure 6.70: Percentage increase in total absorptance for the PV cells with integrated nanorods. The height is equal to three times the diameter for all rods in this thesis. (a) 310 nm PV cell. (b) 880 nm PV cell.

6.35.5 Pyramids

This section gives a summary of the results from the simulations using solid pyramids as nanoparticles. All pyramids have heights equal to their side lenght in this thesis.

310 nm PV cell

All four metals have quite similar results in this group. The absorptance increases with increasing pyramid size for all metals. For the three smallest pyramids with side lengths of 20, 30 and 50 nm, all four metals result in almost equal absorptance. For the fourth pyramid with side length of 75 nm, Al results in higher absorptance while the remaining three metals still result in almost equal absorptance. For the two largest pyramids with side lengths of 100 and 150 nm, Al results in higher absorptance than Pt, while Au and Ag are almost equal and result in the lowest absorptance. The Al pyramid with a side length of 150 nm results in the highest total absorptance value of 0.663, which is a 24.9% increase in absorptance relative to the reference cell without nanoparticles. The results show that the size of the nanorod will most likely not affect which metal is best suited to increase the absorptance of the PV cell. The absorptance increase for all metals and pyramid sizes relative to the reference PV cell without nanoparticles is shown in figure 6.71a.

880 nm PV cell

The absorptance increases with increasing pyramid size for all metals in this group as well, except for Ag which shows a slight drop in absorptance from the second largest to the largest pyramid. For the four smallest pyramids with side lengths of 20, 50, 80 and 150 nm, the total absorptance is almost equal for all four metals used in this thesis. It is only for the two largest pyramids that significant differences are seen. Au and Ag remain quite equal for these two pyramids as well, while Al results in higher absorptance than Au and Ag, and Pt results in even higher absorptance than Al. The Pt pyramid with a side length of 250 nm results in the highest total absorptance with a value of 0.861, which is the highest total absorptance value seen in any simulation in this thesis. It is a 28.3% increase in absorptance relative to the reference cell without nanoparticles. The results again show that the size of the nanopyramid will most likely not affect which metal is best suited to increase the absorptance of the 880 nm PV cell. The absorptance increase for all metals and pyramid sizes relative to the reference PV cell without nanoparticles is shown in figure 6.71b.

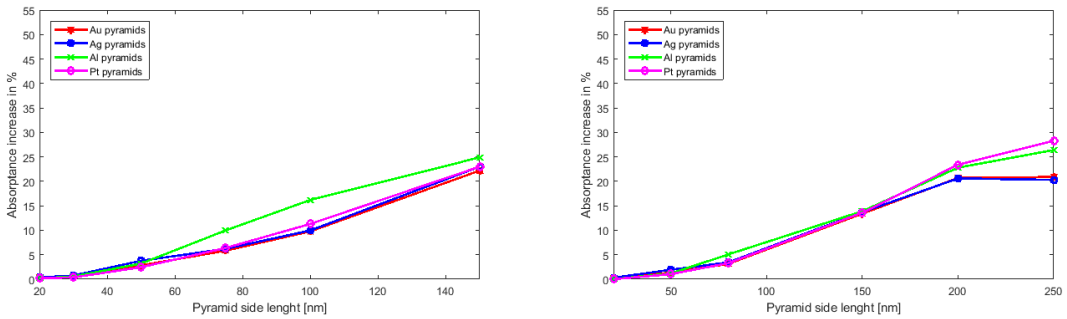

(a) (b)

Figure 6.71: Percentage increase in total absorptance for the PV cells with integrated nanopyramids. The height is equal to the side length for all pyramids in this thesis. (a) 310 nm PV cell. (b) 880 nm PV cell.

6.35.6 Core-Shell and Other Variations

Of the 391 simulations performed in this thesis, approximately half of them used solid nanoparticles placed at the center of the perovskite layer, referred to as standard setup in this thesis. The other half employed various adjustments to investigate whether these adjustments would increase or decrease the total absorptance relative to the simulations using the standard setup. The variations are described in chapter 6.19 and can be summarized as follows: two simulations using nanoparticles with a SiO_2 shell, one simulation placing a solid nanoparticle at the bottom interface of the perovskite layer and one simulation placing a solid nanoparticle at the top interface of the perovskite layer, two simulations placing two nanoparticles close together in either a side by side or a over/under setup. The results of these simulations are summarized in this section.

The results from the simulations in this thesis indicates that it is probably not beneficial to cover the metal nanoparticles with a SiO_2 shell, if the total absorptance of the PV cell is considered. All simulations using core-shell nanoparticles

with a metal core and a SiO_2 shell resulted in decreased absorptance relative to the simulation using the same metal core without a shell, with only two exceptions. The Au pyramids and Ag pyramids with a SiO_2 shell showed a very slight increase in absorptance relative to the standard setup, but the fourteen other simulation groups showed a very significant decrease in absorptance relative to the standard setup. This is consistent with the findings of Carretero-Palacios and co-workers [18] who stated that while core-shell nanoparticles like the ones used in this thesis does increase the total absorptance of a perovskite PV cell, the absorptance will always be higher for uncoated metal nanoparticles.

When it comes to the final four variations which vary the position and the number of the nanoparticles in the PV cell, the results does not show any clear trends. While varying the position and number of nanoparticles will always result in a small change in the total absorptance of the PV cell, it does not result in any drastic changes according to the results in this thesis. There is no clear trend that shows what position and number of particles that results in increased absorptance either. In some groups, placing the nanoparticle at the top interface increases the absorptance slightly, while in other groups it decreases the absorptance slightly. It is the same with the bottom interface position and the double particle setups as well, i.e. in some simulation groups the absorptance increases slightly and in others it decreases slightly. However, these changes could be well suited to optimize the characteristics of perovskite PV cells. Once the material and shape of the nanoparticle has been chosen, simulations and/or experiments can be carried out to find the optimal position of the nanoparticle, and whether it is most beneficial to use a single particle or two smaller particles placed side by side or one above the other. In such a way, these variations can be employed to fine-tune the properties of the PV cell in the desired direction.

6.35.7 Overall

In general, it seems to be most beneficial to use relatively large nanoparticles compared to smaller nanoparticles, if the focus is to increase the total absorptance of the PV cell structure. The only exceptions to this in this thesis are the largest nanocubes in the 880 nm PV cell and the largest Au and Ag nanorods in the 880 nm PV cell. All others show increased absorptance with increasing nanoparticle size. The most natural explanation for this is that the larger nanoparticles covers a larger area of the PV cell. Since the simulation region is the same size in all simulations, a larger nanoparticle covers a larger portion of the simulation region, and this seems to result in a larger total absorptance in most cases. However, there are exceptions to this that seems to indicate that it is not quite that straight-forward. As mentioned above, the two largest nanocubes in the 880 nm PV cell both result in decreased absorptance compared to the third largest nanocube, and the effect is more pronounced for Au and Ag than it is for Al and Pt. The most logical explanation for this is that these nanoparticles are so large that they start to resemble a plane surface due to the periodic boundaries, as explained in chapter 6.7, and this causes a dramatic increase in reflectance with a decrease in absorptance as the natural consequence. Since the effect is more pronounced in Au and Ag, it is most likely better to use Al or Pt for large nanoparticle sizes. Another interesting exception is the fact that in some cases the absorptance actually increases a little when two

smaller nanoparticles are placed one above the other compared to when one larger nanoparticle is used, e.g. chapter 6.25 using Al nanocubes. The total volume of the two smaller nanocubes is the same as the volume of the one larger cube that they are compared to, but since they are placed one above the other, they cover a much smaller portion of the area that is perpendicular to the incident light. Also, the relatively larger nanocube is not one of the larger cubes (the side length is only 80 nm), so there should be no "plane surface effect" as described above for the largest cubes. Consequently, with less area covered it would be expected that the total absorptance in the simulation with the two smaller nanocubes would be lower compared to the simulation with one nanocube covering a larger area, but in fact the total absorptance actually increases a little with the two smaller nanocubes. This indicates that there are other variables that in some cases can be more important than area coverage.

According to equations 4.1 and 4.2, the losses due to photons being absorbed by the nanoparticle will be smaller with relatively large nanoparticles. These equations state that the absorption cross section of a particle is proportional to the volume of the particle, while the scattering cross section is proportional to the square of the volume of the particle. This means that as the volume of the nanoparticle increases, scattering of photons from the nanoparticle will dominate over absorption of photons by the nanoparticle. As discussed in chapters 4.1.1 and 5.2, photons that are absorbed by the nanoparticle will not generate electricity, while photons that are scattered by the nanoparticle could be absorbed by the perovskite layer and consequently generate electricity. This means that there will be less parasitic photon absorption with relatively large nanoparticles, i.e. a larger portion of the increase in total absorptance will be in the perovskite layer. Following this logic, it is reasonable to expect that the actual PCE of the PV cells will benefit more from relatively large nanoparticles than from relatively small nanoparticles.

Since this thesis focuses on maximizing the total absorptance of the PV cell, the best choices related to material and shape of nanoparticle will be dictated mostly by the absorptance values and the absorptance increase. However, when constructing an actual PV cell there could be other considerations that might make it more beneficial to make a different choice. If the maximum total absorptance is desired, then the best choice is the 880 nm PV cell with a Pt nanopyramid with side length and height equal to 250 nm embedded at the center of the perovskite layer. The periodic boundaries means that nanopyramids are placed in an array in the x and y direction with a distance of 50 nm between the base of each pyramid. However, if a thinner PV cell is desired, then the best choice will be the 310 nm PV cell with a Pt nanocube with side lengths equal to 150 nm embedded at the center of the perovskite layer. The periodic boundaries means that the nanocubes extends in the x and y directions with 150 nm between each nanocube. The absorptance of this setup is so high (0.812) that even though the aforementioned Pt pyramid in the 880 nm PV cell has a higher total absorptance (0.861), it might make more sense to choose the 310 nm PV cell with the Pt nanocube since that would require less material for both the nanoparticles, perovskite material and the rest of the PV cell structure. This would reduce the weight and most likely increase the flexibility, as well as reduce material costs, which could result in a more cost-effective PV cell.

There are also other factors affecting the material choice. For both options mentioned above, the Al nanoparticles of the same shape and size result in a total

absorptance that is not that much lower than the Pt nanoparticles. For the 310 nm PV cell the Al nanocube would result in an absorptance of 0.784 instead of 0.812, and for the 880 nm PV cell the Al nanopyramid would result in an absorptance of 0.848 instead of 0.861. Even though this is a little lower, the availability and price of Al versus Pt could very well make it more beneficial to use Al nanoparticles than Pt nanoparticles. The same applies to Al versus Au and Ag, i.e. Al is very likely to be the best choice of material of the four considered in this thesis when considering availability and price.

If other factors make it necessary to use smaller sized nanoparticles, then the differences between shapes and materials are reduced. In most cases, Au or Ag results in the highest absorptance for smaller sized nanoparticles. However, Al could turn out to be a better choice in these cases as well due to availability and price, particularly if mass production is considered. A benefit with smaller particles compared to larger ones, outside of the obvious reduction in nanoparticle material usage, is that it leaves more room to fine-tune the properties of the PV cell by adjusting the position and number of nanoparticles.

Chapter 7

Summary, Conclusion and Future Work

The focus of this thesis has been to investigate the effect of integrated metal nanoparticles on the optical absorptance of perovskite PV cells. This has been a purely theoretical thesis where computer simulations have provided the results rather than experiments. Just under 400 simulations were performed using the software package Lumerical FDTD Solutions, which solves Maxwell's equations in the time domain by using the finite-difference time-domain (FDTD) method. The simulations were divided into groups according to the material and shape of the nanoparticle. In addition to this, variations related to core-shell nanoparticles, position and number of particles were also simulated. The various simulation results were compared to each other and to relevant research articles when available.

The thesis started with an introduction in chapter 1 where the background of the thesis and its objectives were described. Then, a general description of photovoltaic solar cells (PV cells) was given in chapter 2, including history, working principle and different types of PV cells. Following this, a more thorough and detailed description of perovskite PV cells was given in chapter 3. The concept of using nanoparticles to improve the performance of PV cells, often referred to as plasmonic PV cells, was then described in chapter 4, first in general and then specifically for perovskite PV cells. Chapter 5 then provided a description of the working principle of the Lumerical software and the simulation settings used in this thesis. The results of all the simulations was presented, summarized and discussed in chapter 6. This chapter (chapter 7) gives a general summary and conclusion for the thesis.

The advent of fossil fuels has enabled the human race to take great technological strides over the course of the last hundred years, particularly in the latest few decades. However, the enormous emissions of carbon dioxide through the burning of fossil fuels have proven to be the greatest single contributor to the ongoing anthropogenic climate change. There is high consensus in the scientific community that the effects of climate change can become catastrophic if no changes are made. These effects include droughts, famine and extreme weather patterns, which could result in wars, enormous refugee migrations and destabilized societies worldwide. In addition to climate change, fossil fuel combustion also releases gases that cause acid rain and the pollution of air and water. Finally, there is only a finite amount of fossil fuels available from the Earth, which means that it will run out at some point. The consequence of this is that the human race is being forced to make a great shift

over to renewable energy, and it needs to happen as quickly as possible. This is also reflected in several of the Sustainable Development Goals of the United Nations.

Perhaps the most promising of all renewable energy technologies is PV cells. Therefore, the various PV technologies is likely to play a major role in the energy transformation that has already started. One of the most promising of all the PV technologies is the perovskite PV cells. This is a thin film PV cell technology which has shown very good power conversion efficiencies (PCE) in lab experiments, they are easy and relatively cheap to produce, and they are light-weight and flexible which makes them ideal for building integrated PV cells. However, they are still in the development stage and are still experiencing challenges related to long-term stability, hysteresis, and scaling up to large area devices. One of the most promising methods to increase the PCE of these PV cells (and other PV cells) is to utilize the plasmonic effects that arise from the integration of metal nanoparticles in the perovskite PV cells. It is the investigation of how these plasmonic effects influences the amount of light that is absorbed by the PV cell that has been the main objective of this thesis and the simulations performed. For the metal nanoparticles, the materials used were gold (Au), silver (Ag), aluminum (Al) and platinum (Pt), the shapes were spheres, cubes, rods (cylinders) and pyramids. Other variations included covering the metal nanoparticles with a SiO_2 shell, adjusting the vertical position of the nanoparticles, and setting up two and two nanoparticles either side by side or one above the other. The material data for the PV cell layers were imported from research articles. Two different PV cell thicknesses were used: one where the perovskite layer had a thickness of 200 nm and one where the thickness was 500 nm. These were referred to as the 310 nm PV cell and the 880 nm PV cell, which was the total thickness of the two PV cells including hole-transport material (HTM) and electron-transport material (ETM).

The simulation results indicate that the absorptance of the PV cells increases as the size of the nanoparticles increases in most cases. The absorptance increase relative to the reference PV cells without nanoparticles show that the relative increase is higher in the 310 nm PV cells. This supports the claim that thin PV cells will benefit more from plasmonic effects than relatively thicker PV cells. The maximum total absorptance seen in the simulations was achieved by the Pt pyramid with side length and height equal to 250 nm, embedded at the center of the perovskite layer in the 880 nm PV cell. The total absorptance achieved with this setup was 0.861, which means that 86.1% of the incident light in the chosen wavelength interval (300-900 nm) was absorbed by the PV cell structure. The maximum increase in absorptance relative to the reference PV cell without nanoparticles was achieved by the Pt cube with side lengths equal to 150 nm, embedded at the center of the perovskite layer in the 310 nm PV cell. This setup increased the total absorptance by 52.9% relative to the same PV cell without a Pt cube and resulted in a total absorptance of 0.812. For both of these top performing PV cells, the nanoparticle material can be switched from Pt to Al without drastically decreasing the absorptance. Since Al is a much cheaper and more available material than Pt, it could be beneficial to use Al even though the total absorptance is a little lower. The best performing materials for the smaller nanoparticles was usually Au and Ag, but by the same reasoning as above it could be beneficial to use Al instead, particularly for mass production. The core-shell simulations with a SiO_2 shell showed decreased absorptance relative to when the nanoparticle was used without a shell in almost

all cases. The variations related to position and number of nanoparticles showed no clear trends and no major changes in absorptance relative to the standard setup with one nanoparticle at the center of the perovskite layer, but these variations could be useful in an optimization process to fine-tune the properties of the PV cell.

Almost every single simulation in this thesis resulted in increased absorptance through the integration of nanoparticles in the PV cell structure. Only a very few simulations with some of the smallest nanoparticles showed unchanged absorptance, and no simulations resulted in decreased absorptance relative to the PV cells without nanoparticles. These results strongly indicate that the use of metal nanoparticles in perovskite PV cells will increase the total absorptance of these PV cells. Some of the increase in total absorptance is most likely due to photons being absorbed by the metal nanoparticles instead of the perovskite material. These photons will not generate electricity and therefore constitute a loss. However, some of the increase in total absorptance is in the perovskite material and this *will* contribute to the generation of electricity and consequently increase the actual PCE of the PV cell. Thus, the integration of metal nanoparticles in the perovskite layer or at the perovskite boundaries seems to be a very promising route towards increasing the PCE of these PV cells and realizing high-efficiency cost effective thin film PV cells.

As future work it would be very interesting to perform more simulations of different types, as well as experiments, in order to find out how much of the increase in total absorptance is in the perovskite layer and how much of it is lost, e.g. due to photons absorbed by the metal nanoparticles. In this way, the increase in the actual PCE of the PV cells could be quantified. Different methods for maximizing the perovskite absorptance and minimizing the parasitic absorptance by the metal nanoparticles and other layers in the PV cell could also be tested in an optimization process to get the actual PCE of the PV cell as close to its ultimate (ideal) efficiency as possible.

Bibliography

[1] IPCC, "Climate change 2014 - mitigation of climate change," tech. rep., Intergovernmental Panel on Climate Change, 2014.

[2] DNV, "Energy transition outlook 2017," tech. rep., DNV GL, 2017.

[3] REN21, "Renewables 2016: Global status report," tech. rep., Renewable Energy Policy Network for the 21st Century, 2016.

[4] P. G. V. Sampaio and M. O. A. González, "Photovoltaic solar energy: Conceptual framework," *Renewable and Sustainable Energy Reviews*, vol. 74, pp. 590–601, 2017.

[5] P. Hofmann, *Solid State Physics: An Introduction*. Boschstr. 12, 69469 Weinheim, Germany: Wiley-VCH Verlag GmbH and Co. KGaA, 2015.

[6] J. Nelson, *The Physics of Solar Cells*. Covent Garden, London, UK: Imperial College Press, 2003.

[7] NREL, "Best research-cell efficiencies." `https://www.nrel.gov/pv/assets/images/efficiency-chart.png`. Accessed: 2018-03-22.

[8] T. S. Systems, "Standard solar spectra." `https://www.solar-simulator.info/solar-simulator-match.html`. Accessed: 2018-03-22.

[9] N. Kannan and D. Vakeesan, "Solar energy for future world: - a review," *Renewable and Sustainable Energy Reviews*, vol. 62, pp. 1092–1105, 2016.

[10] N.-G. Park, "Perovskite solar cells: an emerging photovoltaic technology," *Materials Today*, vol. 18, pp. 65–72, 2015.

[11] M. I. H. Ansari, A. Qurashi, and M. K. Nazeeruddin, "Frontiers, opportunities and challenges in perovskite solar cells: A critical review," *Journal of Photochemistry and Photobiology C: Photochemistry Reviews*, vol. 35, pp. 1–24, 2018.

[12] I. Mesquita, L. Andrade, and A. Mendes, "Perovskite solar cells: Materials, configurations and stability," *Renewable and Sustainable Energy Reviews*, vol. 82, pp. 2471–2489, 2018.

[13] A. B. Djurisic, F. Z. Liu, H. W. Tam, M. K. Wong, A. Ng, C. Surya, W. Chen, and Z. B. He, "Perovskite solar cells - an overview of critical issues," *Progress in Quantum Electronics*, vol. 53, pp. 1–37, 2017.

[14] F. Enrichi, A. Quandt, and G. C. Righini, "Plasmonic enhanced solar cells: Summary of possible strategies and recent results," *Renewable and Sustainable Energy Reviews*, vol. 82, pp. 2433–2439, 2018.

[15] Y. H. Jang, Y. J. Jang, S. Kim, L. N. Quan, K. Chung, and D. H. Kim, "Plasmonic solar cells: From rational design to mechanism overview," *Chemical Reviews*, vol. 116, pp. 14982–15034, 2016.

[16] Lumerical, "Lumerical FDTD solutions." `https://www.lumerical.com/tcad-products/fdtd/`. Accessed: 2018-04-01.

[17] P. Löper, M. Stuckelberger, B. Niesen, J. Werner, M. Filipic, S.-J. Moon, J.-H. Yum, M. Topic, S. D. Wolf, and C. Ballif, "Complex refractive index spectra of $CH_3NH_3PbI_3$ perovskite thin films determined by spectroscopic ellipsometry and spectrophotometry," *The Journal of Physical Chemistry Letters*, vol. 6, pp. 66–71, 2015.

[18] S. Carretero-Palacios, A. Jimenez-Solano, and H. Miguez, "Plasmonic nanoparticles as light-harvesting enhancers in perovskite solar cells: A user's guide," *ACS Energy Letters*, vol. 1, pp. 323–331, 2016.

[19] S. Carretero-Palacios, M. E. Calvo, and H. Miguez, "Absorption enhancement in organic-inorganic halide perovskite films with embedded plasmonic gold nanoparticles," *The Journal of Physical Chemistry*, vol. 119, pp. 18635–18640, 2015.

[20] UN, "United nations sustainable development goals." `http://www.un.org/sustainabledevelopment/sustainable-development-goals/`. Accessed: 2018-03-17.

[21] S. S. Mali, C. S. Shim, H. Kim, P. S. Patil, and C. K. Hong, "*In situ* processed gold nanoparticle-embedded TiO_2 nanofibers enabling plasmonic perovskite solar cells to exceed the 14% conversion efficiency," *Nanoscale*, vol. 8, pp. 2664–2677, 2016.

[22] M. Tang, L. Zhou, S. Gu, W. Zhu, Y. Wang, J. Xu, Z. Deng, T. Yu, Z. Lu, and J. Zhu, "Fine-tuning the metallic core-shell nanostructures for plasmonic perovskite solar cells," *Applied Physics Letters*, vol. 109, 2016.

[23] B. Cai, Y. Peng, Y.-B. Cheng, and M. Gu, "4-fold photocurrent enhancement in ultrathin nanoplasmonic perovskite solar cells," *Optics Express*, vol. 23, pp. 1700–1706, 2015.

[24] L. Yue, B. Yan, M. Attridge, and Z. Wang, "Light absorption in perovskite solar cell: Fundamentals and plasmonic enhancement of infrared band absorption," *Solar Energy*, vol. 124, pp. 143–152, 2016.

[25] MathWorks, "MATLAB." `https://se.mathworks.com/products/matlab.html`. Accessed: 2018-04-02.

[26] Microsoft, "Excel." `https://products.office.com/nb-no/excel`. Accessed: 2018-04-02.

[27] LaTeX, "The LaTeX Project." `https://www.latex-project.org/`. Accessed: 2018-04-08.

[28] B. Tummers, "Datathief." `https://datathief.org/`. Accessed: 2018-04-20.

[29] Gigahertz-Optik, "Light measurement." `https://light-measurement.com/reflection-absorption/`. Accessed: 2018-06-27.

[30] G. Boyle, *Renewable Energy - Power for a Sustainable Future*. Great Clarendon Street, Oxford OX2 6DP: Oxford University Press, 2012.

[31] M. Kumar and A. Kumar, "Performance assessment and degradation anaysis of photovoltaic technologies: A review," *Renewable and Sustainable Energy Reviews*, vol. 78, pp. 554–587, 2017.

[32] L. E. Chaar, L. Iamont, and N. E. Zein, "Review of photovoltaic technologies," *Renewable and Sustainable Energy Reviews*, vol. 15, pp. 2165–2175, 2011.

[33] IEA, "Snapshot of global photovoltaic markets," tech. rep., International Energy Agency, 2016.

[34] S. J. Fonash, *Solar Cell Device Physics*. 30 Corporate Drive, Suite 400, Burlington, MA 01803, USA: Elsevier, 2010.

[35] V. V. Tyagi, N. A. A. Rahim, N. A. Rahim, and J. A. Selvaraj, "Progress in solar pv technology: Research and achievement," *Renewable and Sustainable Energy Reviews*, vol. 20, pp. 443–461, 2013.

[36] T. D. Lee and A. U. Ebong, "A review of thin film solar cell technologies and challenges," *Renewable and Sustainable Energy Reviews*, vol. 70, pp. 1286–1297, 2017.

[37] M. A. Green, A. Ho-Baillie, and H. J. Snaith, "The emergence of perovskite solar cells," *Nature Photonics*, vol. 8, pp. 506–514, 2014.

[38] M. K. Assadi, S. Bakhoda, R. Saidur, and H. Hanaei, "Recent progress in perovskite solar cells," *Renewable and Sustainable Energy Reviews*, vol. 81, pp. 2812–2822, 2018.

[39] J. Nakazaki and H. Segawa, "Evolution of organometal halide solar cells," *Journal of Photochemistry and Photobiology C: Photochemistry Reviews*, vol. 35, pp. 74–107, 2018.

[40] S. D. Stranks and H. J. Snaith, "Metal-halide perovskites for photovoltaic and light-emitting devices," *Nature Nanotechnology*, vol. 10, pp. 391–402, 2015.

[41] J. M. Ball, S. D. Stranks, M. T. Hörantner, S. Hüttner, W. Zhang, E. J. W. Crossland, I. Ramirez, M. Riede, M. B. Johnston, R. H. Friend, and H. J. Snaith, "Optical properties and limiting photocurrent of thin-film perovskite solar cells," *Energy and Environmental Science*, vol. 8, pp. 602–609, 2015.

[42] M. Filipic, P. Löper, B. Niesen, S. D. Wolf, J. Krc, C. Ballif, and M. Topic, "$CH_3NH_3PbI_3$ perovskite/silicon tandem solar cells: characterization based optical simulations," *Optics Express*, vol. 23, pp. 263–278, 2015.

[43] M. J. Taghavi, M. Houshmand, and M. H. Zandi, "Modeling of optical losses in perovskite solar cells," *Superlattices and Microstructures*, vol. 97, pp. 424–428, 2016.

[44] J. A. Christians, J. S. Manser, and P. V. Kamat, "Best practices in perovskite solar cell efficiency measurements. avoiding the error of *Making Bad Cells Look Good*," *The Journal of Physical Chemistry Letters*, vol. 6, pp. 852–857, 2015.

[45] T. Ibn-Mohammed, S. C. L. Koh, I. M. Reaney, A. Acquaye, G. Schileo, K. B. Mustapha, and R. Greenough, "Perovskite solar cells: An integrated hybrid life cycle assessment and review in comparison with other photovoltaic technologies," *Renewable and Sustainable Energy Reviews*, vol. 80, pp. 1321–1344, 2017.

[46] W. Zhang, M. Anaya, G. Lozano, M. E. Calvo, M. B. Johnston, H. Miguez, and H. J. Snaith, "Highly efficient perovskite solar cells with tunable structural color," *Nano Letters*, vol. 15, pp. 1698–1702, 2015.

[47] B. W. Schneider, N. N. Lal, S. Baker-Finch, and T. P. White, "Pyramidal surface textures for light trapping and antireflection in perovskite-on-silicon tandem solar cells," *Optics Express*, vol. 22, pp. 1422–1430, 2014.

[48] S. A. Maier, *Plasmonics - Fundamentals and Applications*. 233 Spring Street, New York, NY 10013, USA: Springer Science+Business Media LLC, 2007.

[49] K. Ueno, T. Oshikiri, Q. Sun, X. Shi, and H. Misawa, "Solid-state plasmonic solar cells," *Chemical Reviews*, vol. 118, pp. 2955–2993, 2018.

[50] P. Mandal and S. Sharma, "Progress in plasmonic solar cell efficiency improvement: A status review," *Renewable and Sustainable Energy Reviews*, vol. 65, pp. 537–552, 2016.

[51] V. R. A. Holm, B. Y. Zheng, P. M. Denby, B. Holst, N. J. Halas, and M. M. Greve, "Work function-driven hot electron extraction in a bimetallic plasmonic MIM device," *ACS Photonics*, vol. 5, pp. 1202–1207, 2018.

[52] Z. Lu, X. Pan, Y. Ma, Y. Li, L. Zheng, D. Zhang, Q. Xu, Z. Chen, S. Wang, B. Qu, F. Liu, Y. Huang, L. Xiao, and Q. Gong, "Plasmonic-enhanced perovskite solar cells using alloy popcorn nanoparticles," *RSC Advances*, vol. 5, pp. 11175–11179, 2015.

[53] W. Zhang, M. Saliba, S. D. Stranks, Y. Sun, X. Shi, U. Wiesner, and H. J. Snaith, "Enhancement of perovskite-based solar cells employing core-shell metal nanoparticles," *Nano Letters*, vol. 13, pp. 4505–4510, 2013.

[54] A. E. Shalan, T. Oshikiri, H. Sawayanagi, K. Nakamura, K. Ueno, Q. Sun, H.-P. Wu, E. W.-G. Diau, and H. Misawa, "Versatile plasmonic-effects at the interface of inverted perovskite solar cells," *Nanoscale*, vol. 9, pp. 1229–1236, 2017.

[55] M. M. Tavakoli, K.-H. Tsui, Q. Zhang, J. He, Y. Yao, D. Li, and Z. Fan, "Highly efficient flexible perovskite solar cells with antireflection and self-cleaning nanostructures," *ACS Nano*, vol. 9, pp. 10287–10295, 2015.

[56] Z. Xie, S. Sun, W. Wang, L. Qin, Y. Yan, R. Hou, and G. G. Qin, "Simulation study on improving efficiencies of perovskite solar cell: Introducing nano textures on it," *Optics Communications*, vol. 410, pp. 117–122, 2018.

[57] H. Nourolahi, A. Behjat, S. M. M. H. Zarch, and M. A. Bolorizadeh, "Silver nanoparticle plasmonic effects on hole-transport material-free mesoporous heterojunction perovskite solar cells," *Solar Energy*, vol. 139, pp. 475–483, 2016.

[58] G. M. Kim and T. Tatsuma, "Semi-transparent perovskite solar cells developed by considering human luminosity function," *Scientific Reports*, vol. 7, pp. 10699–10705, 2017.

[59] M. A. Mohebpour, M. Saffari, H. R. Soleimani, and M. B. Tagani, "High performance of mixed halide perovskite solar cells: Role of halogen atom and plasmonic nanoparticles on the ideal current density of cell," *Physica E: Low-dimensional Systems and Nanostructures*, vol. 97, pp. 282–289, 2018.

[60] H. Yu, J. Roh, J. Yun, and J. Jang, "Synergistic effects of three-dimensional orchid-like TiO_2 nanowire networks and plasmonic nanoparticles for highly efficient mesoscopic perovskite solar cells," *Journal of Materials Chemistry A*, vol. 4, pp. 7322–7329, 2016.

[61] N. Fu, Z. Y. Bao, Y.-L. Zhang, G. Zhang, S. Ke, P. Lin, J. Dai, H. Huang, and D. Y. Lei, "Panchromatic thin perovskite solar cells with broadband plasmonic absorption enhancement and efficient light scattering management by au@ag core-shell nanocuboids," *Nano Energy*, vol. 41, pp. 654–664, 2017.

[62] D. J. Griffiths, *Introduction to Electrodynamics*. Edinburgh Gate, Harlow, Essex CM20 2JE, England: Pearson Education Limited, 2014.

[63] X. Ziang, L. Shifeng, Q. Laixiang, P. Shuping, W. Wei, Y. Yu, Y. Li, C. Zhijian, W. Shufeng, D. Honglin, Y. Minghui, and G. G. Qin, "Refractive index and extinction coefficient of $CH_3NH_3PbI_3$ studied by spectroscopic ellipsometry," *Optical Materials Express*, vol. 5, pp. 29–43, 2014.

[64] S. E. Han and G. Chen, "Optical absorption enhancement in silicon nanohole arrays for solar photovoltaics," *Nano Letters*, vol. 10, pp. 1012–1015, 2010.

[65] W. Shockley and H. J. Queisser, "Detailed balance limit of efficiency of pn junction solar cells," *Journal of Applied Physics*, vol. 32, pp. 510–519, 1961.

[66] V. R. A. Holm, M. M. Greve, and B. Holst, "A theoretical investigation of the optical properties of metal nanoparticles in water for photo thermal conversion enhancement," *Energy Conversion and Management*, vol. 149, pp. 536–542, 2017.

Appendix A

Calculation and Plotting Methods

The general method used to calculate total absorptance, reflectance and transmittance, as well as to create plots, was to import the simulation data from Lumerical FDTD Solutions into MATLAB (to create plots) and Microsoft Excel (to calculate total absorptance, reflectance and transmittance).

Each simulation in Lumerical FDTD Solutions recorded both reflectance and transmittance for the given PV cell as a function of the wavelength of the incident light. A total of 601 datapoints were used, which means that the data available from each simulation was a reflectance value and a transmittance value taken at 601 different points spread throughout the wavelength interval that was used in this thesis (300-900 nm). For each simulation, the "Export script to MATLAB" function was used. This script was modified slightly to plot the absorptance versus wavelength (instead of reflectance and transmittance). This was done simply by plotting 1 minus reflectance and transmittance on the y-axis instead of reflectance and transmittance directly. An example of the script used is given below.

MATLAB script example 1, start

```
load ('D:/Dropbox/Skoledokumenter/Mastergrad/Masteroppgaven/
MATLAB filer/Filer til masteroppgaven/simulation_391.mat');
ax1 = axes;
plot(lum.x0, (1-lum.y0-lum.y1))
set(get(ax1, 'XLabel'), 'String', 'lambda(nm)')
set(get(ax1, 'XLabel'), 'FontSize', 16)
set(get(ax1, 'XLabel'), 'FontWeight', 'bold')
set(ax1, 'XLim', [300 900])
set(ax1, 'YLim', [0 1])
set(ax1,'XGrid', 'on')
set(ax1,'YGrid', 'on')
```

MATLAB script example 1, end

These plots containing the result of a single simulation is not included in the thesis, but they were used as a way of visually checking the result after each simulation. Then the dataset was accessed in MATLAB and copied into an Excel spreadsheet. 601 reflectance values, 601 transmittance values and 601 wavelength values were combined in this spreadsheet to calculate the total absorptance, reflectance and transmittance for each simulation. To calculate the total reflectance and total transmittance, a simple numerical integration method based on finding the area under the curve was used. In this method, each of the 601 reflectance and

transmittance values were multiplied with the distance between the wavelength value at that specific datapoint and the wavelength value at the next closest datapoint. These products were then summed and divided by 600 (since the total wavelength interval consisted of 600 sections) to give the total reflectance and the total transmittance. This was done separately for reflectance and transmittance. Finally, the total absorptance can be calculated simply by subtracting the total reflectance and total transmittance from 1. The calculated values for total absorptance, reflectance and transmittance for each simulation were then copied into another spreadsheet to have an easy overview of the results from all the simulations in one table. These values are the ones given in the various tables in this thesis.

The following method were used to create the different plots in this thesis: The datasets with wavelength, reflectance and transmittance values for each simulation that was going to be included in the plot (usually 6-8 simulations in one plot) was copied into an Excel spreadsheet. This spreadsheet was then used as the datasource for the given plot in MATLAB. An example of the script written for these plots is given below.

MATLAB script example 2, start

```
dataset_2=xlsread('Plot_2.xlsx','A1:WC17');

x=dataset_2(1,:);

y1r=dataset_2(2,:);
y1t=dataset_2(3,:);

y2r=dataset_2(4,:);
y2t=dataset_2(5,:);

y3r=dataset_2(6,:);
y3t=dataset_2(7,:);

y4r=dataset_2(8,:);
y4t=dataset_2(9,:);

y5r=dataset_2(10,:);
y5t=dataset_2(11,:);

y6r=dataset_2(12,:);
y6t=dataset_2(13,:);

y7r=dataset_2(14,:);
y7t=dataset_2(15,:);

y8r=dataset_2(16,:);
y8t=dataset_2(17,:);

plot(x,1-y1r-y1t,x,1-y2r-y2t,x,1-y3r-y3t,x,1-y4r-y4t,x,1-y5r-y5t,
x,1-y6r-y6t,x,1-y7r-y7t,x,1-y8r-y8t)
```

```
xlabel('Wavelength [nm]')
ylabel('Absorptance')
legend('d=20 nm','d=30 nm','d=50 nm','d=75 nm','d=100 nm',
'd=125 nm','d=150 nm','no nanoparticle','Location','southwest')
```

MATLAB script example 2, end

The plots in section 6.1, where the simulation model used in this thesis is compared to existing work, were created by using the same method. The only difference is that the dataset for the graphs showing the results from existing work were taken from existing research articles by using the shareware Datathief. These datasets were then copied into the Excel spreadsheet which was used as the data-source in the MATLAB plot, in the same way as described above. An example of the script written for these plots is given below.

MATLAB script example 3, start

```
dataset_comp_5=xlsread('comp_5.xlsx','A1:B27');
load ('D:/Dropbox/Skoledokumenter/Mastergrad/Masteroppgaven/
MATLAB filer/Filer til masteroppgaven/comparison_5.mat');

x=dataset_comp_5(:,1);

y=dataset_comp_5(:,2);

plot(x,y,lum.x0,(1-lum.y0-lum.y1))

xlabel('Wavelength [nm]')
ylabel('Absorptance')
xlim([410 780])
ylim([0 1])
legend('Simulation result Carretero-Palacios et al.',
'Simulation result in this thesis','Location','Southwest')
```

MATLAB script example 3, end